FHWA-NJ-2005-013

Monitoring the Construction of the Doremus Avenue Bridge Structure

FINAL REPORT

May 2010

Submitted by

Hani Nassif, Ph.D., P.E.[1]
(PI) Associate Professor

Nakin Suksawang, Ph.D.[2]
Assistant Professor

Joe Davis, Ph.D., P.E. [1]
Research Associate

Mayrai Gindy, Ph.D.[3]
Assistant Professor

Talat Salama, Ph.D., P.E.[4]
Assistant Professor

[1]Dept. of Civil & Environmental Engineering
623 Bowser Road
Rutgers, The State University
Piscataway, NJ 08854-8014

[2]Dept. of Civil Engineering and Construction
Florida International University
1501 West Bradley Ave.
Miami, FL 61625

[3]Dept. of Civil & Environmental Engineering
University of Rhode Island
1 Lippitt Road, 201 Bliss Hall
Kingston, RI 02881

[4]Dept. of Civil Engineering and Construction
University of Alabama
Birmingham, AL

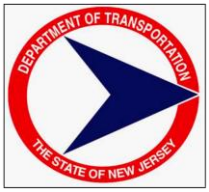

NJDOT Research Project Manager
Mr. W. Lad Szalaj

In cooperation with

New Jersey
Department of Transportation
Bureau of Research
And
U. S. Department of Transportation
Federal Highway Administration

DISCLAIMER STATEMENT

“The contents of this report reflect the views of the author(s), who is (are) responsible for the facts and the accuracy of the data presented herein. The contents do not necessarily reflect the official views or policies of the New Jersey Department of Transportation or the Federal Highway Administration. This report does not constitute a standard, specification, or regulation.”

TECHNICAL REPORT
STANDARD TITLE PAGE

1. Report No. FHWA NJ-2005-013	2.Government Accession No.	3. Recipient's Catalog No.
4. Title and Subtitle Monitoring of the Construction of the Doremus Avenue Bridge Structure		5. Report Date May 2010 6. Performing Organization Code CAIT/Rutgers
7. Author(s) Hani Nassif (PI), Nakin Suksawang, Joe Davis, Mayrai Gindy, Talat Salama		8. Performing Organization Report No.
9. Performing Organization Name and Address Dept. of Civil & Environmental Engineering Center for Advanced Infrastructure & Transportation Rutgers, The State University Piscataway, NJ 08854-8014		10. Work Unit No. 11. Contract or Grant No.
12. Sponsoring Agency Name and Address New Jersey Department of Transportation PO BOX 600 Trenton, NJ 08625 Federal Highway Administration U.S. Department of Transportation Washington, D.C.		13. Type of Report and Period Covered Draft Report 08/31/01 – 12/31/2006 14. Sponsoring Agency Code
15. Supplementary Notes		

16. Abstract

Starting in 2007, the American Association of State Highway and Transportation Officials (AASHTO) adopted the Load and Resistance Factored Design (LRFD) Bridge Design Specifications as the mandatory standard by which all future bridge structures should be designed. New Jersey committed itself to adopting the LRFD Specifications in January 2000. The LRFD Specifications consider the variability in the behavior of structural elements through extensive statistical analyses and, therefore, continue to be improved. However, many of the Specifications' design approaches and methodologies have been adopted with limited or virtually no experimental validation. Hence, there became a need to validate these new design procedures and models as well as the behavior of LRFD designed bridge structures.

The main objective of this study was to validate the AASHTO LRFD Specifications through field-testing of the Doremus Avenue Bridge- New Jersey's first AASHTO LRFD (1998) design. In addition, long-term monitoring of the bridge fatigue life was also implemented. In particular, the study evaluates the AASHTO criteria for composite design with respect to the requirements for shear connectors, the effects of designing for deflection control as well as using higher concrete strengths on deck stiffness and stresses. Results included new simplified equations for calculating Girder Distribution Factors (GDF) and effective flange width criteria in addition to establishing major live load spectra for various WIM NJ sites. Deflection measurements and simulation using Extreme Value Theory (EVT) shows that the 75-year maximum deflection is within the NJDOT deflection limit of L/1000. However, future research is needed to establish if the L/1000 limit is indirectly helping to control vibration of the superstructure. Moreover, a new procedure for predicting the remaining fatigue life is established using WIM truck data, rain flow, and structural analyses.

17. Key Words Bridge Structure, Deflection, Fatigue, LRFD, Distribution Factor, Impact Factor, Field Testing	18. Distribution Statement		
19. Security Classif (of this report) Unclassified	20. Security Classif. (of this page) Unclassified	21. No of Pages 155	22. Price

Form DOT F 1700.7 (8-69)

ACKNOWLEDGMENTS

The authors thank the New Jersey Department of Transportation (NJDOT) and staff for their help and support of this project: W. Lad Szalaj, NJDOT project manager; Jose Lopez (retired); Harry Capers, Jr. (retired); Nick Vittilo (retired); Richard Dunne; and Xiaohua “Hannah” Cheng for their help and assistance throughout the project. Also, the assistance of students Duygu Yuksel, Maqbool Mohamad, Nuno Chao, Kevin Robine, David Fusco, Pat Jameison, Amer Mohamad, Chris Eftychiatis, and Jim Ordija are thankfully acknowledged. The help of Scott Spencer and Rob Hansen of Slattery-Skanska and their accommodations and help with field-testing and instrumentation are greatly appreciated. In particular, much gratitude to Warren Vincentz, NJDOT resident engineer, for his help with the work for field instrumentation during Stage I construction.

TABLE OF CONTENTS

LIST OF FIGURES

LIST OF TABLES

EXECUTIVE SUMMARY

The American Association of State Highway and Transportation Officials (AASHTO) Load and Resistance Factored Design (LRFD) Bridge Design Specification was mandated by the Federal Highway Administration (FHWA) in the year 2007. All new bridges are to be designed and constructed according to AASHTO LRFD Specifications to be eligible for federal funding. New Jersey committed itself to adopting the AASHTO LRFD Specifications in January 2000. The AASHTO LRFD Specifications consider and ascertain the variability in the behavior of structural elements through extensive statistical analyses; therefore they continue to be refined. Many of the code's design approaches and methodologies have been adopted with limited or virtually no experimental validation. Therefore, it is believed that there is a need to validate the new design procedures and models as well as the resultant AASHTO LRFD bridge structure designs.

The primary objective of this study is to validate the AASHTO LRFD Specifications through field testing of the Doremus Avenue Bridge- New Jersey's first AASHTO LRFD (1998) design. In addition, long-term monitoring of the bridge fatigue life was also implemented.

The following is a summary of the results for the six main objectives that are described in this report:

Live-Load Distribution Factor

The Live-Load Distribution Factor (LDF) is one of the significant changes made in the AASHTO LRFD Specifications. In the AASHTO Standard Specifications, the LDF is based on a simple "*S*-over" equation, where the girder spacing (*S*) is divided by a constant depending on the bridge type; e.g., for steel I-girder, the constant is 5.5 ft. However, in the AASHTO LRFD Specifications, the LDF is calculated by using several power equations (i.e., $LDF = ax^n$) depending on the bridge type, and are based on regression analysis. These power equations involve several parameters, which complicate the design calculation. Additionally, some of these parameters are often unknown to the bridge engineer when designing new bridges. Thus, a simpler and accurate LDF equation is proposed in this study.

The Research Team (RT) has proposed new equations that are a modified version of the AASHTO Standard Specification LDF simple "*S*-over" formula. However, rather than dividing *S* by a constant, an equation is proposed to replace the constant. The following equations represent the denominator of the "*S*-over" equation for girder bridges (e.g., steel I-beam, prestressed concrete I-beam, and concrete spread box beam).
One lane,

$$D = 8.4 + \frac{S}{1.4} + \frac{L}{C}$$ Eq. (1)

Two lanes,

$$D = 7.0 + \frac{S}{3.0} + \frac{L}{C}$$ Eq. (2)

where *L* is the span length (ft) and *C* is given as 28 for the steel I-beam, 50 for the prestressed concrete I-beam, and 20 for the concrete spread box beam.

Effective Flange Width

There are no significant changes to the effective flange width (b_e) calculations in the AASHTO LRFD specifications. However, the validity of these calculations needs to be confirmed. Moreover, the National Cooperative High Research Program (NCHRP 12-57) recently questioned the validity of using the current code provisions for b_e especially for longer and wider structures that are now being built. Additionally, with the emergence of new high-performance material, there becomes a need to reexamine code design provisions and assess the validity of such assumptions. The accuracy in calculating the effective slab width has a direct effect on the computed ultimate moment as well as serviceability limit states, such as deflection and overloading.

In this study, a linear equation for the effective flange width, b_e, is proposed as follows:

$$b_e / b_s = 1 - 0.5\left(\frac{b_s}{L}\right) \text{ for } b_s / L > 0.25$$ Eq. (3)

Where $b_e = b_s$ for $\left(\frac{b_s}{L}\right) \leq 0.25$, b_s is the girder spacing, and L is the span length.

Deflection Limits

The AASHTO LRFD specifications made the use of deflection limits optional. However, the New Jersey Department of Transportation (NJDOT) as well as many state transportation departments still set a limit for all their state bridge designs. In this study, reliability-based analysis and simulation techniques were used to analyze measured field data. Based on the results, it is predicted that the deflection limit set by NJDOT will not be exceeded in 75 years. The reason for this is quite obvious as deflection limits used by NJDOT and many other states are based on human perception of vibration rather than on a serviceability limit state. In this study, the current deflection limits are verified using a new rational approach for predicting the bridge deflection. The new rational approach was developed by the use of extreme value theory. The predicted bridge deflection can be determined at different stages of its lifetime and compared to

the NJDOT limit. This approach is additionally used for the fatigue prediction which is also conducted in this study.

Dynamic Amplification Factor

The dynamic amplification factor in the AASHTO LRFD Specifications was simplified and reduced by multiplying the truck part of the HL-93 by 33 percent and by 15 percent for the strength limit state and the fatigue limit state, respectively. In this study, the dynamic impact factor was measured and evaluated using detailed grillage models that include road roughness and truck models. The results were compared with those from other dynamic tests of existing steel girder bridges in Michigan. For all tested bridges, the dynamic impact factor does not exceed 20 percent for trucks with a minimum gross vehicle weight (GVW) of 60 kips.

Truck Load Model

A permanent weight-in-motion (WIM) system was installed at the bridge site to collect data on traffic crossing the Doremus Avenue Bridge. The Doremus Avenue Bridge is a major crossing and entrance for trucks loading and unloading goods and containers into and from the Port of Elizabeth, near Newark, NJ. The WIM data was compared with other Strategic Highway Research Program (SHRP) WIM sites throughout the State of New Jersey. According to WIM data, a significant number of overloaded trucks are crossing the bridge. Traditionally, these overloads were considered errors in the system and were taken out of the WIM data. However, because the girder stresses were also monitored at the Doremus Avenue Bridge, the overloads were confirmed with stress readings. Trucks with GVW exceeding 200 kips were recorded as crossing over Doremus Avenue. Thus, new load models should be proposed for bridge rating analysis.

Fatigue Load Model

Estimation of the remaining fatigue life of an existing bridge involves evaluating fatigue resistance (capacity) and load spectra. Fatigue resistance depends on the type of detail, the degree of corrosion, and other deterioration. Load analysis requires knowledge of load history (accumulated damage), current load spectra, and prediction of future loads. The observed traffic stream is compared with the nominal fatigue evaluation model to gauge its effectiveness in predicting fatigue damage at Doremus Avenue. The effect of measurement duration is also studied to determine the minimum sample size needed for a stable and accurate fatigue life estimation. The procedures developed can be extended to simulate bridge live loads with site-specific WIM data applied to structural models. The resulting simulated stresses are then extrapolated, reducing or eliminating the need for labor-intensive field instrumentation.

BACKGROUND

The Doremus Avenue Bridge is part of an integrated roadway infrastructure system that is to carry heavyweight truck traffic. It is New Jersey's first bridge to be designed and constructed according to the American Association of State Highway and Transportation Officials (AASHTO) Load and Resistance Factor Design (LRFD) Specifications (1998). It is expected that in 2010, nearly 15,000 trucks will use the bridge every day, resulting in two million truck trips for a hauling capacity of 1.4 million containers. During the final scope development and preliminary design phases of the project, the New Jersey Department of Transportation (NJDOT) design practice specified the use of Working Stress Design (WSD). With the introduction of AASHTO's LRFD Specifications, NJDOT decided to evaluate the merits of this new design methodology through the redesign of the Doremus Avenue Bridge Replacement Project.

Construction of the Doremus Avenue Bridge was divided into two stages: construction of a five-girder bridge adjacent to the existing structure (Stage I), demolition and replacement of the existing structure by another five-girder bridge (Stage II). Phase I of the research project involved evaluating the analytical behavior of the Doremus Avenue Bridge and developing a technical specification and instrumentation plan. This study identifies the procedure(s) and parameters that were used in the bridge instrumentation and analysis. The identification process was implemented in two phases: (1) development of a detailed Finite Element Model that incorporated various parameters and (2) planning and optimization of instrumentation schemes and sensor locations.

The evaluation process aims at assessing the new AASHTO LRFD design procedures and identifying what NJDOT hopes to establish as future bridge design guidelines. The instrumentation schemes were implemented during the construction phase, which permitted measuring the "undisturbed" behavior of the bridge and establishing the structure's "finger prints" before opening the bridge to traffic. The three-span continuous unit was fully instrumented to monitor actual stress levels, both during and after the completion of the structure for three years. In addition, a weigh-in-motion (WIM) system was permanently installed in the south approach roadway to accurately gather vehicle-loading information. The second phase of the project involved instrumenting the bridge and collecting data from field tests before opening the bridge to traffic. Static as well as dynamic tests were performed to calibrate sensors and collect data pertaining to help answer some of the questions posed in the objectives listed in the next section.

OBJECTIVES

The primary objective of this study is to validate the LRFD Specifications (1998) by means of instrumentation, field-testing, and condition monitoring of the new Doremus Avenue Bridge. The following six main objectives are described in this report:

1- Verify the LRFD live-load distribution factor specification and develop new simplified equations.
2- Evaluate and develop a prediction model for the effective flange width in the bridge deck.
3- Verify New Jersey Department of Transportation's deflection limits and develop provisions for designing and formulating deflection and related serviceability limit states.
4- Verify the LRFD dynamic amplification factor specification.
5- Develop a truckload model using a permanent WIM system. Compare the live-load spectra to other WIM sites in New Jersey.
6- Develop a fatigue load mode to estimate the remaining service damage.

BRIDGE SUPERSTRUCTURE

Figure 1 shows a plan view of the first unit of the Doremus Avenue Bridge that was selected for instrumentation of its three continuous spans due to easier access. The three spans were instrumented with a comprehensive sensor network organized to monitor the bridge superstructure under controlled test conditions as well as normal truck traffic.

Instrumentation

The sensor network included two major data acquisition systems: a long-term monitoring system, a fatigue system, more than 300 sensors, and wireless communication capabilities. The sensors included a WIM system to gather actual truckload information, strain transducers, a Linear Variable Differential Transformer (LVDT), a Laser Doppler Vibrometer (LDV) to measure girder deflection and velocity, and accelerometers and geophones to measure bridge vibration. A schematic diagram of the sensor network is shown in Figure 2.

Two data acquisition systems and one data logger were used to collect data from various sensors installed on the bridge. The two data acquisition systems consisted of the Structural Testing System (STS) from Bridge Diagnostic, Inc., and the CR9000 (fatigue system) from Campbell Scientific, Inc. The data logger, model CR10X, was also available from Campbell Scientific, Inc. The STS was used solely for measuring the strain output from the strain transducers and for static and dynamic live load testing. The system had 64 input channels, while also having the capability to simultaneously take all 64 channels at 100 samples per second, which is appropriate for bridge structures. The advantage of this system is that each sensor can be tagged with an identification number, allowing the sensors to be wired in any order.

The CR9000, the fatigue system, was used for monitoring the bridge response to heavy trucks passing over the bridge as well as for recording the stress range and performing rainflow analysis. The system was permanently installed at the bridge to automatically gather long-term measurements. The system has 24 input channels that are designed for connecting 22 strain transducers and 2 LVDTs. The twenty-two strain transducers were strategically selected to represent fatigue critical sections as well as the stress of each girder. The system also collected data simultaneously at 100 samples per second. For monitoring the bridge response under the effect of a heavy load, the fatigue system constantly received the information on the gross vehicle weight (GVW) from the WIM system and then calculated whether the gross vehicle exceeded a pre-determined limit. If the vehicle exceeded this limit, (e.g., weight limit was set to be above the fatigue truck about 65 kips) the system then collected the strain and deflection data of the bridge. Moreover, the system also separated the recorded data according to the lane direction. For the northbound lanes, the data was collected one second before and 13 seconds after the fatigue system determined a heavy truck was present in the lane. The reason for collecting the data one second before the triggering condition was to adjust for communication delays so that whole records of the bridge response caused by the vehicle could be preserved. On the other hand, for southbound lanes, all the data was pretriggered because the vehicle passed over the bending plate after it passed over the bridge.

Figure 3 shows the fatigue system installed in a protective stainless steel cabinet located on the crash wall of Pier 2. The CR10X is also a permanent long-term monitoring system. It is used solely for collecting data from the vibrating wire strain gage (VWSG). The system has 96 VWSG input channels and it collects data sequentially at 5-minute intervals. However, the data is stored only every hour in addition to storing only the minimum and maximum values within that hour. In conjunction to the VWSGs, a temperature and humidity probe is connected to the data logger to record ambient conditions. Figure 4 shows the CR10X system used in the long-term monitoring of data from VWSG's.

Strain sensors were installed at the maximum positive moment positions, with some transducers installed at pier locations along all three spans to measure the greatest load effect. The LVDT and LDV systems were positioned to measure the response at the two most heavily loaded girders, specifically Girder 4 and Girder 8 of Span 3. Span 3 was chosen because of easy accessibility under the bridge. Figure 5 shows the overall instrumentation plan and the location of various sensors.

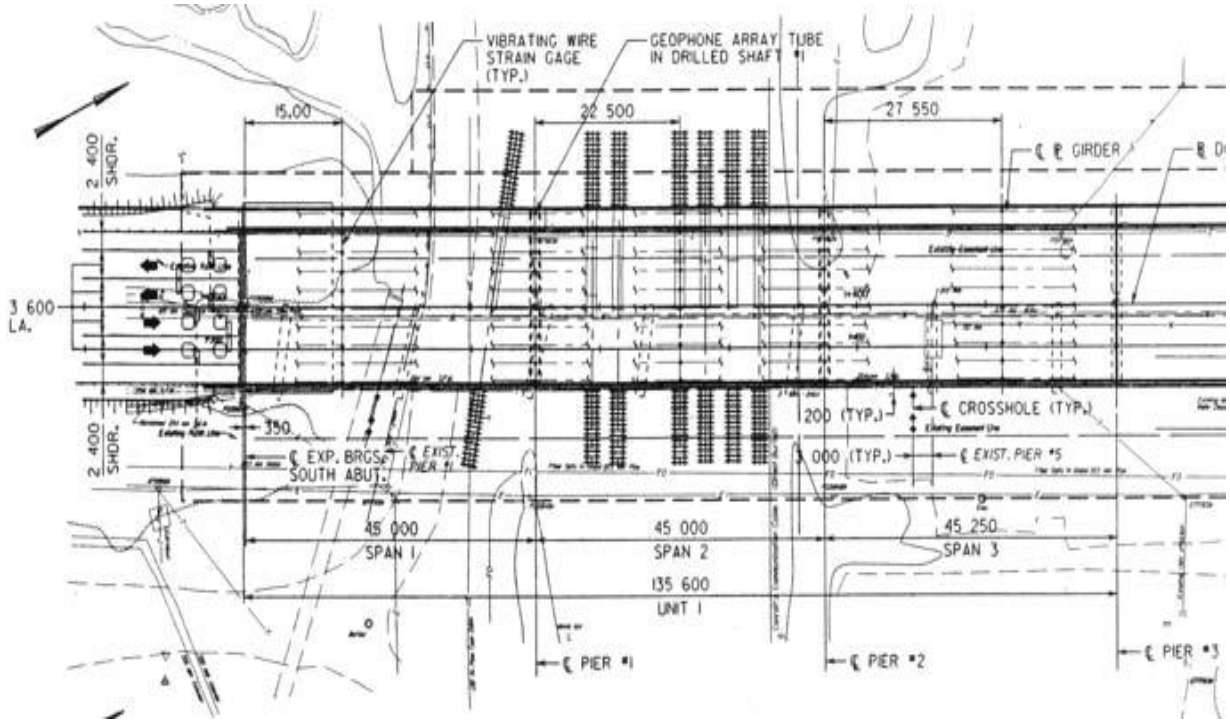

Figure 1. Plan view of the Doremus Avenue Bridge, unit 1, spans 1, 2, and 3.

Strain Gauges

Moment reactions of the bridge can be computed because of known stresses of the welded steel plate girder configuration. It is expected that live load will cause only elastic bending. The stress in the bridge girder can be calculated by multiplying the modulus of elasticity by the strain. The modulus of elasticity of steel is well established, with a value of 29,000 ksi. The strain in the welded steel plate girder is measured with strain transducers. The most common type of strain gauge is a quarter bridge uniaxial foil strain gauge. Though this type of gauge has been used successfully in the laboratory, it is not used in this study because of its impracticality. The gauge installation requires a great deal of preparation, and in the field necessary preparation becomes difficult (e.g., the harsh environment in the field). One problem is the mounting surface. In this case, the bottom flange of the welded plate girder needs to be smooth and clean. This is not only time-consuming but also very difficult to do since weathering steel was used for bridge construction. The second problem is that the bonding material takes a minimum of 24 hours to cure and during cold winter months it may take even longer. However, despite these two disadvantages, the main reason for not using the quarter bridge uniaxial foil strain gauge is the lead wire length limitation. Long lead wire increases the gauge resistance, which leads to incorrect measurements.

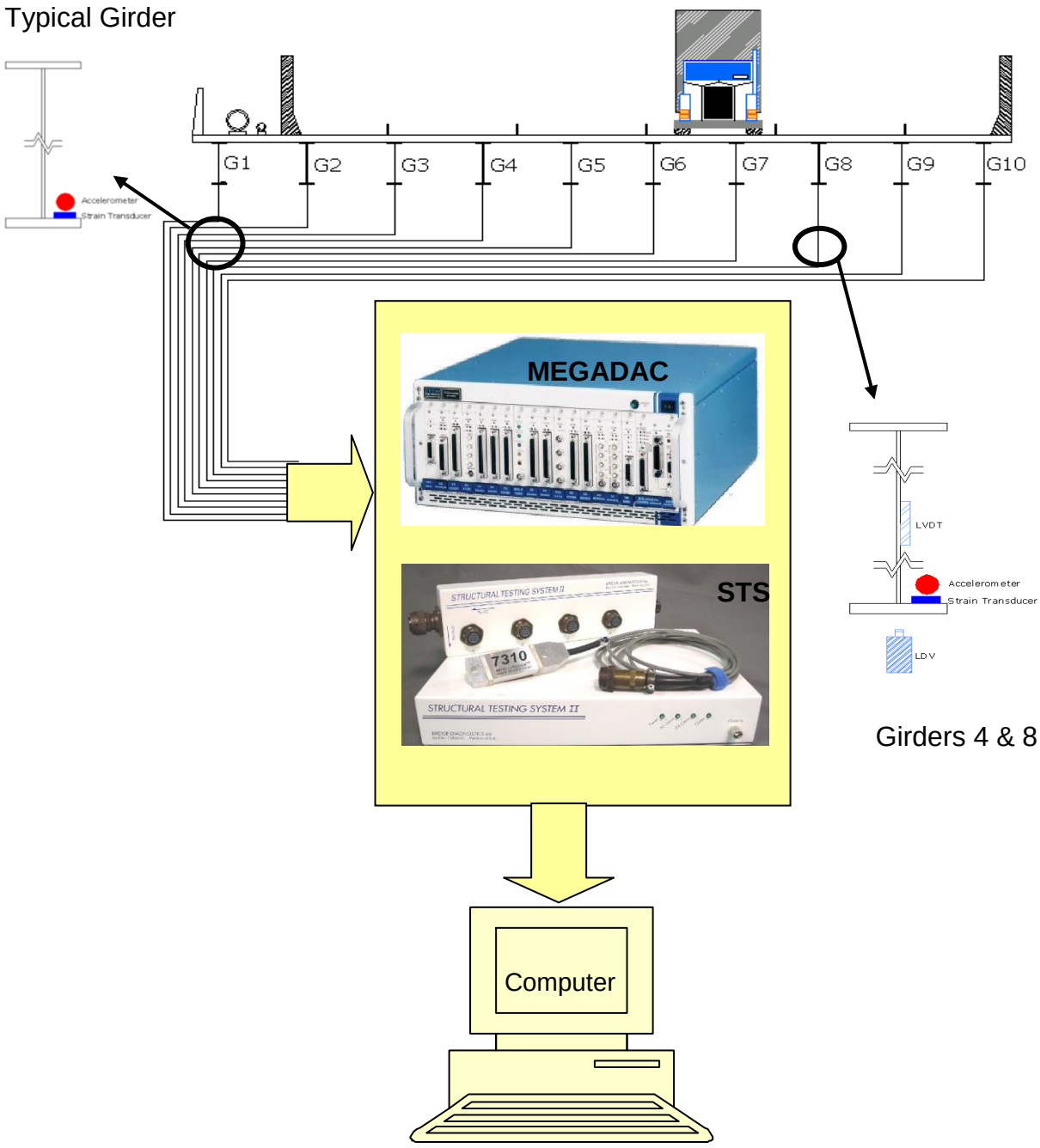

Figure 2. Sensor network components

Figure 3. Fatigue system

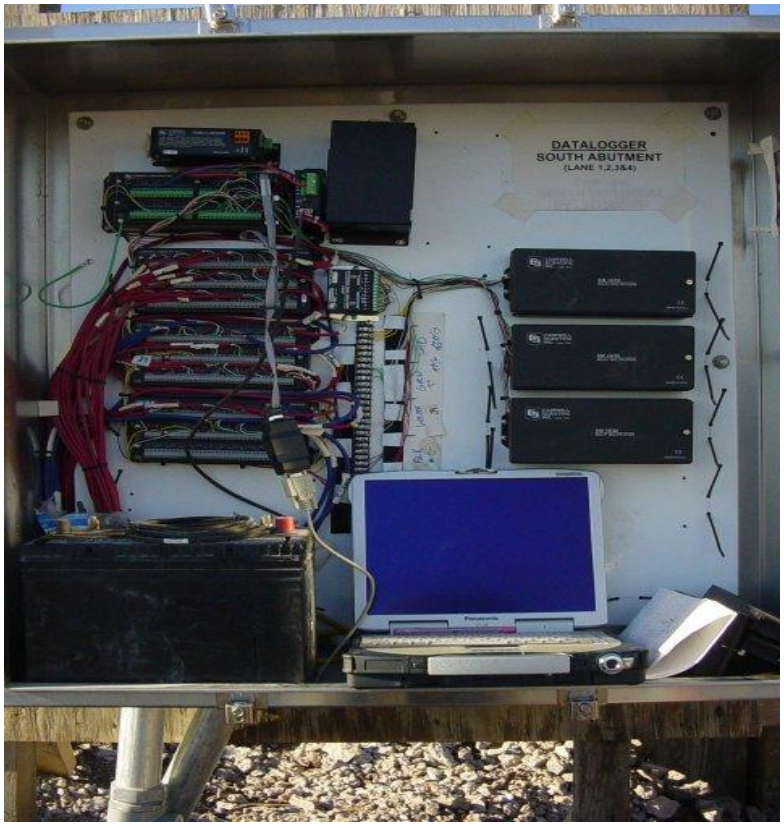

Figure 4. Long-term monitoring system

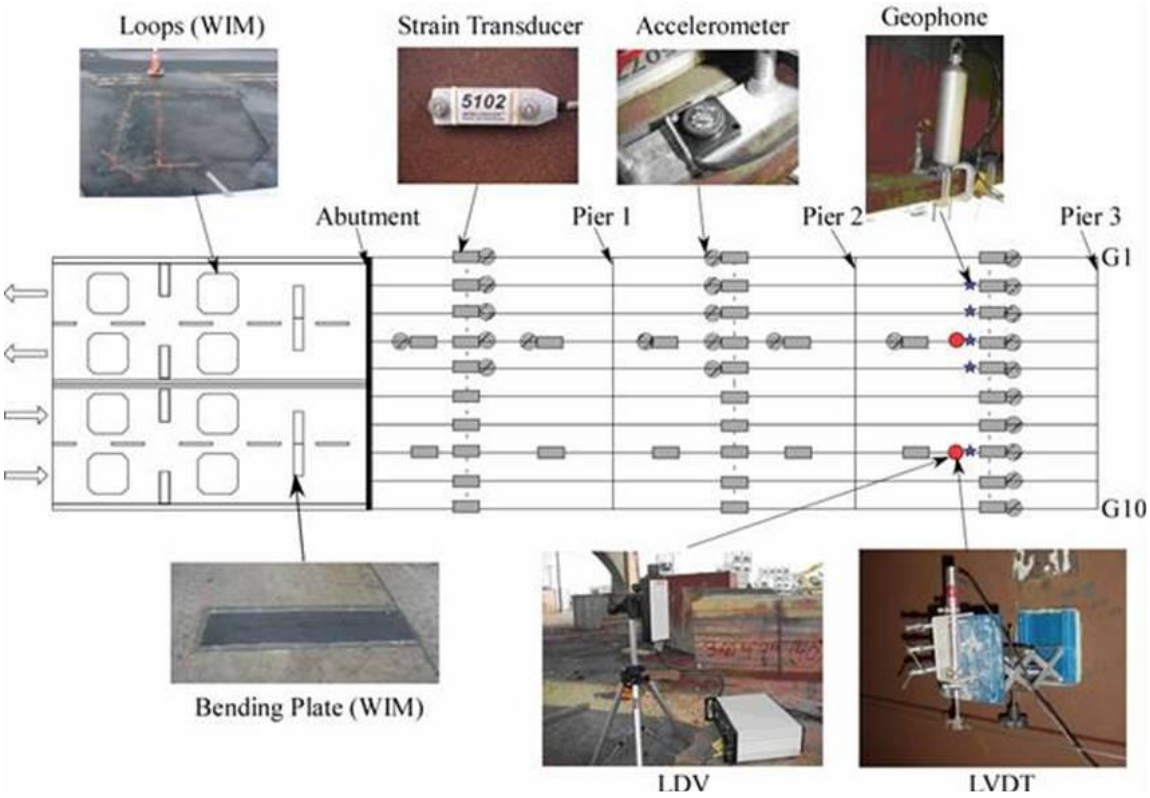

Figure 5. Instrumentation plan for Unit I of the Doremus Avenue Bridge: strain transducers

To avoid these problems, a strain transducer was used instead of the quarter bridge uniaxial foil gauge. The strain transducer, usually found in load cells, consists of a full Wheatstone bridge strain transducer. The advantage of using a full Wheatstone bridge is that rather than using the gauge resistance to measure the strain, the strain is measured by the voltage output. The strain transducer is calibrated with a strain gauge by inputting a known excitation voltage and applying a known strain and then recording the output voltage. The strain is therefore computed using a scale factor to convert the output voltage into strain. Thus, the increased resistance caused by the long lead wire will not significantly affect the strain measurement. If the lead wire is short and properly installed, the quarter bridge uniaxial strain gauge can give more accurate readings.

The bridge was instrumented with strain transducers (made by Bridge Diagnostics Inc. (BDI)) at the position of maximum positive and negative moments. A total of 36 demountable strain transducers were installed during the Stage I construction. Twenty-five of them were installed in the transverse direction at the position of the maximum positive bending moment of each span and at the position of the maximum negative bending moment positions (the end of Span 1 and Span 2). Four strain transducers were installed to monitor the cross diaphragm in the first span. The remaining transducers were installed longitudinally on the fourth girder throughout the three spans

to obtain the strain profile of the most heavily loaded girder. In Stage II Construction, an additional 24 strain transducers were installed at the same position as Stage I. Fifteen sensors were installed at the position of maximum moment and the rest where installed along the eighth girder to monitor the strain profile of the most heavily loaded girder. The demountable strain transducers were attached on the upper surface of the bottom flange of the girder with ¼-in. threaded bolts and nuts. The lead wires of each gauge were bundled together and routed to the data acquisition system located at the crash wall of Pier 2. The wires ran along the cable tray located on the fourth and eight girders for Tests I and II, respectively. Figure 5 shows the location of the strain transducers installed on the bridge. Figure 6 shows the installation and final orientation of a typical strain transducer.

(a) (b)

Figure 6. (a) Gauge installation and (b) mounted strain transducer

Vibrating Wire Strain Gauge

In addition to the strain transducers, 96 VWSGs were also embedded inside the concrete deck. These gauges, shown in Figure 7, consisted of standard 4-in. embedded gauges, sister-rebar gauges, and weldable gauges. The standard gauges were used primarily for measuring the early-age and drying shrinkage of the concrete deck as well as the imposed static load. The sister-rebar gauges were also used to measure the drying shrinkage as well as the imposed static load. The advantage of sister-rebar gauges is their ruggedness. A construction worker could step on the gauges without damaging them. Weldable gauges were used to measure the strain in the top flange of the steel plate girder. All three types of gauges were also equipped with an embedded thermistor that measured the temperature of concrete to compensate for thermal effects on the strain readings.

These gauges are very different from the strain transducer because they do not rely on electrical output measurement and thereby being unaffected by the change in the cable

resistance or other electrical disturbances. The strain is measured using the vibrating wire principle by recording the resonant frequency of a wire with a different tension. In the VWSG, a wire that is enclosed in a protective case is attached to the two end blocks with a calibrated tension. The two end blocks are free to move so that as the concrete shrinks or expands, the end blocks are compressed or extended respectively. When the end blocks move, the wire tension changes, thereby changing the resonant frequency of the wire. The changes in the resonant frequency are then converted into corresponding strain readings. Hence, these gauges could be attached to long lead wires and, together with their long-term performance and ruggedness, the gauges have an edge over other gauges when being installed in the field.

The primary use of these gauges was for long-term monitoring of the concrete shrinkage as their readings did not affect the dynamic live load. However, their readings were collected during static live load testing to determine the contribution of the concrete slab in determining the effective flange width and the location of the neutral axis. These gauges were installed at the position of maximum positive and negative moments as well as parallel to the top reinforcement over the steel plate girder. Some gauges were also installed parallel to the bottom reinforcement as well as on the top flange of the welded plate girder.

(a)

(b)

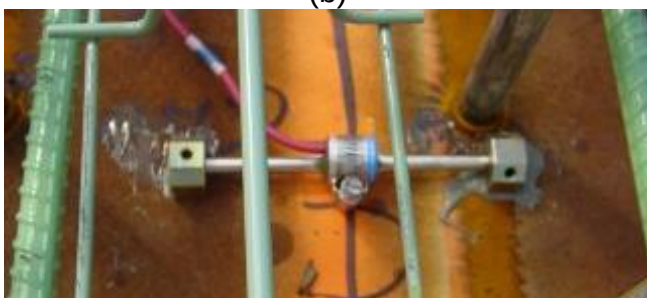

(c)

Figure 7. (a) Standard 4-in. VWSG, (b) sister-rebar, and (c) weldable VWSG

Linear Variable Differential Transformer

An LVDT was used to measure the deflection of the girder. Since LVDT is a contact sensor, a base or reference point was needed so that the LVDT arm would be compressed or extended as the bridge deflected. A stainless steel aircraft reference cable was used as the reference point. The stainless steel aircraft reference cable was mounted to the end diaphragms adjacent to the selected girder using angles. A 12-in. turnbuckle was used to tighten the cable to a proper tension. In addition, to account for creep and temperature effects on the cables, a spring was attached to one end of the cable to maintain proper tension. The LVDT was attached to the girder using a telescopic laboratory platform. The platform was mounted on the centerline of the web of the selected girder with high-strength epoxy as shown in Figure 8. Two LVDTs were installed on the two most heavily loaded Girders, 4 and 8, at the position of maximum positive moment of Span 3.

Laser Doppler Vibrometer

The LDV system, provided by Polytec PI, Inc., is a noncontact system that measures surface vibrations based on laser interferometry and provides both velocity and displacements. The vibrometer consists of a modular controller (OFV-3001) and a helium neon (Class II) laser sensor head (OFV-353), which is rated for distances ranging from 450 mm to 250 m (18 in. to 820 ft) when used with reflective tape. The controller provides signals and power to the sensor head and processes the vibration signals. The signals are then electronically converted by decoders within the controller to a velocity and displacement in analog or digital form.

The LDV, shown in Figure 9 is based on detection of the Doppler shift of laser light that is scattered from the test object to independently determine its vibration velocity and displacement. The Doppler shift refers to the frequency shift of the light that is reflected back from the vibrating object to the source. An object moving away from the sensor head will reflect light that has a longer wavelength (lower frequency) than it had when it was emitted. Similarly, an object moving toward the sensor head will reflect light that has a shorter wavelength (higher frequency) than it had when it was emitted. The measured frequency shift of the wave is given by $f_D = 2v/\lambda$, where v is the velocity of the object and λ is the wavelength of the emitted wave.

An optical interferometer is used to mix the scattered light with a reference beam, with a known frequency f_o and phase angle φ_o, to determine the Doppler frequency shift. The helium neon laser beam is split by a beam splitter (BS1) into two parts: a reference and a measurement beam. The measurement beam then passes through beam splitter BS2 and is focused on the vibrating object. The reflected beam is merged with the reference beam by another beam splitter BS3 and is directed back to the laser head. A Bragg cell is used to determine the direction of motion of the vibrating object.

The phase and frequency of the laser beam that is scattered back from the object of interest are compared with the internal reference beam. This frequency difference is proportional to the instantaneous velocity. The phase difference is proportional to the instantaneous position of the object as given by $\Delta\varphi = 2\pi \frac{\Delta L}{\lambda}$, where ΔL is the path length difference between the reflected and reference (constant path length) beams, which is related to the wavelength of the reference beam.

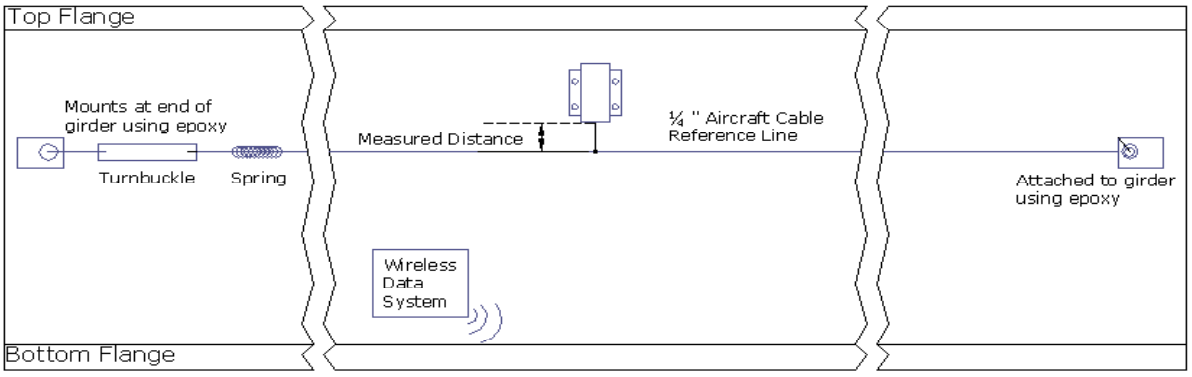

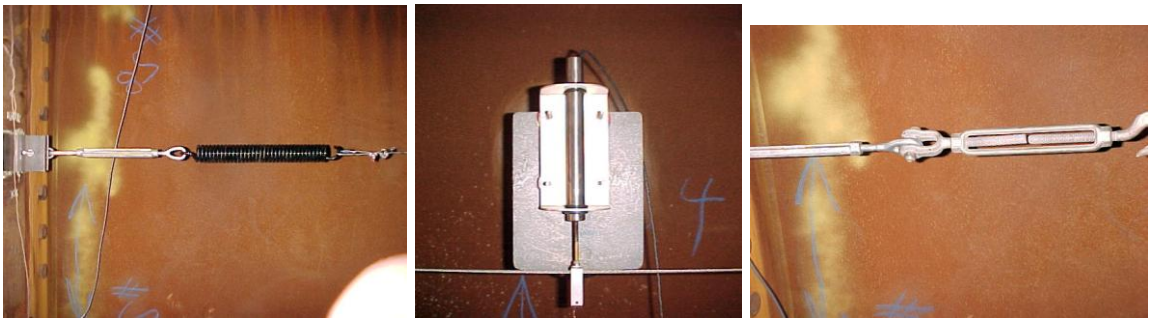

(a) (b) (c)

Figure 8. LVDT cable system: (a) heavy-duty spring, (b) LVDT, and (c) turnbuckle

Since the laser vibrometer measures the differential displacement between its optical laser head and the bridge girder, the unit needs to be mounted on a support that is free of vibration. As a result, the system is often set up on the ground under the bridge structure. This limits its usefulness as a long-term monitoring system, as it is impractical to leave the unit unattended for a long period of time. Therefore, the LDV is used only to verify the results of the long-term LVDT system.

During live load testing, the laser head was placed on a tripod and pointed toward retroreflective tape that was glued with an elastic epoxy to the bottom flanges of Girders 4 and 8 at the same location as the permanent LVDT systems. This setup allows

deflection measurements of one location to be collected simultaneously by two independent systems.

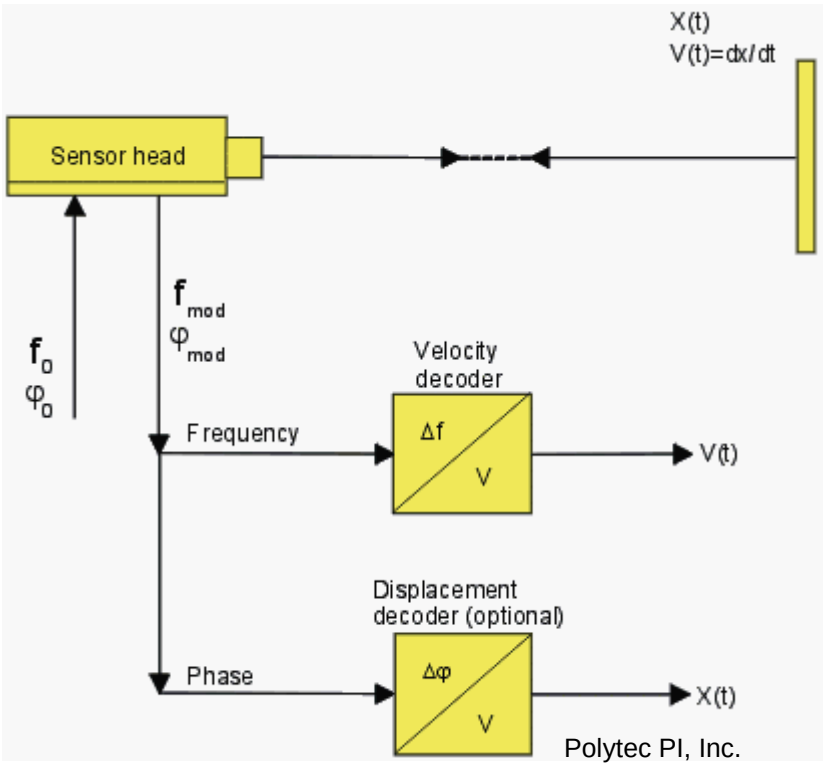

(a)

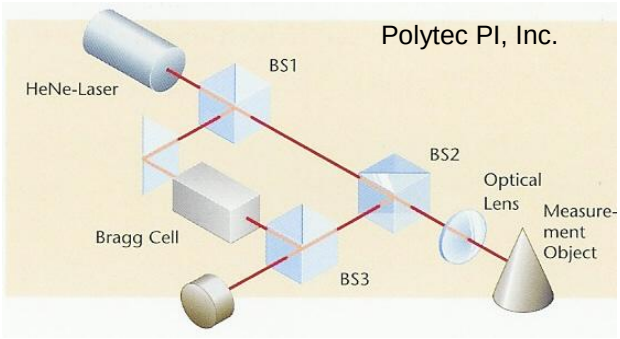

(b)

(c)

Figure 9. LDV system: (a) vibrometer signals, (b) laser beam path (Polytec PI), and (c) field setup

Accelerometers

The purpose of using accelerometers is to indirectly measure the deflection of each girder under various test truck loadings. Twenty accelerometer sensors, provided by Dytran Instruments, Inc., were installed at maximum positive moment positions across

all girders of Stage I, for all three spans along the length of Girder 4, as well as on Girder 8 at Span 3. The sensors are relatively small—approximately 1 in. diameter and 2 in. tall—and are attached to the girders via a magnetic base. Ten additional accelerometers, manufactured by Kistler Instrument Corporation, were installed on Girders 4 and 6–10 at the maximum positive moment position of Span 3. These sensors use a three-layer silicon variable capacitance-sensing element capable of measuring low-level acceleration in a low-frequency environment (0–250 Hz). This characteristic becomes very important during signal processing of the recorded acceleration in predicting displacements. Figure 10 shows the three types of accelerometer used in the instrumentation and data collection.

(a) (b)

Figure 10. Accelerometers: (a) uniaxial Dytran (model 3192A) and (b) low-frequency Kistler (models 8330A2.5 and 8305A)

The accelerometers are connected to the data acquisition system, MEGADAC, manufactured by Optim Electronics. MEGADAC is equipped with input modules and offers up to 48 channels operating at speeds of up to 25,000 samples per second. The system program and test setup are done through Optim's Test Control Software (TCS), which allows for, among other features, the formation of a user-defined sensor library and a real-time display of collected measurements.

Geophones

Five geophone sensors, provided by Mark Products, Inc., were installed at the maximum positive moment position of Span 3 on Girders 2–5 and 8 to measure girder velocity due to vertical vibration. These sensors are low-frequency three-directional geophones. Figure 11 shows the field setup of the geophones along with other sensors (accelerometers and strain transducers) installed at the same location.

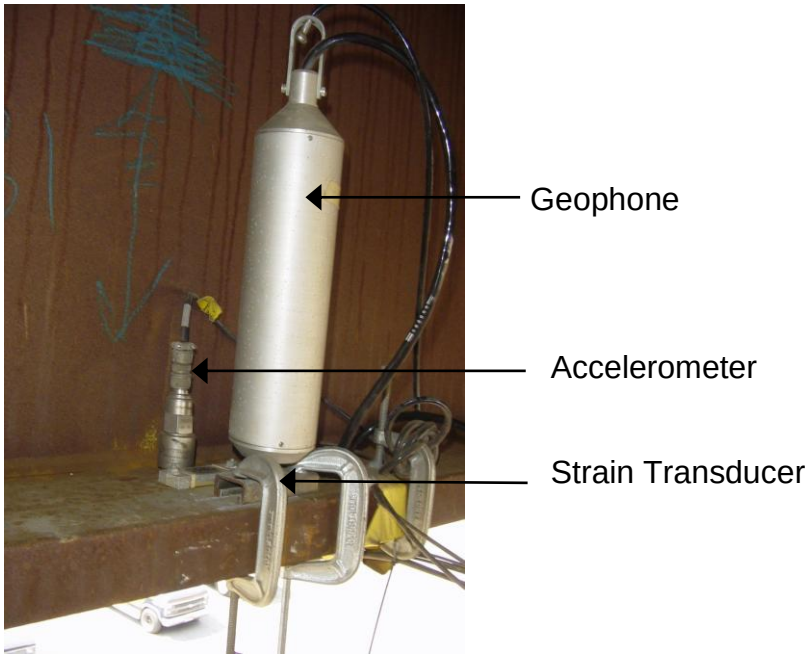

Figure 11. Field setup of geophone sensors

Weigh-in-Motion

All the sensors described herein were used to detect the bridge live load or long-term response. The bridge response provided important information about the bridge carrying capacity; however, it is important to note that the applied load was also needed to analyze the bridge. Moreover, the data obtained from these sensors needed to be validated so that the readings had no interference. A WIM system was used to detect the live load (mainly truck loads) traveling on the bridge. The WIM system was designed to weigh a passing vehicle traveling at normal traffic speed.

Three main technologies are used for assessing the truck weight: a piezoelectric sensor, a single load cell sensor, and a bending plate sensor. The piezoelectric is the least expensive sensor of the three and is the most inaccurate as well as the least durable. It is about 10 ft long (other lengths are also available depending on the application) and about 1/2-in. wide. As a vehicle passes over the sensor, an electrical signal is sent from the sensor to a WIM system. The electrical signal is then transferred to a load reading.

The single load cell sensor is the most expensive but also the most accurate. It uses a dynamic rated (fatigue rated) load cell to measure the load. The load cell is embedded in the pavement under a steel plate. As the vehicle passes over the steel plate, the plate compresses onto the load cell, which registers the load to the WIM system.

The bending plate system used in this project utilizes strain gauges to transmit the load. A strain gauge is attached to a steel plate. As the steel plate bends, a signal is transmitted to the WIM system converting the signal into load. The system is less expensive than the single load cell system, but provides equivalent accuracy. To obtain this accuracy, two sensors were installed so an average value could be obtained. In addition, for the system to determine the speed and the vehicle, two inductive loops were also installed so that the WIM system could distinguish one vehicle from another.

Eight bending plates and inductive loops, two in each lane, were installed on the south approach slab of the Doremus Avenue Bridge. A staggered bending plate setup, shown in Figure 12 was used so that the two bending plates in each lane could detect the left and right wheels of each axle. The two inductive loops in each lane were spaced 16 ft apart, leaving sufficient distance to calculate the speed of the vehicle. The WIM system was installed in a stainless steel electrical box located on the east side of the approach slab. The data from the WIM system was also transmitted to a fatigue data acquisition system located on Pier 2.

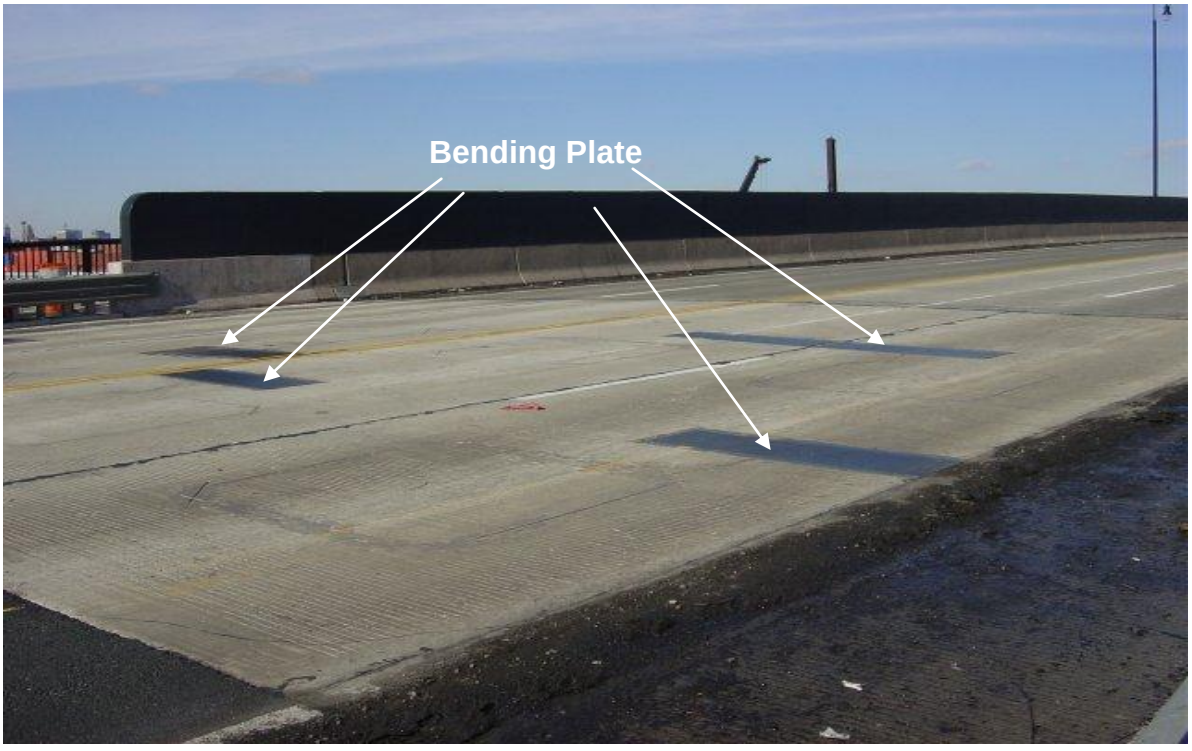

Figure 12. Installed bending plates and inductive loops on the Doremus Avenue approach slab

Material Properties

To evaluate the bridge models, the material properties of the bridge must be known. These materials include weathering steel girders, rebars, and concrete slab. The steel girder and rebar are manufacturered materials with controlled properties that do not significantly change from one to another nor over time. For the steel girder and rebar, the modulus of elasticity were assumed to be 29×10^6 psi. The yield strength of the steel girder and rebar were also assumed to be 50 and 60 ksi, respectively.

Concrete, on the other hand, is not a uniform material because it varies quite significantly from batch to batch. To obtain a good representation of the concrete properties for each pour, samples were prepared and tested in accordance with American Society of Testing and Materials (ASTM) standards. The concrete samples were also stored and cured according to the field conditions. Figure 13a shows the pouring of the deck slab using concrete pumps and hand-held vibrators as a method of consolidation. Figure 13b shows similar consolidation methods using a vibrating table. The specimens consisted of 4- × 8-in. cylinders as specified by NJDOT. After the concrete was cast, a curing compound was applied to the top of the exposed surface of cylinders (Figure 13c) and later covered with wet burlap and thin plastic sheeting (Figure 13d). After 24 hours, the specimens were placed under the wet burlap on top of the concrete deck (Figure 14) to ensure that they were under the same curing regime as the deck slab.

Testing

The compression test was performed in accordance with ASTM C39. For each pour, 21 plain concrete cylinders were cast and matched-cured in the field. Three specimens were tested when the concrete reached the ages of 1, 3, 7, 14, 28, 56, and 90 days using a Forney 1-million-pound compression machine. Steel caps with neoprene inserts were placed on the top and bottom of the concrete specimen to ensure alignment and pressure distribution on the concrete.

In addition to the compression test, the modulus of elasticity was also tested in accordance with ASTM C469 using 4- × 8–in. cylinders for a 28-day setup. For each cylinder, a minimum of three repetitive tests was performed. The first repetition was for seating the concrete materials, while the other two represented the actual testing results. Unlike compression tests, the cylinder was capped with a high-strength capping compound to prevent measuring the strain from the neoprene pads.

The modulus of elasticity test setup consisted of three, ultraprecision linear ball bearing LVDTs with a gauge length of ±0.020 in. and a resolution of 0.000004 in., which is capable of measuring 1 microstrain (i.e., the original length is 4 in.). The three LVDTs

were positioned around the specimen at an angle of 120 degrees. The average reading was used to calculate the strain in the specimen. The load was recorded with a 200-kip load cell. All the sensors were connected and recorded using the Megadac data acquisition system described earlier. Figure 15 illustrates the modulus of elasticity test setup.

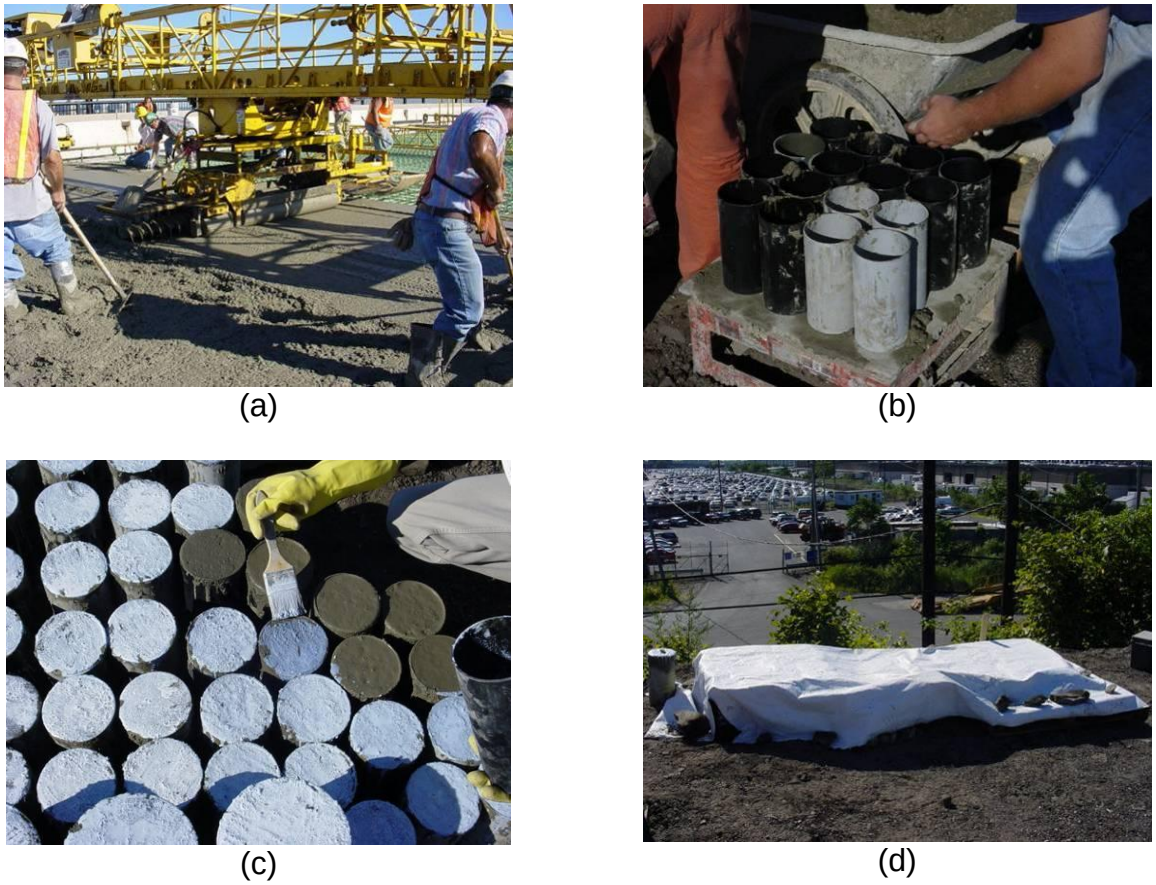

(a) (b)

(c) (d)

Figure 13. Concrete sampling: (a) pouring deck slab, (b) consolidating specimens, (c) applying curing compound, and (d) covering specimens with wet burlap

Figure 16 illustrates typical compressive strength values at various ages of the concrete deck slab. The 28-day compressive strength of the deck slab was 7,500 psi. The concrete strength increase significantly dropped after 56 days. However, because the bridge was subjected to loading prior to 56 days, the 28-day compressive strength value was used. It should be noted that there was only a 10 percent increase in compressive strength, hereby not significantly affecting the models.

Figure 14. Field matched-cured specimen

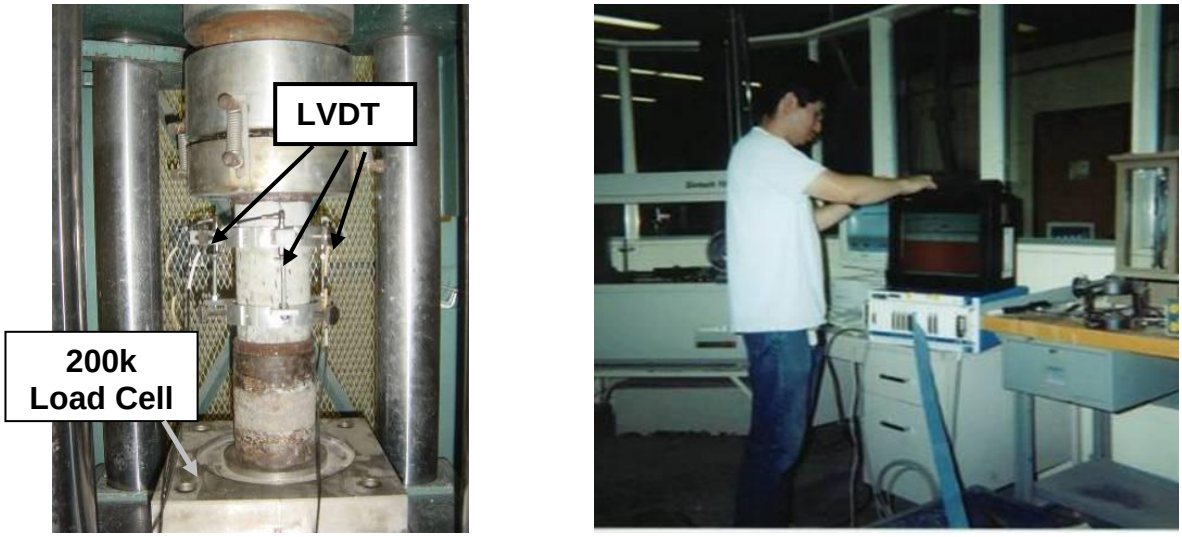

Figure 15. Modulus of elasticity test setup

Figure 17 illustrates the modulus of elasticity of the concrete deck slab at 28 days, which gives a value of 4.24×10^6 psi. The experimental value is slightly lower than the modulus of elasticity equation recommended by the American Concrete Institute (ACI) 318, resulting in a modulus of elasticity of 4.94×10^6 psi or 16 percent higher. ACI 363 has a better modulus of elasticity prediction, with a value of 4.46×10^6 psi which is 5

percent higher. This confirmed the ACI 363 recommendation that its equation should be used in lieu of ACI 318 when the compressive strength of concrete is higher than 6,000 psi.

FIELD TESTING

The bridge was loaded statically and dynamically to validate its behavior to live load. To simulate the design truck, five-axle trucks (
Figure **18**) were utilized for the load test. Five and six different trucks were used to perform the load test in Stages I and II, respectively. Their axle configurations and weight are tabulated in Table 1 and Table 2 for Stages I and II, respectively. The trucks consisted of flatbed trailer trucks or dump trucks. The flatbed trailer trucks were loaded using New Jersey barriers, whereas the dump trucks were loaded with aggregates to obtain approximately 72,000 lb of GVW. The weight of the truck was obtained from a weight station; the front axle was weighed separately, the second and third axles were weighed together as a set, as were the fourth and fifth axles. Thus, to obtain the weight of an individual axle, the weight of the set of axles was assumed to be evenly distributed.

Static Load Test

The static load test was performed to eliminate the dynamic amplification caused by the road roughness and truck suspension. The test was conducted by placing the third axle of the truck at the position of the maximum positive moment. For the static tests, only the strain from the strain transducers and VWSG were recorded. It should be noted that the initial zero readings needed to be recorded prior to performing the test.

The static test was performed at both stages of construction. Stage I was conducted before the bridge was opened to traffic; whereas in Stage II, traffic on the instrumented portion of the bridge was temporarily closed for approximately 10 minutes to perform each loading case. The load cases consisted of loading the bridge at the positions of maximum positive and negative moments for one- and two-lane loading. In addition, special load cases consisting of two trucks following each other in the same lane, two staggered trucks, and two trucks positioned on different spans were also studied. The special load cases were performed to understand the bridge response to normal truck traffic, which eases the data processing for the long-term health monitoring of the bridge structure. Figure 19 shows special static loading cases performed in both stages of construction.

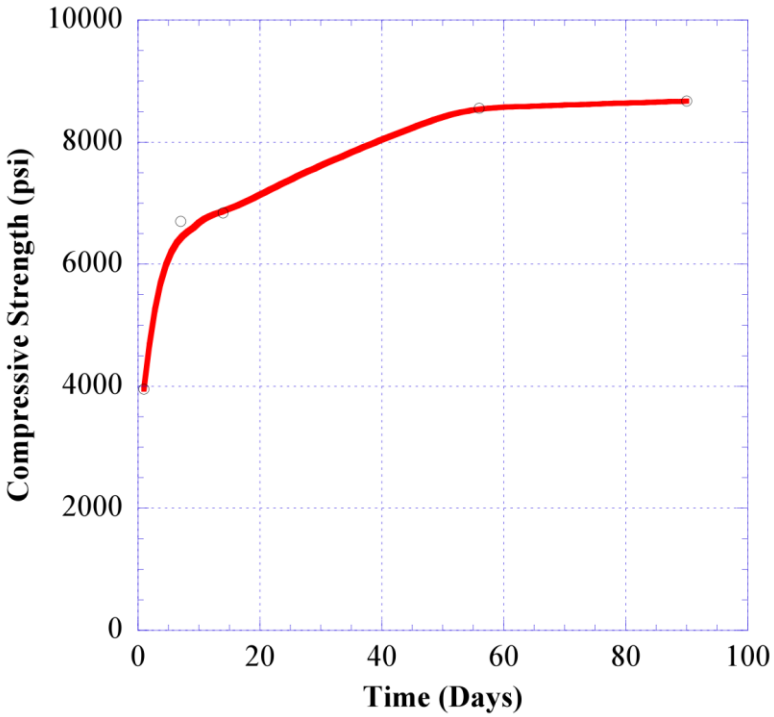

Figure 16. Compressive strength of the Doremus Avenue Bridge deck slab

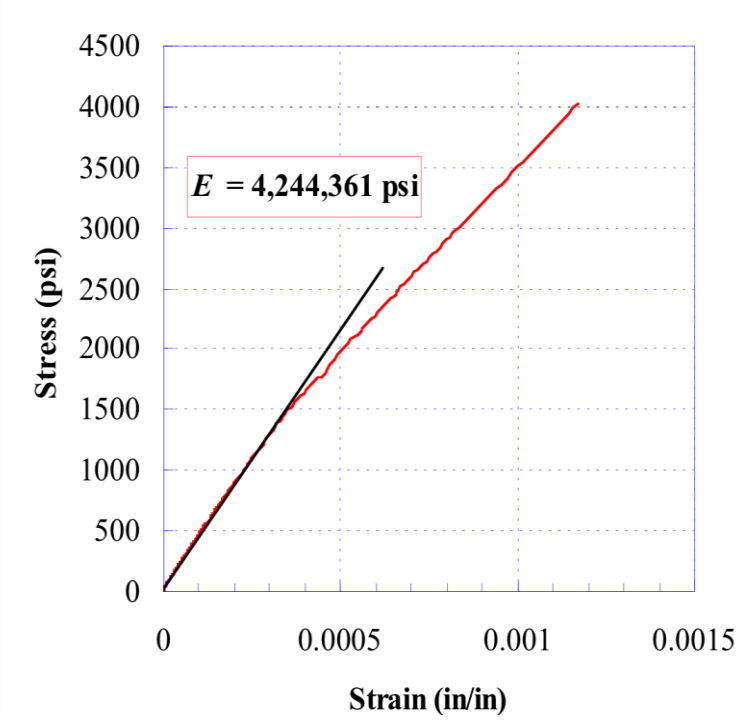

Figure 17. Modulus of elasticity of the Doremus Avenue Bridge deck slab

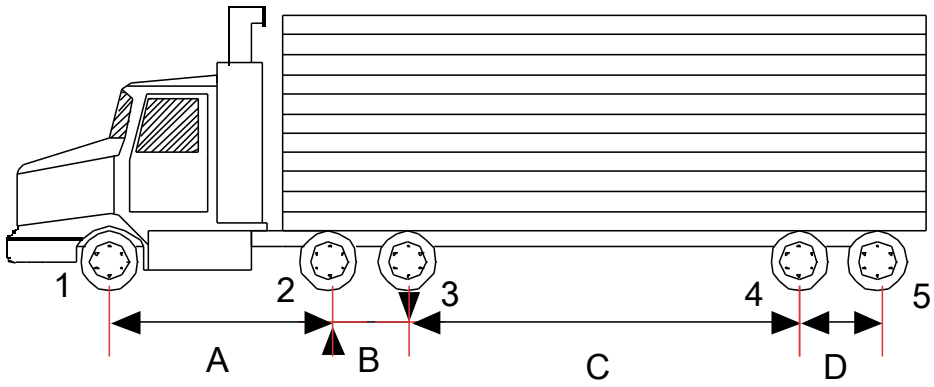

Figure 18. Standard truck configurations

Table 1. Truck configuration for Stage I testing

Test Dates	**12/7/01**		**12/14/01**		**12/21/01**
Truck #	**A1-1**	**A1-2**	**A2-1**	**A2-2**	**A3**
Axle 1 (kip)	8.68	10.86	9.19	12.10	9.13
Axle 2 (kip)	17.60	17.94	12.43	15.67	12.88
Axle 3 (kip)	17.60	17.94	12.43	15.67	12.88
Axle 4 (kip)	15.33	14.90	14.43	14.93	15.49
Axle 5 (kip)	15.33	14.90	14.43	14.93	15.49
GVW (kip)	74.54	76.54	62.91	73.3	65.87
Spacing A	12’-2”	15’-1”	13’-5”	17’-4”	13’-5”
Spacing B	4’-4”	4’-7”	4’-7”	4’-7”	4’-4”
Spacing C	28’-3”	28’-3”	28’-6”	27’-7”	27’-6”
Spacing D	4’-4”	4’-4”	4’-4”	4’-4”	4’-4”

Table 2. Truck configuration for Stage II testing

Test Dates	7/10/03		12/1/03		12/12/03	
Truck #	**B1-1**	**B1-2**	**B2-1**	**B2-2**	**B3-1**	**B3-3**
Axle 1 (kip)	10.76	10.34	10.00	10.78	9.34	9.32
Axle 2 (kip)	15.74	13.87	12.21	9.31	14.22	21.08
Axle 3 (kip)	15.74	13.87	12.21	9.31	14.22	21.08
Axle 4 (kip)	17.05	19.26	18.90	19.57	20.73	12.48
Axle 5 (kip)	17.05	19.26	18.90	19.57	20.73	12.48
GVW (kip)	**76.34**	**76.6**	**72.22**	**68.54**	**79.24**	**76.44**
Spacing A	14’-8”	13’-4”	13’-4”	13’-5”	13’-5”	12’-4”
Spacing B	4’-7”	4’-5”	4’-5”	4’-4”	4’-5”	4’-4”
Spacing C	23’-4”	23’-6”	18’-3”	22’-11”	18’-9”	23’-10”
Spacing D	4’-6”	4’-7”	4’-2”	4’-6”	4’-4”	4’-7”

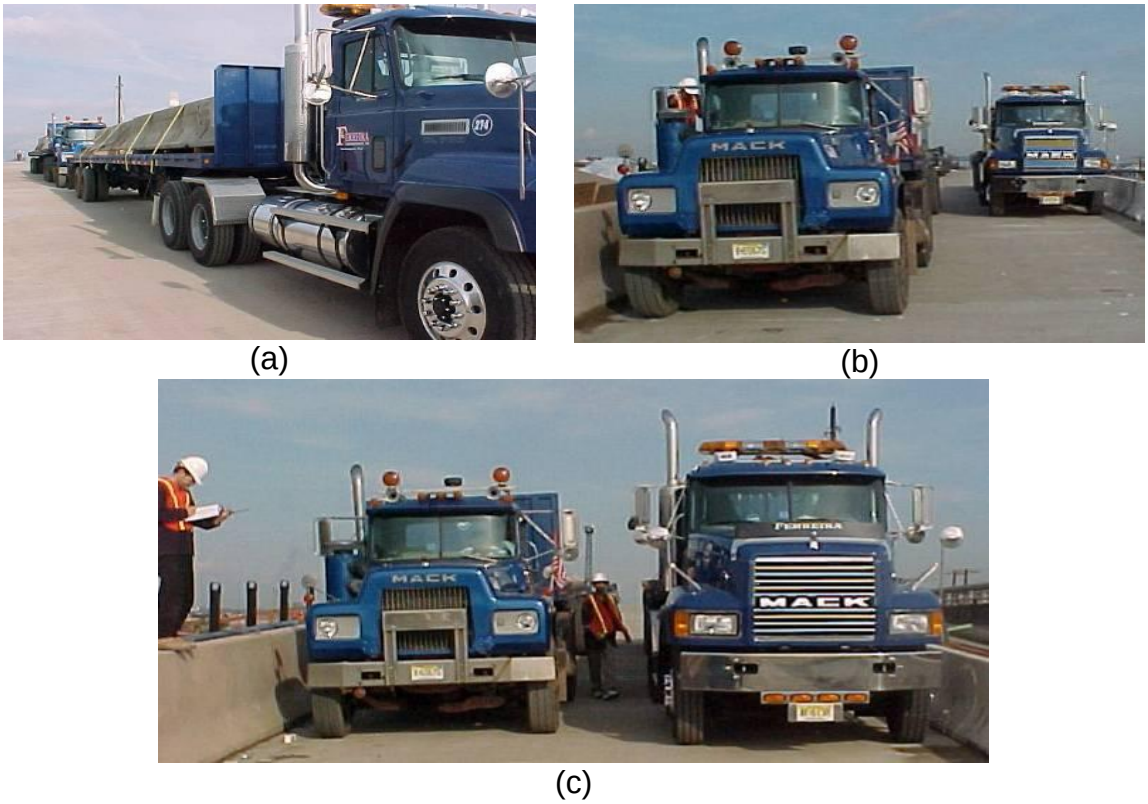

(a) (b)

(c)

Figure 19. Static load cases: (a) following, (b) staggered, and (c) side-by-side

The static load test for the Stage I construction was performed mainly on December 7, 2001, just before the bridge was opened to traffic. More tests were performed a week later on December 14, 2001, using different trucks to confirm previous test results. These tests were conducted by positioning the truck(s) at locations that caused maximum bridge live-load response (i.e., at the position of maximum positive and negative moment). Various load cases were investigated including one lane, two lanes, two following trucks, and two staggered trucks.

Figure 20 shows the Girder Distribution Factor (GDF) of one- and-two lane loading cases on Span 1. The trucks consisted of A1-1 and A1-2 (Table 1) with similar GVWs of 74,540 and 76,540 lb, respectively. The GDF is calculated from the measured strain and compared with code provisions, specifically AASHTO (denoted by S/14 and S/11 in Figure 20 through Figure 32 for one-and-two lane loads, respectively), and AASHTO LRFD (denoted as LRFD–1 Lane and LRFD–2 Lanes in Figure 20 through Figure 32). The two code provisions are conservative in predicting the GDF. The AASHTO value is significantly more conservative with a deviation of approximately 40 percent of the field test results. The deviation for AASHTO LRFD is approximately 12 percent. Only at the peak, the AASHTO LRFD provision is close to the measured GDF value occurring at the most loaded girder, G4.

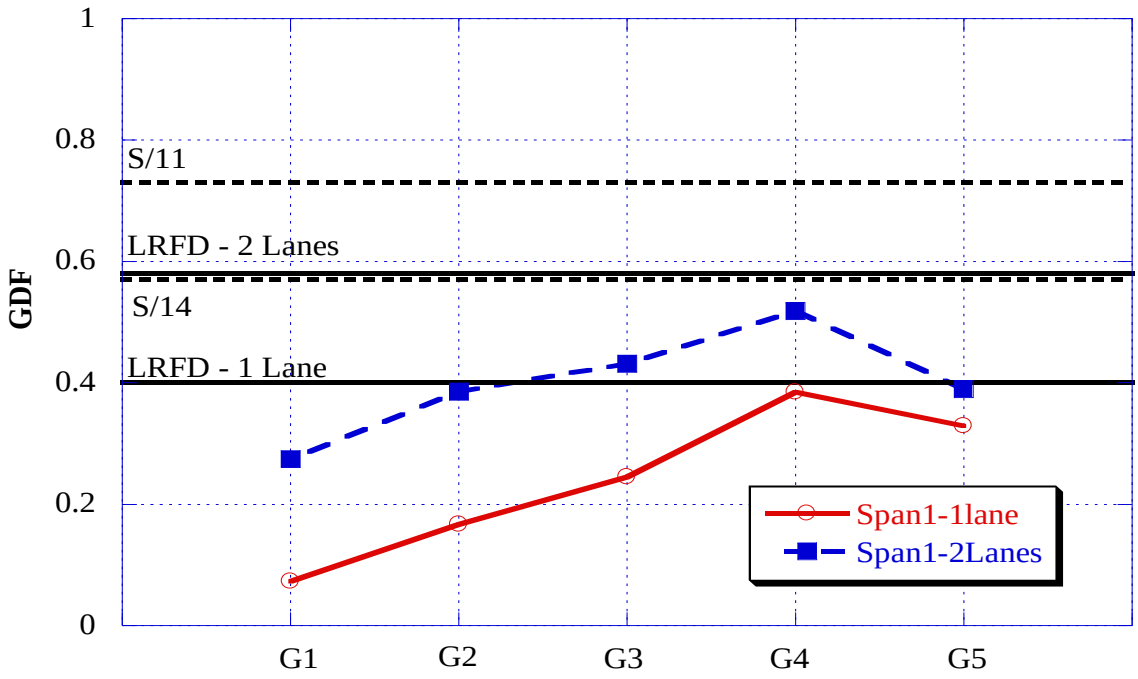

Figure 20. GDF obtained at a distance of 64 ft from abutment of Stage I construction when Trucks A1-1 and/or A1-2 are placed on Span 1

Figure 21 shows similar GDFs of one- and two-lane load cases on Span 1 but with different trucks consisting of A2-1 and A2-2 (Table 1) with GVWs of 62,910 and 73,300 lb, respectively. Similar bridge responses are observed in terms of GDF with very little deviation, especially for the peak GDF values. The same observations are made for other spans as illustrated in Figure 22 through Figure 25.

In addition to the positive moment, the GDF caused by the negative moment is also evaluated. Figure 26 and Figure 27 illustrate the GDFs for Spans 1 and 3, or at distances of 64 ft and 378 ft-11 in. from the abutment, respectively. In both cases, the trucks are positioned in Span 2, causing a negative moment in Spans 1 and 3. Similar trends are observed in both cases, where the G5 had the highest GDF values. Likewise, the measured GDFs were significantly close to AASHTO LRFD code provisions at peak for span 1 when the trucks were placed on Span 2. On the other hand, GDFs were lower at peak compared to both code provisions for Span 3 when the trucks were placed on Span 2. Figure 28 and Figure 29 also show the negative moment GDFs for Span 2 or at a distance of 221 ft- 5 in. from the abutment. Unlike the negative moment GDFs for Spans 1 and 3, the GDFs are evenly distributed and are significantly lower than the code provisions.

Special load cases were also performed on the bridge, which included two following and two staggered trucks. The following case is performed so that the two trucks are on a single span, causing the maximum bridge response in the corresponding span. The staggered case is conducted similarly to the two-lane load case, but with one truck moved forward so that they are staggered. show the measured GDF value of each girder as well as the truck locations for Spans 1, 2, and 3. These load cases did not have a significant influence on the GDF, since they were both lower than the GDF obtained from two lanes. Interestingly, the GDFs of both load cases were very close. The staggered case also correlates well with the two-lane load but is significantly lower.

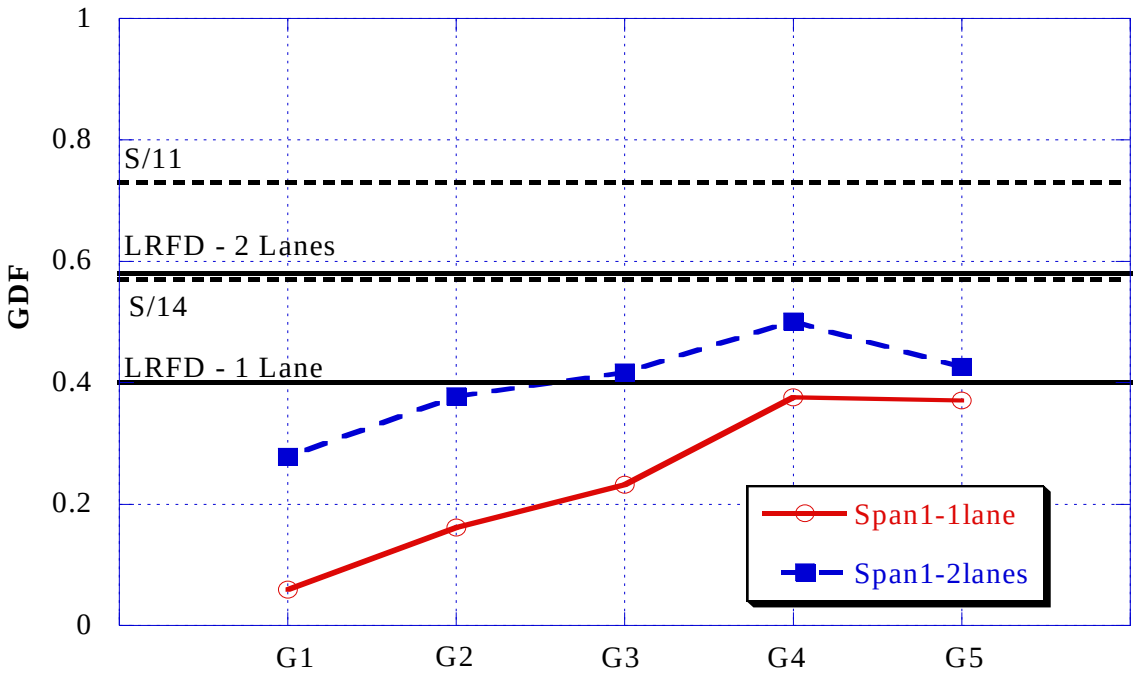

Figure 21. GDF obtained at a distance of 64 ft from abutment of Stage I construction when Trucks A2-1 and/or A2-2 are placed on Span 1

The effect of the truck transverse position is also investigated. The truck is moved transversely so that the truck would be positioned in the left, middle, and right lanes. Figure 33 illustrates the distance of the truck near wheel to the center of Girder 1. The truck wheel lies on top of Girder 3 for both left- and middle-lane loading cases. The only difference between the two cases was that the near wheel lies on top of Girder 3 for middle-lane loading, instead of the far wheel for left-lane loading. Figure 34 to Figure 36 show the effect of truck transverse position on GDF for Spans 1 to 3. A similar trend is observed in all spans. The GDF is controlled by the right lane when the wheel load is closest to the exterior girder (i.e., Girder 5).

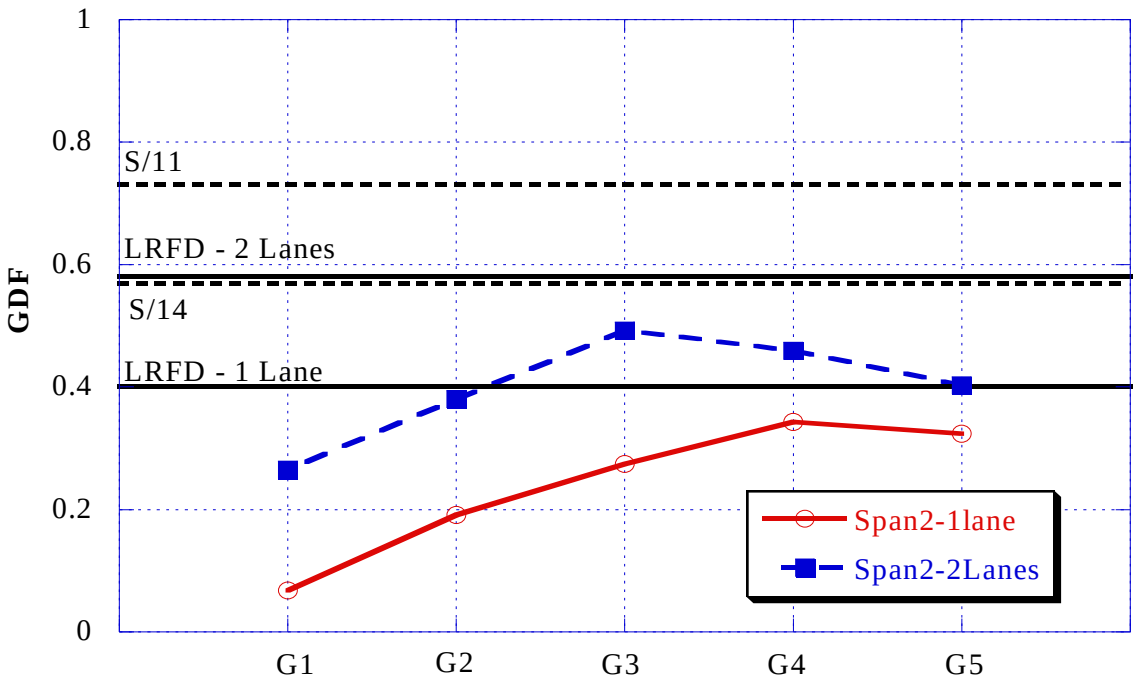

Figure 22. GDF obtained at a distance of 221 ft 5 in. from abutment of Stage I construction when Trucks A1-1 and/or A1-2 are placed on Span 2

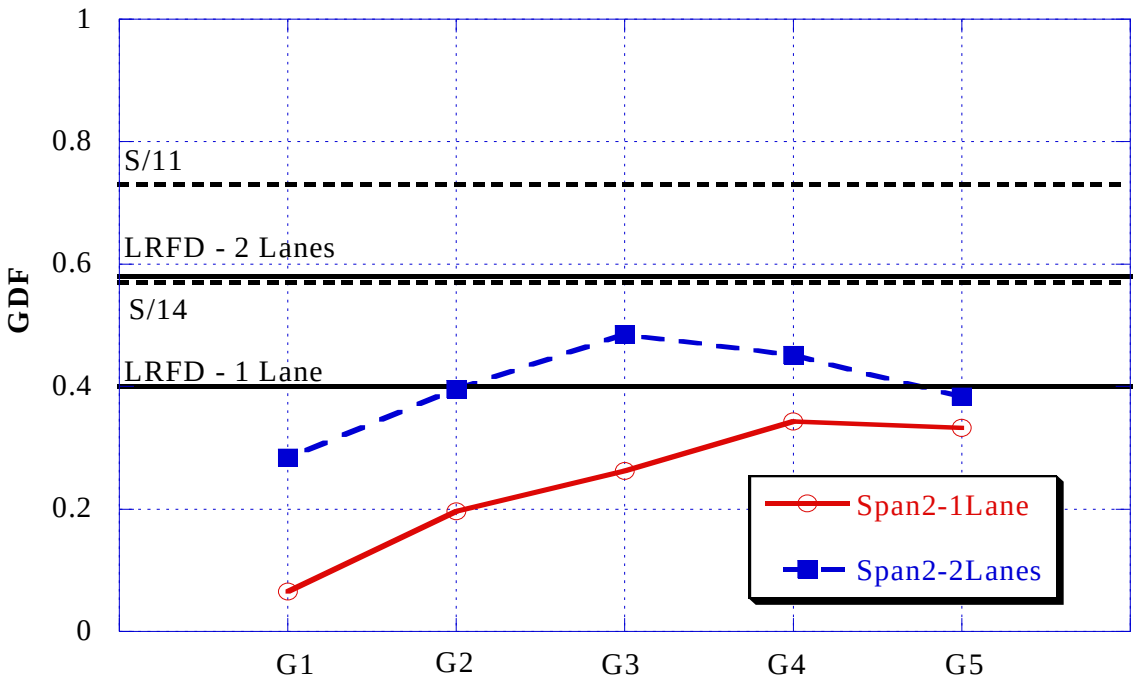

Figure 23. GDF obtained at a distance of 221 ft 5 in. from abutment of Stage I construction when Trucks A2-1 and/or A2-2 are placed on Span 2

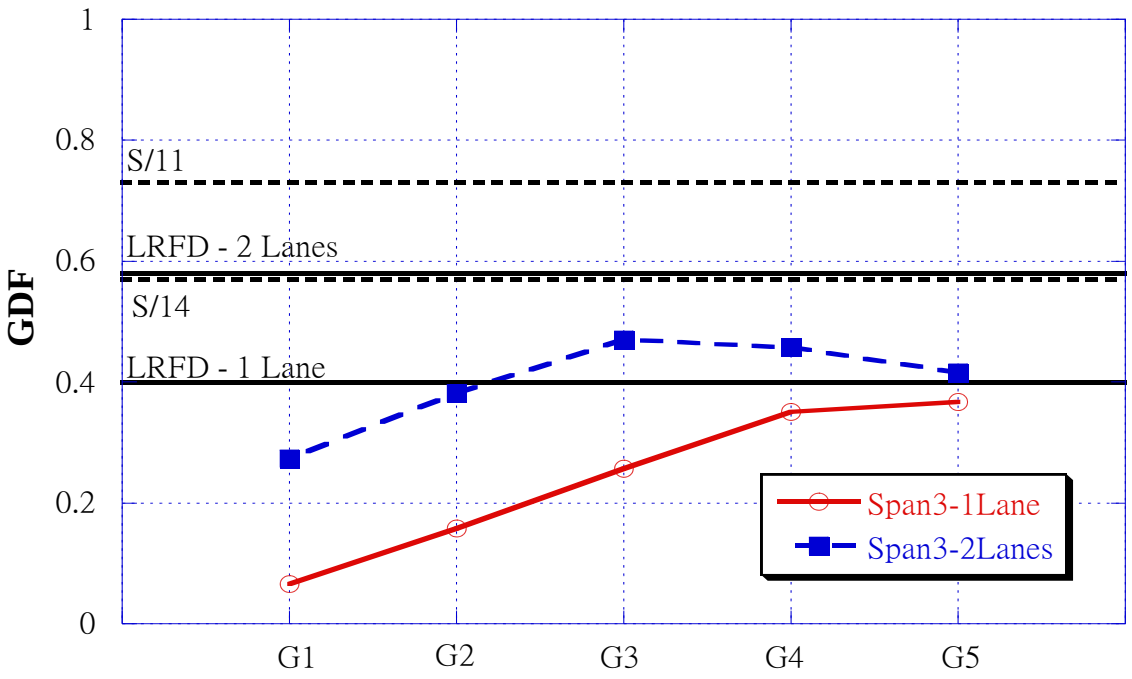

Figure 24. GDF obtained at a distance of 378 ft 11 in. from abutment of Stage I construction when Trucks A1-1 and/or A1-2 are placed on Span 3

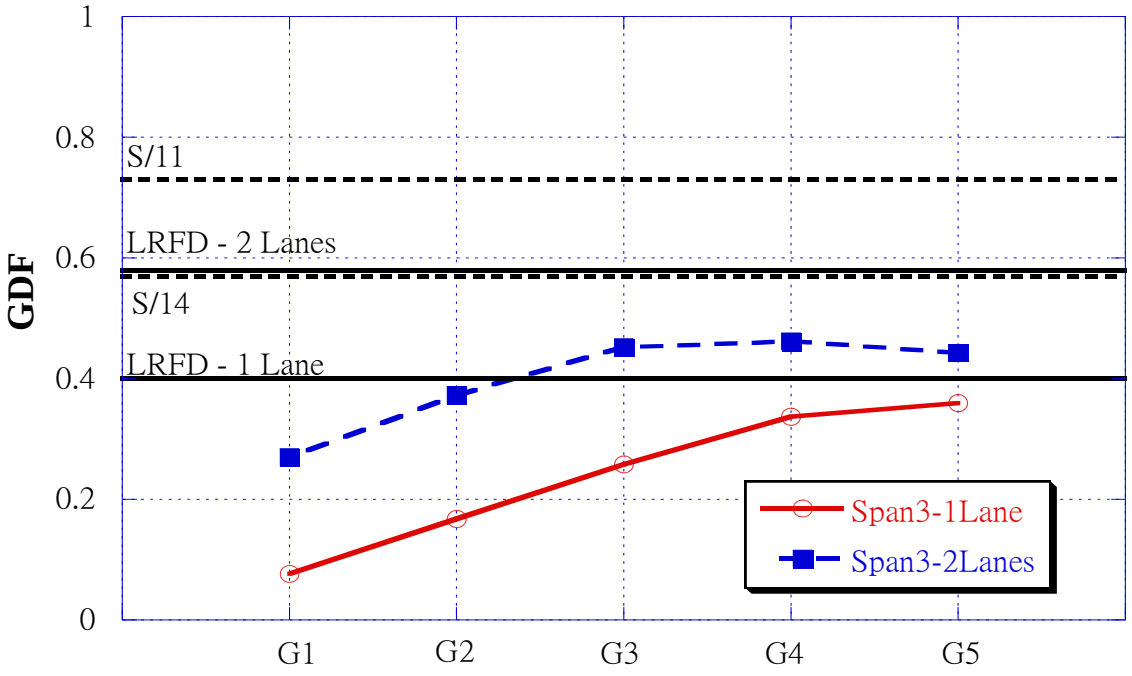

Figure 25. GDF obtained at a distance of 378 ft 11 in. from abutment of Stage I construction when Trucks A2-1 and/or A2-2 are placed on Span 3

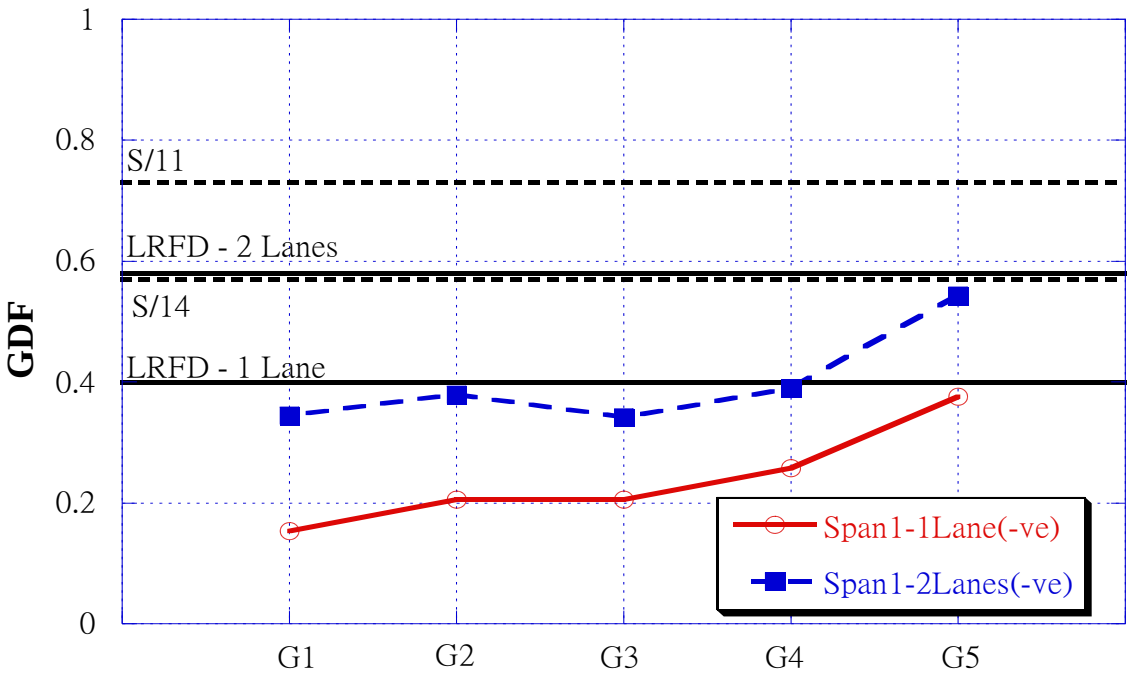

Figure 26. GDF obtained at a distance of 64 ft from abutment of Stage I construction when Trucks A1-1 and/or A1-2 are placed on Span 2

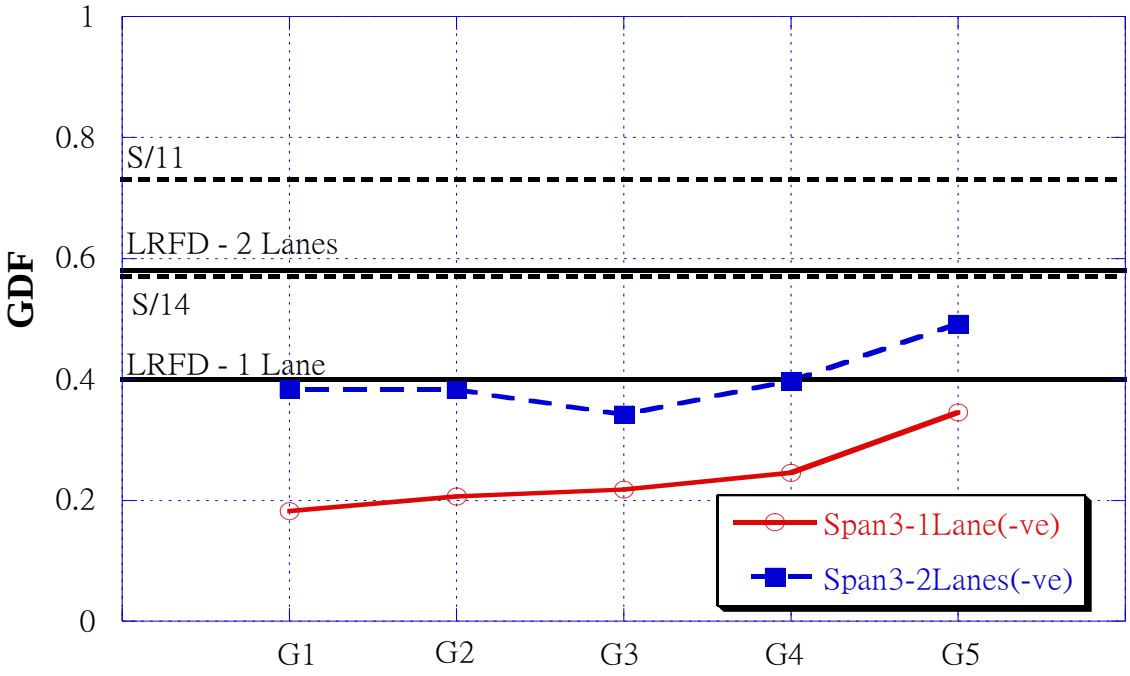

Figure 27. GDF obtained at a distance of 378 ft 11 in. from abutment of Stage I construction when Trucks A1-1 and/or A1-2 are placed on Span 2

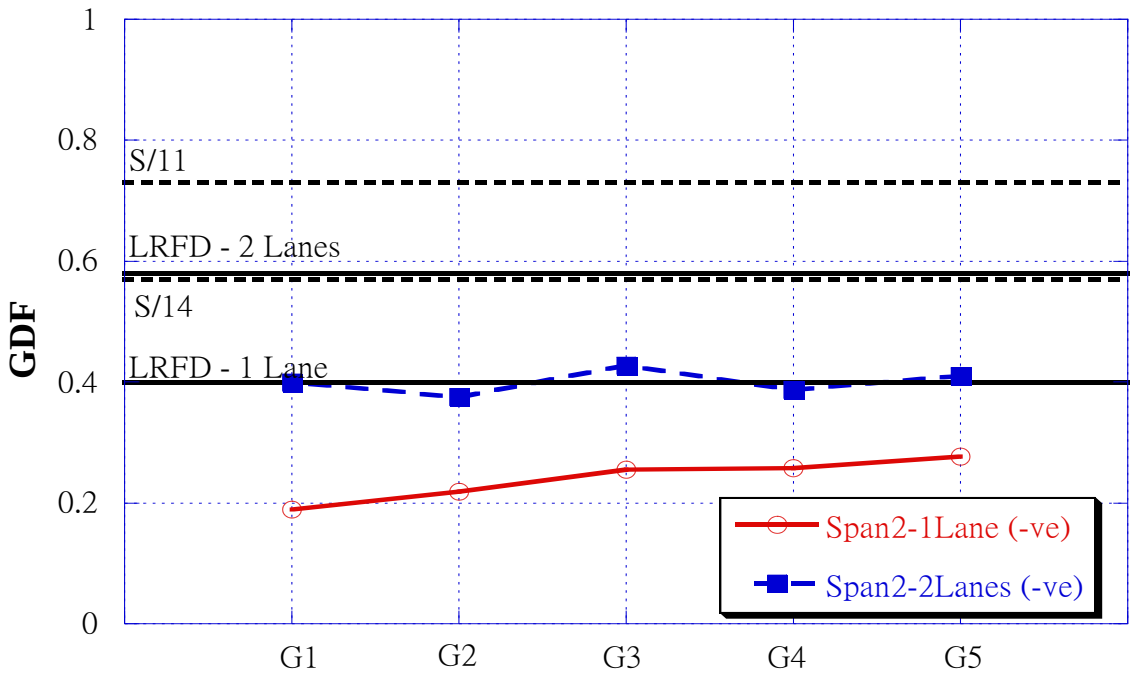

Figure 28. GDF obtained at a distance of 221 ft 5 in. from abutment of Stage I construction when Trucks A1-1 and/or A1-2 are placed on Span 1

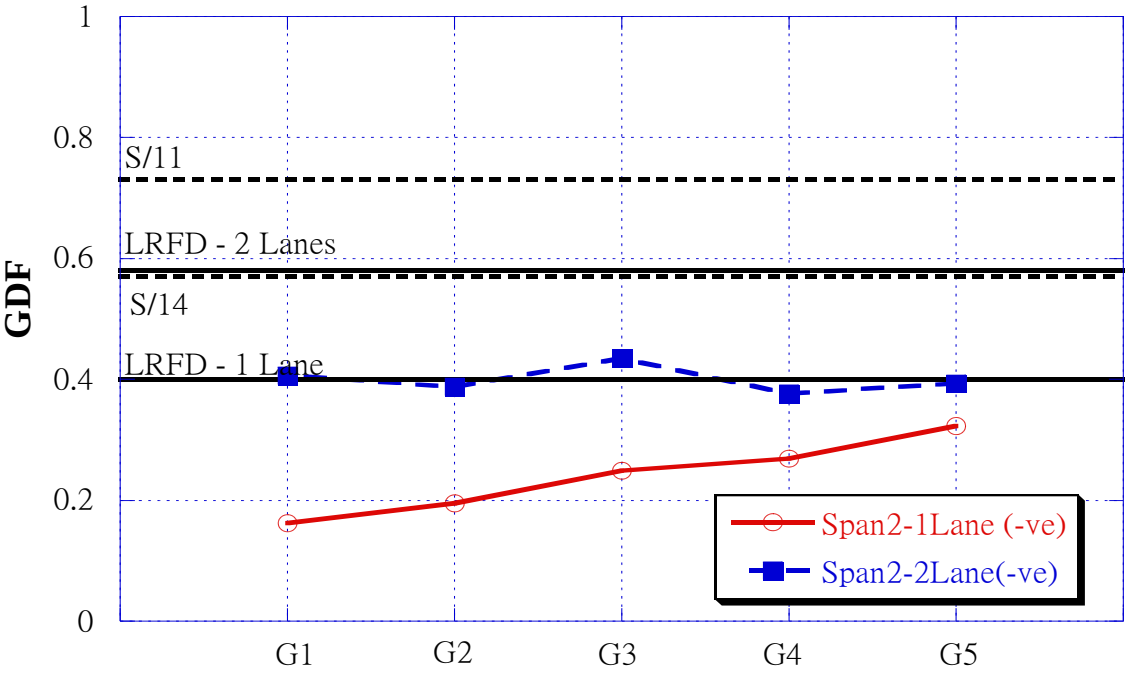

Figure 29. GDF obtained at a distance of 221 ft 5 in. from abutment of Stage I construction when Trucks A1-1 and/or A1-2 are placed on Span 3

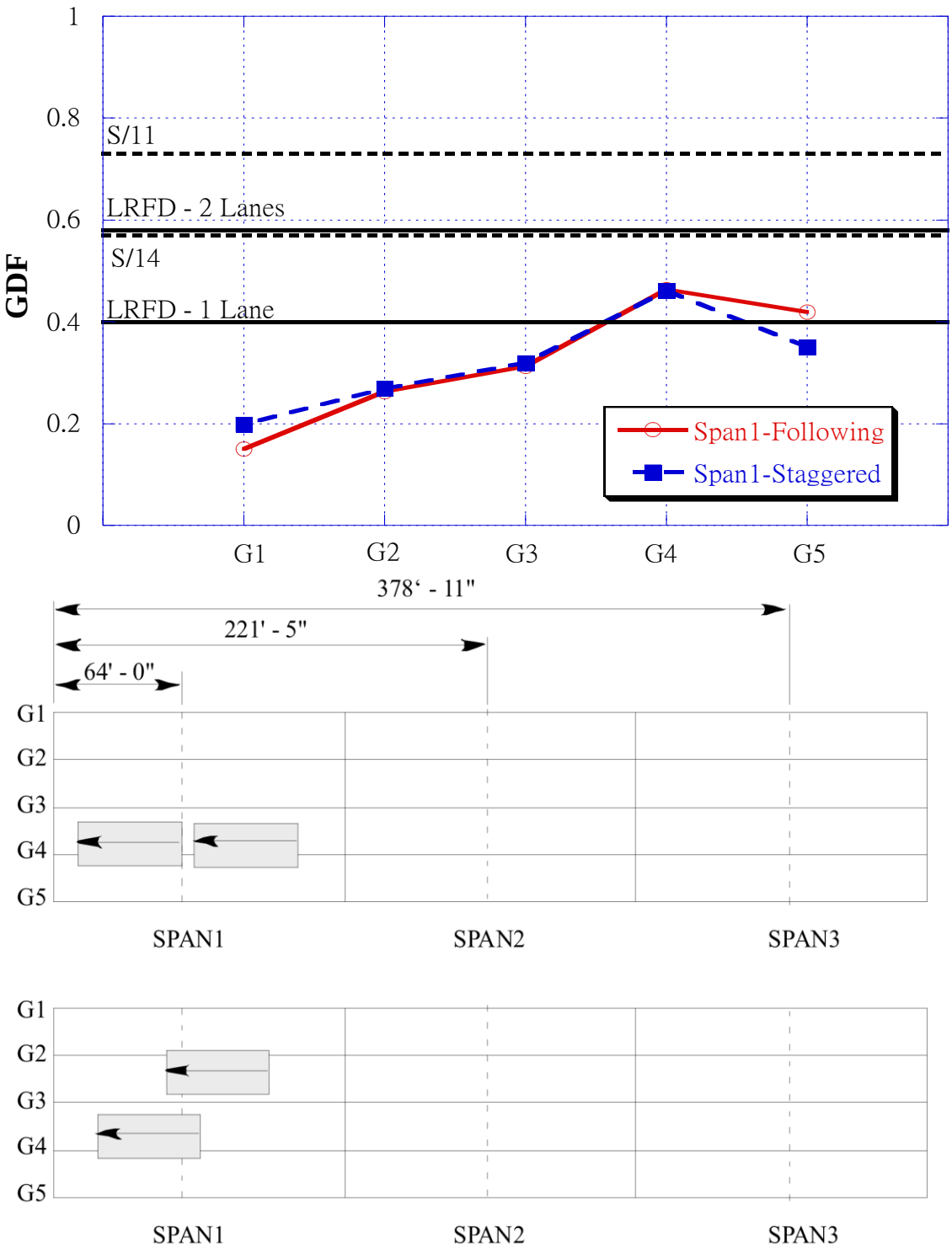

Figure 30. GDF obtained at a distance of 64 ft from abutment of Stage I construction when Trucks A1-1 and A1-2 are following or staggered

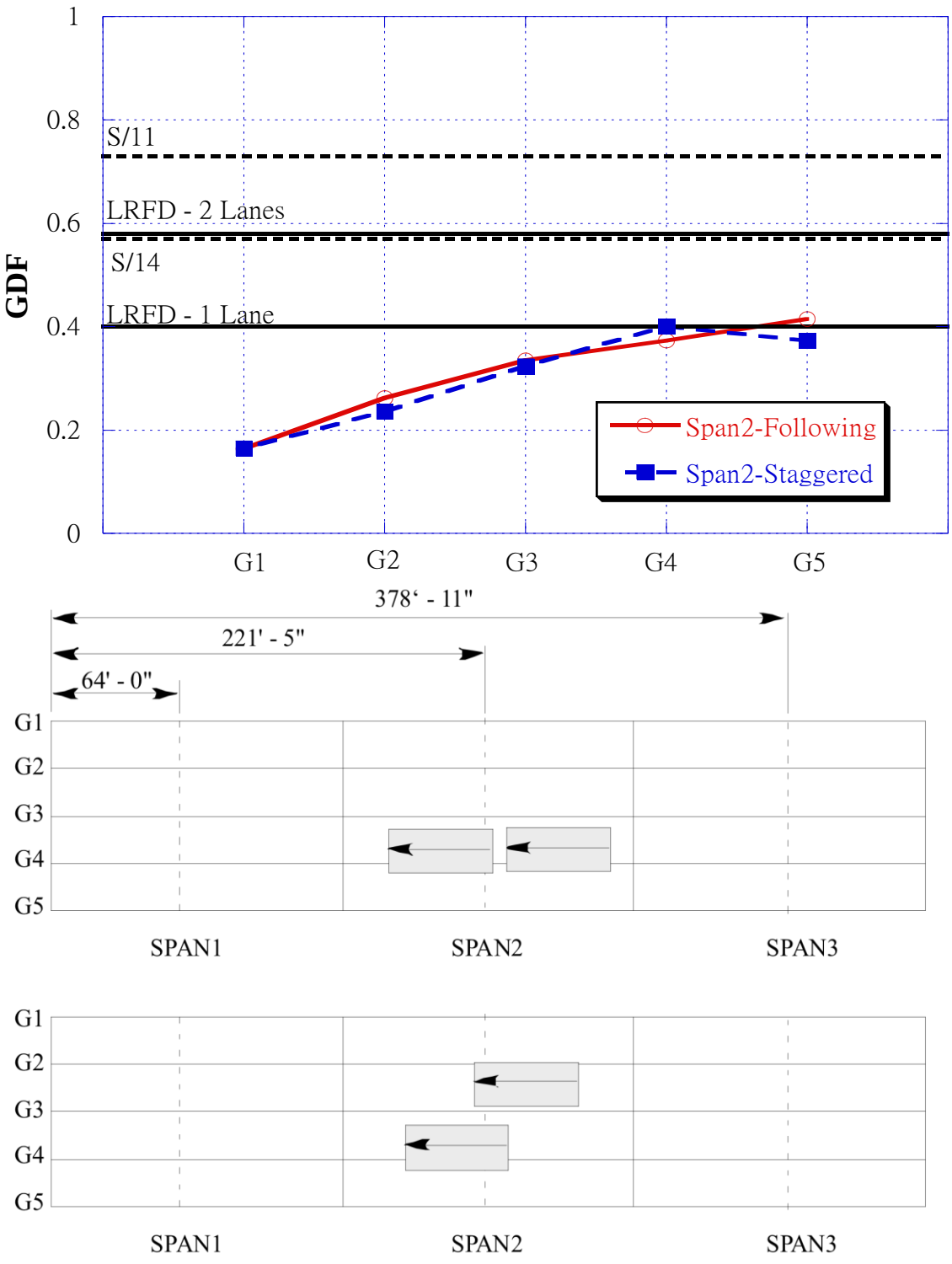

Figure 31. GDF obtained at a distance of 221 ft 5 in. from abutment of Stage I construction when Trucks A1-1 and A1-2 are following or staggered

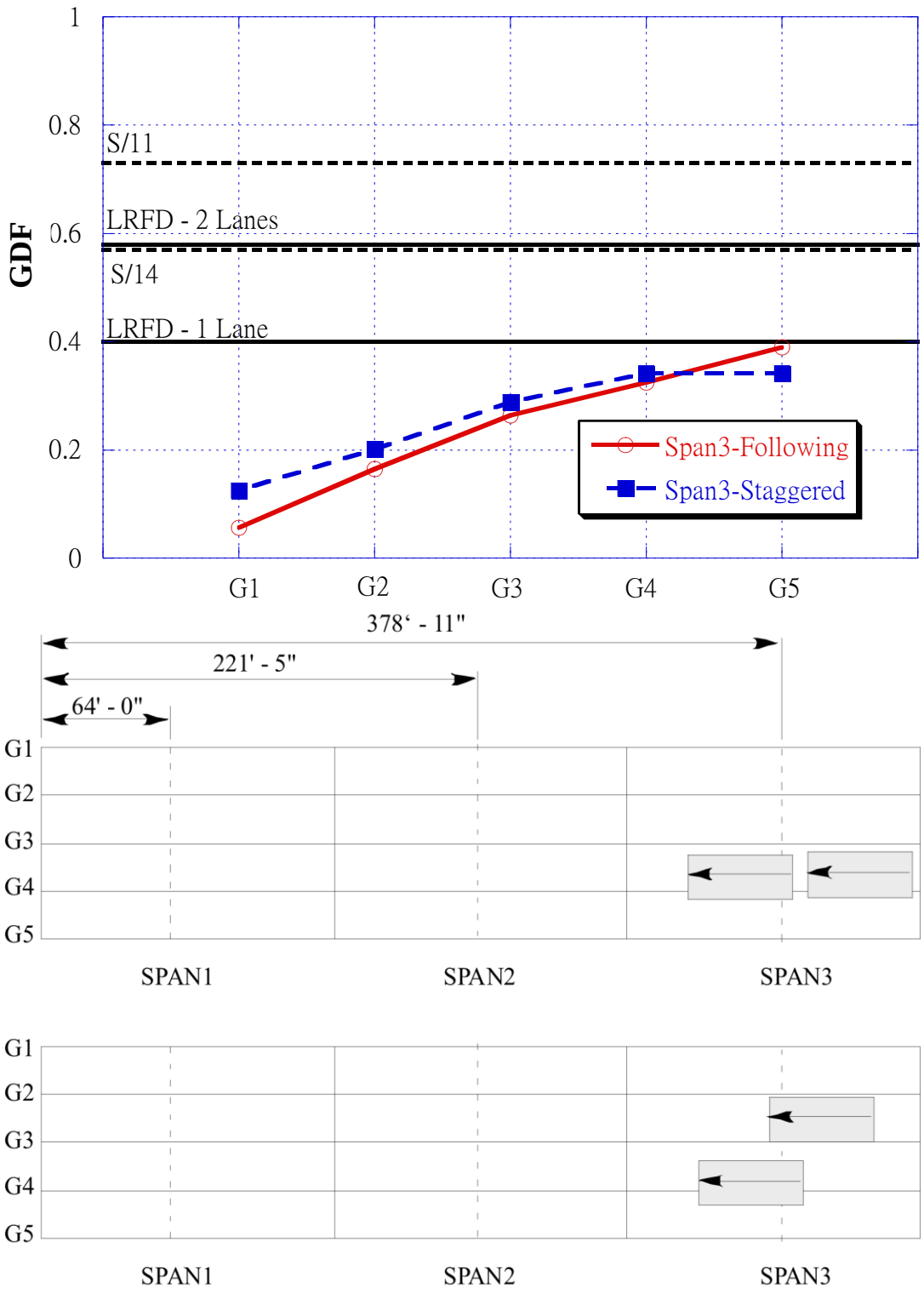

Figure 32. GDF obtained at a distance of 378 ft 11 in. from abutment of Stage I construction when Trucks A1-1 and A1-2 are following or staggered

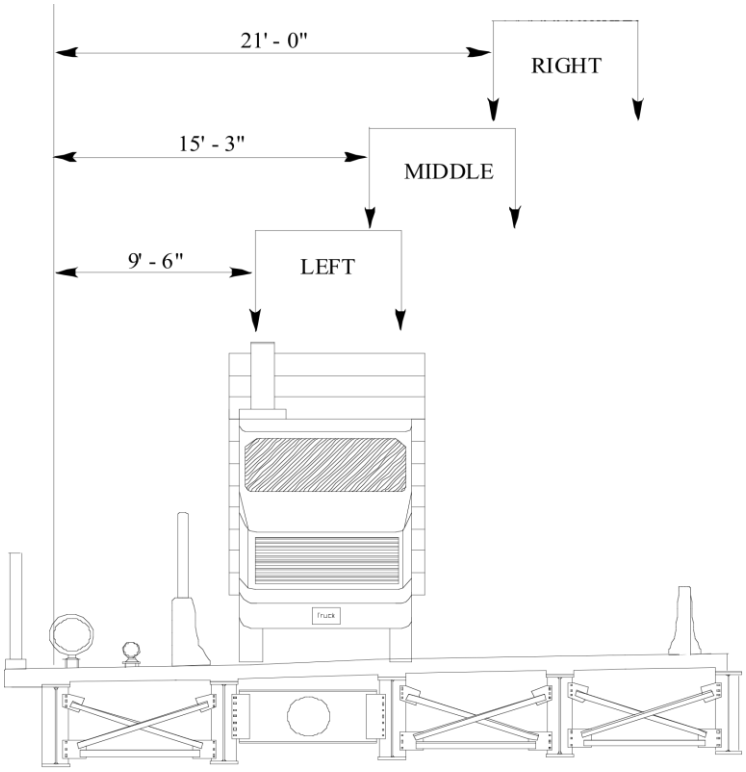

Figure 33. Transverse truck distances

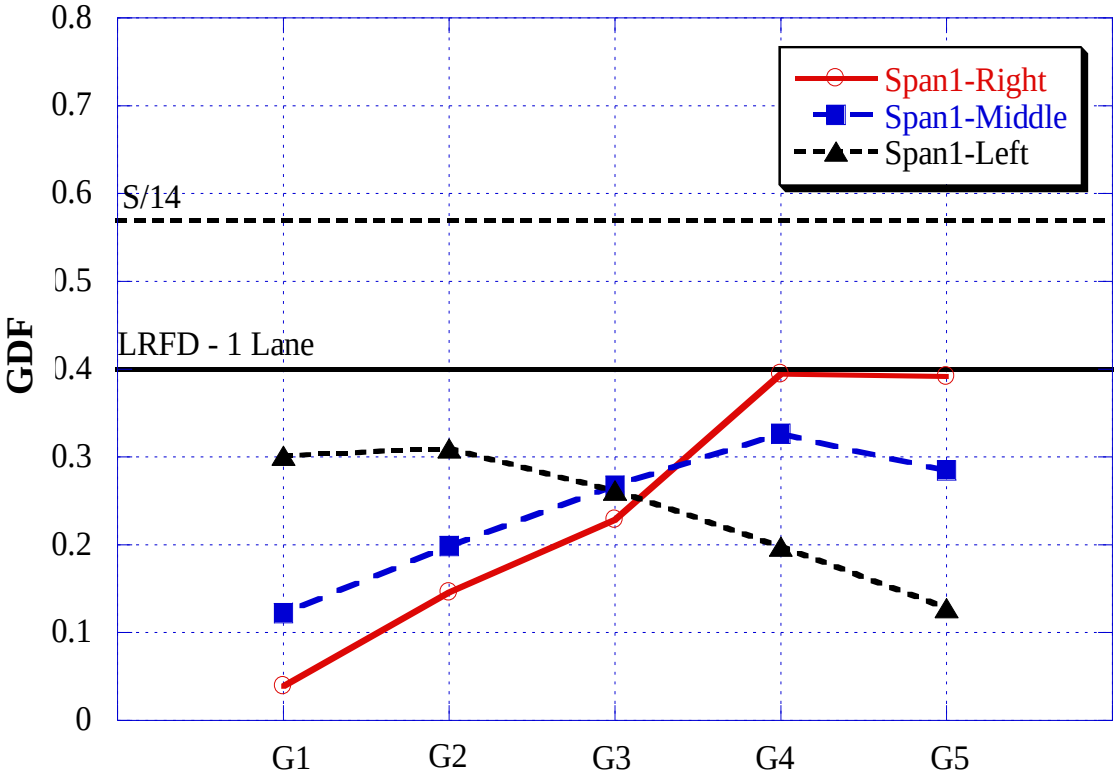

Figure 34. Effect of transverse truck positions on GDF on Span 1

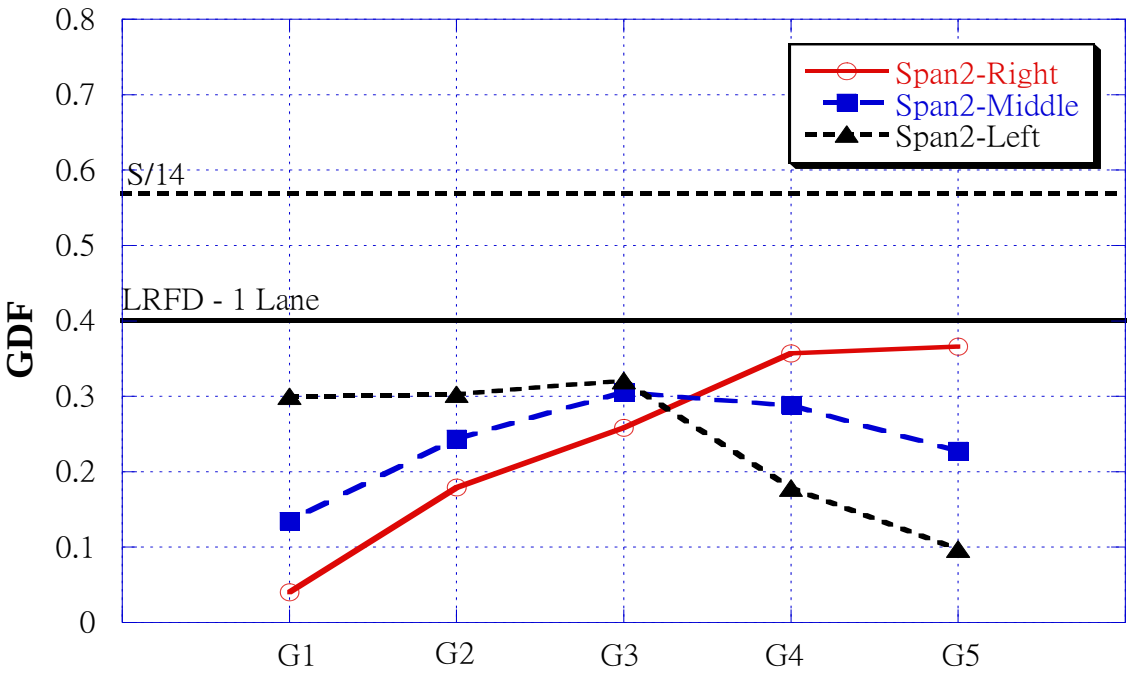

Figure 35. Effect of transverse truck position on GDF on Span 2

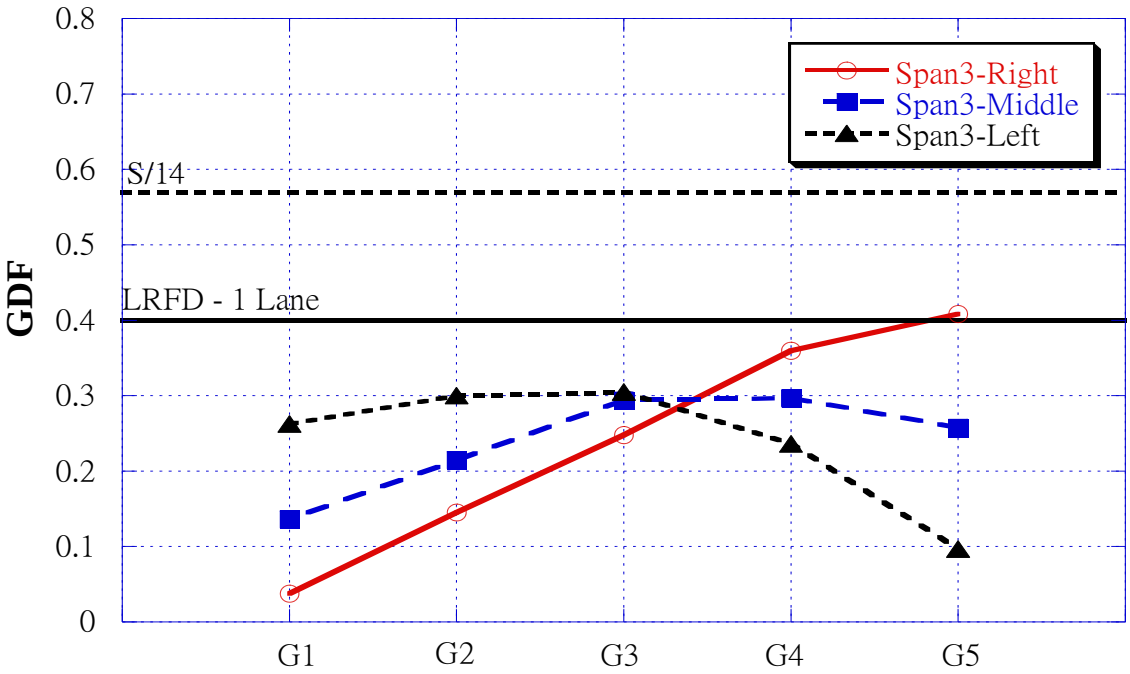

Figure 36. Effect of transverse truck positions on GDF on Span 3

Stage II Static Load Tests

The Stage II static load tests were performed on two occasions: July 10, 2003 (with no LMC), and December 1, 2003 (with LMC). The first test was done immediately after the Stage II construction. The second test was done immediately after the bridge latex-modified concrete overlay (LMC) was poured onto the deck slab. A 1- to 2–in. layer of LMC was poured on top of the deck to provide a specified clear cover for the reinforcing steel. Thus, the effect of the LMC layer was also investigated.

For the test on July 10, 2003, the bridge was loaded with Trucks B1-1 and B1-2. Both trucks had a GVW of approximately 76,000 lb. Figure 37 through Figure 39 show the GDF at Spans 1, 2, and 3, respectively. The trucks were positioned so that one wheel lies on top of Girders 7 and 9 (Figure 37). Similar to Stage I, the GDFs in Span 1 with values of 0.34 and 0.43 for one- and two-lane loading, respectively, were slightly higher than for other spans that have GDF values of 0.35 and 0.38 for one- and two-lane loading. Two trucks were also positioned side by side, four feet apart to conform to AASHTO LRFD loading as shown in Figure 40. The GDF increased slightly from 0.43 to 0.46, but was significantly lower than the code specifications. Moreover, these values were lower than the GDF obtained in Stage I, which was expected because Stage II construction had shorter girder spacing.

Figure 41 and Figure 42 show the effect of LMC on GDF for one- and two-lane loading, respectively. In both load cases, the GDFs were reduced by approximately 31 percent with values of 0.25 and 0.35 for one- and two-lane loading, respectively, as compared with no LMC. These values decreased because of the increased slab thickness and concrete compressive strength.

A summary of the GDF results is shown in Table 3**.** It is seen that the distribution factor given in AASHTO LRFD is correct, but conservative for different loading cases and positions.

Table 3. Summary of GDF results

Code	**Stage I**		**Stage II**	
	One Lane	**Two Lanes**	**One Lane**	**Two Lanes**
AASHTO	0.57	0.73	0.55	0.70
AASHTO LRFD	0.40	0.58	0.39	0.57
Field test	0.39	0.52	0.34	0.46
Field test (LMC)	N/A	N/A	0.25	0.35

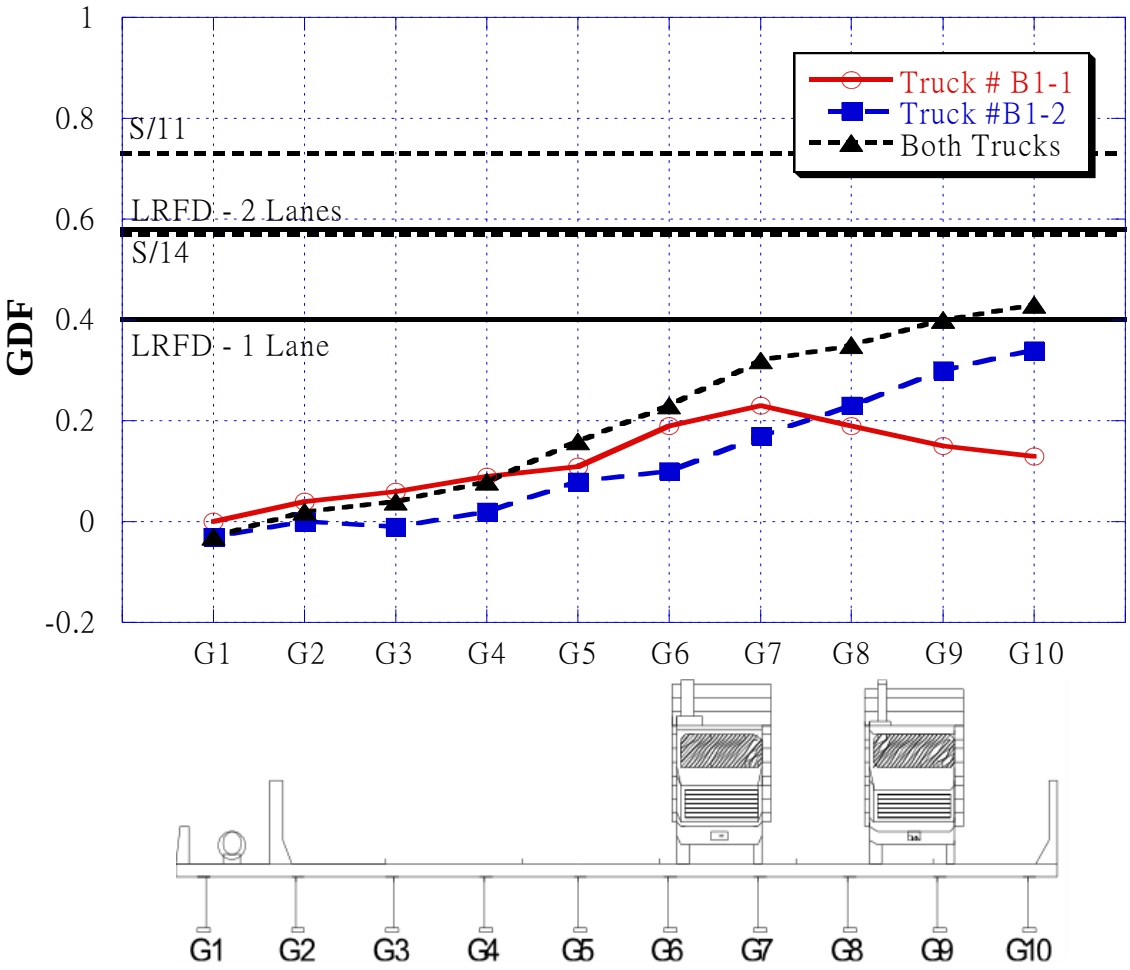

Figure 37. GDF obtained at a distance of 64 ft from the abutment when Trucks B1-1 and B1-2 were placed on Span 1

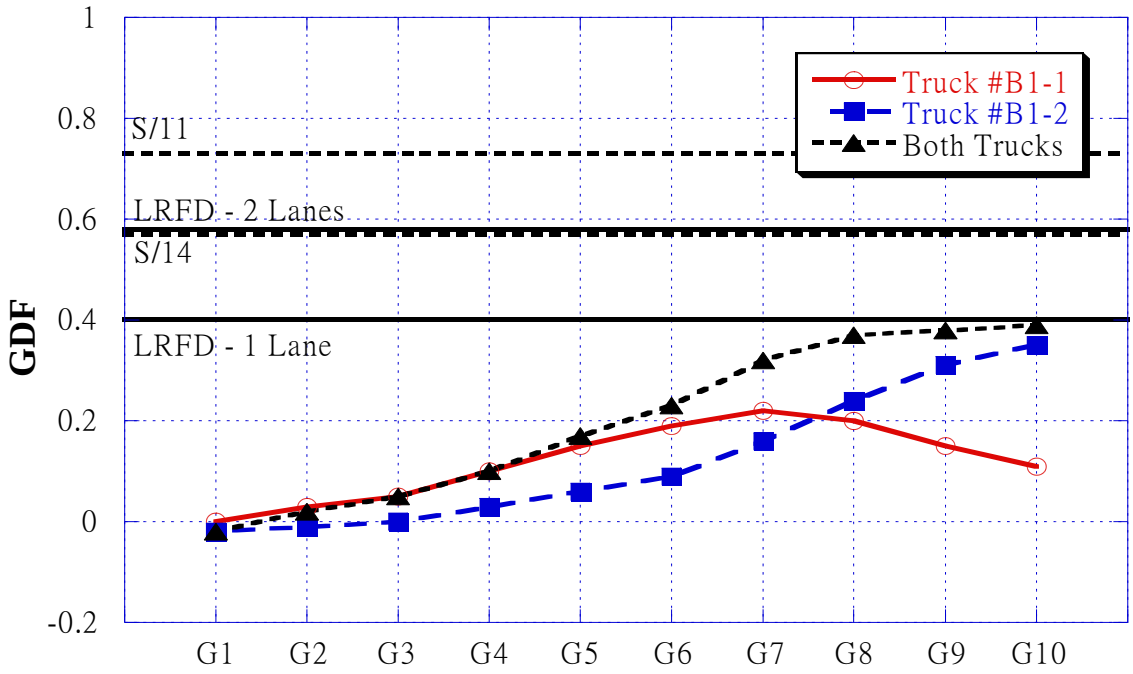

Figure 38. GDF obtained at a distance of 221 ft 5 in. from the abutment when Trucks B1-1 and B1-2 were placed on Span 2

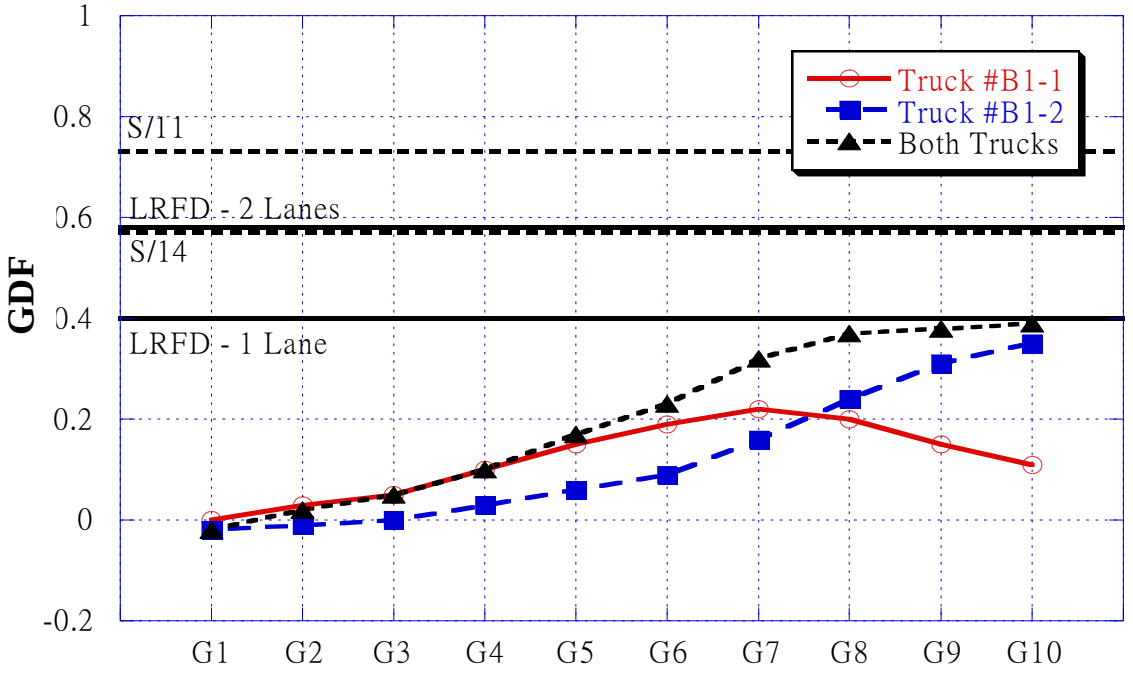

Figure 39. GDF obtained at a distance of 378 ft 11 in. from the abutment when Trucks B1-1 and B1-2 were placed on Span 3

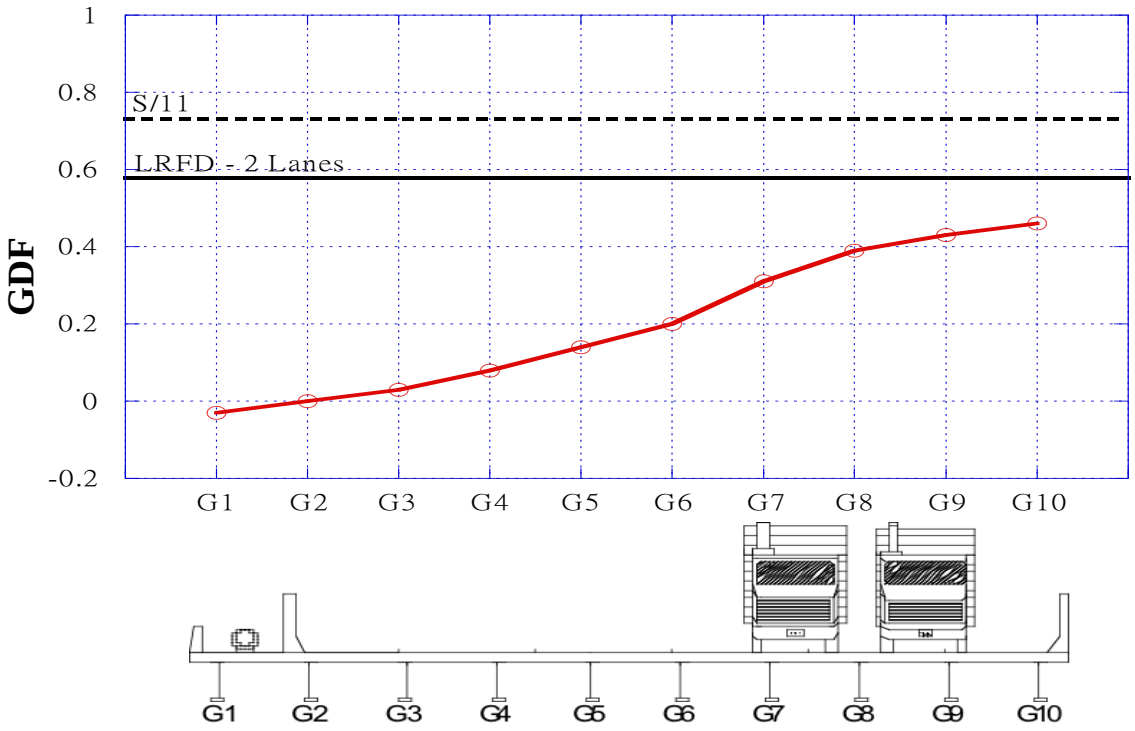

Figure 40. GDF of Stage II construction with two-lane load

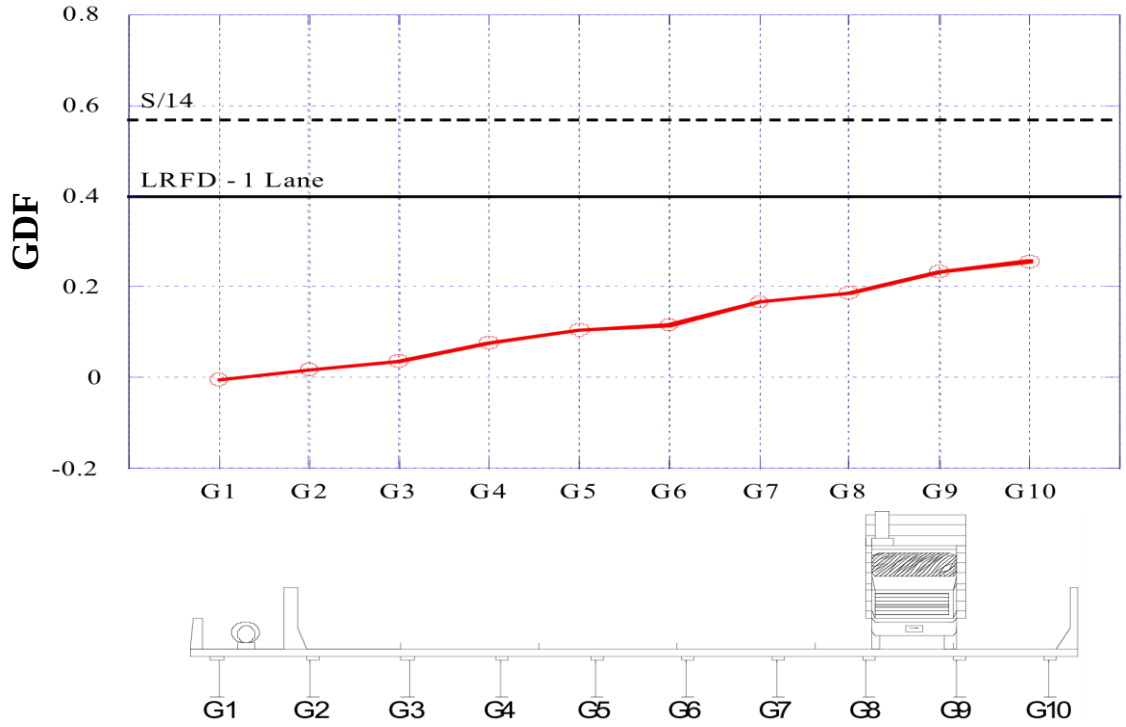

Figure 41. GDF of Stage II construction with one-lane load

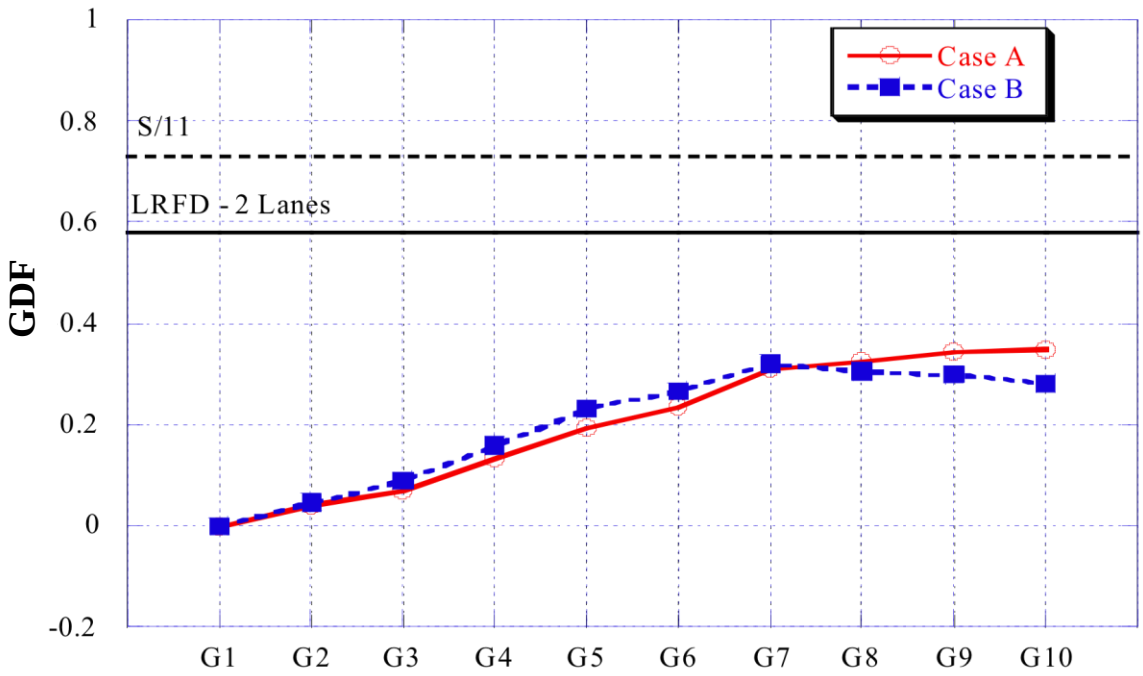

Case A:

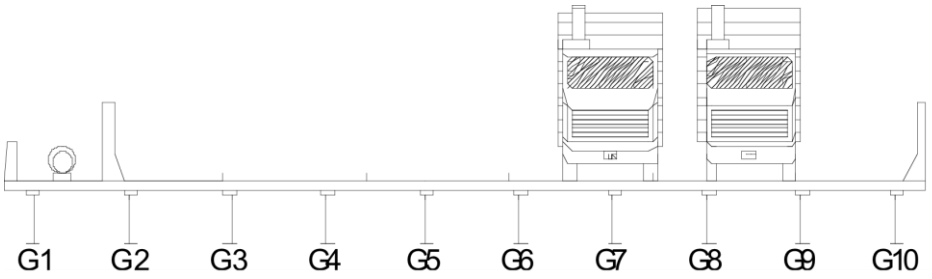

Case B:

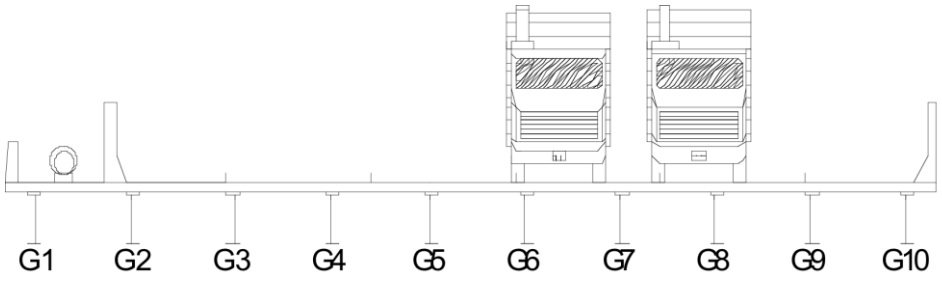

Figure 42. Effect of LMC on GDF with two-lane load cases

BRIDGE MODELS

Three analytical models—semi-continuum, grillage analogy, and Finite Element Model—were used to verify the field test results and validate the LRFD specification. All analytical methods can be used to model girder bridges with a high degree of accuracy; however, different assumptions and techniques must be made and understood by the engineer. These assumptions and techniques consist of the idealizations of various bridge components (e.g., concrete deck, girders, and diaphragms). Moreover, some modeling techniques are limited to bridge geometry, skew angle, and material properties. Therefore, it is important for an engineer to have a good understanding of the theories, assumptions, and limitations of each analytical method. The following section discusses and compares these methods in more detail.

Semi-Continuum Bridge Model

The semi-continuum bridge model used in analysis of the Doremus Avenue Bridge is based on the FORTRAN programs SECAN I and II developed by Jaeger and Bakht (1989, 1990). Jaeger and Bakht have extensively used the semi-continuum model for analyzing girder bridges. They also used the semicontinuum method for calibrating the GDF formulas for the Ontario Highway Bridge Design Code (OHBDC). The SECAN I and II programs are very similar (i.e., they both use semi-continuum theory). They account for the torsional rigidities in both longitudinal and transverse directions, but SECAN I can be used only to model simple span bridges, whereas SECAN II allows a total of ten intermediate supports to be placed between the end supports, making it a continuous supported bridge. However, SECAN I and II are limited to the number of girders and geometry of the bridge (i.e., they can be used only to model right bridges). Moreover, secondary bridge components, such as parapets and diaphragms, cannot be directly incorporated into the models. Therefore, to overcome these limitations, certain assumptions must be made. Two of the most important parameters of the semi-continuum model are the flexural stiffness, *EI,* and torsional stiffness *GJ*. For the concrete slab, both *EI* and *GJ* are well defined because it has a constant thickness in the longitudinal and transverse direction. On the other hand, computation of *EI* and *GJ* for the I-girder is more complex. The variable girder cross section along the length of the beam and the different cross sections of the interior and exterior girders contribute to this complexity. Additionally, the contribution of secondary components (e.g., edge stiffeners and diaphragms) increases the stiffness of the girder. Thus, to accurately model the bridge using the semi-continuum model, the variable and increased stiffness must be incorporated into the model.

Weighted-Average and Harmonic Analysis

The SECAN program allows the user to input different values of *EI* and *GJ* for different girders. However, the stiffness parameters are assumed constant along the length of the beam. Thus, for bridges with variable girder cross-sections (e.g., steel plate girder

bridges or W-shaped steel girder bridges with cover plates), constant values of *EI* and *GJ* need to be derived. Two methods were introduced by Gindy (2004), who used the SECAN program exclusively to find the bridge response of the Doremus Avenue Bridge, located Newark, New Jersey. The two methods consist of weighted-average and harmonic analysis.

Weighted-Average Analysis is a simple method that transforms the girder section into an equivalent section of constant flange thickness based on the length of each uniform section. The mathematical expression is given as:

$$t_{\mathrm{e}} = \sum_{i=1}^{i=n} t_i L_i; \qquad b_{\mathrm{e}} = \sum_{i=1}^{i=n} b_i L_i; \qquad \text{Eq. (4)}$$

where t_e and b_e are the equivalent top and bottom flange thicknesses, respectively;, and t_i and b_i are actual constant top and bottom flange thicknesses over length L_i for n sections of constant cross section. The moment of inertia and torsional rigidity could then be calculated using t_e and b_e.

The harmonic series analysis is a method suggested by Jaeger and Bakht (1989), which is very similar in theory to that of the externally applied loads. This method uses a harmonic series to express the moment of inertia denoted as *I(x)* for a simply supported beam at a distance *x* from the left-hand support as follows:

$$I(x) = I^{(1)} \sin\frac{\pi x}{L} + I^{(2)} \sin\frac{2\pi x}{L} + I^{(3)} \sin\frac{3\pi x}{L} + \ldots \qquad n = 1,2,3,\ldots \qquad \text{Eq. (5)}$$

where $I^{(n)}$ denotes the nth moment of inertia. The expressions for the coefficients are found by multiplying both sides of the above equation by $\sin(\pi x/L)$ and integrating with respect to *x* over the span length. Similarly, by considering an equivalent beam with a constant moment of inertia, and assuming that it closely represents the beam with a varying moment of inertia, the following expression can be found for the equivalent moment of inertia:

$$I_e = \frac{\pi}{2L} \int_0^L I(x) \sin\left(\frac{\pi x}{L}\right) dx \qquad \text{Eq. (6)}$$

For a stepwise varying moment of inertia, the equivalent moment of inertia is as follows:

$$I_e = I^{(1)}\left(1 - \cos\frac{\pi a_1}{L}\right) + I^{(2)}\left(\cos\frac{\pi a_1}{L} - \cos\frac{\pi a_2}{L}\right) + I^{(3)}\left(\cos\frac{\pi a_2}{L} - \cos\frac{\pi a_3}{L}\right) + \ldots \qquad \text{Eq. (7)}$$

where a_i is the distance from the left-hand support to the beginning of the ith section and $I^{(i)}$ is the moment of inertia of the ith increment of constant cross-section.

Table 4 shows the moment of inertia computed for the Doremus Avenue Bridge using the two methods. The moment of inertia calculated using weighted-average analysis is slightly smaller than the harmonic series (by approximately four percent). Thus, the weighted-average method was used to compute the equivalent constant section of all bridges because of the simplicity of the method.

Table 4. Computation of moment of inertia by using Weighted-Average and Harmonic Series Analyses (Gindy 2004)

Girder	Weighted Average I (10^5 in.^{4})	Harmonic Series I (10^5 in.^{4})	Ratio
G1	2.71	2.83	0.96
G2	1.83	1.87	0.97
G3	0.91	0.94	0.96
G4	0.91	0.94	0.96
G5	1.06	1.15	0.93

Grillage Model

The grillage model is based on a FORTRAN program, 3DBVRG, developed by Nassif and Liu (1996, 2004) to determine the dynamic and static stresses, deflections, and dynamic load factors of I-girder bridges. The program was later improved by Nassif, Liu, and Ertekin (2003) to include the ability to analyze continuous-span bridges. The model was also adopted by Yuksel (2004) to model the Doremus Avenue Bridge.

The grillage analogy is based on the idealization of a bridge structure in terms of one-dimensional beams organized in a grid system. The longitudinal beams generally represent the bridge I-girders, whereas the transverse beams represent the deck slab. For girder bridges, the longitudinal beams are usually placed coinciding with the girder centerline and the transverse beams are divided evenly along the longitudinal beams to represent the deck slabs. It is very important to provide enough transverse beams to gain an acceptable level of accuracy. A rule of thumb is to have the grid aspect ratio equal to 1.0, and it should not exceed an aspect ratio of 1.5 (West 1973). An aspect ratio of 1.15 was used to model the Doremus Avenue Bridge (Yuksel 2004).

Similar to the semi-continuum model, the longitudinal moment of inertia of the I-girder is calculated in the same manner as with weighted-average analysis. The composite action is also considered using Article 4.6.2.6.1 and Commentary C4.6.2.6.1-1 (AASHTO LRFD 2004) previously described. In addition, the concrete slab torsional constant is added to that of the I-girder because the concrete slab resists torque in both longitudinal and transverse directions. Thus, the torsional constant J_T values for the longitudinal grillage elements are calculated as follows:

$$J_T = J_{beam} + J_{slab} \qquad \text{Eq. (8)}$$

where J_{beam} and J_{slab} are the torsional constants of the beam and slab, respectively. The torsional constants of the beam are calculated by using Commentary C4.6.2.2.1-1 and C4.6.2.2.1-2 (AASHTO 2005) and are expressed as follows:

For thin-walled open beam,

$$J_{beam} = \frac{1}{3}\sum bt^3 \qquad \text{Eq. (9)}$$

where b and t are the width and thickness of the plate element, respectively, A is the area of the cross section, and I_p is the polar moment of inertia.

The torsional constant of the slab is calculated with the following expression:

$$J_{slab} = \frac{b_e t_e^{\,3}}{6} \qquad \text{Eq. (10)}$$

where b_e and t_e are the width and thickness of the equivalent transverse beams, respectively. In the transverse direction, only the moment of inertia and torsional constant of the slab are used. The width of the slab is computed using the tributary area of the transverse beams (i.e., for interior beams, the width is the distance of the grid in the transverse direction; for exterior beams, the width is one-half the distance of the grid).

Finite Element Model

A general-purpose finite element (FE) program, ABAQUS, was used to perform the analytical study. ABAQUS includes a variety of routines that are suited for civil engineering application. The program contains many concrete engineering properties such as the stress–strain profile, failure ratio, and tension stiffening and modeling of reinforcing bars in concrete.

Two different idealizations of the Doremus Avenue Bridge were developed: the Shell-Beam (SB) and the Shell-Shell (SS) models. Both FE models utilized shell elements to construct the concrete slab and different elements to represent the bridge girder. The SB model used beam elements to represent the bridge girders, whereas the SS model used shell elements. The SS model provided better connectivity between the bridge deck slabs to the bridge girder.

For both models, the concrete slab was created using a general-purpose four-node shell element (S4) with six degrees of freedom at each node. The 28-day compressive strength, modulus of elasticity, and modulus of rupture of match-cured or field-cured samples were used for the material properties of the concrete deck slabs. The modulus of elasticity used was equal to 34,500 MPa (5,000 ksi) with a Poisson ratio of 0.17. The compressive strength was 55 MPa (8 ksi) and the modulus of rupture was 4 MPa (0.6 ksi). The reinforced bars in the concrete were also modeled by using a “rebar” element provided by ABAQUS. The reinforcing bar properties were defined by a similar reinforcing bar tested in the laboratory with a modulus of elasticity of 200 GPa (29,000 ksi), a Poisson ratio of 0.3, and a yield strength of 400 MPa (60 ksi) at 0.2 percent. The aspect ratio for the shell element was kept to a maximum of 1:1.5 to minimize distortions.

For the SB model, the girders were modeled using a two-node beam element (B3) with six degrees of freedom at each node. The actual cross section of the girder was considered because the girders have varying thicknesses. The modulus of elasticity, Poisson ratio, and yield strength were taken from the steel manual with values of 200 GPa (29,000 ksi), 0.3, and 350 MPa (50 ksi), respectively. The beam element and the shell element of the slab were connected using a multiple point constraint (TIE MPC) where the active degrees of the beam and shell nodes were equal. In addition, the concrete barrier, end stiffeners, and steel rails were modeled using the same beam element with their respective material properties.

For the concrete barrier, the same concrete properties were used as was for the concrete deck slab. The steel rails used the same material properties as the steel bridge girder. For simplicity, the barriers were idealized as an equivalent rectangle beam rather than using the actual geometry. In addition, the diaphragms were also modeled using two-node beam elements where the nodes were also shared by the girders. For the cross diaphragms, an equivalent steel I-girder was used. The holes in the diaphragms were disregarded to simplify the models, as the diaphragms did not contribute significantly to the change in the slab or the girder moments. Furthermore, boundary conditions were used instead of modeling the abutments and the piers. A roller boundary condition was used to represent the south abutment, Pier 1, as well as Pier 3. The second pier was represented by a pin boundary condition. The pin boundary condition restricts the vertical and horizontal movements of the bridge at the support. The boundary condition was set only on the beam element (i.e., the bridge girder).

To eliminate the connecting elements or TIE MPC, the SS model was developed. The SS model used only a general-purpose four-node shell element to model the entire bridge with the exception of the diaphragm, which was modeled using a two-node beam element. The same material properties from the SB model were also utilized in the SS model. The concrete barrier, stiffeners, and steel rails were all included in the model using the four-node shell elements. The actual geometry of the cross diaphragms was considered in the SS model. Similarly, boundary condition was also used to represent the abutments and piers. The boundary condition was set on the nodes of the bottom flange elements. Figure 43a and Figure 43b illustrate the FE models of the SB and SS models, respectively.

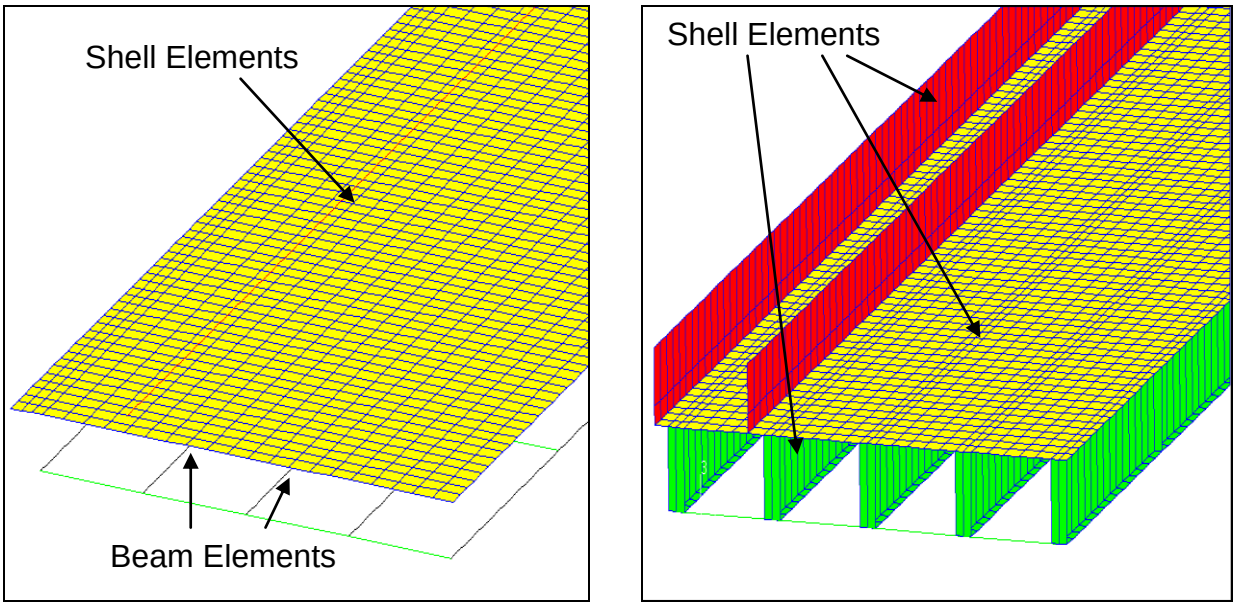

(a) (b)

Figure 43. FE Models: (a) Shell-Beam (SB) (b) Shell-Shell (SS)

Comparison of Analytical Models

Semi-Continuum Model

Gindy (2004) extensively used the semi-continuum model for analyzing the Doremus Avenue Bridge and compared the girder stresses for the cases described above. Only half the bridge (i.e., Girders 6 to 10) is modeled and the response of the girder with the maximum bending moment (i.e., Girder 8) is reported. Figure 44 compares stresses in Girder 8 for live load testing of a one-lane load. The stresses, obtained in Spans 1 and 3 using the semi-continuum model, relate well with the field measurements. In Span 2, the semi-continuum model under predicted the peak stresses by approximately 36 percent. Despite the large variation in stresses, overall, the model provides an accurate bridge response, as long as the correct assumption about the cross section is made.

Grillage Model

Yuksel (2004) used grillage analogy to model the Doremus Avenue Bridge. The grillage program used was developed by Nassif and Liu to incorporate dynamic responses, such as road roughness and vehicle suspension. Figure 45 through Figure 47 compare all ten girder stresses using the grillage model with the test results. The dynamic stresses are used for the comparison rather than the static stresses, because the former stresses include truck suspension and road roughness. Overall, the grillage model provides very accurate results for all spans, especially for Girders 8 and 9. The largest deviation is in Girder 10, where the stresses obtained from the grillage model are significantly lower than the measured data due to the contribution of the parapet to the overall stiffness in the model. Nevertheless, the grillage model is one of the best methods for calculating girder stresses.

FE Model

Figure 48 through Figure 50 compare Stage II live load testing of one-lane load using the FE method, which relates well with all ten girders, unlike the grillage method that under predicted stresses in Girder 10. Part of the reason is that rather than assuming the stiffness and moment of inertia for the parapet, the parapet and other secondary elements (e.g., utility pipes and steel rails) are included in the model as separate assemblies (parts). One disadvantage of the FE method is the lengthy computation time and difficulty in modeling the bridge.

As a summary of the above, the FE Method is the most accurate among other approaches when comparing the stresses between experimental and analytical models. However, the computational effort in using the FE method is more involved than that of the semi-continuum or the grillage approaches.

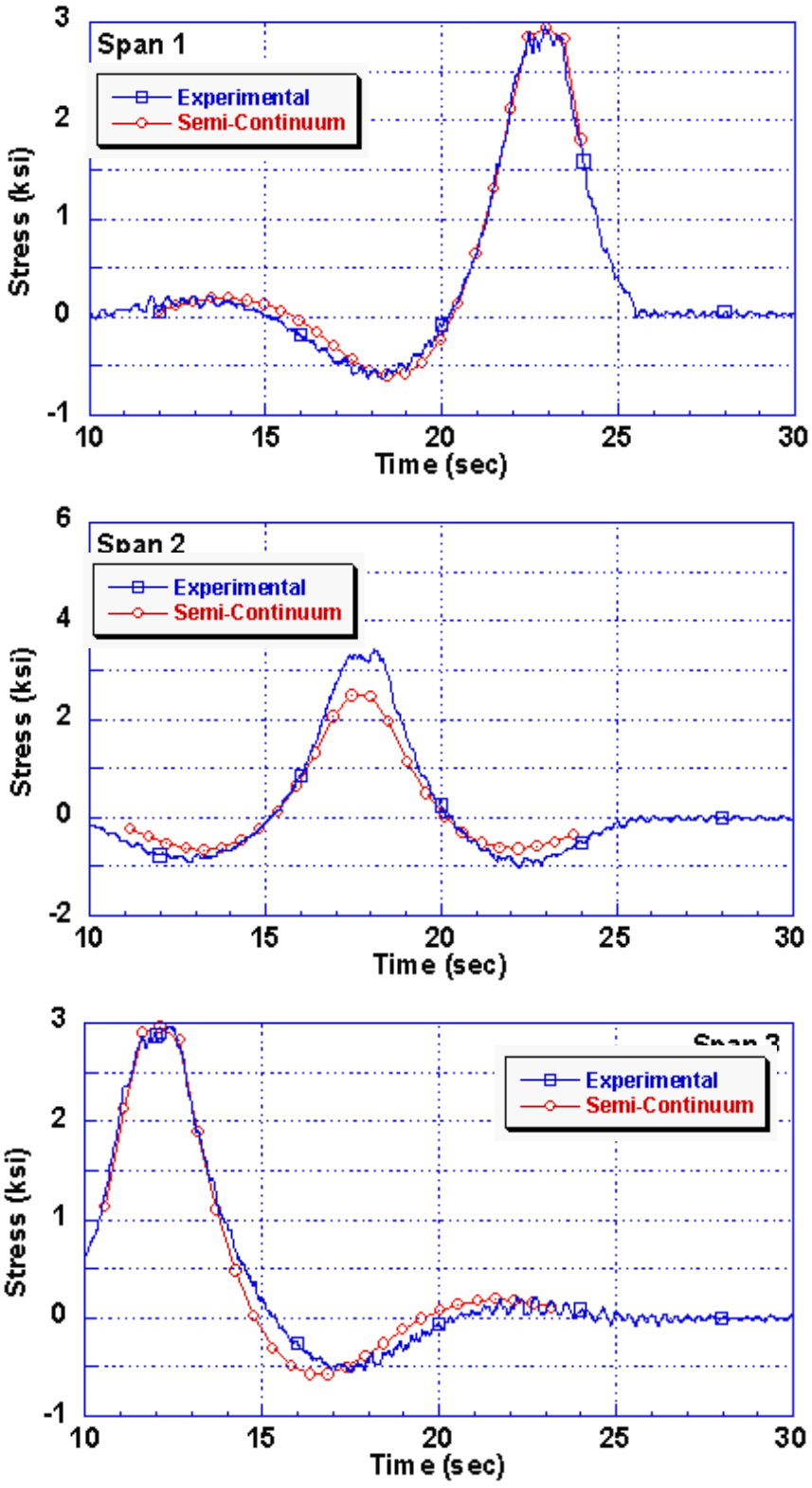

Figure 44. Comparison of Girder 8 stress for Stage II live load testing of two-lane load using the Semi-Continuum Method (Gindy 2004)

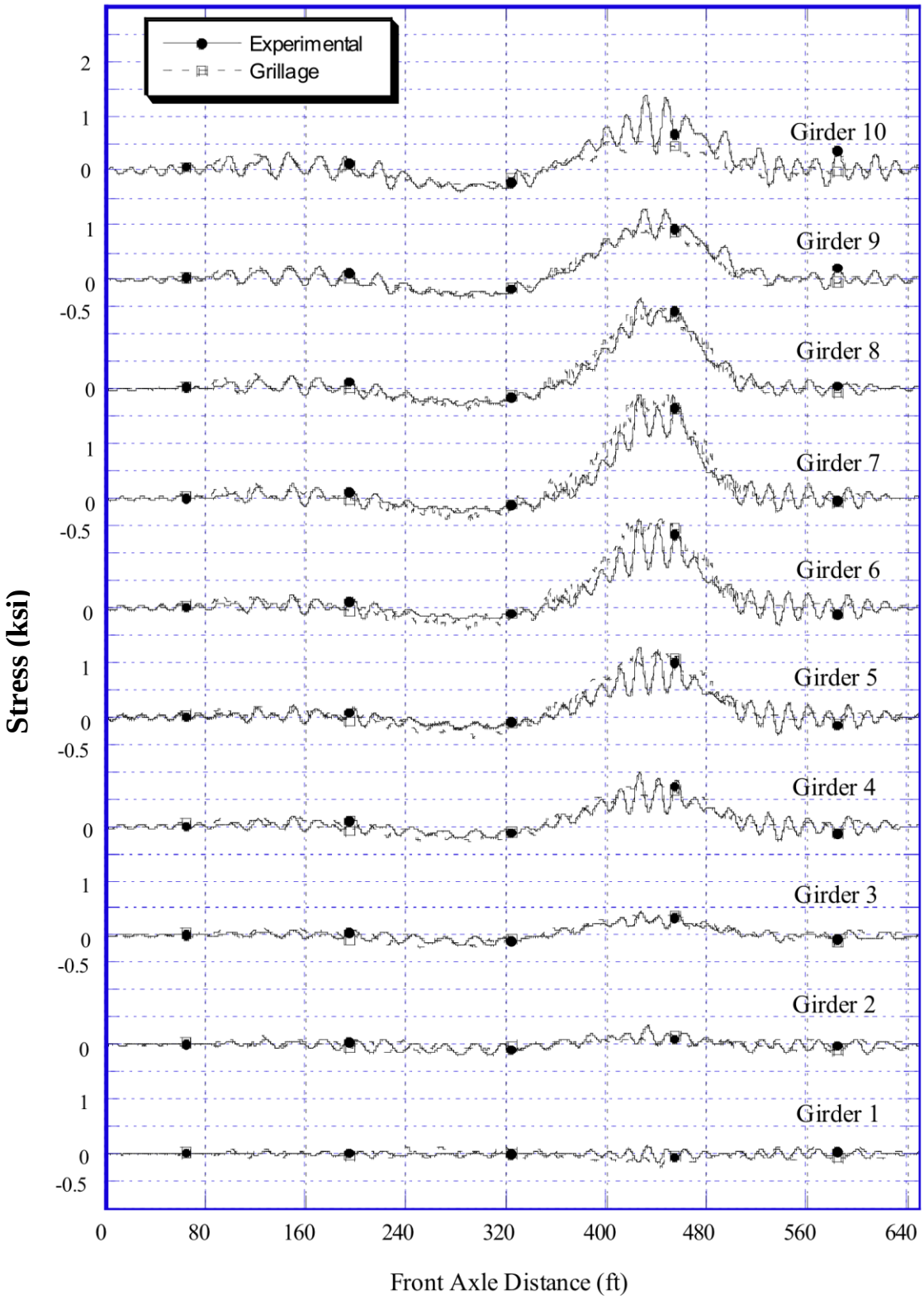

Figure 45. Comparison of girder stresses for Span 1 for Stage II live load testing of one-lane Load using Grillage method (Yuksel 2004)

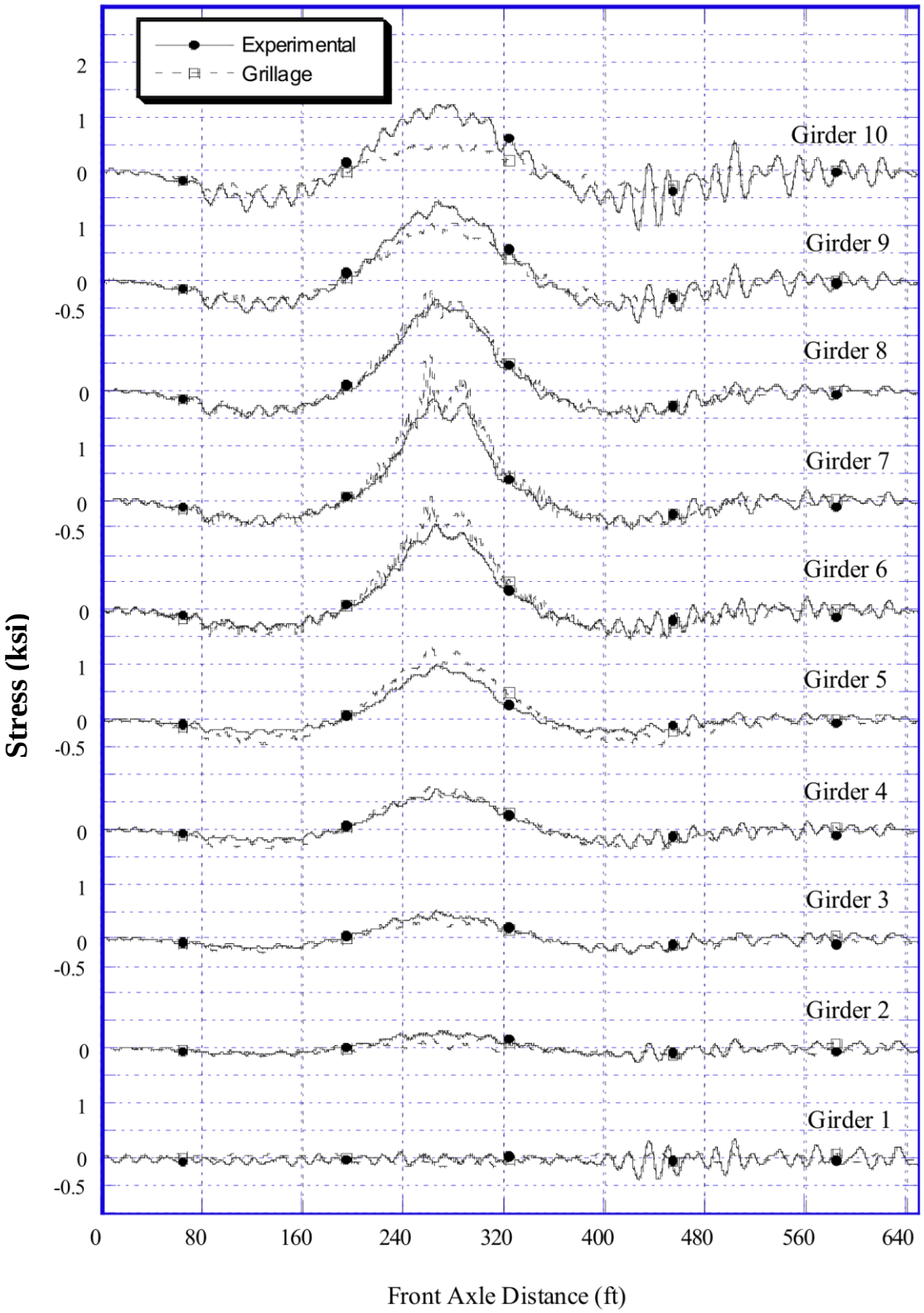

Figure 46. Comparison of girder stresses for Span 2 for Stage II live load testing of one-lane load using Grillage Method (Yuksel 2004)

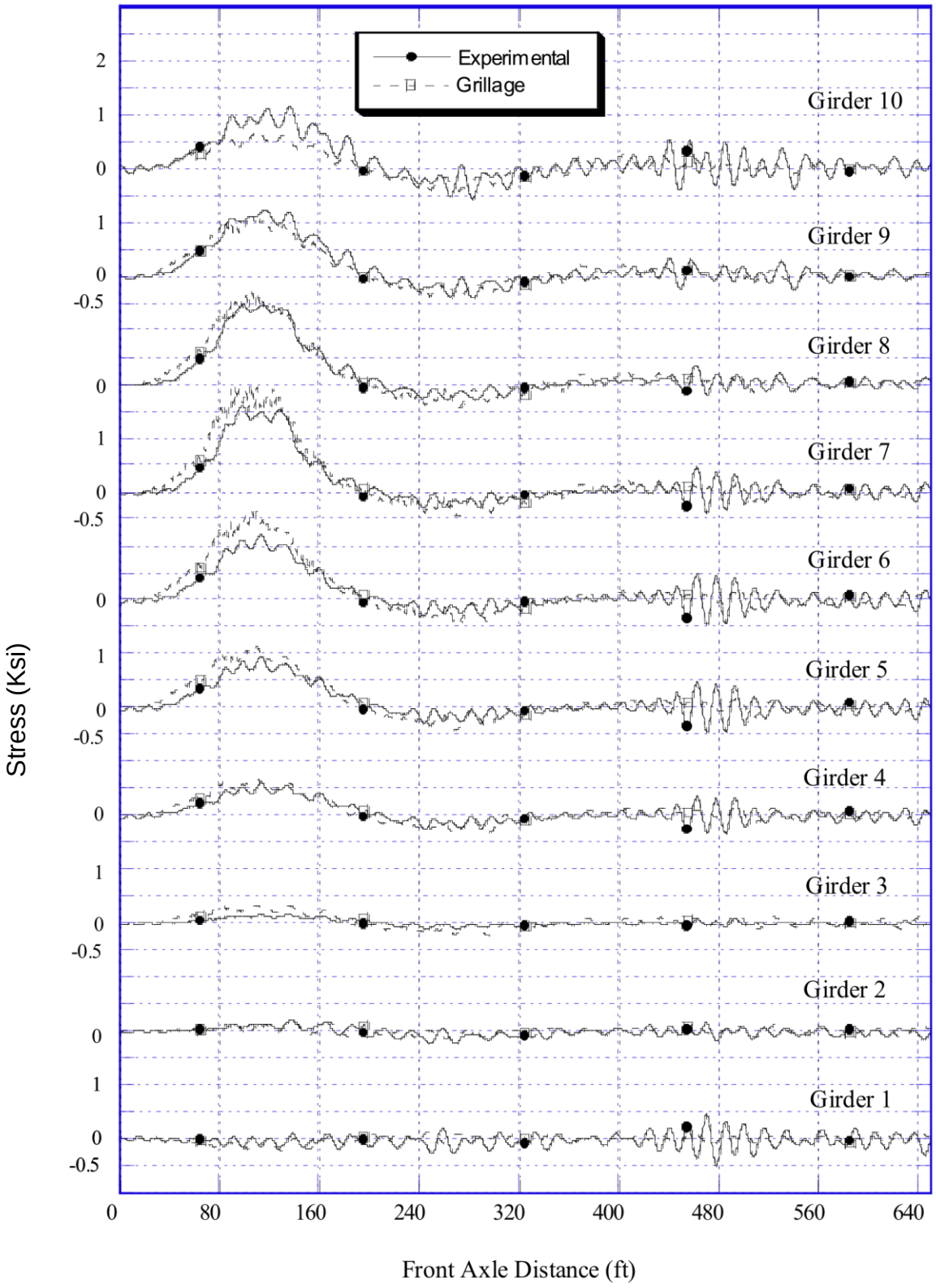

Figure 47. Comparison of girder stresses for Span 3 for Stage II live load testing of one-lane load using Grillage Method (Yuksel 2004)

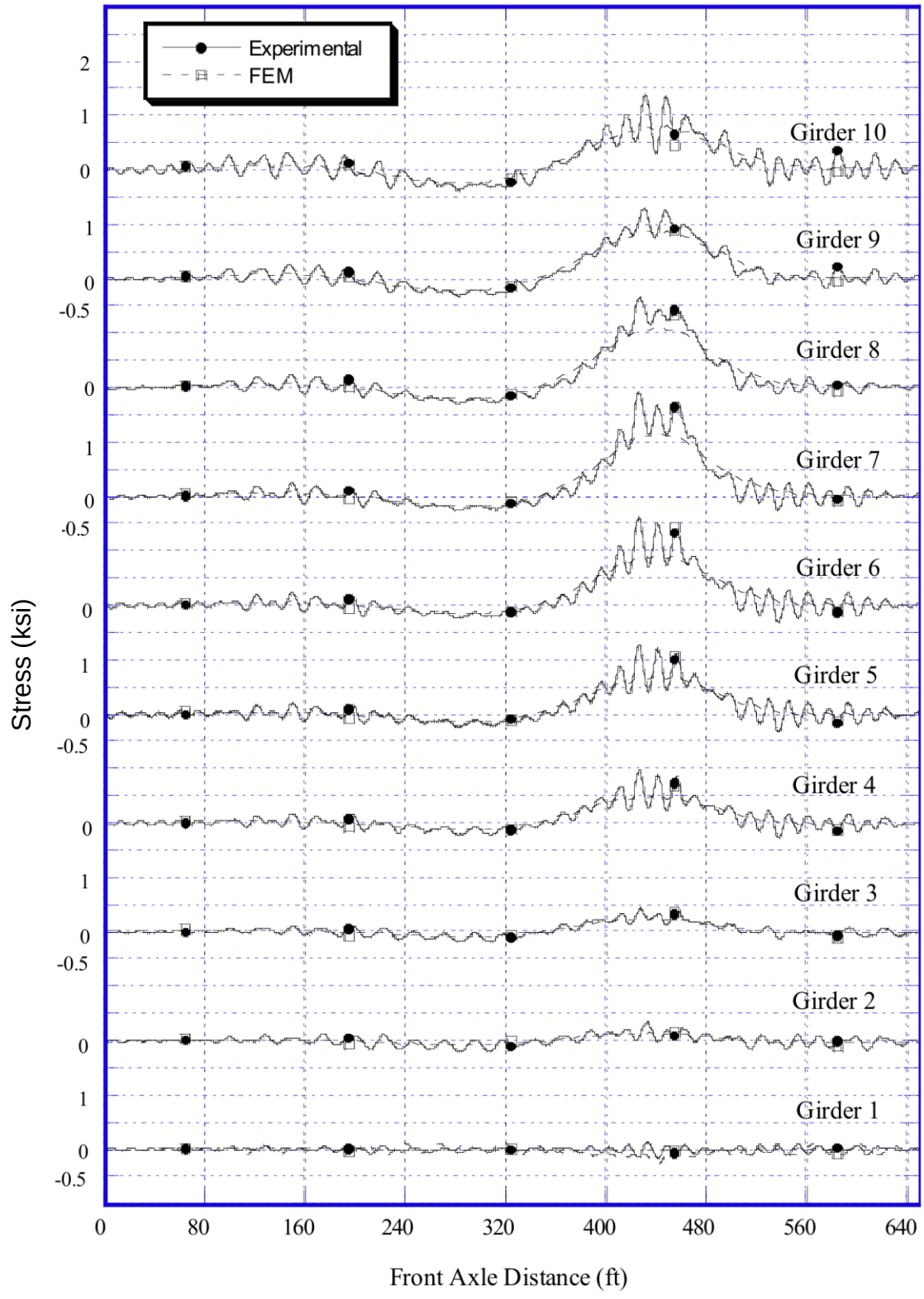

Figure 48. Comparison of girder stresses for Span 1 for Stage II live load testing of one-lane load using FE method

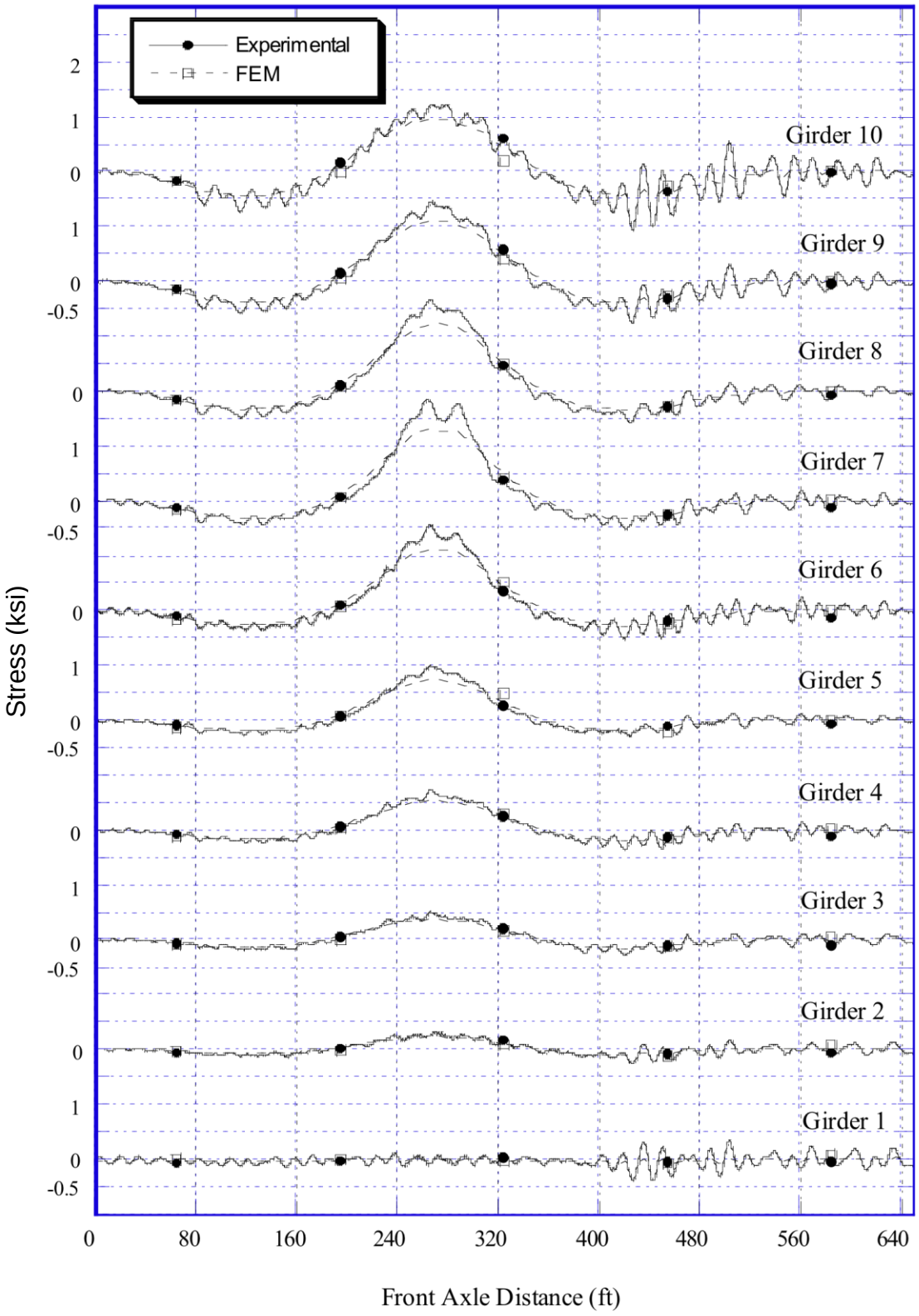

Figure 49. Comparison of girder stresses for Span 2 for Stage II live load testing of one-lane load using FE method

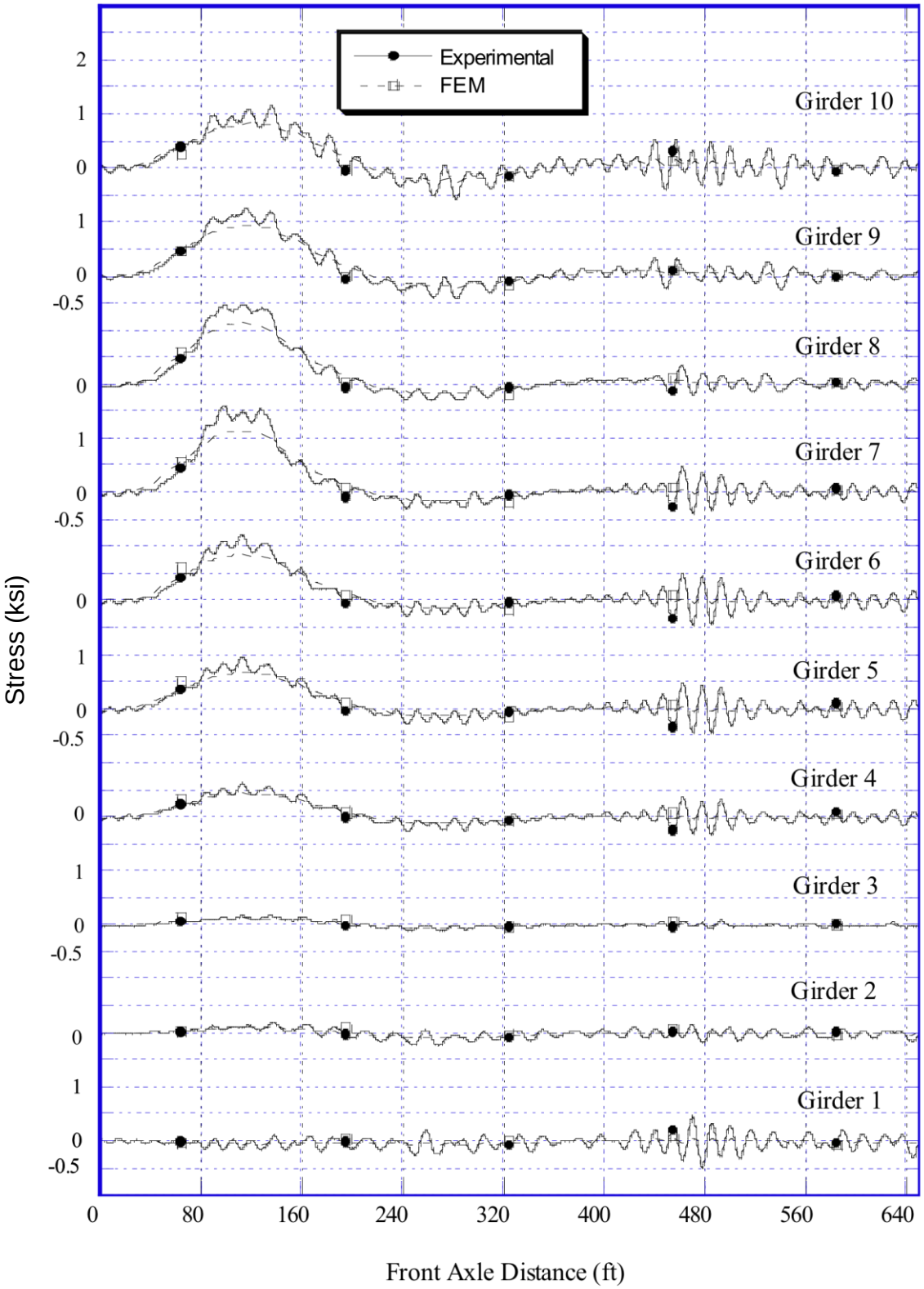

Figure 50. Comparison of girder stresses for Span 3 for Stage II live load testing of one-lane load using FE method

LIVE-LOAD GIRDER DISTRIBUTION FACTOR

Literature Review

There are two main live-load girder distribution factor equations (hereafter referred to as GDFs) for slab-on-girder bridges that are widely accepted by bridge engineers in the United States: 1) American Association of State Highway Transportation Officials (AASHTO) Standard Specifications (AASHTO 1996) and 2) AASHTO Load and Resistance Factor Design (LRFD) Bridge Design Specifications (AASHTO 2002). The AASHTO Standard Specification (referred to as Load Factor Design (LFD)), also known as the "*S*-over" distribution factors, is based on the experimental and analytical study of I-beam bridges at the University of Illinois (Newmark and Siess 1954). This is a very simple method where GDF is determined by dividing the girder spacing *S* over a constant *D*, which is based on the type of bridge. For steel and prestressed I-beam, the constant *D* is given as 3.35 m (11 ft) for multiple-lane loads. The AASHTO LRFD Bridge Design Specifications (referred to as LRFD) is a newer, more accurate, and complex method that included various parameters based on the geometry of the bridge. The equation was developed as part of the National Cooperative Highway Research Program NCHRP 12-26 using finite element analysis (Zokaie et al. 1991) and later adopted by AASHTO in 1994. It should be noted that there are no changes to the GDF equations for slab-on-girder bridges in the second and third editions of the AASHTO LRFD (AASHTO 1998, 2002).

After the adoption of the NCHRP 12-26 GDF equations in the LRFD, several studies compared the LFD (Load Factor Design) and LRFD GDF equations with finite element (FE) analysis or actual field tests. Schwarz and Laman (2001) investigated the response of live load on three prestressed girder bridges. In their study, they compared the LFD and LRFD GDF equations with experimental data for single- and multilane loads. The results showed that both equations over predicted the GDF. In addition, the LRFD GDF equations were more conservative than the LFD equations for shorter-span bridges but were less conservative for medium- and long-span bridges.

Chen and Aswad (1996) also studied and compared the LRFD GDF of prestressed concrete bridges with FE analysis. They studied 10 types of prestressed concrete girder bridges with three span lengths: 27.4, 35.0, and 42.7 m (90, 115, and 140 ft). The LRFD GDF equations were more conservative than the results obtained from FE analysis in all cases and more so for interior girders. They also suggested that if the FE analysis were used for long-span bridges, the release strength of the prestressed girder could have been reduced or alternatively the span of the bridge could have been increased, resulting in a cost savings for the owner of the bridge.

Barr et al. (2001) drew the same conclusions in their study of prestressed girder bridges. They showed that the GDF calculated using LRFD was more conservative than

FE analysis. The degree of conservatism of the LRFD could be as high as 28 percent when compared with the FE analysis that had been validated with an actual live-load test. However, when comparing bridges with configurations similar to the one developed by NCHRP 12-26 (i.e., simply supported), without lift or diaphragms, the difference between the LRFD and the FE analysis was reduced to only 6 percent. They also recommended the use of FE analysis over the LRFD equations because it reduced the required release strength of the girder, and alternatively the bridge could be designed for a 39 percent higher live load.

Mabsout et al. (1997a) reported similar results by analyzing steel girder bridges using FE analysis. They compared the GDF obtained from FE analysis and field tests with the LFD and LRFD GDF equations. The results showed that both equations over predicted the GDF compared with results obtained from FE analysis and field tests. They also investigated the effect of railing and sidewalk on GDF (Mabsout et al. 1997b). They showed that when the sidewalk and/or railing were constructed integrally with the bridge deck, the stiffness of the exterior girder increased, resulting in lower GDF in the interior girders. Eamon and Nowak (2002) confirmed this conclusion in their study of the effect of sidewalks and barriers on the GDF using FE analysis. The influence of the bridge diaphragm was also investigated. It had little effect on the GDF, whereas the sidewalks and barriers reduced the GDF by 10 to 40 percent.

LFD and LRFD are not the only two methods used for calculating GDF. Other GDF equations were developed by various researchers and were shown to be accurate by the corresponding authors. However, most of these equations were not fully understood nor ever examined by others. The objective of this study was also to evaluate the available GDF equations to actual field tests of a newly constructed Doremus Avenue Bridge, which is New Jersey's initial LRFD design. Additionally, FE models were developed to evaluate the field test results and used to perform a parametric study of 30 bridges with girder spacing varying from 1.22 to 4.88 m (4 to 16 ft) and span length varying from 6.10 to 61.0 m (20 to 200 ft).

Live-Load Distribution Factor Calculation

The live-load distribution factor (also known as GDF for girder bridges) was validated using FE method, as its results compare well with the field test results. The reason for not directly using the field test data to validate the GDF is because the LRFD load model (HL93 truck) represents not an actual truck but a truck that the bridge is designed for. Thus, HL93 design trucks were used in the analysis at the position of maximum positive and negative moment. The GDF was then calculated with the following formula:

$$GDF = \frac{N_L m M_{\max}}{\sum M} \quad \text{Eq. (11)}$$

where N_L is the number of loaded lanes, m is the multiple presence factor, M_{max} is the maximum girder bending moment, and $\sum M$ is the sum of all girder bending moments.

The FE method results were compared with the AASHTO LRFD as well as other provisions and available formulas, including AASHTO LFD (1996) and Puckett et al. (2005; NCHRP 12-62 Simplified Live Load Distribution Formula) as well as Rutgers simplified equations (Suksawang 2006). In addition to Doremus Avenue Bridges, four additional bridges: I-94E, I-94W, M14, and US-23 were also evaluated. These bridges were tested and validated by the FE method.

Table 5 through Table 7 show values for the GDF obtained with the FE method and the twelve equations as well as Rutgers simplified GDF equations, (shown later) for interior girders, exterior girders, and the governing load case. The best available GDF equations are determined by finding the equations with the lowest error sum of squares (SSE), calculated as follows:

$$SSE = \sum_{i=1}^{n} (GDF_i - GDF_{FEM})^2 \quad \text{Eq. (12)}$$

where GDFi and GDF_{FEM} are the GDFs obtained from the available equations and FE method, respectively. For a one-lane load, AASHTO LRFD (2004) has the lowest SSE for interior girder, exterior girder, and the governing case. This equation also performs well for two-lane loading with the lowest SSE in exterior girder and the governing case. The Marx et al. (1986) and Shahawy and Huang (2001) equations perform better than AASHTO LRFD (2004) in the interior girder for two-lane loads. The Puckett et al. (2005) GDF equations developed as part of NCHRP 12-62 to replace AASHTO LRFD (2004) have the highest SSE in the interior and exterior girders for both one- and two-lane loads. Moreover, in the governing case, the Puckett et al. (2005) GDF equations did not perform as well as the AASHTO (1996) GDF equations. In all cases, the Rutgers simplified (2006) equations had the best performance with the lowest SSE.

Proposed GDF Equation

The proposed equation was developed to eliminate the dependency on the girder moment of inertia as required by the AASHTO LRFD to calculate the GDF. Designers use Table 2.5.2.6.3-1 the Traditional Minimum Depths for Constant Depth Superstructures in AASHTO LRFD Bridge Design Specifications (2008) to estimate an initial value for the minimum section required. However, since this initial value can

change during the design iterations, his makes the design process more cumbersome and iterative. The Rutgers simplified equation relates the girder cross-section in terms of span length and thereby eliminates the girder cross-section from the GDF equation. The proposed GDF equations for both interior and exterior girders are as follows:

$$GDF = \frac{S}{D} \qquad \text{Eq. (13)}$$

where S is the girder spacing (ft) and D is given by the following equations:

one-lane load,

$$D = 8.4 + \frac{S}{1.4} + \frac{l}{C} \qquad \text{Eq. (14a)}$$

However, based on a second-degree polynomial relationship between moment of inertia and span length $\left(I_{equiv} = \frac{L^2}{500}\right)$, another form of Eq. (14a) for concrete spread box beams can be used as follows:

$$D = 12.0 + \frac{S}{25} + \sqrt{l} \qquad \text{Eq. (14b)}$$

two-lane load,

$$D = 7.0 + \frac{S}{3.0} + \frac{l}{C} \text{ or} \qquad \text{Eq. (14c)}$$

$$D = 7.0 + \frac{S}{3.7} + \frac{\sqrt{l}}{2} \text{ for concrete spread box using } \left(I_{equiv.} = \frac{l^2}{500}\right) \qquad \text{Eq. (14d)}$$

where *l* is the span length (ft) and C is given as 28 for a steel I-beam, 50 for a prestressed concrete I-beam, and 20 for a concrete spread box beam.

Table 5. Comparison of GDF Equations for tested bridges (interior girder)

Number of Loaded Lane	GDF Equations	Bridge					SSE
		I94E	I94W	M14	US23	Doremus	
One (Interior Girder)	FEM	0.48	0.47	0.31	0.35	0.32	--
	AASHTO (1996)	0.36	0.41	0.43	0.45	0.57	0.11
	AASHTO LRFD (2004)	0.39	0.42	0.40	0.40	0.40	**0.03**
	Shahawy & Huang (2001)	0.36	0.40	0.40	0.50	0.59	0.12
	Puckett et al. (2005)	0.36	0.40	0.45	0.40	0.60	0.12
	Rutgers-Simplified (2006)	0.38	0.40	0.41	0.40	0.41	**0.04**
Two (Interior Girder)	FEM	0.51	0.53	0.42	0.46	0.48	--
	AASHTO (1996)	0.45	0.53	0.55	0.57	0.73	0.09
	Newmark & Siess (1942)	0.38	0.50	0.44	0.58	0.63	0.05
	Sanders & Ellenby (1970)	0.47	0.55	0.57	0.58	0.72	0.10
	Bakht et al. (1979)	0.35	0.41	0.42	0.44	0.56	0.05
	Marx et al. (1986)	0.47	0.54	0.52	0.54	0.52	**0.02**
	AASHTO LRFD (2004)	0.49	0.55	0.53	0.55	0.58	0.03
	Tarhini & Frederick (1992)	0.51	0.50	0.51	0.48	0.89	0.18
	Shahawy & Huang (2001)	0.40	0.47	0.45	0.46	0.53	**0.02**
	Phuvoravan et al. (2004)	0.56	0.57	0.58	0.56	0.63	0.06
	Henry Method (Huo et al., 2004)	0.37	0.41	0.41	0.50	0.52	0.04
	Mod. Henry (Huo et al., 2004)	0.34	0.38	0.38	0.46	0.47	0.06
	Puckett et al. (2005)	0.52	0.58	0.58	0.60	0.72	0.10
	Rutgers-Simplified (2006)	0.51	0.54	0.55	0.53	0.54	**0.02**

Table 6. Comparison of GDF Equations for tested bridges (exterior girder)

Number of Loaded Lane	GDF Equations	Bridge					SSE
		I94E	I94W	M14	US23	Doremus	
One (Exterior Girder)	FEM	0.32	0.37	0.39	0.40	0.42	--
	AASHTO LRFD (2004)	0.39	0.42	0.40	0.40	0.55	**0.03**
	Pucket et al. (2005)	0.46	0.40	0.45	0.49	0.63	0.08
	Rutgers-Simplified (2006)	0.38	0.40	0.41	0.40	0.41	**0.00**
Two (Exterior Girder)	FEM	0.39	0.55	0.46	0.57	0.55	--
	Marx et al. (1986)	0.32	0.37	0.40	0.43	0.58	0.06
	AASHTO LRFD (2004)	0.49	0.50	0.53	0.55	0.58	**0.02**
	Puckett et al. (2005)	0.52	0.58	0.58	0.60	0.72	0.06
	Rutgers-Simplified (2006)	0.51	0.54	0.55	0.53	0.54	**0.02**

Table 7. Comparison of the governing GDF for tested bridges

Number of Loaded Lane	GDF Equations	Bridge					SSE
		I94E	I94W	M14	US23	Doremus	
One (Governing Case)	FEM	0.48	0.47	0.39	0.40	0.42	--
	AASHTO (1996)	0.36	0.41	0.43	0.45	0.57	0.05
	AASHTO LRFD (2004)	0.39	0.42	0.40	0.40	0.55	**0.03**
	Shahawy & Huang (2001)	0.36	0.40	0.40	0.50	0.59	0.06
	Puckett et al. (2005)	0.46	0.40	0.45	0.49	0.63	0.06
	Rutgers-Simplified (2006)	0.38	0.40	0.41	0.40	0.41	**0.02**
Two (Governing Case)	FEM	0.51	0.55	0.46	0.57	0.55	--
	AASHTO (1996)	0.45	0.53	0.55	0.57	0.73	0.04
	Newmark & Siess (1942)	0.38	0.50	0.44	0.58	0.63	0.03
	Sanders & Ellenby (1970)	0.47	0.55	0.57	0.58	0.72	0.04
	Bakht et al. (1979)	0.35	0.41	0.42	0.44	0.56	0.06
	Marx et al. (1986)	0.47	0.54	0.52	0.54	0.58	**0.01**
	AASHTO LRFD (2004)	0.49	0.55	0.53	0.55	0.58	**0.01**
	Tarhini & Frederick (1992)	0.51	0.50	0.51	0.48	0.89	0.13
	Shahawy & Huang (2001)	0.40	0.47	0.45	0.46	0.53	0.03
	Phuvoravan et al. (2004)	0.56	0.57	0.58	0.56	0.63	0.02
	Henry Method (Huo et al., 2004)	0.37	0.41	0.41	0.50	0.52	0.05
	Mod. Henry (Huo et al., 2004)	0.34	0.38	0.38	0.46	0.47	0.08
	Puckett et al. (2005)	0.52	0.58	0.58	0.60	0.72	0.05
	Rutgers-Simplified (2006)	0.51	0.54	0.55	0.53	0.54	**0.01**

EFFECTIVE FLANGE WIDTH

Literature Review

Earlier theoretical and experimental work to evaluate the stress distribution in flanged composite beams was performed by Schule (1909), Bortsch (1921), and later by von Karman (1923). Metzer (1929), Timoshenko and Goodier (1970), and Cook (1977) addressed the shear lag in flanged sections and derived equations to calculate the equivalent stress block that replaces the entire stress distribution over an infinite flange width. However, for bridge beams, Wegmuller (1977) studied the overloading behavior of composite steel bridges through the development of a numerical model to include cracking of concrete and the effect of reinforcement. The analysis used nonlinear plate bending elements with an accuracy of up to 20 percent. Cheung and Chan (1978) analyzed various bridge types by using the finite strip method to determine the effective width. It was concluded that the major factors affecting b_e were girder spacing and span length. The equation was given by the polynomial $B_E / B = \sum_{i-1}^{\infty} A_i (L/B)^i$ calculated using the first four terms of the polynomial constant A_i.

Buckle et al. (1985) used the FE method to model bridges with layered plate elements and filament beam elements to compare results with those from destructive field tests. Song and Scordelis (1990) developed a harmonic shear-lag analysis using plane stress elasticity for the stresses in flanges. The study, however, neglected inelastic behavior including cracking in concrete. Sedlacek and Bild (1993) presented specifications to calculate b_e based on the advanced bending theory assuming linear elastic behavior.

Recently, Elhelbawey et al. (1999) field-tested bridges and showed that the effective flange width depends on the neutral axis location. They concluded that the neutral axis value was independent of the magnitude and configuration of loading. They also reported that in a few cases b_e was larger than the girder spacing, suggesting a reduction in the design modular ratio n.

Determination of Effective Flange Width

Two main approaches were developed to determine the effective flange width, b_e: the neutral axis approach and the stress distribution approach. The neutral axis approach is applied by equating the sum of tension forces and the sum of compression forces to zero. Figure 51 shows the internal forces over the depth of the cross section of Girder 4 of the Doremus Avenue Bridge at the maximum moment location of Span 1 for Tests 1 and 2. The strain values are obtained from the FE analysis and plotted to obtain the position of the neutral axis. It is also observed that the neutral axis location does not vary with load configuration and position.

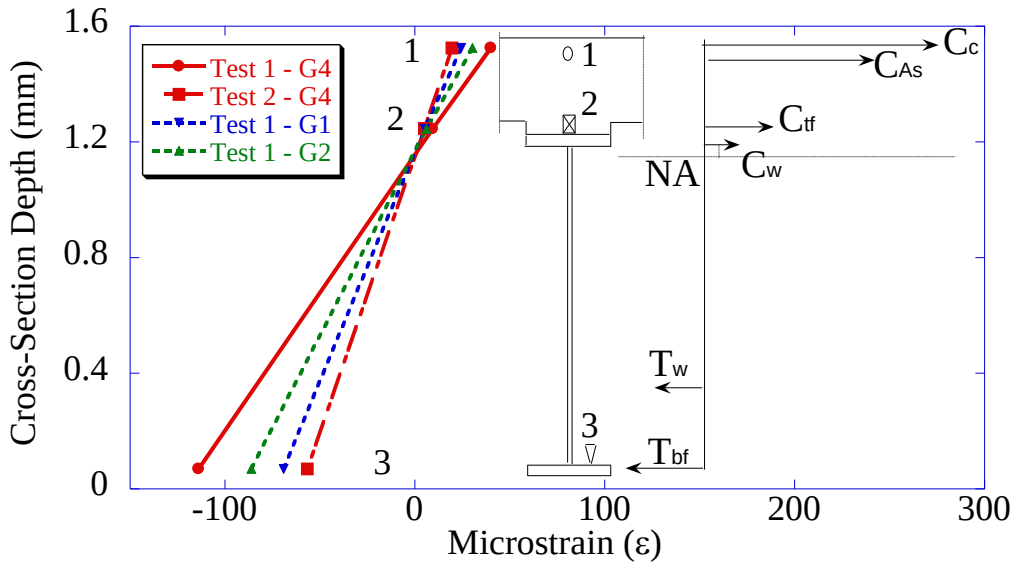

Figure 51. Neutral axis location on Span 1

The internal forces are determined from the stress distribution in each material. By applying force equilibrium, the effective flange width, b_e, is found as illustrated in Figure 51. By rearranging and having b_e on one side, the following equation is obtained:

$$b_e = \frac{(T_{bf} + T_w) - (C_w + C_{tf} + C_{As})}{t_s(\sigma_{ct} + \sigma_{cb})/2} \qquad \text{Eq. (15)}$$

where σ_{ct} is stress at the top of the slab and σ_{cb} is stress at the bottom of the slab. With this approach, the ratios of b_e/b_s were 0.95 and 0.96, respectively.

The second approach obtains the exact stress distribution in the concrete slab from the FE method. It was found that b_e/b_s obtained from this approach was 0.98. Furthermore, it was found that this ratio obtained experimentally was 1.0. Since the stress distribution over the slab is a more accurate and direct method of calculating the effective flange width, the second approach was utilized in the parametric study performed.

The developed and validated FE method was used in the analysis of various types of bridges- box and I-girders. The bridges were designed in accordance with AASHTO LRFD specifications, and the HS20 truck was used for the parametric study. The truck was placed on simply supported bridges at the location of the maximum longitudinal moment. The parameters considered were the effects of various truck loadings, slab thickness (t_s), concrete strength (f_c'), steel girder strength (F_y), span length (b_s), and girder spacing (L).

The effect of these parameters on b_e is studied by using the dimensions of 10 I-girder and 4 box-girder bridges. All bridges were designed according to AASHTO LRFD and had girder steel strength (F_y) of 50 ksi (345 MPa); the concrete slab had a strength (f_c') of 4.35 ksi (30 MPa) and a thickness of 9.8 in. (250 mm). Maximum girder spacing allowed by the code is 16 ft (4.9 m). For the box-girder bridges, the two top flanges were 15.7 x 0.79 in. (400 x 20 mm) each, and the two webs as well as the bottom flanges were 14 mm (0.55 in.) thick.

Various truck loadings were applied to the bridge to find the loading that would induce the critical value of b_e. Loading type (1) was that of a 2.17 times HS20 truck loading, loading type (2) was a transverse line loading, and loading type (3) was a multiple of HS20 trucks. Loading types (2) and (3) were incremented until the stress levels obtained were similar to those of loading type (1). Figure 53 shows the longitudinal stress distribution due to two of the loading cases, (a) and (b). The critical loading is that of a single truck of 2.17 times HS20 loading. Therefore, this loading was used for the parametric study.

The effect of the parameters t_s, f_c', and F_y were studied. There is no significant change in b_e as a result of increasing those variables, but it is dependent on b_s and L. Figure 52 shows that as the b_s/L ratio increases, the b_e/b_s ratio decreases linearly. A linear equation was developed from the graph of the form:

$b_e/b_s = 1 - 0.5\left(\frac{b_s}{L}\right)$ for $b_s/L > 0.25$ and $b_e = b_s$ for $b_s/L \leq 0.25$

It is also observed from Figure 52 that the AASHTO and the Canadian codes, compared with the FE method results, are conservative for short-span bridges, while the proposed equation is satisfactory.

Moreover, the value of b_e has a direct effect on the design moment capacity and serviceability limit states of the bridge. Figure 53 and Figure 54 are plotted showing the percentage gain in moment and deflection, respectively, by comparing FE method, proposed equation, and Canadian code with the AASHTO LRFD code. It is concluded that the proposed equation is always satisfactory compared with the FE method-where it is observed that as b_s/L increases, the moment capacity increases by about 8 percent for I-girder bridges and by 6 percent for box-girder bridges compared with AASHTO LRFD. Moreover, compared to AASHTO LRFD, a decrease in deflection of 12 percent is observed for both I-girder bridges and box-girder bridges.

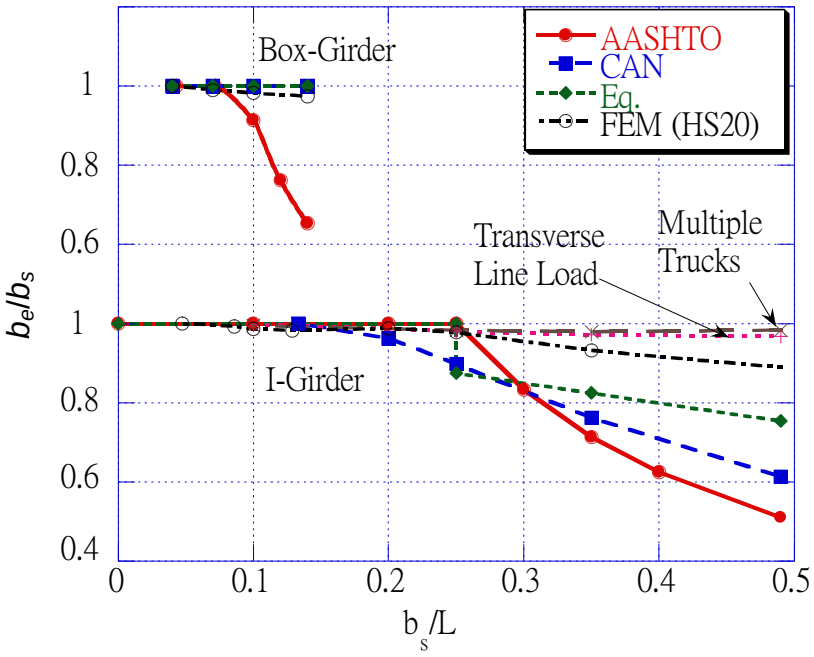

Figure 52. Relationship of b_e/b_s and b_s/L for Codes, proposed equation, and FE method

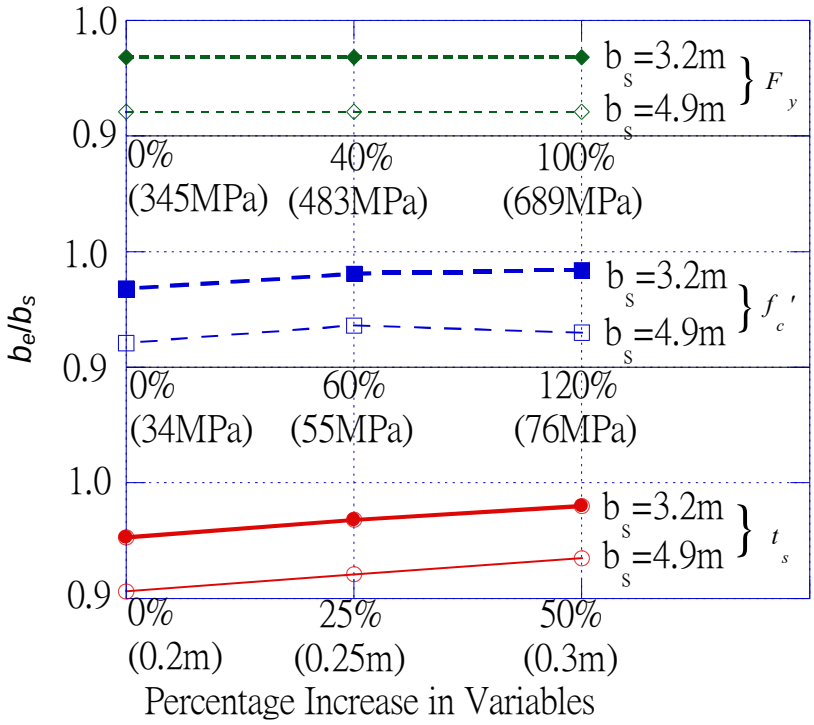

Figure 53. b_e/b_s versus percentage increase in variables t_s, f_c', F_y for I-girder of 125-ft (38-m) length

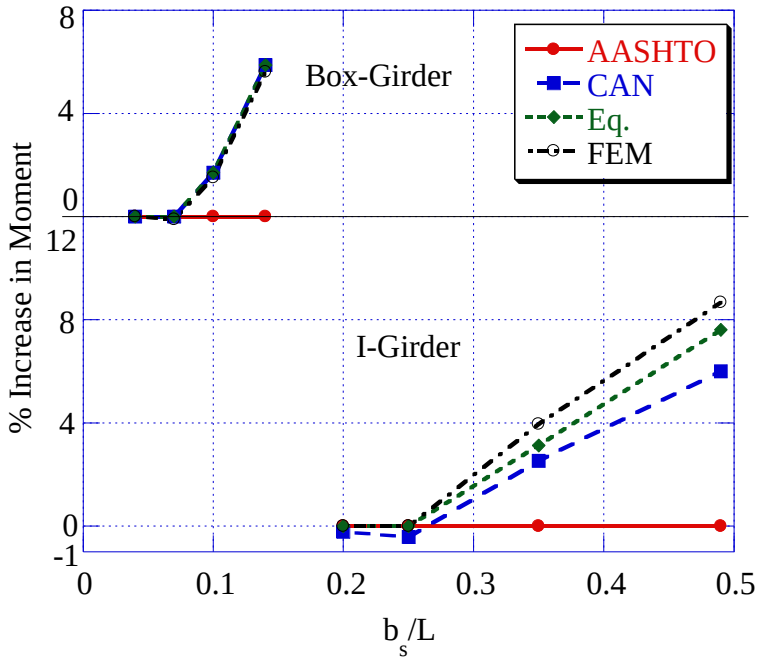

Figure 54. Percentage difference in moment versus b_s/L relationships for all bridges compared with AASHTO LRFD code

DEFLECTION LIMITS

Literature Review

Since the study by the American Society of Civil engineers more than 45 years ago, many changes have occurred that affect bridge flexibility and the imposed vertical deflections. Live loads have become heavier, and more innovative materials have been introduced. With the increased use of high-performance steel, the deflection limits may become a controlling design issue. This can have serious economic implications, since a larger steel section will be required to comply only with serviceability criteria rather than ultimate.

Conflicting views have been presented on the necessity of live-load deflections in the literature. Roeder, Barth, and Bergman (2002) presented a comprehensive literature review of past research on the effects of bridge deflections on structural performance and bridge vibration. They looked at four main types of concrete bridge deck deterioration—namely, spalling, surface scaling, transverse, and longitudinal cracking. After a review of existing research, they concluded that there was little support for deflection limits as a method of controlling structural damage. However, as the original intent of the limits indicates, limiting live-load deflection as a means of controlling bridge vibration was found not to be the best method where human perception plays a large role. Human response was found to depend on a combination of maximum deflection, maximum acceleration, and natural frequency.

Boothby and Laman (1999) evaluated the cumulative damage caused by vehicle loading to bridge concrete decks. They looked at the bridge deck life due to fatigue as a comparison with the expected lifetime available for environmental factors. Although they did indicate contradictions in the literature with regard to the influence of vehicle loading on bridge deck fatigue, they concluded that compared with environmental factors, mechanical loading had an insignificant effect on bridge deck damage.

Burke (2001) examined the impact of optional live-load deflection limits on the long-term integrity of bridge decks. He argued that if deflection limits are not mandated, the effective service life of reinforced concrete deck slabs could become considerably less than their replacement interval of 30 years. Burke noted that with the adoption of new materials (such as high-strength ASTM A588 and A572 steel), construction and analysis methods, composite design, load factor design, and extra-wide beam spacings, superstructure flexibility had progressively increased. He suggested that before any changes in deflection limitations are made on a national level, long-term effects of flexibility on aging reinforced concrete bridge decks should be studied first.

With increased use of composites in bridge design and rehabilitation, excessive vertical deflections may become a concern. Hayes et al. (2000) evaluated the performance of a glue-laminated timber deck on composite girders through laboratory and field tests. The composite beams were composed of E-glass and carbon fiber in a vinyl resin. Field tests indicated a maximum service load deflection of $L/400$ for an HS20 loading. This value is twice the Code allowable $(L/800)$ limit.

Demitz, Mertz, and Gillespie (2003) introduced a method for determining deflection limits for bridges constructed with advanced composite materials. Stiffness limitations were proposed on limiting response accelerations caused by truck traffic as an equivalent to vertical deflection limits. It was suggested that resulting vibrations and accelerations be evaluated against human tolerance curves.

It is clear that more research is required to justify the removal of mandated live-load deflection limits. In the meantime, state highway departments are specifying their own deflection criteria, which may often be arbitrary.

In a current nationwide survey of bridge engineers about professional practices with regard to live-load deflection limits, large variations in the state-imposed limits were observed. The survey also revealed variation in the type of loads and load combinations used in deflection calculations. Impact and load factors were applied in some states while not in others. The method of computing deflections and the type of distribution factors were also identified as being variable among states.

Extreme Value Theory

The characteristics of the upper and lower tail of a statistical distribution are critical when addressing questions about the behavior of extreme events. By nature, extreme events do not readily occur and are often scarce in observed experimental records. Thus, the traditional practice of fitting a probability distribution to the overall observed data set serves only to statistically describe the central region of the data, and may not be adequate for the extreme tail behavior where the data is scarce. In contrast, extreme value techniques provide a robust means of estimating the probabilities of events that are more extreme than those observed, irrespective of the parent distribution. This feature makes extreme value theory models appealing, for they accurately describe extremes without prior knowledge of their stochastic behavior.

Maximum girder deflection measurements captured by the long-term monitoring system were analyzed for an 8-month (with some gaps) duration. Gaps were removed, resulting in 5 complete months (150 days) of data. The maximum deflection measurements captured by the LVDT system are plotted in Figure 55 along with details of the greatest bridge response (Case 2378) captured during that time period. The maximum observed deflection (nearly 0.8 in) is less than the NJDOT Code $_{L/1000}$ limit of 1.38 inches.

Case 2378 involves an overloaded eight-axle truck weighing nearly 2.5 times the New Jersey legal weight limit of 80,000 lb. Closer evaluation of the truck configuration suggests that the truck is also in violation of the legal restrictions for single (22,400 lb) and tandem (34,000 lb) axles.

Two closely related extreme models are considered for estimation of maximum live-load deflection at various return periods. The Generalized Extreme Value (GEV) distribution models the maximum occurrences observed during repeated time intervals or blocks (i.e., daily maxima) and the Generalized Pareto Distribution (GPD) models all observed events that are greater than a specified high value. Often, near or far future values are extrapolated based on time-limited data sets (i.e., 1 day, 1 week, or 1 month). The most pertinent levels, however, are those that are most likely to occur within a longer period of time than what has been observed. For bridges, this level is the design service life of 75 years.

It is observed that on average there are 1,500 truck-loading events (single and multiple truck presence) that occur each day, 20 of which are considered extreme and are registered by the system. Maximum girder deflections corresponding to various return periods are estimated based on captured measurements for 2-week and for 1-, 2-, 3-, 4-, and 5-month durations. Details of the models may be found in papers by Nassif and Gindy (2005a, 2005b, 2007). The effect of using different short time history durations for future predictions is also investigated.

The maximum girder deflections based on the fitted GPD model are identified on the 2-month time series plot for various return periods, including the bridge service life of 75 years in Figure 56. It is estimated that the maximum girder deflection will be 24 mm (0.94 in.).

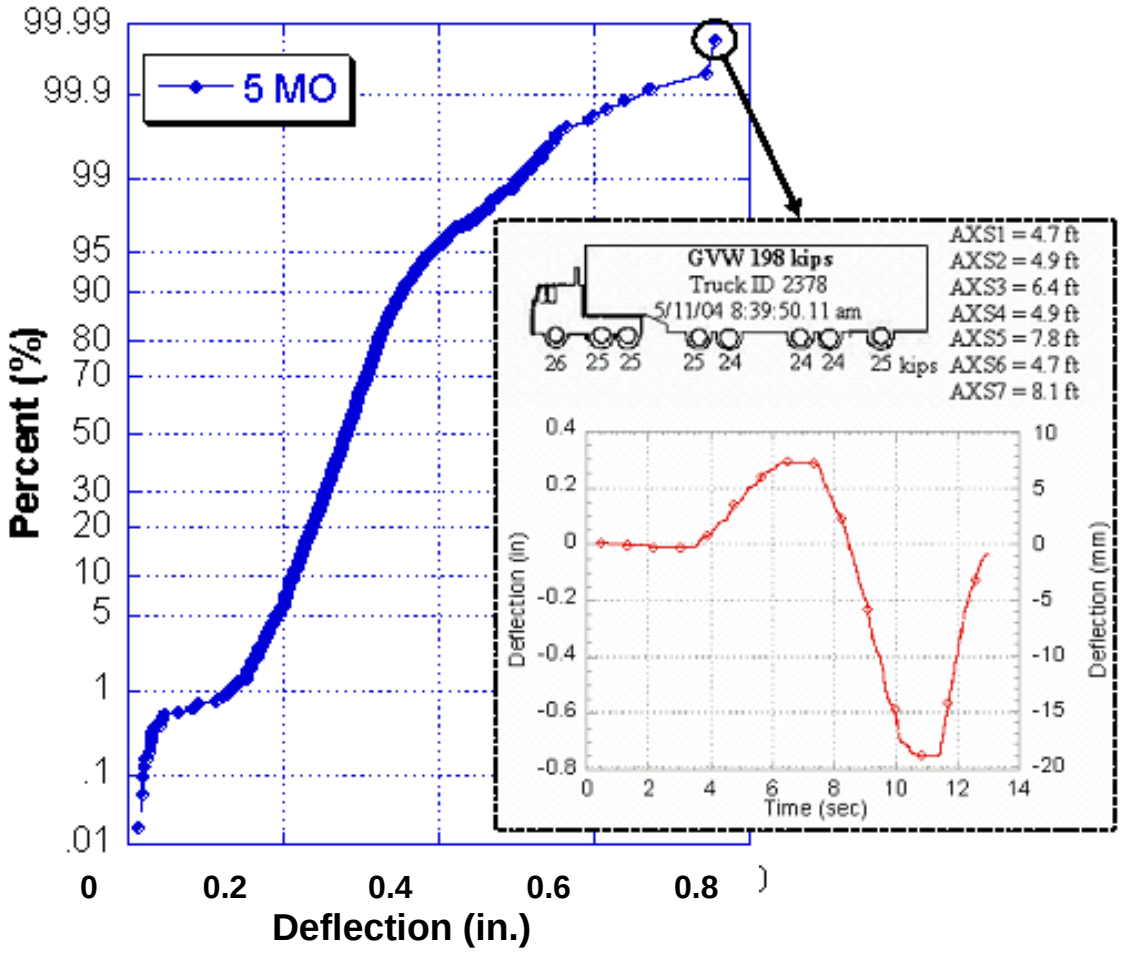

Figure 55. Maximum Girder 8 deflections collected by long-term monitoring system

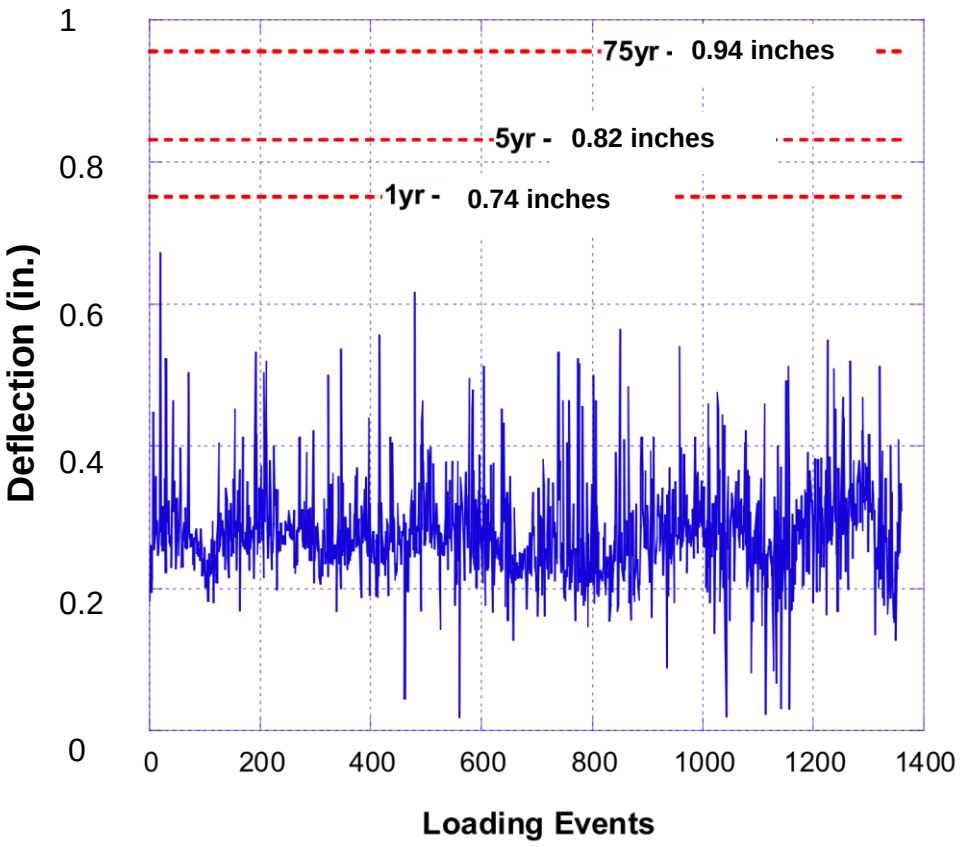

Figure 56. Time series of maximum girder deflection for 2-month period

Reliability Analysis

Reliability analysis is based on distinguishing between the desired (success) and undesired (failure) performance of a structure. Mathematically, structural reliability is described using a limit state function, $g(.)$, expressed in terms of the resistance and load effect for a specified performance, and is given by:

$$g = R - Q \qquad \text{Eq. (16)}$$

The boundary between desired and undesired performance is described by:

$$\begin{aligned} g(.) &< 0 \quad failure \\ g(.) &= 0 \quad boundary \\ g(.) &> 0 \quad success \end{aligned} \qquad \text{Eq. (17)}$$

It is the area for which $g < 0$, load effect exceeds resistance that is of most concern, and is referred to as the probability of failure, P_f. One measure of P_f is the reliability index, defined as:

$$\beta = \frac{\mu_g}{\sigma_g} = \frac{\mu_R - \mu_Q}{\sqrt{\sigma_R^2 + \sigma_Q^2}} \qquad \text{Eq. (18)}$$

and it is related to by:

$$\beta = -\Phi^{-1}(P_f) \qquad \text{Eq. (19)}$$

where $\Phi^{-1}(.)$ is the inverse cumulative standard normal distribution function. Generally, the reliability index measures how far the limit state function mean is from failure in terms of the number of standard deviations. The further the central tendency is from zero, the failure boundary, the lower is the probability of failure and the greater is the index.

For live-load deflection, resistance is taken as the code-specified limit and the load effect taken as the 75-year maximum deflection estimated with the GPD model. Deflection limits are specified as $L/800$ and $L/1000$ for the LRFD Code and the State of New Jersey, respectively. Span length is defined as the distance between dead-load contraflexure points, 115 ft (35.1 m) for Span 3. The resistance is then 1.73 in. (44 mm) as given by the code, and 1.38 in. (35 mm) as given by the state department of New Jersey, and is taken as deterministic (zero standard error). The maximum 75-year girder deflection for Span 3 is estimated as 24 mm (0.94 in) with a 20 percent coefficient of variation (*COV*), defined as the ratio of standard error to mean estimate. Errors in return level estimates depend on the accuracy of model parameters and are assumed to follow a normal distribution. It follows then that the limit state function also follows a normal distribution.

The reliability index is computed to be 4.17 using Eq. 19 for the LRFD code and 2.29 for the New Jersey limit as shown in Figure 57. The ultimate limit state in the LRFD code is calibrated for a reliability index of 3.5. This suggests that, for the same girder section, since the NJDOT limit is more conservative than that of the LRFD, the probability of the NJ limit being exceeded is higher (i.e., lower reliability).

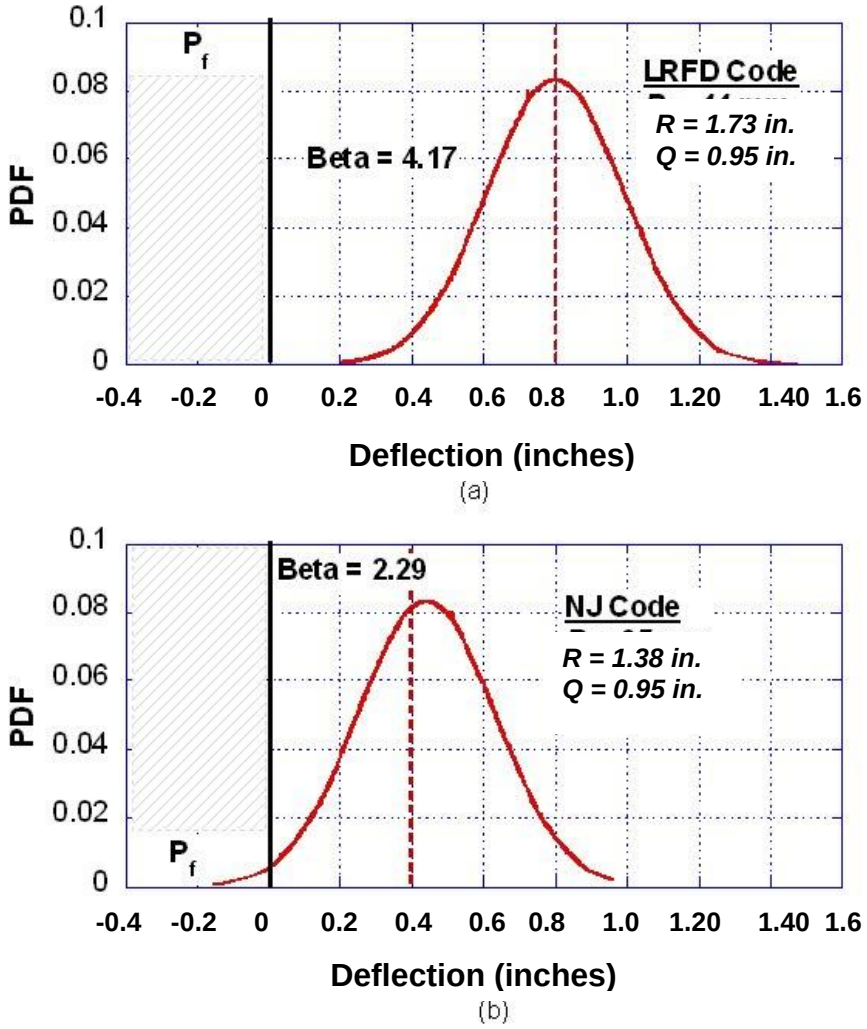

Figure 57. Reliability index: (a) LRFD code and (b) New Jersey limit

LIVE-LOAD MODEL

The live-load distribution of Class 9, as classified by Federal Highway Administration (FHWA) truck designation to denote five-axle trucks, is shown in Figure 58a and b. In the figure, the trucks have an average GVW of 31 kips and the curve follows a lognormal distribution. Yet, there exists many trucks that are heavier than 31 kips, ranging from 90 to 100 kips. In addition, there seem to be heavier trucks traveling in the summer and winter months, i.e., June and July and November and January (excluding December), respectively.

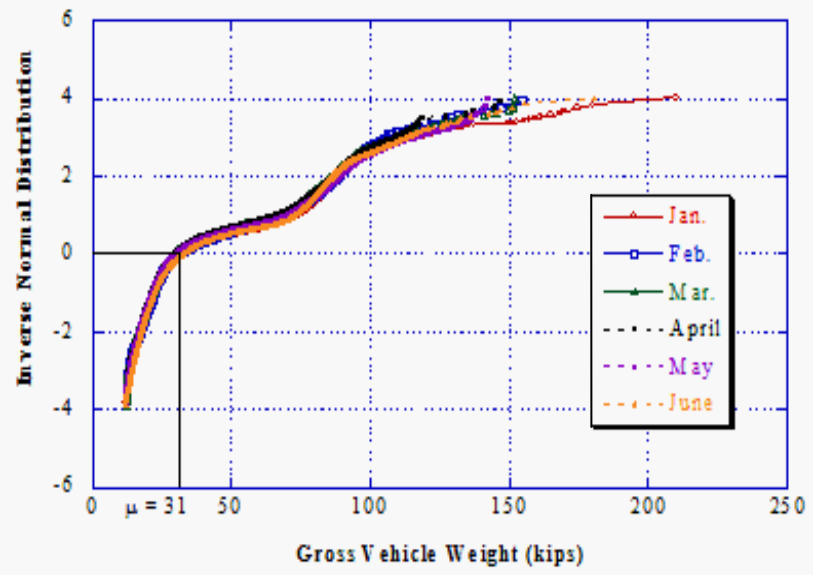

(a)

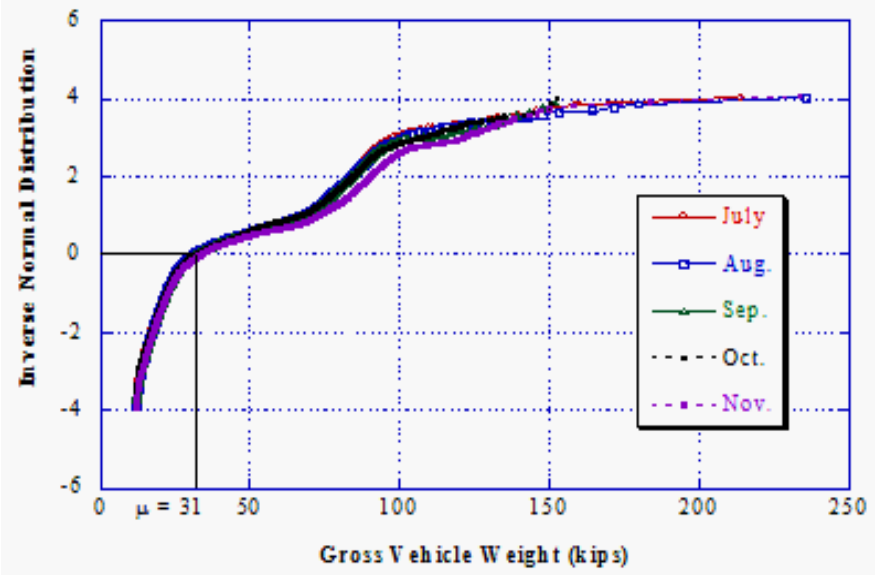

(b)

Figure 58. Live-load distribution of Class 9 vehicle from the months of (a) January to June and (b) July to November

Characterization of Live-Load from NJDOT WIM Sites

Many State DOTs and FHWA have recognized the need for reliable truck weight data since many states allow considerably heavier truck loads than the federal mandated legal limit of 80 kips (356 kN). The continuous increase in the weight and frequency of overloaded vehicles can result in lower safety reserve of bridges, which can often lead to fatigue and other problems. Hence, there is a real need to characterize the actual load spectra on state and federal highway bridges. This can work directly to alleviate the

uncertainty in the evaluation of bridge load carrying capacity, prediction of deterioration (corrosion) rates, and remaining life (fatigue).

For many years, trucks were measured at a limited number of stationary scales (truck weigh stations) that are located on major highways. However, there has been a justified concern that the heaviest trucks knowingly avoid the scales (Nowak, Nassif, and DeFrain 1993) and, as a result, bias the weigh station data toward less heavy vehicles. On the other hand, WIM systems are capable of measuring truck characteristics such as vehicle gross weights, axle weights, axle spacings, and vehicle class of actual traffic at full highway speeds. WIM sensors—typically a piezoelectric strip, load cell, or bending plate—are directly installed in the roadway surface. As a result, the sensors are relatively undetectable by roadway users and provide unbiased truck weight data (Moses et al. 1987, Kim et al. 1996, Laman and Nowak 1997, Katz and Rakha 2002).

Many states have initiated and adopted comprehensive programs to collect truck weight data from various locations. Data collected through these initiatives have contributed to efficient traffic flow planning as well as roadway and pavement design. In the case of bridges, however, truck weight data and event statistics have not been fully utilized in design and practice. Development of the AASHTO LRFD Bridge Design code (AASHTO 2002) was based on a 1975 truck weight survey from Ontario, Canada, which consisted of 9,250 trucks that appeared to be heavily loaded (Nowak, 1994). This relatively limited data set is now 30 years old and, given the continuous change in the trucking industry, these statistics have undoubtedly changed.

In this study, a statistical basis is developed for the live-load model for the State of New Jersey bridges The database includes WIM data collected from 33 sites located throughout the State of New Jersey over an 11-year period (1993–2003, with some gaps). The WIM sites represent a variety of location-specific characteristics, including truck volume, roadway; type (major/minor arterials), area type (urban/rural), and number of lanes as shown in Figure 59. The sites are divided into three categories based on truck volume; (1) Light-; (2) Average-; and (3) Heavy-. Due to the size of the database, approximately one million truck records per month, WIM data is statistically analyzed to evaluate the truck traffic characteristics. Based on the WIM data collected at the Doremus Avenue Bridge (ADTT approx. 2000), the site is considered as “Average”.

Table 8. State of New Jersey WIM site descriptions

	Site ID	Site Name	County	Travel Direction	No. of Lanes	FHWA Functional Class	ADTT
LIGHT VOLUME	068*	NJ-68	Burlington	NB	1	06	103
	130*	US-130	Salem	NB	1	16	190
	072*	NJ-72	Burlington	EB	1	02	489
	31C*	NJ-31	Warren	NB	1	02	821
	01D*	US-1&9 (EX)	Essex	SB	3	12	123
	280*	I-280	Essex	WB	3	11	251
	31B*	NJ-31	Hunterdon	NB	2	02	1,323
	78B*	I-78	Somerset	WB	3	01	2,108
	01C*	US-1&9 (LO)	Essex	SB	4	12	2,711
	052	NJ-52	Cape May	NB	2	14	148
	40B	US-40	Atlantic	EB	2	14	248
	022	US-22	Hunterdon	EB	2	06	268
	202*	US-202	Hunterdon	NB	2	02	306
	073	NJ-73	Camden	NB	2	14	325
	034	NJ-34	Monmouth	NB	2	06	365
	15*	NJ-15	Morris	NB	2	12	384
	68A	NJ-68	Burlington	NB	2	06	391
	046	US-46	Morris	EB	2	02	410
	031	NJ-31	Hunterdon	NB	2	02	523
	22B	US-22	Somerset	EB	2	16	649
	CLR	CO-653	Hudson	NB	2	16	799
AVERAGE VOLUME	40A	US-40	Salem	EB	2	02	1,039
	13B	US-130	Burlington	NB	2	14	1,092
	01A*	US-1	Middlesex	NB	2	14	1,145
	34B	NJ-34	Monmouth	NB	2	06	1,342
	13A	US-130	Middlesex	NB	2	06	1,345
	18B	NJ-18	Monmouth	NB	2	02	1,657
	NJT	NJTPK	Salem	NB	2	12	2,209
	552*	NJ-55	Gloucester	NB	2	12	2,379
	195*	I-195	Monmouth	EB	2	01	2,430
	018	NJ-18	Monmouth	NB	2	12	2,969
HEAVY VOLUME	A87†	I-287	Morris	NB	3	01	4,743
	287*	I-287	Bergen	NB	2	11	5,921

** Not used in multiple presence statistics*

† Only 2 lanes are used for multiple presence statistics

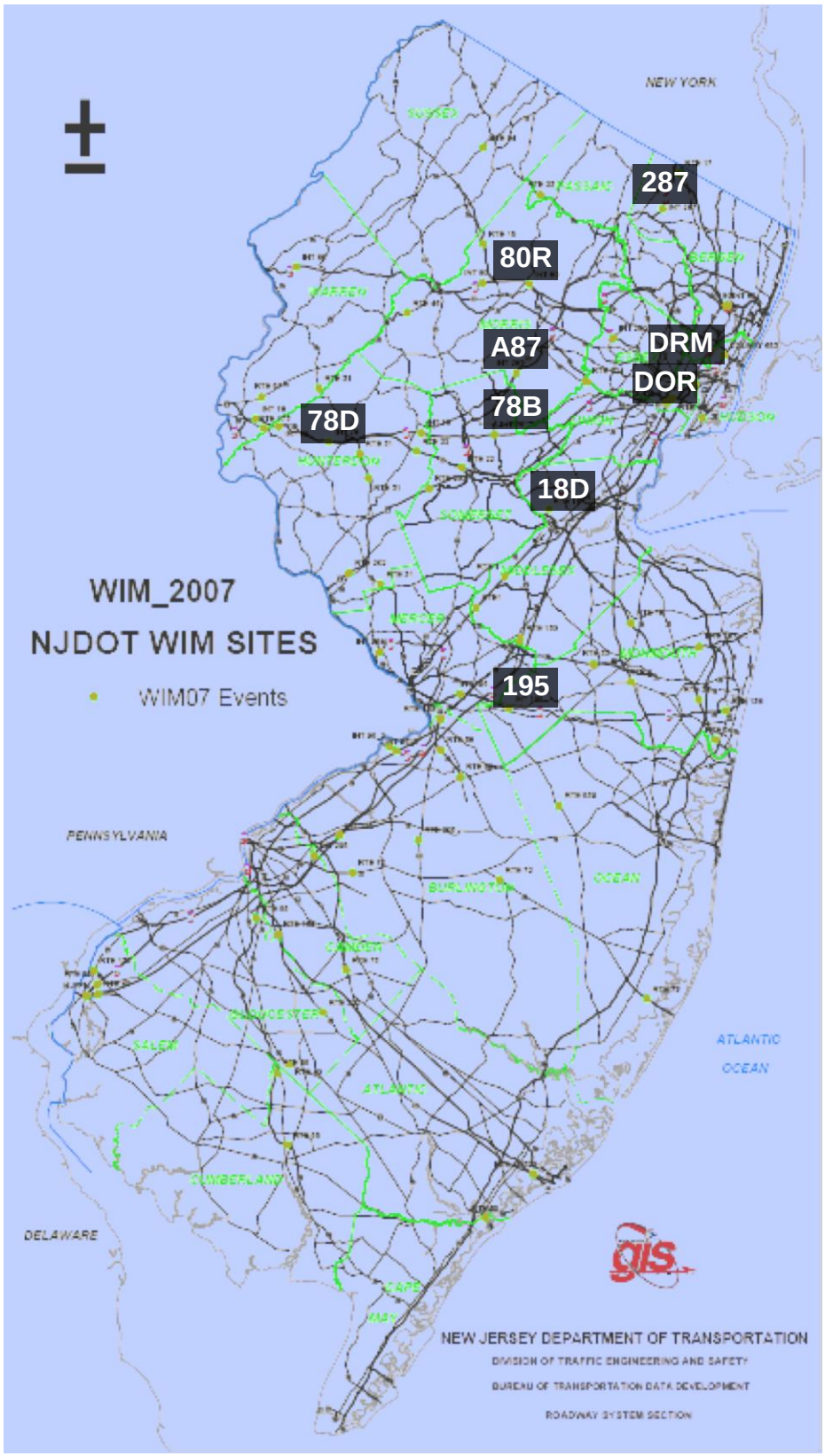

Figure 59. Selected New Jersey WIM sites shown in rectangles (NJDOT 2007)

Site Variation

Several researchers (Laman and Nowak 1997, Ghosn and Moses 1986, Kim, Sokolik, and Nowak, 1997) have noted that truck loading is site specific and dependent of truck volume, local industry, economic activity, law enforcement, and traffic flow control which may cause heavy truck queues. This has also been recognized by the LRFD code, which, despite having a calibrated live-load model, highlights consideration for site-specific modifications to design live loads. Thus, it is important to account for uncertainty due to site variation in statistical modeling.

The composition of the truck population is statistically investigated in terms of truck type, percent of trucks operating at heavy loads, and total truck weight. This analysis was carried out for each of the 33 WIM sites for the month of June 2003. This data set included 1,146,879 truck records. Trucks were classified using the FHWA 13, a category vehicle classification scheme as shown in Figures 60 and 61. The percentage of Class 5–8 vehicles decreased with increasing truck volume, while the number of Class 10–13 vehicles increased. This indicates that heavy-volume sites will experience fewer single-unit trucks (four or fewer axles) and more single- and multitrailer trucks (five or more axles, with the exception of Class 8 vehicles). In fact, about 61 percent of the truck population at light-volume sites can be described as Class 5–8 vehicles, compared with only 17 percent for heavy-volume sites. In addition, a relatively large percentage of trucks at heavy-volume sites are Class 11 (five or fewer, multi-trailer trucks), accounting for almost 4 percent of the population. It is also observed that Class 9 vehicles are by far the most frequently occurring truck type for all site conditions. Their number tends to increase with increasing truck volume—38, 57, and 78 percent of the population for light-, average-, and heavy-volume sites, respectively.

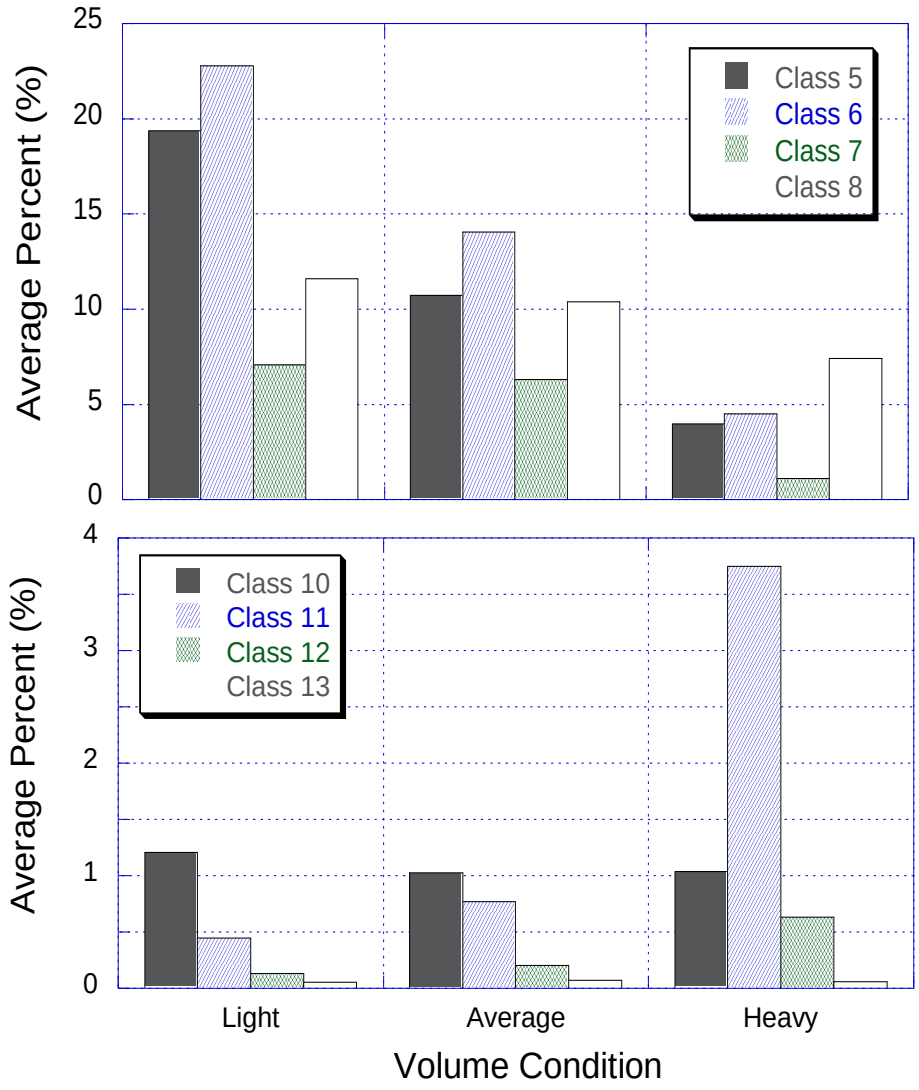

Figure 60. Vehicle type by site volume condition (33 sites, June 2003)

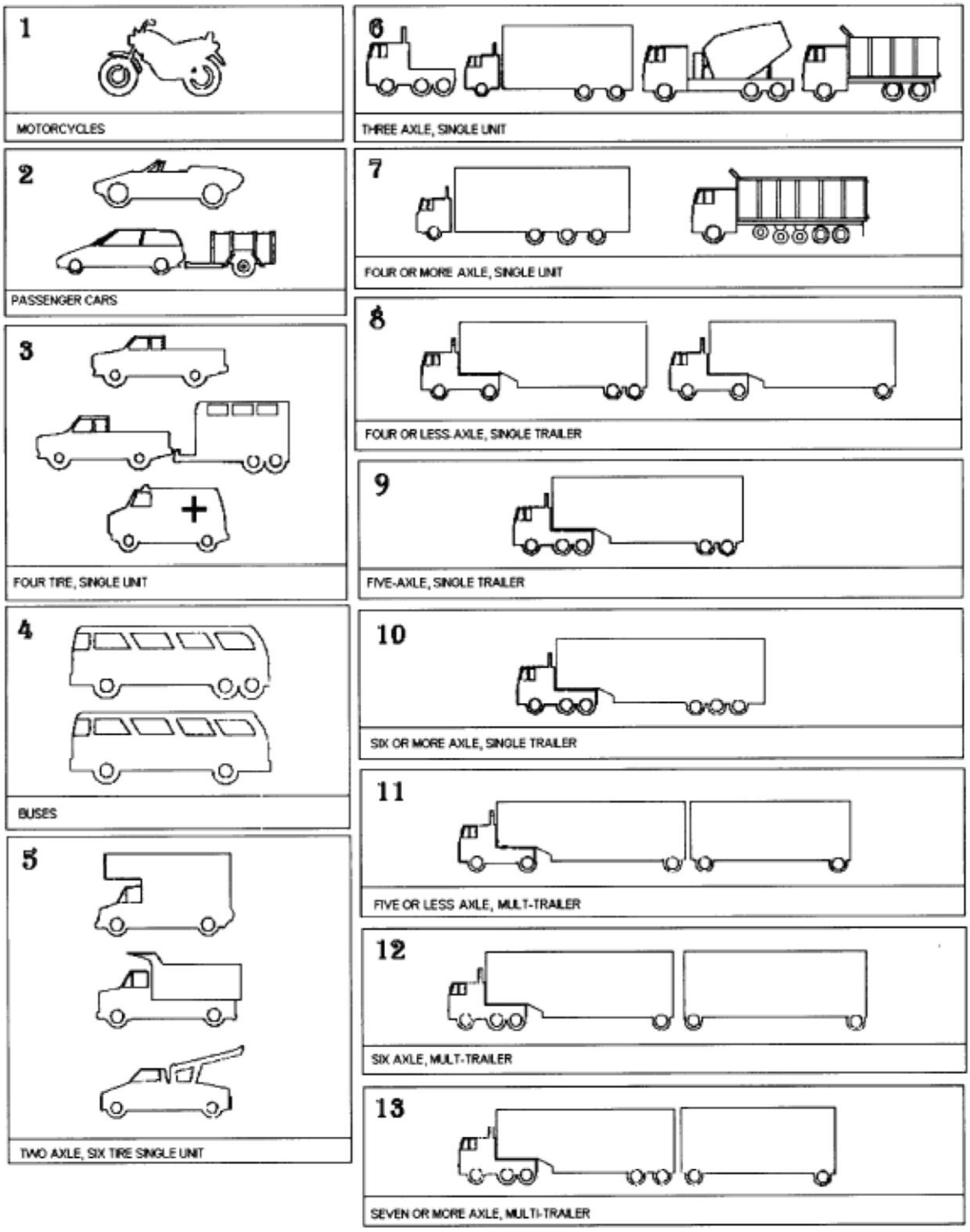

Figure 61. Federal Highway Administration (FHWA) vehicle classification scheme (http://www.dot.state.oh.us/)

The number of trucks operating at loads exceeding 80 kips (356 kN, the legal load for most states) is also investigated. Figure 62 shows the percentage of overloaded trucks as a function of Average Daily Truck Traffic (ADTT). There does not appear to be a discernible strong trend. However, if the overloaded percentage is expressed in terms of volume condition, it is seen that with increasing truck volume, more trucks are likely to be overloaded, reaching an average of 12 percent for the two heavy-volume sites. If all sites are considered (with the exception of Site 1 (i.e., I-287), which needs to be investigated further), the average rate of overloading is 8.3 percent. It is important to note that some of these trucks may be permit vehicles and therefore carry legal loads.

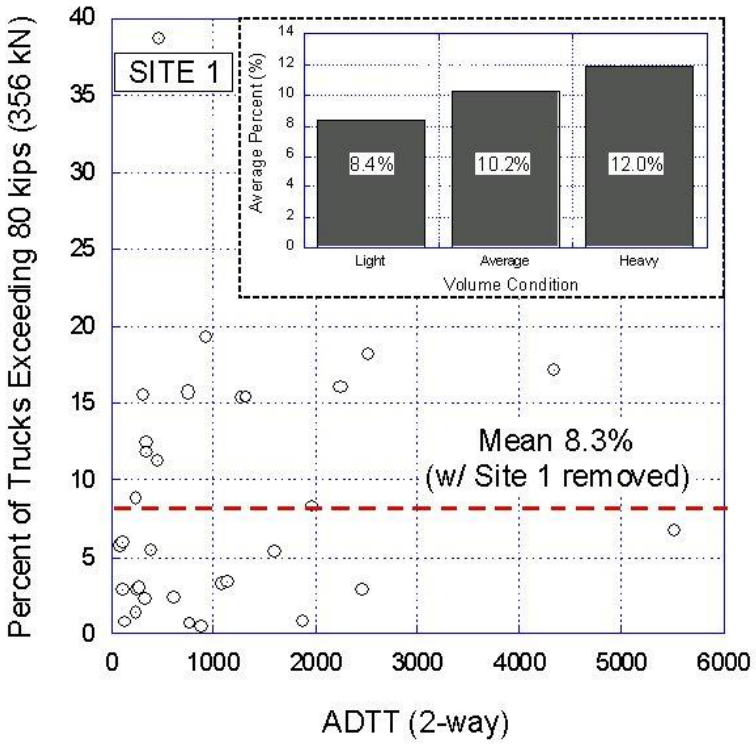

Figure 62. Overloaded trucks by site volume condition (33 sites, June 2003)

Finally, truck weight variation from one site to another is investigated. One approach in comparing truck weight statistics is to compare the 95th percentile (W_{95}) of the total weight. This parameter describes the level for which 95 percent of trucks weigh less. Due to site variation, the distributions of the mean, 95th percentile, and maximum observed truck weights are expressed as random variables with an approximate normal distribution The mean and coefficient of variation (COV) for each parameter are computed as follows: mean (46 kips, 15 percent), W_{95} (81 kips, 18 percent), and maximum observed (170 kips, 18 percent). The 18 percent COV of the W_{95} parameter compares well with that determined by other researchers; 17 to 20 percent (Nowak 1999) and 20 percent (Ghosn and Moses 1986). In addition, the average of all statistics increased with increasing truck volume, indicating that heavy-volume sites are likely to see more trucks that are heavier.

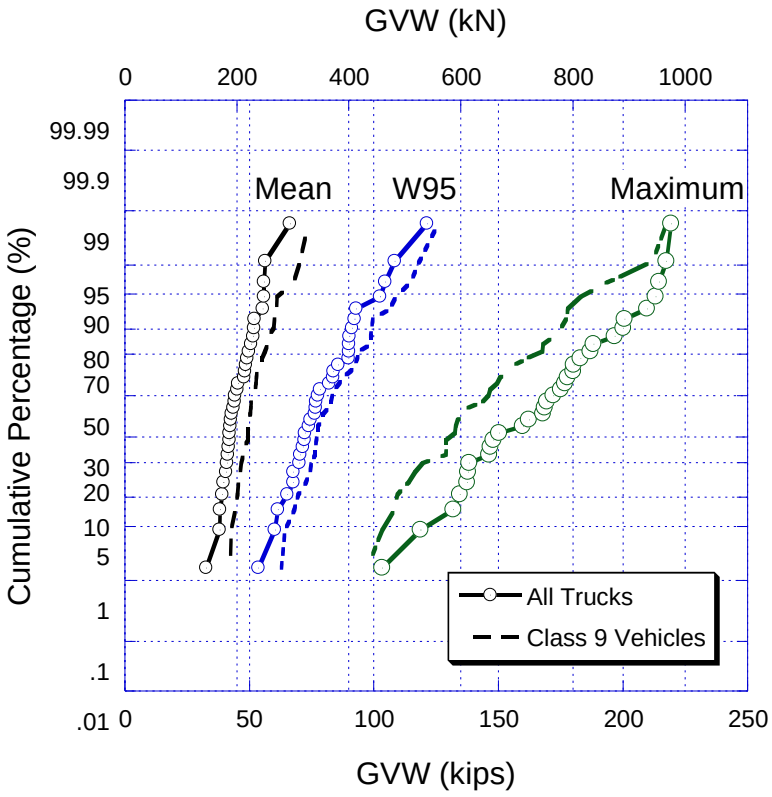

Figure 63. Total truck weight statistics' distributions (33 sites, June 2003)

Statistical distributions for the GVW parameters of Class 9 vehicles are also plotted in Figure 63. The mean and W_{95} truck weights were greater (averaging 53 and 87 kips) than those of the total truck population, whereas the maximum observed weights (average of 148 kips) were considerably smaller. This is because the large number of smaller trucks at light-volume sites tends to decrease the mean and the 95th percentile, while the maximum observed truck weights are often due to trucks larger than a Class 9 vehicle.

Time Variation

The US truck population is a dynamic system, continuously evolving in truck body characteristics, extent, type of freight transported, as well as payload weight. The FHWA estimates that commercial truck travel has doubled over the past two decades, with combination truck travel increasing at a faster rate than that for single-unit trucks (FHWA 2004). These time variations—i.e., seasonal or annual—are particularly important for truck traffic simulation and for the development of bridge live-load models. Often, time-limited data (2 weeks, 1 month) is used as the basis for simulation of longer time periods and extrapolation of bridge effects to 75 years (the economic service life of bridges). It has been found that the time and length of the base data set do affect future

predictions (Gindy and Nassif 2005). Due to the availability of truck records in this database for such an extent and time span, a rare opportunity to model truck trends was available.

Time variations of the truck population are investigated in terms of truck volume, type, and weight. This analysis is conducted on one of the 33 WIM sites, Site 195, a four-lane Interstate highway in a rural area categorized as an average-volume site. The data set includes 83 months during the period 1993–2003, consisting of more than 2.8 million records. The results presented here focus strictly on annual trends.

Figure 64 shows the ADTT over time, which illustrates a steady increase of about 7.7 percent. The percentage of trucks above 80 kips (356 kN) remains relatively constant at about 13 percent. This, coupled with an increasing truck volume, indicates that there are more overloaded trucks in recent years at this site. The variation in truck type (vehicle class) over time is analyzed. Class 7 vehicles (four or more axles, single-unit trucks) were observed to have increased dramatically from 3 percent in 1993 to about 13 percent in 2003. There is also a slight increase in multi-trailer trucks with six or more axles (Classes 12 and 13). All other vehicle classes remained relatively constant. This indicates that more single-unit and multitrailer trucks are operating with a larger number of axles. Truck weight variation over time is analyzed for two groups: all truck records and Class 9 vehicles. The mean, W_{95}, and maximum observed total truck weight for all trucks are plotted in Figure 65. The maximum observed weight increases slightly at a rate of about 3.5 kips/year, while the mean and W_{95} remain relatively constant (49 and 89 kips, respectively). This was also true for Class 9 vehicles, with the maximum weight observed increasing at a lower rate of 1.2 kips/year.

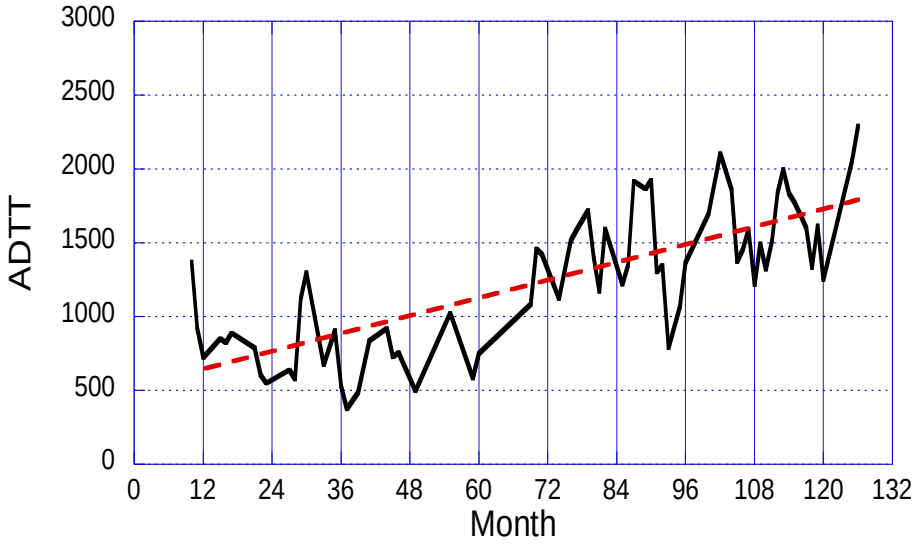

Figure 64. Truck volume variation during 1993–2003 (Site 195)

The total weights of Class 9 vehicles over the 10-year duration are plotted on Normal Probability Paper (NPP) in Figure 66. The variation in weight can be attributed to the heaviest 5 percent of the data. This portion of the data is analyzed separately to refine weight trends. It is observed that the percent of trucks in the upper 5 percent (by weight) nearly doubles over the past 10 years (4 percent in 1994 to 8 percent in 2003). The mean and W_{95} also increase slightly, indicating that more trucks with larger loads constitute the truck population in the last few years.

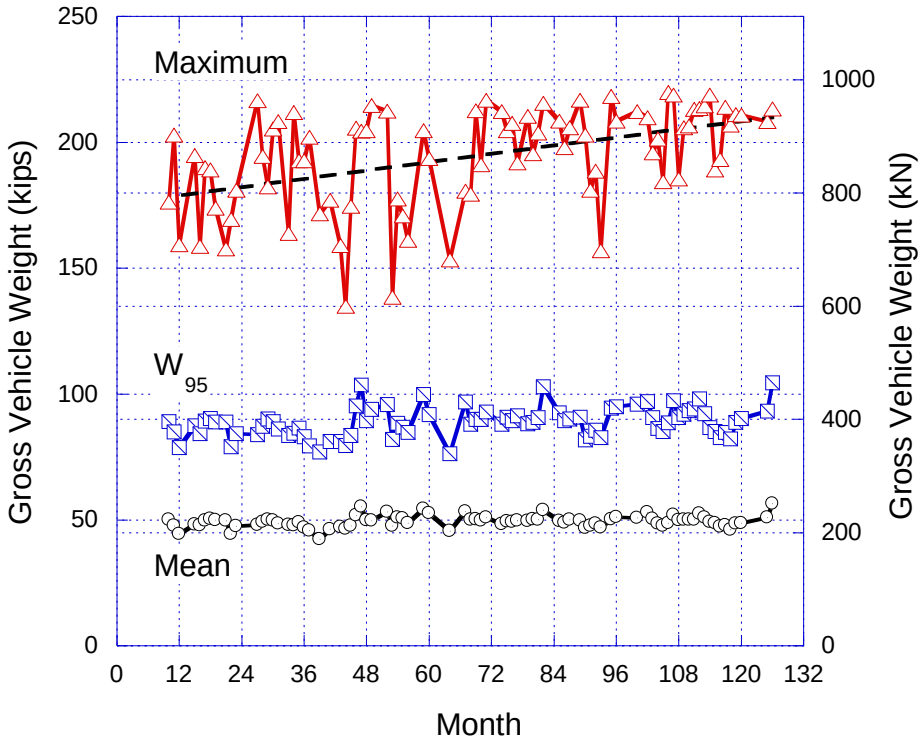

Figure 65. Truck weight variation during 1993–2003 (Site 195)

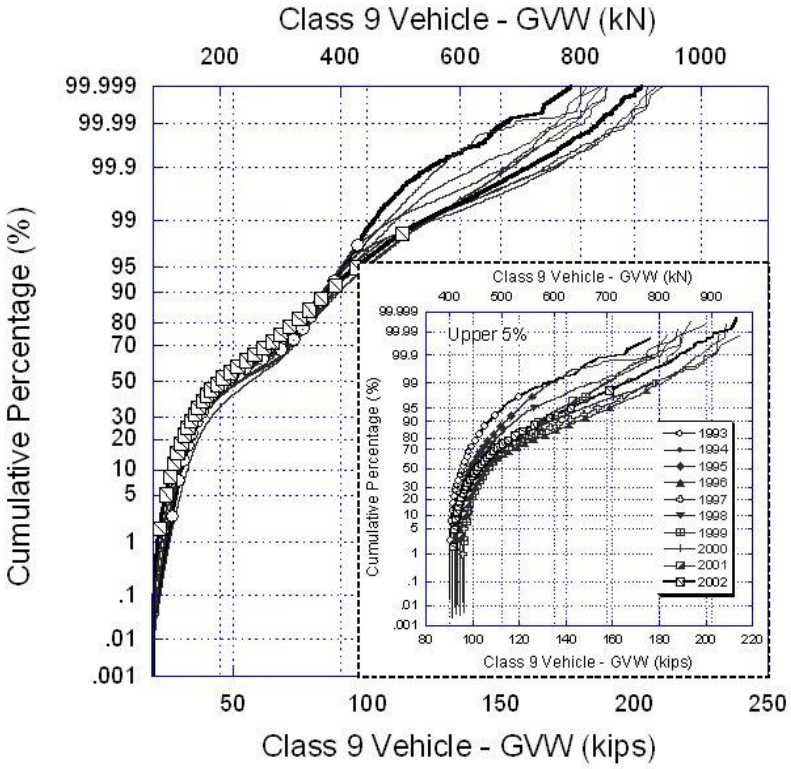

Figure 66. Total truck weight for Class 9 vehicles (Site 195)

Live-Load Variation

Time and site variation should be taken into account in truck traffic simulation and stochastic analysis. This becomes particularly important when time-limited data sets are used as the basis for modeling. The importance of the size of the data set (i.e., 2 weeks, 1 month) and the time the data collected (i.e., weekday/weekend, January/June) are now considered.

Actual monthly truck records occurring at Site 195 were used to compute the maximum bending moment of a simply supported bridge with a 60-ft span. Figure 67 shows the moments induced by trucks for different lengths of time plotted on NPP and expressed as a ratio of the 1989 AASHTO HS20 design loading. Table 9 shows the ratios of the moment and shear load effects between HL-93 and HS20 type of loadings. Table 9 can be used to find the moment induced by various WIM trucks, shown in Figure 67 earlier, with respect to HL-93. Extrapolation of future effects using the NPP method indicates heavy dependence on which month (during the same year or in different years) is used as the basis, and less on the length of the data set. This is because, for longer observation periods, most of the data describes the central region of the distribution while only a few contribute to the upper tail. Additionally, the effect of the upper tail becomes less noticeable because of the relation to the much larger data set size.

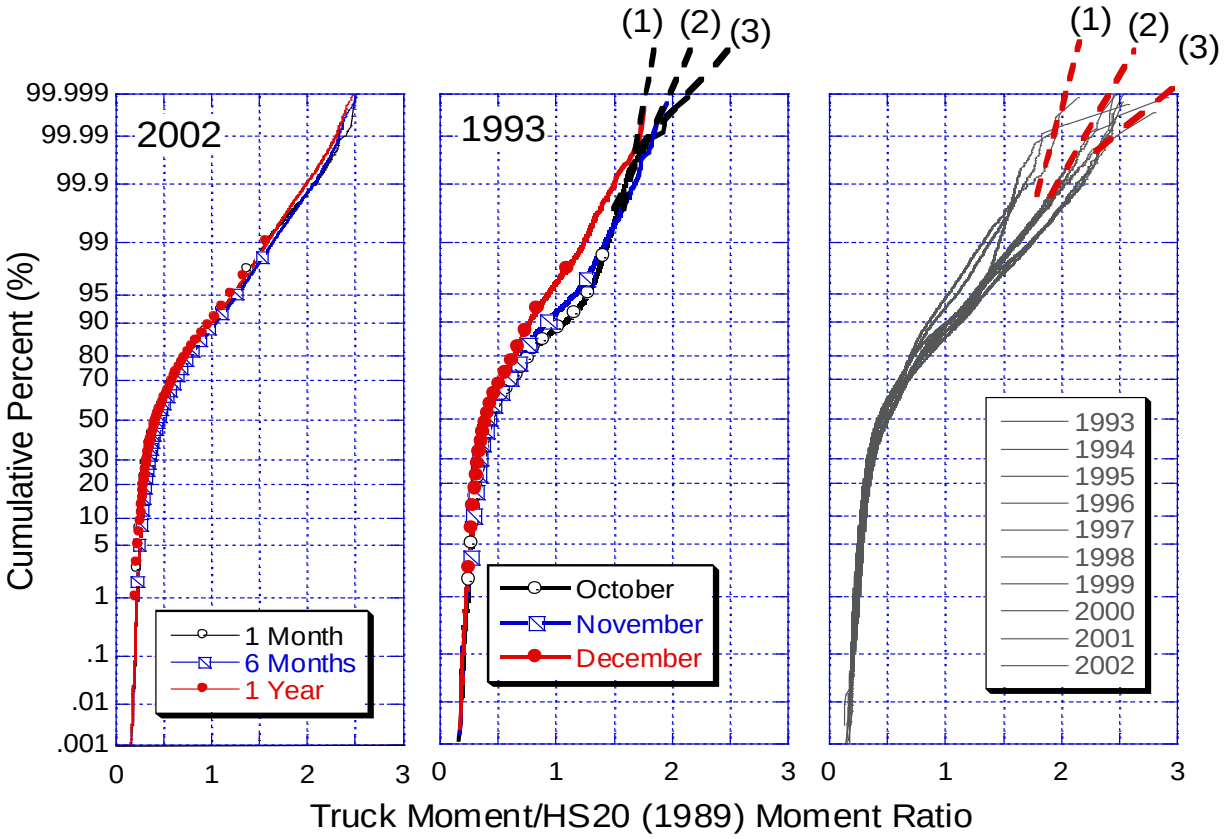

Figure 67. Bridge live-load effects and extrapolation based on various time periods (Site 195)

Table 9. Shear and Moment Ratios For HL-93 and HS20 Loadings

Span Length	Moment (kip-ft)		Moment Ratio	Shear (kips)		Shear Ratio
(ft)	HL93	HS20	HL93/HS20	HL93	HS20	HL93/HS20
20	232	160	1.45	51	42	1.24
40	578	450	1.29	68	55	1.23
60	1088	807	1.35	80	61	1.32
80	1672	1165	q.44	89	64	1.40
100	2320	1524	1.52	97	65	1.49
120	3032	1883	1.61	105	66	1.58
140	3808	2243	1.70	112	71	1.58
160	4648	2768	1.68	119	77	1.54
180	5552	3402	1.63	126	84	1.51
200	6520	4100	1.59	133	90	1.47
220	7552	4862	1.55	140	96	1.45
240	8648	5688	1.52	146	103	1.42
260	9808	6578	1.49	153	109	1.40
280	11032	7532	1.46	159	116	1.38
300	12320	8550	1.44	166	122	1.36
Average	**5254**	**3447**	**1.51**	**116**	**81**	**1.42**
Minimum	**232**	**160**	**1.29**	**51**	**42**	**1.23**
Maximum	**12320**	**8550**	**1.70**	**166**	**122**	**1.58**
STD	**3926**	**2673**	**0.12**	**34**	**24**	**0.11**

The following conclusions were drawn from this portion of the study:

- Heavy-volume sites will experience fewer single-unit trucks and more single- and multitrailer trucks. Class 11 vehicles (five axles or fewer, multitrailer trucks) are mostly observed at heavy-volume sites, constituting 4 percent of the truck population.
- One-third of the truck population at light-volume sites can be described as Class 9 vehicles compared with 80 percent at heavy-volume sites.
- Heavy-volume sites are likely to include more trucks that are heavier, with 12 percent above 80 kips (356 kN). Considering all sites, an average of 8 percent of trucks exceed 80 kips (356 kN) and the average W_{95} is found to be 81 kips (360 kN) with a COV of 18 percent.
- Over 10 years, the ADTT was found to increase 2.3 percent annually at Site 195.
- The percentage of truck types remained relatively constant except for Class 7 (four or more axles, single-unit trucks), which increased considerably in the last few years.
- The maximum truck weight observed over the last decade increased at about 3.5 kips/year.
- More trucks with heavier loads constituted the truck population in recent years. The percentage of trucks in the top 5 percent (by weight) of the data nearly doubled over the past decade.

The major parameters in the evaluation of existing bridges and in the design of new bridges are magnitude and frequency of loads. The truckload statistics and trends resulting from this study are used to describe the live-load spectra from a 10-year perspective. It provides an opportunity for reflection and forms a stronger foundation for future predictions.

Quality Control of WIM Data

WIM data, like any other measured scientific data, must be quality checked before casual use. There are many causes for poor quality of WIM data (Southgate 2000):

(1) Suboptimal WIM site choice: rough pavement, road curvature, slowing, and accelerating traffic
(2) Settings or dimensions: inaccurate sensor location, improper installation, and incorrect settings
(3) Time-out settings too long: the system is adding closely following trucks together as a single record
(4) Calibration drift over time: electronics tend to lose their calibration set point over time
(5) Temperature: piezosensors use the impulse of the axle loads to load; at higher temperatures the asphalt is softer and offers less resistance, thereby reducing the sensor reading.

There are several methods to check for WIM data quality as well as to adjust the data to proper calibration. Auto-calibration functions are built into most systems. These functions use the relationship of the first or steering axle to the gross weight of a typical five-axle tractor trailer (Class 9). To test calibration, techniques have been developed to check the calibration of WIM systems based on an extensive database of past results and physical characteristics of trucks (Southgate 2000).

WIM Data Filtering

After quality control checks have been completed, further steps need to be taken to reduce the amount of erroneous or otherwise insignificant data. Filters were developed to remove the known permit loads, insignificant data (such as trucks weighing less than 15 kips), and erroneous data (such as single-axle weights more than 40 kips or axle spaces less than 2 ft). A disqualification file was created for each of the filter criteria. Any data that was removed from the mainstream set was counted and placed in the respective disqualification file. The filter criterion is based on known trends, permit configurations furnished by a state transportation agency, or engineering judgment.

After filtering the WIM data for this Doremus Avenue study, a counter tallied the qualified trucks. Typically, approximately 75 percent of the raw data passed the filters and was included in the analysis. The qualifying percentage may be lower if the original data contained passenger cars and a large proportion of light trucks. The disqualified trucks were tallied according to the disqualification criteria and stored in a separate file. The most common disqualification occurred for GVW under 15 kips. The next section details the permit configurations for NJDOT.

NJDOT Permit Loads

NJDOT specifies a permit vehicle in the *Bridge Design Manual* (NJDOT 2002) that provides an envelope for the maximum expected load for design or evaluation. The eight-axle (200 kip) permit vehicle is shown in Figure 68. The configuration of the permit truck replicates a four-axle single-body Class 7 (dump truck) towing a four-axle trailer. The first axle, weighing 16 kips, represents the steering axle. The second axle, weighing 16 kips, represents the auxiliary drop axle found on most single-body dump trucks. The load effect envelope for simple moment is given in Figure 69. The maximum simple moment ratio for the NJDOT permit truck was 2.43 times HS20 for a span of 140 ft.

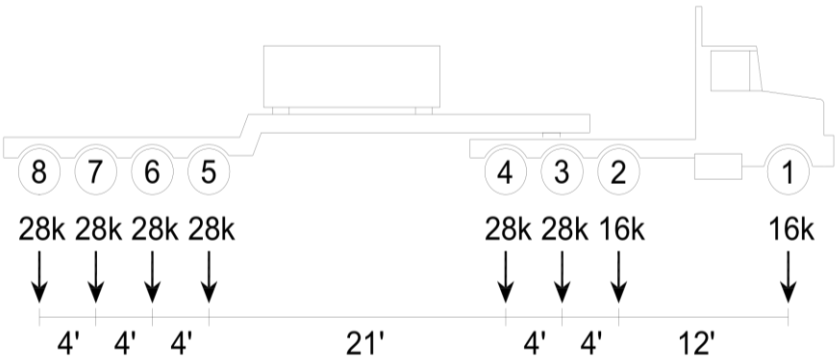

Figure 68. Permit vehicle from NJDOT *Bridge Design Manual* (NJDOT 2002)

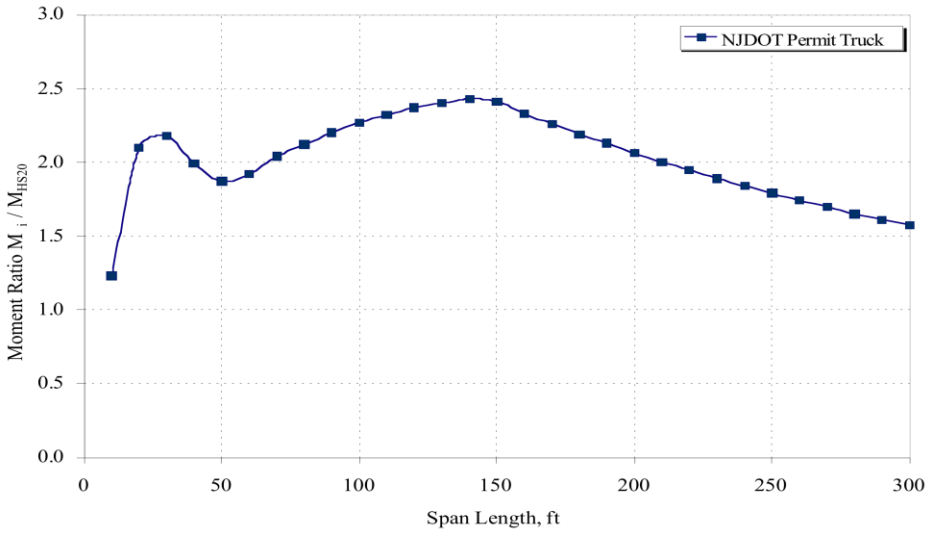

Figure 69. Simple moment envelope for NJDOT permit truck

NJDOT requires commercial carriers to obtain authorizations when moving extra-legal loads or excessively large truck configurations, specifically above 80 kips. Each carrier submits a permit application that describes in detail the following: carrier information, proposed route, number of movements, number of axles, length, gross weight, individual axle weights, axle spacing, axle width, and number of tires per axle. The number of permitted movements is important when considering damage due to overload such as concrete cracking and fatigue damage. Most permits are issued with a finite number of permitted movements to limit the damage to structures along the route. The moment envelope of each permit application is checked against the NJDOT permit vehicle. If the application truck causes moments or shears greater than the permit vehicle allowance, permission for a permit is denied. Furthermore, the proposed route may be amended to avoid aging or deteriorating structures. Table 10 shows ten NJDOT permit applications in the vicinity of the site area between 2003 and 2004 by axle weight and axle spacing.

Table 10. NJDOT permit applications in the vicinity of Doremus Avenue between 2003 and 2004: (a) axle weights and (b) axle spacing

Ref No.	Permit Date	GVW (k)	Length (ft)	Axles	W1 (k)	W2 (k)	W3 (k)	W4 (k)	W5 (k)	W6 (k)	W7 (k)	W8 (k)	W9 (k)	W10 (k)	W11 (k)	W12 (k)
1	6/13/2003	172	105	9	12	20	20	20	20	20	20	20	20			
2	7/9/2003	180	110	10	12	16	16	16	20	20	20	20	20	20		
3	12/11/2003	164	110	9	12	19	19	19	19	19	19	19	19			
4	1/2/2004	188	110	10	15	13	14	14	22	22	22	22	22	22		
5	1/5/2004	197	110	9	13	23	23	23	23	23	23	23	23			
6	2/23/2004	199	110	11	12	16	16	16	23	23	17.7	17.7	17.7	20	20	
7	3/18/2004	172	106	9	12	20	20	20	20	20	20	20	20			
8	3/26/2004	173	110	9	13	20	20	20	20	20	20	20	20			
9	4/30/2004	181	110	9	13	21	21	21	21	21	21	21	21			
10	10/6/2004	172.5	110	9	12.5	20	20	20	20	20	20	20	20			

(a)

Ref No.	Permit Date	GVW (k)	Length (ft)	Axles	S1-2 (ft)	S2-3 (ft)	S3-4 (ft)	S4-5 (ft)	S5-6 (ft)	S6-7 (ft)	S7-8 (ft)	S8-9 (ft)	S9-10 (ft)	S10-11 (ft)	S11-12 (ft)
1	6/13/2003	172	105	9	19.0	4.5	14.1	4.5	36.0	4.5	14.0	4.5			
2	7/9/2003	180	110	10	17.7	4.3	4.3	13.8	4.5	38.8	4.5	14.1	4.5		
3	12/11/2003	164	110	9	21.2	4.5	13.5	4.5	35.0	4.5	13.5	4.5			
4	1/2/2004	188	110	10	17.0	4.3	4.3	13.5	4.5	37.7	4.5	13.5	4.5		
5	1/5/2004	197	110	9	22.1	5.1	14.5	4.5	34.5	4.5	14.1	4.5			
6	2/23/2004	199	110	11	17.1	5.1	5.1	16.5	5.1	27.7	5.1	5.1	14.1	5.1	
7	3/18/2004	172	106	9	17.5	4.5	15.4	4.1	32.4	4.2	12.8	4.2			
8	3/26/2004	173	110	9	21.8	4.5	13.5	4.5	38.2	4.5	13.5	4.5			
9	4/30/2004	181	110	9	21.2	4.5	14.3	4.5	35.3	4.5	14.0	4.5			
10	10/6/2004	172.5	110	9	17.3	4.6	14.5	4.5	34.3	4.5	13.6	4.5			

(b)

To predict the stress levels caused by these permit application trucks, the weight and spacing information was inputted and ran with the semi-continuum model of Doremus Avenue (Figure 70). Because most of the approved routes from the permit applications indicate vehicles heading southbound on Doremus Avenue, all permit simulations are assumed to be in the southbound right lane (Lane D). The stress in the bottom flange of Girder 4 (G4) will be considered, since the Lane D truck aligns over it. A location at the maximum positive moment position of Span 3 is considered as the truck travels from Span 3 to Span 1 in Lane D.

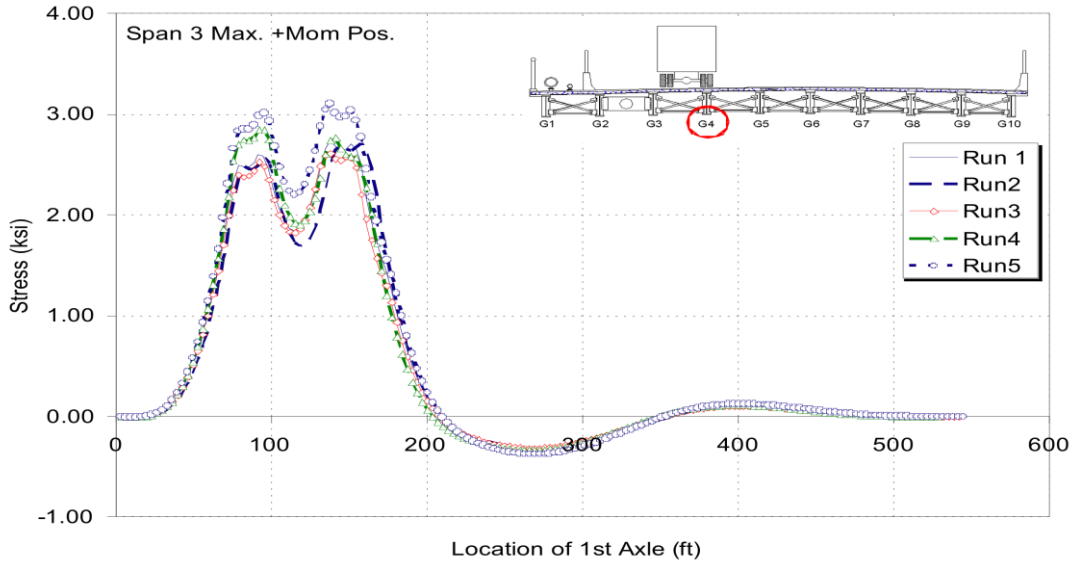

(a)

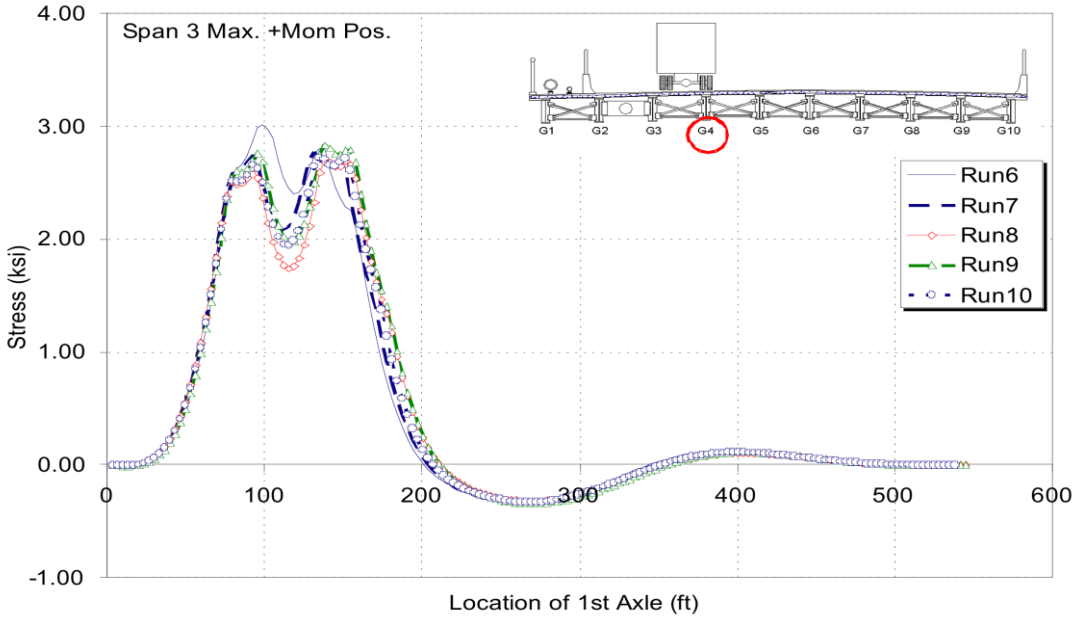

(b)

Figure 70. Semi-continuum Girder 4 stress predictions for Doremus Avenue permit trucks in Lane D

The plots in Figure 70a and Figure 70b show the semi-continuum stress predictions for Girder 4 Span 3 given Permit Trucks 1 to 5 (indicated by Runs 1-5) and 6 to 10 (indicated by Runs 6-10), respectively. All 10-permit trucks exhibit similar twin peaked stress profiles during their passage. In addition, the magnitude of Girder 4 stress is similar for all known permit trucks, with a maximum stress of 3.11 ksi for Permit Truck 5 in Figure 70a. A configuration of a typical 7-axle and 13-axle permit applicant truck is shown in Figure 71.

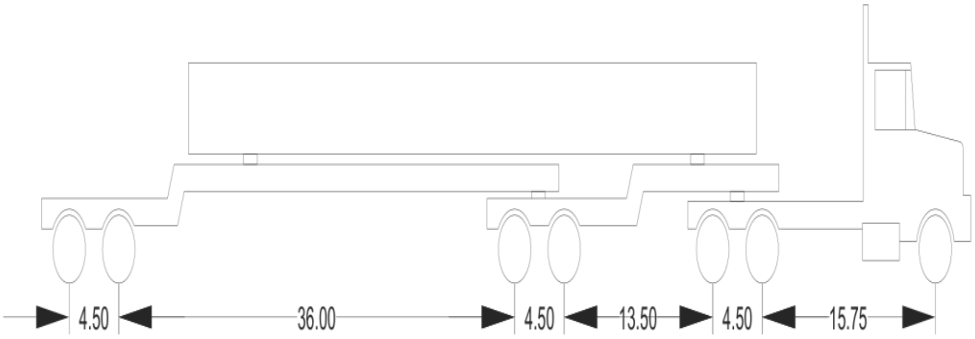

(a)

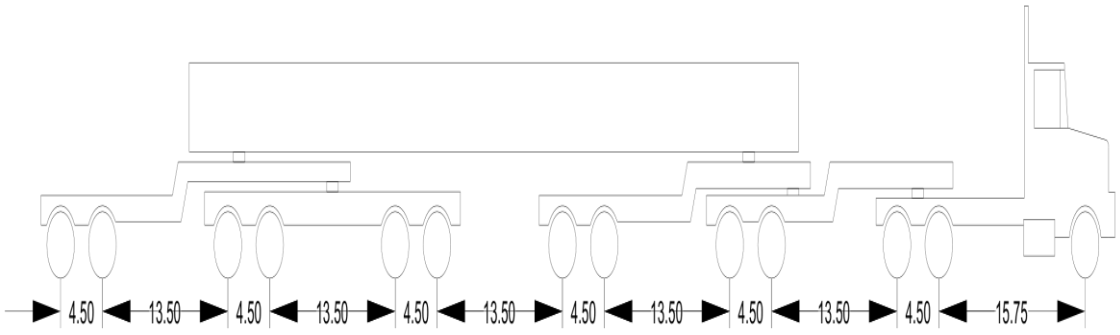

(b)

Figure 71. Typical permit applicant truck configurations: (a) with 7 axles and (b) with 13 axles

New Jersey WIM Site Characteristics

The gross weight histograms for New Jersey WIM sites and Doremus Avenue Bridge are given in Figure 72 for the dominant Class 9 truck type. Class 9 is the dominant truck type for all sites but Site 18D, where the dominant type is Class 6. The bi-modal weight distribution is evident at the following sites: 18D, 78B, 78D, 195, DRM, and DOR. These sites contain a mixture of loaded and unloaded trucks. It is possible that a distribution center is near the Interstate sites. The bi-modal gross weight distribution for sites DOR (Figure 72i) and DRM (Figure 72h) is undoubtedly related to their proximity to Port Newark. Near the port, trucks travel with a loaded container, empty container, or without a container. Furthermore, Doremus Avenue is a short, local connector where the economics of empty trucks are insignificant. Regional routes such as Interstate 80 (Site 80R, (Figure 72d) and Interstate 287 (Site A87, Figure 72f) show a single continuous distribution of truck weights.

The percentage of overweight vehicles by site is given in Table 11. Because the legal gross weight limit without a permit is 80 kips, any filtered vehicle over 80 kips is

considered to be overweight. Overweight vehicles make up most of the upper tail of the load effects used to determine the maximum 75-year levels in design. Therefore, the percentage of overweight vehicles and their trend dictate the load factors for each site. Table 11 shows that at 7 percent, southbound Doremus Avenue Bridge contains the highest proportion of overweight vehicles. On Interstate sites such as 78B, 80R, 195, A87, and 287, 4 to 5 percent of vehicles are overweight. The directionality of truck flow can be seen in the difference between northbound (DOR12) and southbound (DOR34) Doremus Avenue at the bridge. Nearly three times more overweight vehicles are traveling south (7 percent) over the Doremus Avenue Bridge than are traveling north (2 percent). The reason may be related to the proximity to the port. Southbound trucks (DOR34) are heading into the port carrying items for export, which typically consist of bulk scrap metal and other materials. Northbound trucks (DOR12) exiting the port, carry more highly regulated containers that are less likely to be overweight because of port oversight and controls.

Truck Multiple Presence (MP)

Truck superposition is defined as the presence of two or more trucks occurring simultaneously. The maximum load effect is often controlled by a truck superposition, such as the two lanes loaded design case in AASHTO LRFD. The multiple presence is reported in terms of two main quantities: (1) the frequency of each type of occurrence as a percentage of the total truck population and (2) the frequency of each type of occurrence with two trucks above a chosen “heavy” threshold. Truck superposition is site specific and is influenced by traffic density, speed, truck population, and number of lanes. MP statistics are reported only for qualified trucks and exclude all passenger vehicles, light trucks, and erroneous records.

The configurations of MP are described by the following events: single, side by side, following, staggered, and other. The next sections describe in detail the criteria and significance of each truck superposition.

Single Event

A single event is defined as an event when a truck occurs with no trucks in the adjacent lanes so that the load effect on any particular girder results from one truck only. The basic case of a single event is one truck occurring on a span with no other traffic (Figure **73**a). Because only one truck is acting on the span, any load effects are attributed to this truck. In multi-lane, multi-girder bridges the compounding effect of loading distant lanes are negligible due to the distribution of load to many girders. For example, consider a 10-girder bridge where the moment is being considered at Girder 1, and a truck load is applied over Girder 10. The effect of the load applied over Girder 10 on the moment at Girder 1 is negligible because the distant load is distributed to Girders 10, 9, 8, and so on. The residual moment leftover for Girder 1 is nearly zero. For a multi-lane

bridge, there may be several single events at one time, provided that the loading is not in adjacent lanes.

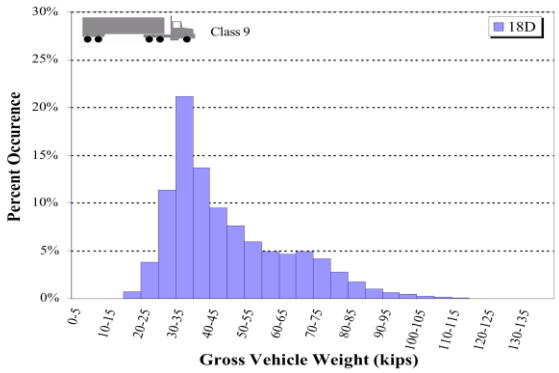

(a) SITE 18D

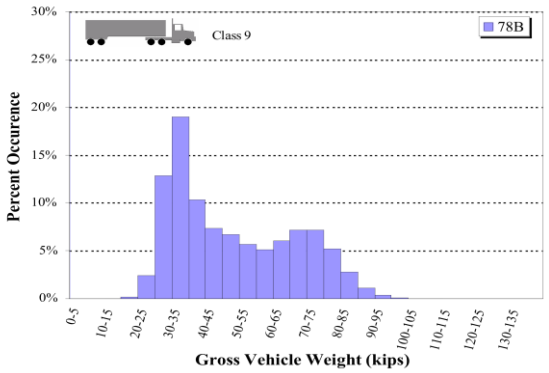

(b) SITE 78B

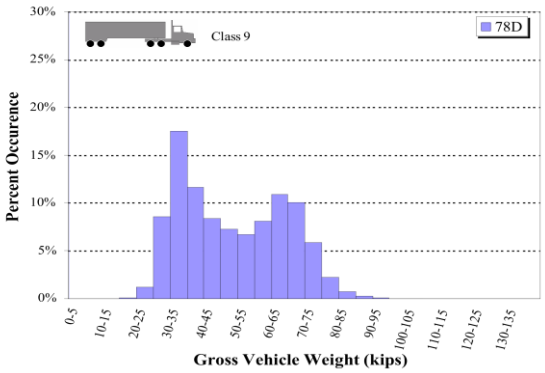

(c) SITE 78D

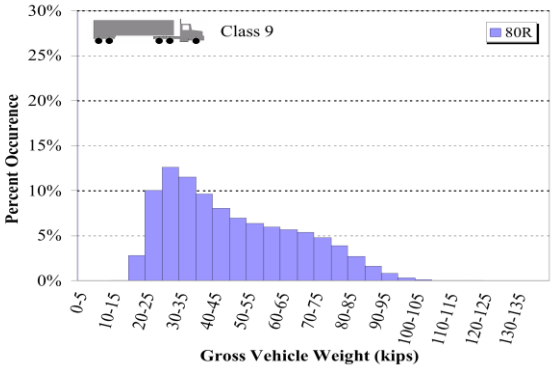

(d) SITE 80R

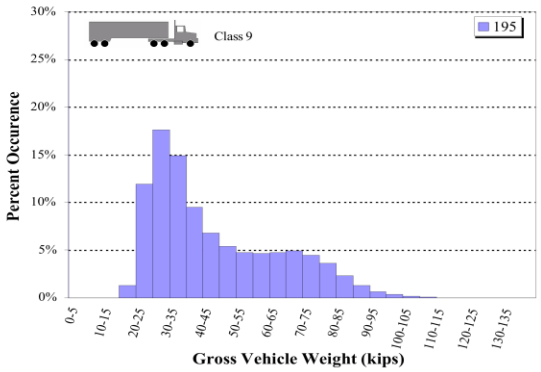

(e) SITE 195

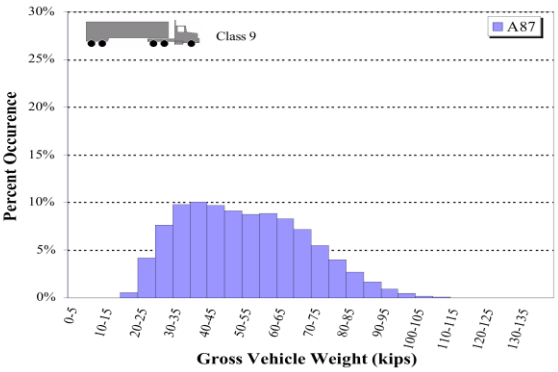

(f) SITE A87

Figure 72. Class 9 GVW histograms for New Jersey WIM sites (continues on next page)

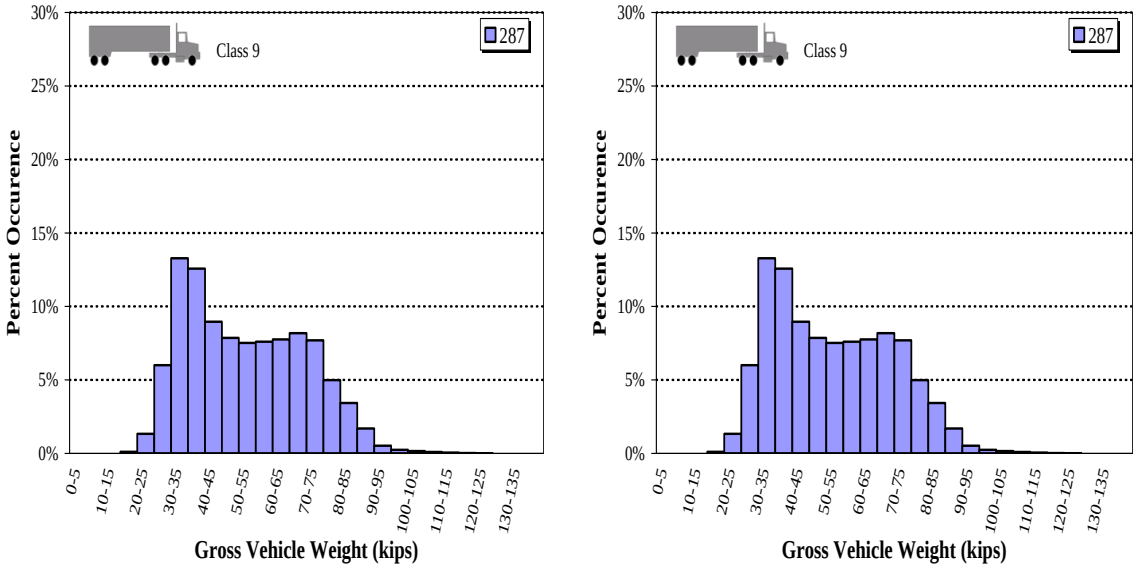

(g) SITE 287 (h) SITE DRM

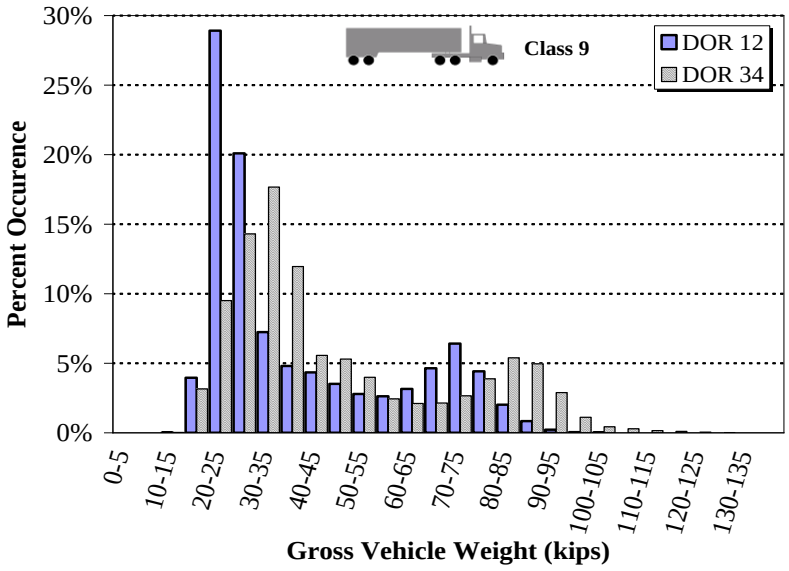

(i) DOREMUS AVENUE BRIDGE (DOR)

Figure 72. Class 9 GVW histograms for New Jersey WIM sites (Continued)

Figure **73**b shows an example of two simultaneous single events on a four-lane bridge. The truck in Lane 1 (nearest to the bottom) is nearly parallel to the truck in Lane 3. This MP event would be considered a side-by-side event if the second truck was in Lane 2. However, since the loaded truck is not in the adjacent lane, this event would be classified as two single events. The single event is the simplest of all MP events, whereas the more severe case of loading, the side-by-side event, is described next.

Table 11. Truck volumes and percentage of overweight trucks (above 80kips) for New Jersey WIM sites

Site	Qualified ADTT	Percent Overweight
18D	577	2%
78B	2017	4%
78D	14783	1%
80R	7849	5%
195	2225	4%
287	6515	5%
A87	3526	5%
DOR 12	1485	2%
DOR 34	1306	7%
DRM	2017	4%

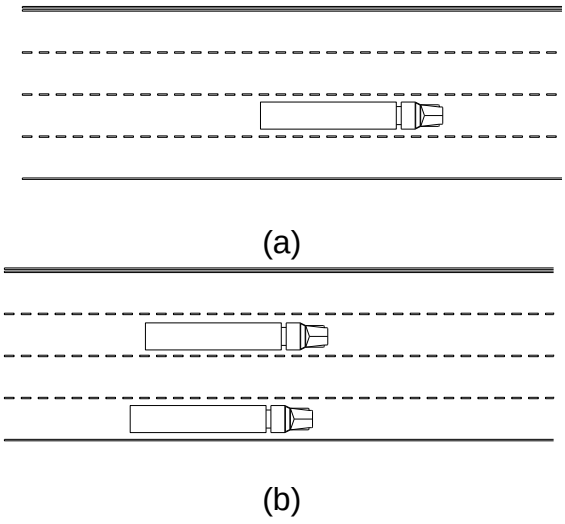

(a)

(b)

Figure 73. Typical truck configurations for (a) the single event with one truck and (b) multiple single events where the load effect on any one girder is equivalent to that due to one truck.

Side-by-Side Event

The side-by-side event describes the case in which two trucks are traveling parallel in adjacent lanes. To qualify, the second truck must overlap the leading truck by at least one-half of the leading truck's length (Figure **74**). Therefore, the range of acceptable for side-by-side events starts with two trucks traveling perfectly parallel and ends with an allowable truck overlap of less than one-half of the first truck's length. This tolerance allows for a range over which side-by-side events may cause the same effect. Modeling

of a long span (about 150 ft) steel girder bridge has shown that two trucks positioned in adjacent lanes with a longitudinal offset, as much as one entire truck length, produce the same moment as two perfectly parallel side-by-side trucks.

The side-by-side event represents the two-lane loaded design case in AASHTO LRFD (AASHTO 2004). Two-lanes loaded usually controls the girder design for interior members. Therefore, quantification of the maximum expected side-by-side load intensity is needed. In addition, the frequency of the side-by-side MP case must be found. The MP algorithm also includes a statement (not shown herein) that evaluates the weights of any identified side-by-side event and tallies all cases that have two truck weights above a chosen “heavy” threshold. The goal is to measure the frequency of side-by-side events as well as the weights associated with those events.

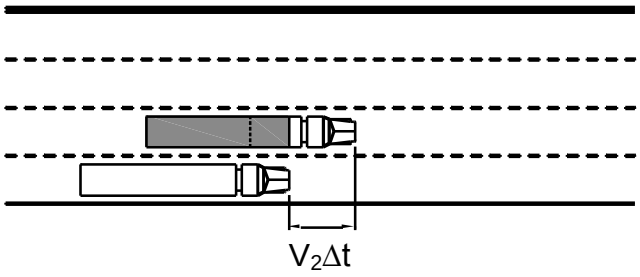

Figure 74. Typical truck configuration for side-by-side event where two trucks travel in adjacent lanes with an overlap of one-half of the first truck’s length

Staggered Event

Two trucks traveling in adjacent lanes, such that both trucks are entirely on the span and the overlap is less than one-half of the leading truck length, is considered a staggered event. Figure 76 shows the typical staggered truck configuration. The lower bound for this case is an overlap of less than one-half the leading truck lengths and the upper bound is that the entire length of both trucks must be within the span but not necessarily overlapping. Similar to the side-by-side event, the effect of different degrees of stagger has been modeled on the Doremus Avenue Bridge with three spans at 147 ft. The results (not shown herein) reveal that the load effect for the lower-bound stagger case (overlap about one-half length) generates the same moment as the perfect side-by-side case. Furthermore, the stagger event, where the clear distance is about one-half the leading truck lengths, also generates nearly the same moment as the perfect side-by-side case. Therefore, for long-span bridges a portion of the staggered truck events may be included in the side-by-side occurrences when calculating the maximum load event. As in the side-by-side case, the weights of the staggered truck are evaluated and compared with a chosen heavy threshold.

Following Event

When two trucks are traveling closely in the same lane they are said to be in a following configuration. The upper bound for the following event is when the distance from the front of the leading truck to the end of the following truck is less than the span length. The clear distance, as shown in Figure 76a between two vehicles in the same lane is normally defined by transportation engineers as the headway distance. However, in terms of load effect, the headway is taken as the distance from the last axle of the leading truck to the first axle of the following truck as in Figure 76b (Nowak 1999). Truck parameters in terms of axle position are more relevant to the study of live-load effects as this is where the forces are transferred to the structure. Furthermore, many WIM systems measure the vehicle lengths based on the inductive loop sensors, which report the body length. The body of a truck always overhangs the first and last wheels. This contributes to error in vehicle length, which is an important parameter in each MP case. Therefore, the vehicle length, for the purpose of evaluating truck MP, is taken as the summation of the axle spacing as shown in Figure 76b. As with all MP cases, the vehicle weights for the following events are compared with a selected heavy threshold. Following events, where both vehicle weights are above the heavy threshold, are tallied as heavy following.

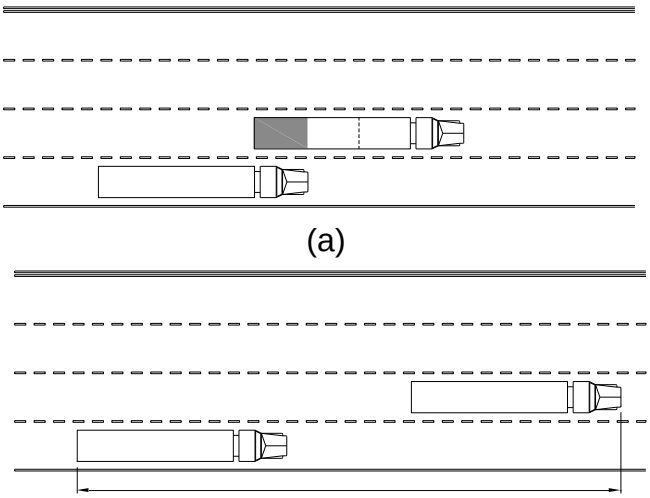

Figure 75. Typical truck configuration for staggered event: (a) stagger with overlap and (b) stagger with clear distance

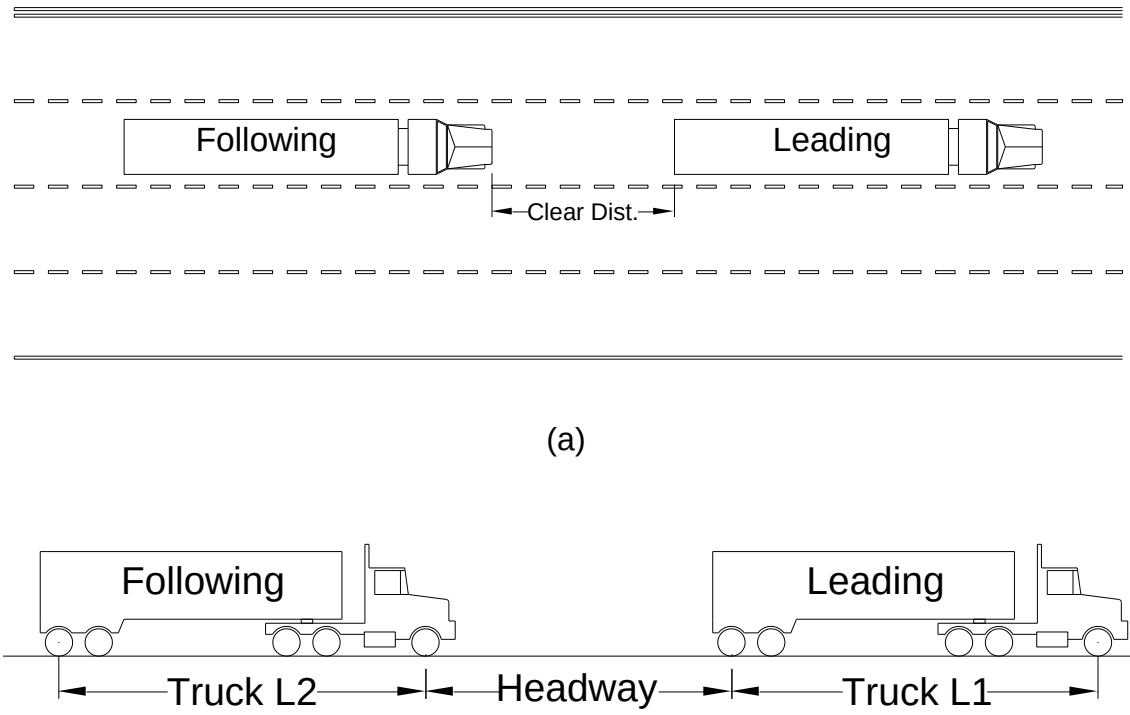

Figure 76. Example of (a) clear distance between trucks and (b) where the headway for the following event is defined as the distance between the last axle of the leading truck and the first axle of the following truck

Other Events

The “other event” describes the case in which more than one Multiple Presence (MP) event occurs simultaneously over a given span length. The probabilities used to forecast the maximum load event for the design of bridges are based on two trucks occurring at the same time. Since the frequency of occurrence and the load effect (in terms of load distribution) for the common MP cases are known, approximation of the maximum lifetime load effect can be estimated. While more than two trucks may occur on a given span simultaneously, the probabilities for each of these events decrease because of the limited number of combinations that are possible. Estimating the load effect of each of the compound MP cases becomes difficult without the use of complex two-dimensional computer modeling. Examples of some of the other MP cases are shown in Figure **77**.

Multiple Presence Detection Algorithm

A computer program was written to evaluate the WIM data for MP. As discussed earlier, a timestamp to the nearest 1/100th of a second resolution is needed to differentiate the cases of MP. The location of any vehicle can be described with the following

information: (1) lane of travel, (2) time or arrival or timestamp to the nearest 1/100th second, and (3) speed of travel. Using these three parameters, the location of each vehicle relative to others can be established. Additional information such as gross weight and length are used to refine the qualifications for each event. A fictitious span length is chosen over which to consider the MP cases. The span comes into consideration when setting an upper bound for the event criteria. For example, in the event that two trucks are following, such that the length from the first axle of the first truck to the last axle of the second truck is 190 ft, the event would be counted as a following event on a fictitious span length of 200 ft. However, the same two trucks would not qualify for following on a 100-ft span because the two trucks would not fit entirely on the span.

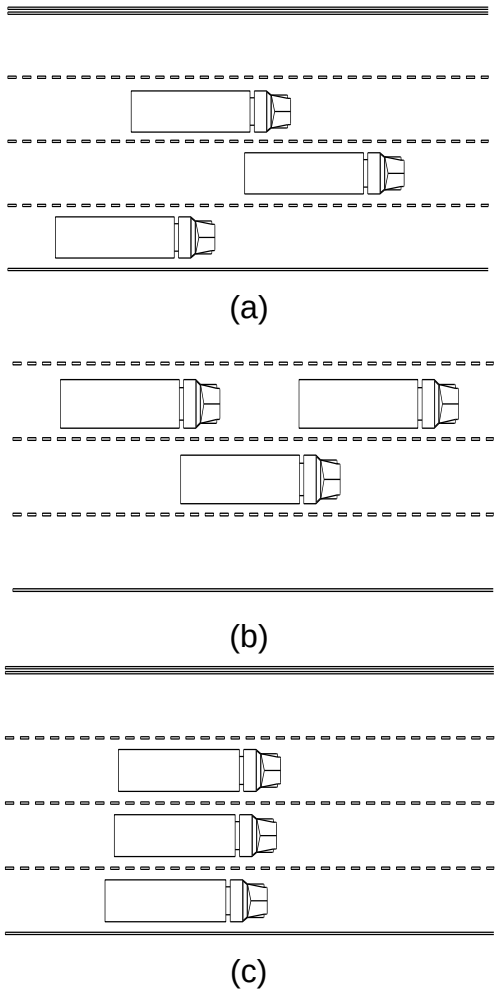

Figure 77. Examples of compound configurations classified as other: (a) double stagger, (b) following and stagger, and (c) triple side-by-side

Multiple Presence Results by Site

A principle input into the forecast of future maximum live loads is the frequency of vehicle superposition or MP. Using the procedures and algorithms outlined previously, the frequency of MP for each site was determined. There are two main parameters to MP, as outlined by Nowak (1999): frequency of each configuration and the weights (or degree of correlation) associated with each event. Again, the key modes of superposition are as follows: side-by-side, staggered, and following. The frequency of each configuration can be determined from the relative positions of the vehicles in the traffic stream. The relationship of the vehicle weights is also determined from the data. For each occurrence of superposition, the weights of the vehicles involved were stored to an array, and the heaviest observed case for each type of MP is also stored. The frequency of the “heavy-heavy” MP influences the maximum expected load intensity during the service life of a bridge.

General Multiple Presence Statistics by Site

The MP statistics in terms of percentages of following, side-by-side, staggered, and other events need to quantify the amount of truck superposition on a given roadway. MP is calculated based on incremental span lengths to gauge the effect for different bridges. Events such as following, staggered, and other depend greatly on the considered span length. The percentages reported are the number of events divided by the total number of qualified trucks in the sample. Each event for following, side-by-side, and staggered contains only two trucks. Compound occurrences such as following with another truck in a staggered condition (involving three or more trucks) are classified as other. The number of other events is sensitive to span length as the probability of seeing three or more trucks on a bridge increases with span length. The trends for the MP events by span take into account the losses due to compound occurrences. For example, the percentage of side-by-side events is greatest for shorter spans and decreases as span length increases. This is due to additional trucks being present on the bridge and causing a compound occurrence. By definition, the percentages of following and staggered are low for small spans. For staggered and following events to occur, the entire length of both trucks must be within the span length. Given that trucks must maintain minimum headways at highway speeds, two following trucks typically occupy 150 ft from the front of the first truck to the rear of the following truck.

All MP results given are based on qualified trucks that have passed the filters. The percentages shown are calculated as the total number of events divided by the total number of trucks qualified.. The case of other may include three or more trucks.

Multiple Presence Statistics for New Jersey WIM Sites

The MP statistics for the Doremus Avenue Bridge (DOR) and New Jersey WIM Sites 287 and 80R are given in Figure 78, Figure 79, and Figure 80, respectively. The MP statistics by span, shown in Figure 81, Figure 82, and Figure 83, are given for northbound and southbound directions separately. The side-by-side event is the most common MP at 1.5 percent up to a span of 80 ft. Thereafter, the stagger event becomes more common. The MP statistics for side-by-side and stagger are greater in the northbound direction than in the southbound direction. The northbound lanes approaching the Doremus Avenue Bridge are subject to an uphill grade of approximately 4 percent over a distance of about 1,500 ft. The grade causes a reduction in truck speeds as they drive uphill towards the bridge (northbound). The speed of loaded trucks is reduced more than the speed for empty trucks. Therefore, an increase in the number of superposition events is expected as the number of passing events increases on the grade. The frequency of following events is greater for the southbound lanes than for the northbound lanes. This is due to the traffic patterns near the end of Doremus Avenue. Doremus Avenue ends at Port Street approximately 3,000 ft south of the bridge. At this intersection most trucks turn right onto Port Street since all other directions have no outlet to other routes.

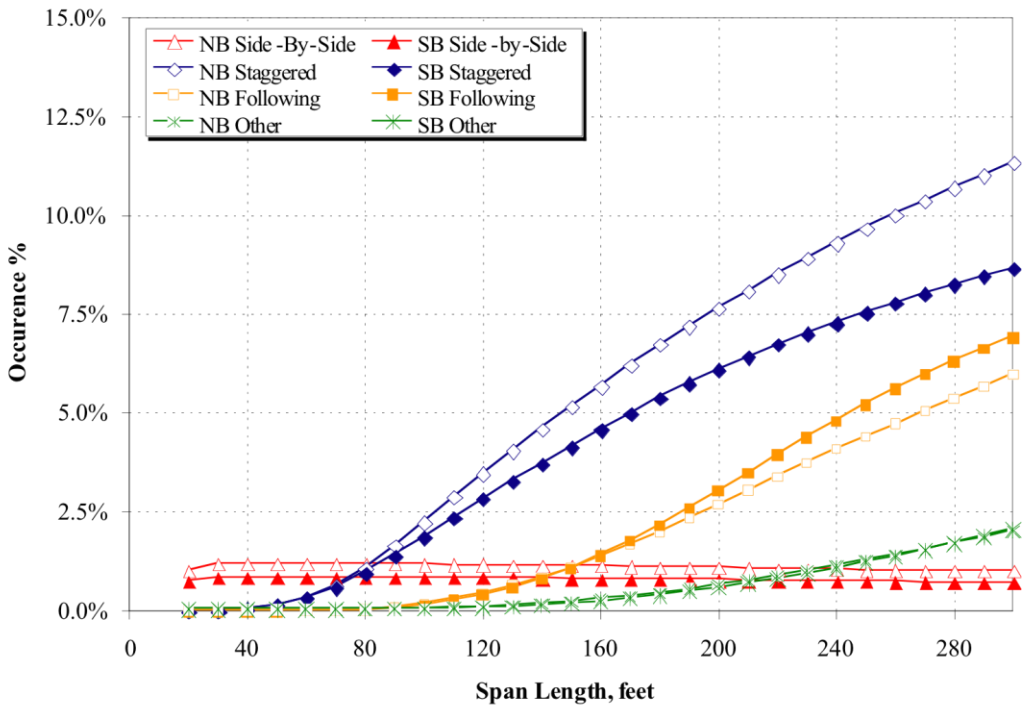

Figure 78. Doremus Avenue Bridge: MP statistics by span for northbound Lanes 1 & 2 and southbound Lanes 3 & 4

Since Doremus Avenue is instrumented for the applied loads (WIM) and bridge response (stresses and deflections), direct comparisons can be made between the

frequency of MP events and the bridge response. The WIM data and calculated MP frequency correspond to an actual bridge with a span length of 147 ft (45 m). Therefore, the MP statistics for the actual Doremus Avenue Bridge are given in Table 12. The overall MP statistics are low as Doremus Avenue is a local roadway with relatively low ADTTs of 1,485 and 1,306 for northbound and southbound traffic, respectively.

Table 12. MP statistics for the Doremus Avenue Bridge for a span length of 147 ft (45 m)

Doremus Ave Bridge (DOR) Span L = 147ft (45m)	Follow Event %	Sideby Event %	Stagger Event %	Other Event %	Single Event %
Northbound Lanes (1&2)	1.1%	1.2%	5.2%	0.2%	92.4%
Southbound Lanes (3&4)	1.1%	0.8%	4.1%	0.2%	93.8%

Computer simulation, using Doremus Avenue as a test case, has shown that a portion of stagger events cause girder stresses similar to those caused by side-by-side events. Therefore, a portion of the stagger events may be added to the side-by-side percentages when calculating the future load effects due to two trucks.

The MP statistics by span for Site 287 are given in Figure 79. The results are similar to Doremus Avenue percentages for side-by-side and following events. The stagger results are higher than those for Doremus Avenue. Because MP frequency is related to traffic volume the higher stagger percentages are reasonable. The maximum single direction ADTT for Site 287 is 3,220 trucks/day, while Doremus Avenue has an ADTT, of 1,485 trucks/day. Also, the curves in Figure 79 indicate that the MP frequency is greater for northbound than southbound traffic in terms of stagger, following, and other events. MP frequency is related to traffic volume, grade, and other site-specific factors. The northbound ADTT is 3,295 trucks/day, while the southbound ADTT is 3,220 trucks/day. The difference is not significant enough to conclude that traffic volume is the sole factor contributing to MP events. Further investigation is needed to determine whether other site-specific factors such as grade, lane merge, and exiting traffic are contributing to the increased MP.

New Jersey WIM Site 80R has some of the highest MP statistics of any other NJ site. Figure 80 shows the MP frequency curves for the eastbound and westbound directions of Interstate 80. The maximum side-by-side percentage of 2.5 percent is larger than any other New Jersey WIM site studied. The MP frequency for the eastbound direction (Lanes 1, 2, and 3) is significantly greater than for the westbound direction (Lanes 4, 5, and 6) for all types of MP events. This is due to a greater eastbound traffic volume of 4,246 trucks/day compared with a westbound volume of 3,603 trucks/day. The high percentages of side-by-side events, coupled with high stagger percentages, make Site 80R the most critical for MP of any New Jersey WIM site.

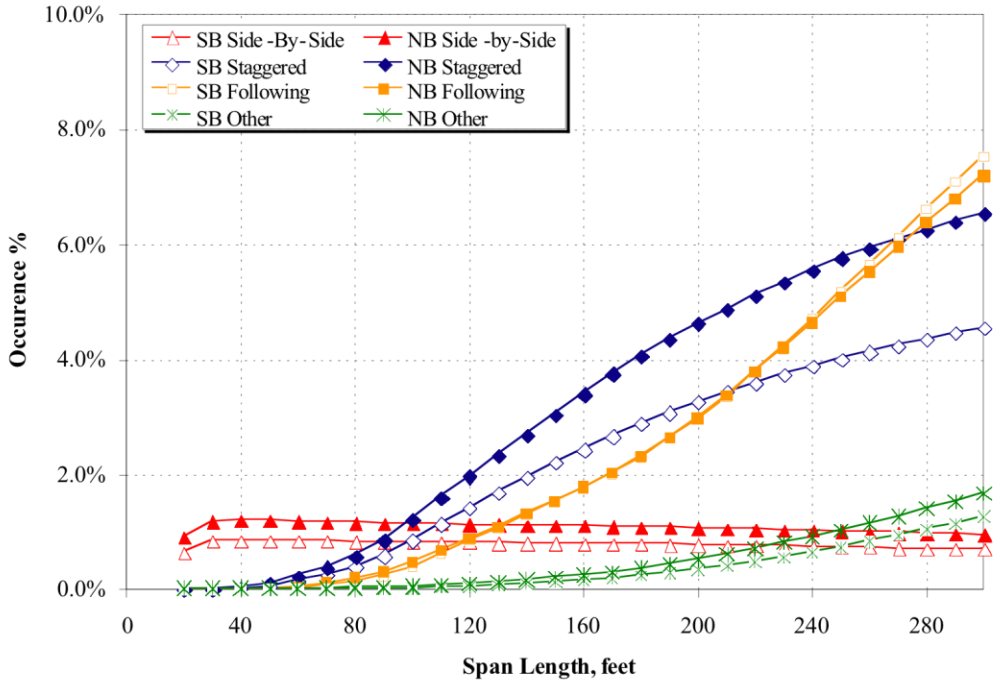

Figure 79. New Jersey WIM Site 287: MP statistics by span for northbound and southbound lanes

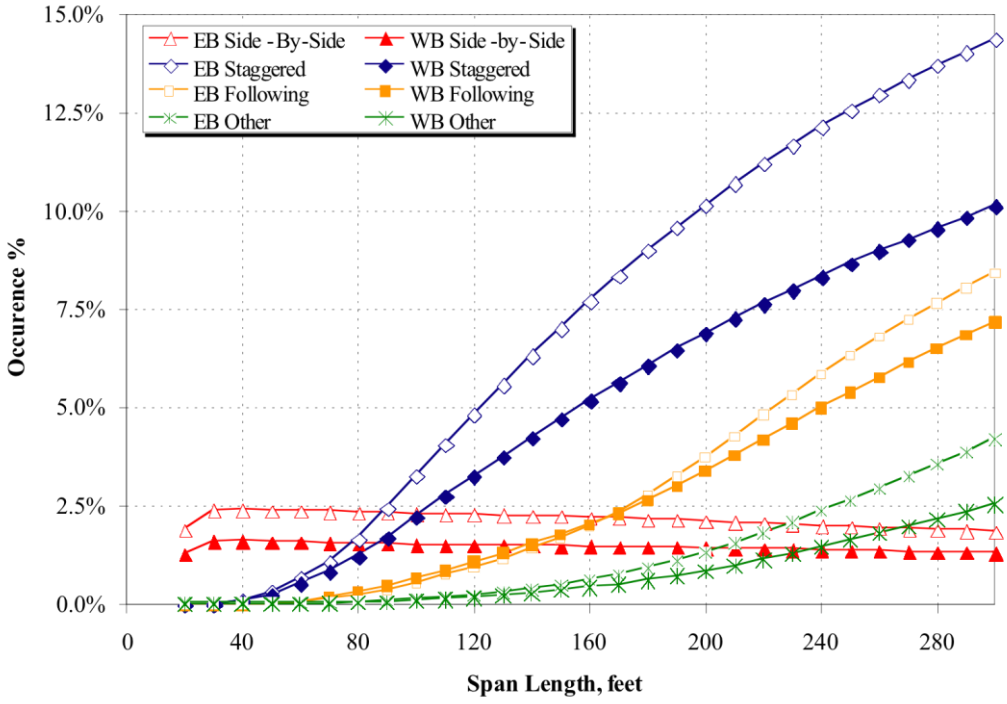

Figure 80. New Jersey WIM Site 80R: MP statistics by span for eastbound and westbound lanes

Events Involving Two Heavy Trucks

The following analysis is a breakdown of the MP results in terms of the weights of each truck involved. These “heavy-heavy” plots represent the portion of the general MP results where each truck weight is equal to or greater than the given threshold weight. Most trucks involved in a MP event are “light” (weighing less than 60 kips each). To determine the maximum expected load event in 75 years, information is needed about the two heaviest trucks that are expected to occur together as two trucks following, side-by-side, or staggered. The percent occurrence for the “heavy-heavy” MP plots represents a subset of the MP events in which each truck weight is equal to or greater than the threshold weight. Recall that the LRFD code assumption for overall side-by-side trucks was 6.67 percent (Nowak 1999). The assumptions further state that 3.3 percent of these side-by-side events involve two trucks that are heavy. WIM data was analyzed to compare the frequency of two heavy trucks occurring in various MP configurations to verify the code assumptions.

Heavy MP Statistics for Doremus Avenue Bridge

The “heavy-heavy” statistics for side-by-side, staggered, and following are shown in Figure 81, Figure 82, and Figure 83, respectively. Each figure contains curves for each direction: northbound (Lanes 1 & 2) and southbound (Lanes 3 & 4). Figure 81 shows the proportion of side-by-side events where the GVW of each truck involved is greater than or equal to the threshold weight. It is shown that most side-by-side events, about 97 percent, involve two trucks each weighing less than 60 kips. The most extreme side-by-side event for the Doremus Avenue Bridge involved two trucks, each weighing 92 kips, in the southbound lanes. Extreme side-by-side events are rare considering only 0.8 to 1.2 percent of trucks occur side by side, and that less than 0.1 percent of these cases involve two trucks weighing more than 90 kips. The heaviest occurrences of side-by-side (Figure 81) and stagger (Figure 82) occurred in the southbound lanes. As stated earlier, the southbound lanes have a higher average weight or are more frequently traveled by the dominant Class 9 trucks than the northbound lanes. As the overall truck population is heavier southbound, heavier MP events are expected in that direction.

The data in Figure 83 show that very few heavy trucks are involved in following events at the Doremus Avenue Bridge. The most extreme following event involved two northbound trucks, each weighing at least 82 kip.

Detailed counts for each of the extreme MP cases are listed in Table 13. The heavy-heavy counts listed are used along with the total number of base events to calculate the percent occurrence of extreme MP events.

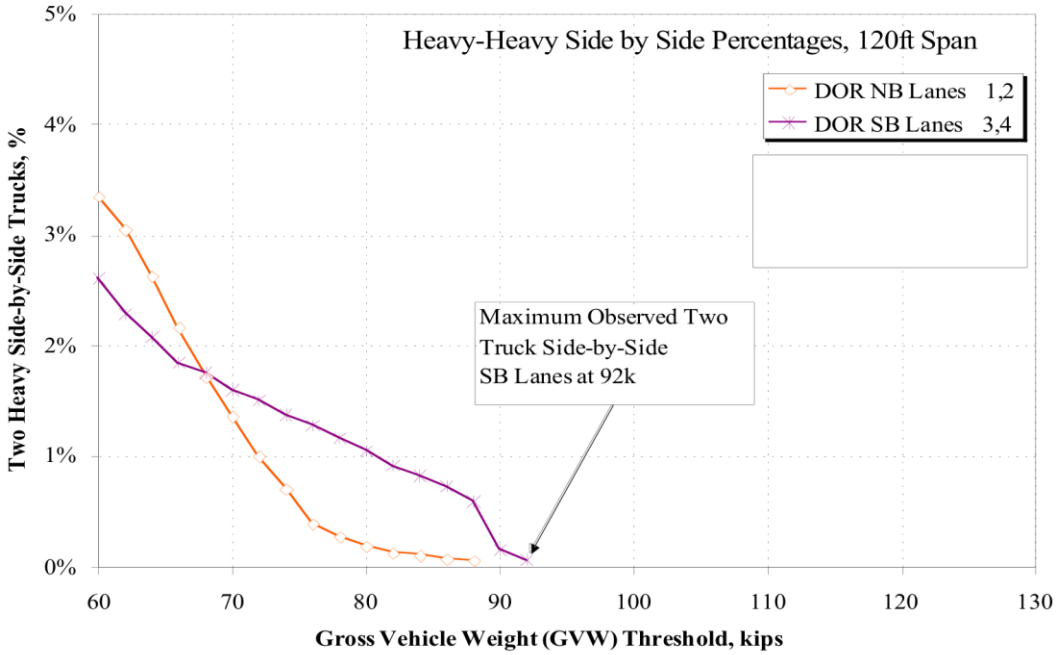

Figure 81. Doremus Avenue Bridge: variation of side-by-side event statistics for two heavy trucks using different “heavy” weight thresholds for a span of 120 ft

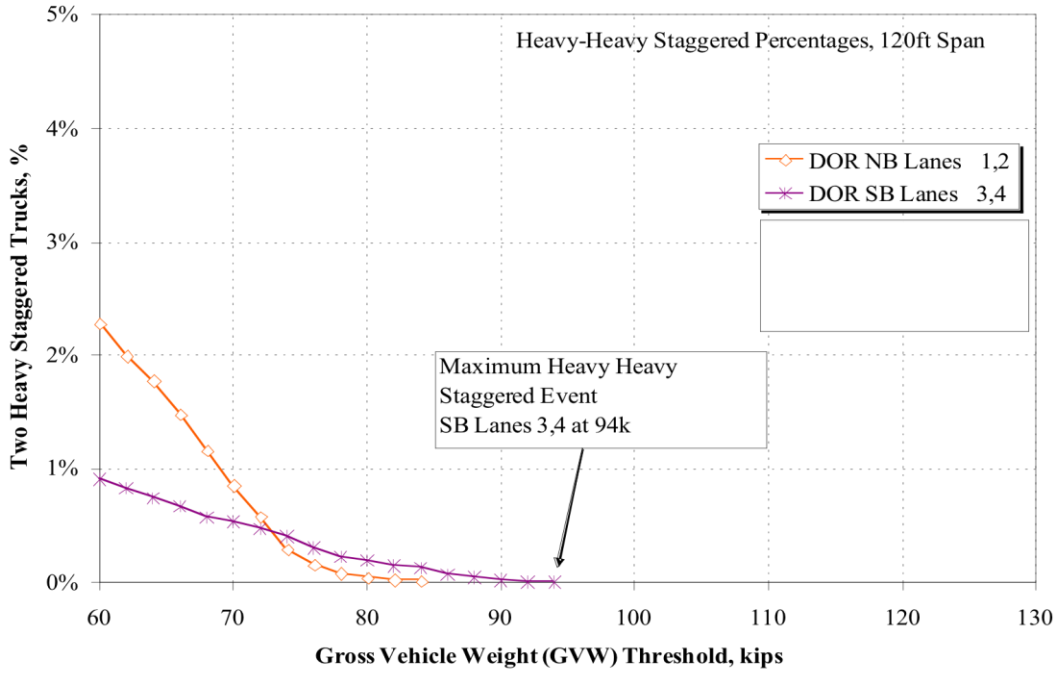

Figure 82. Doremus Avenue Bridge: variation of staggered event statistics for two heavy trucks using different “heavy” weight thresholds for a span of 120 ft

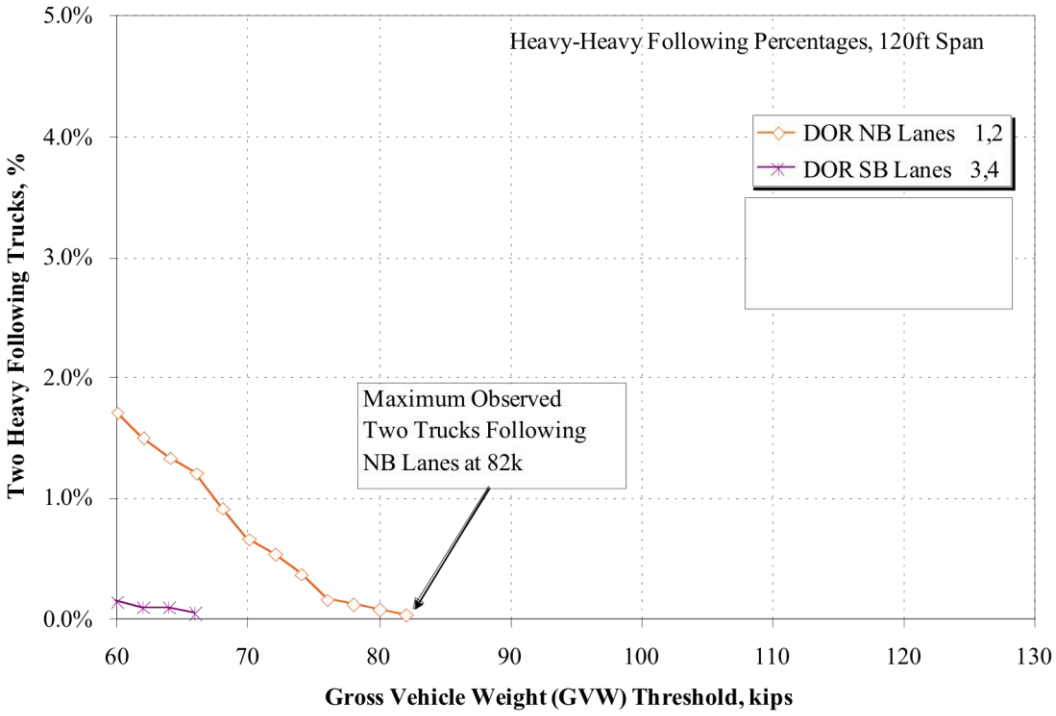

Figure 83. Doremus Avenue Bridge: variation of following event statistics for two heavy trucks using different "heavy" weight thresholds for a span of 120 ft

Table 13. Doremus Avenue Bridge: summary of MP events involving two heavy trucks of different weight

120ft Span	Heavy Side-by-Side		Heavy Staggered		Heavy Following	
Threshold GVW, k	Doremus Lanes 1,2	Doremus Lanes 3,4	Doremus Lanes 1,2	Doremus Lanes 3,4	Doremus Lanes 1,2	Doremus Lanes 3,4
60	204	114	412	134	41	3
62	186	100	360	122	36	2
64	160	91	321	110	32	2
66	132	81	267	99	29	1
68	105	77	210	85	22	
70	83	70	155	79	16	
72	61	66	105	70	13	
74	43	60	53	60	9	
76	24	56	29	45	4	
78	17	51	15	33	3	
80	12	46	8	29	2	
82	8	40	5	22	1	
84	7	36	3	19		
86	5	32		11		
88	4	26		7		
90		7		3		
92		3		1		
94				1		
Total Base Events	**6087**	**4372**	**18027**	**14698**	**2389**	**2085**
Maximum Obs. Wt(k)	**88**	**92**	**84**	**94**	**82**	**66**

Heavy MP Statistics for New Jersey WIM Site 287

Similarly, variation of side-by-side, following, and staggered event statistics for two heavy trucks for NJ WIM Site 287 is presented in Figure 84, Figure 85, and Figure 86, respectively. Table 14 provides a summary of MP events involving two heavy trucks for this NJ site.

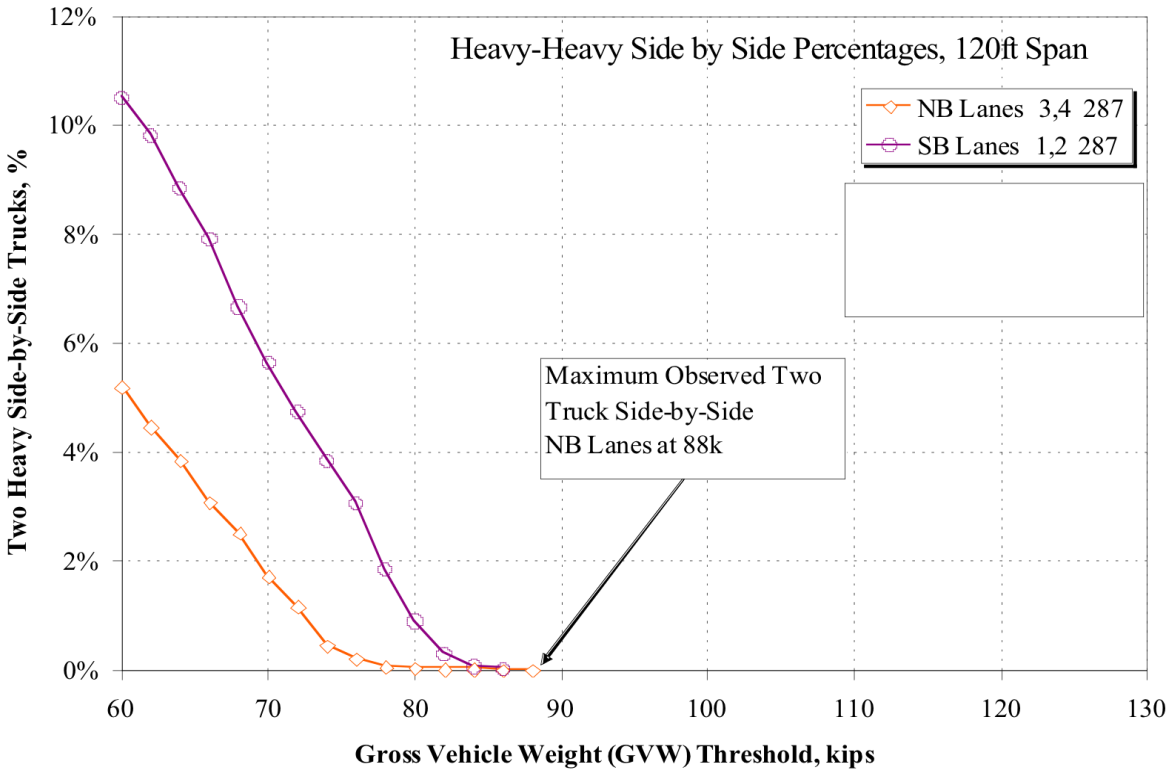

Figure 84. New Jersey WIM Site 287: variation of side-by-side event statistics for two heavy trucks using different “heavy” weight thresholds for a span of 120 ft

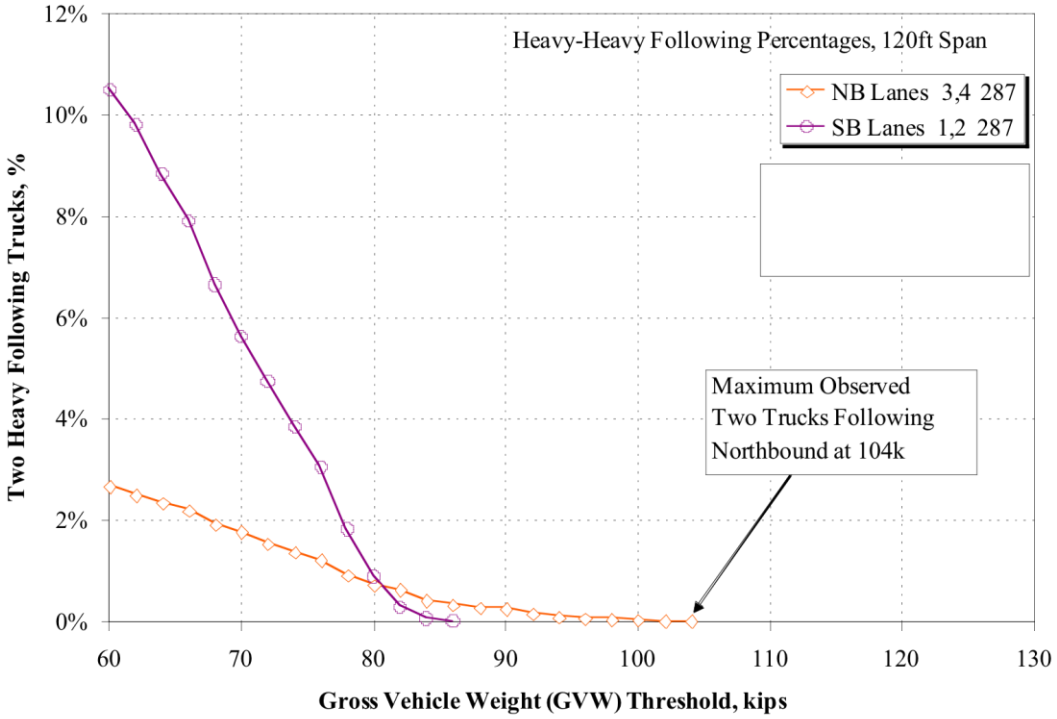

Figure 85. New Jersey WIM Site 287: variation of following event statistics for two heavy trucks using different “heavy” weight thresholds for a span of 120 ft

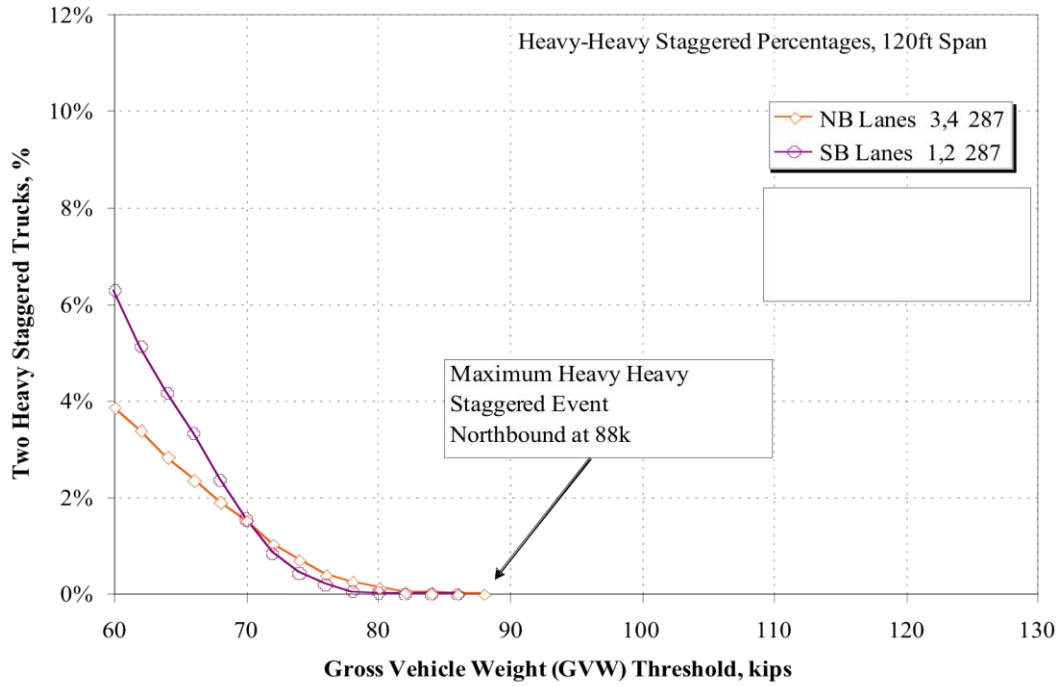

Figure 86. New Jersey WIM Site 287: variation of staggered event statistics for two heavy trucks using different “heavy” weight thresholds for a span of 120 ft

Table 14. New Jersey WIM Site 287: summary of MP events involving two heavy trucks at different weight thresholds

120ft Span Threshold GVW, k	Heavy Side-by-Side Site 287 SB LN 1,2	Heavy Side-by-Side Site 287 NB LN 3,4	Heavy Staggered Site 287 SB LN 1,2	Heavy Staggered Site 287 NB LN 3,4	Heavy Following Site 287 SB LN 1,2	Heavy Following Site 287 NB LN 3,4
60	267	633	344	790	142	597
62	229	517	302	642	133	558
64	198	414	253	523	125	502
66	158	314	211	418	117	450
68	129	231	171	298	102	378
70	88	158	136	196	94	320
72	60	90	93	108	82	269
74	23	46	65	56	73	219
76	11	15	37	26	65	174
78	3	2	24	7	49	104
80	2	1	13	3	39	51
82	1	1	5	1	34	17
84	1		3	1	23	4
86			1	1	18	1
88			1		15	
90					14	
92					9	
94					5	
96					4	
98					3	
100					2	
102					1	
104					1	
106						
Total Base Events	**5132**	**7232**	**8867**	**12529**	**5304**	**5680**
Maximum Obs. Wt(k)	**84**	**82**	**88**	**86**	**104**	**86**

Heavy MP Statistics for New Jersey WIM Site 80R

Similarly, Figure 87, Figure 88, and Figure 89 show variations of side-by-side, following, and staggered statistical events for NJ WIM Site 80R, respectively.
Table 15 shows a summary of MP events involving two heavy trucks at varying weight thresholds for Site 80R.

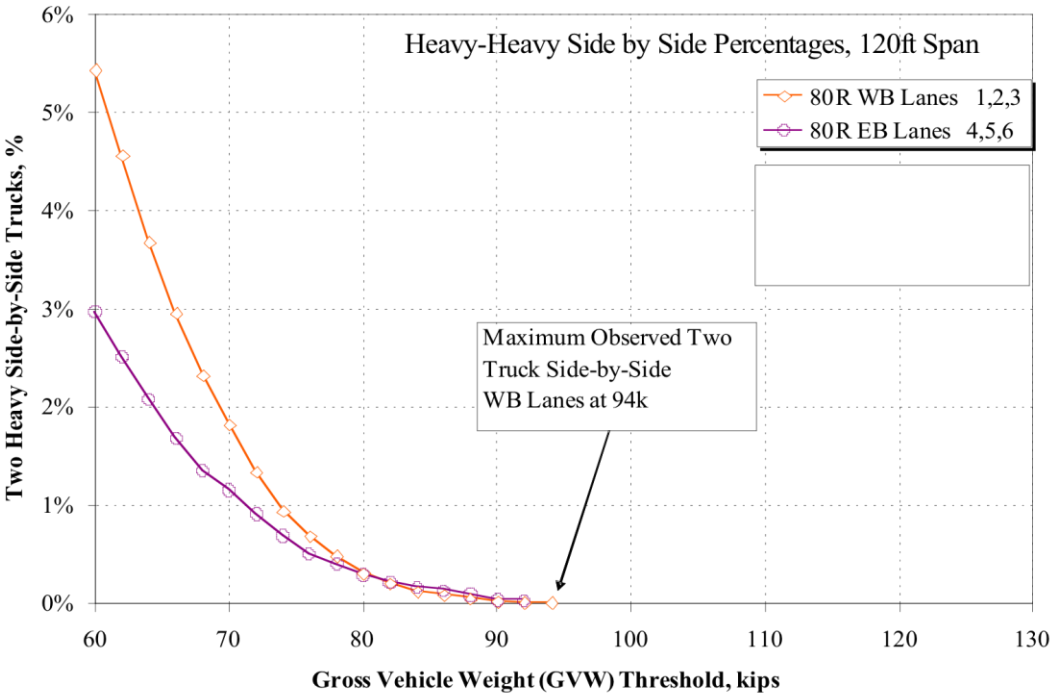

Figure 87. New Jersey WIM Site 80R: variation of side-by-side event statistics for two heavy trucks using different “heavy” weight thresholds for a span of 120 ft

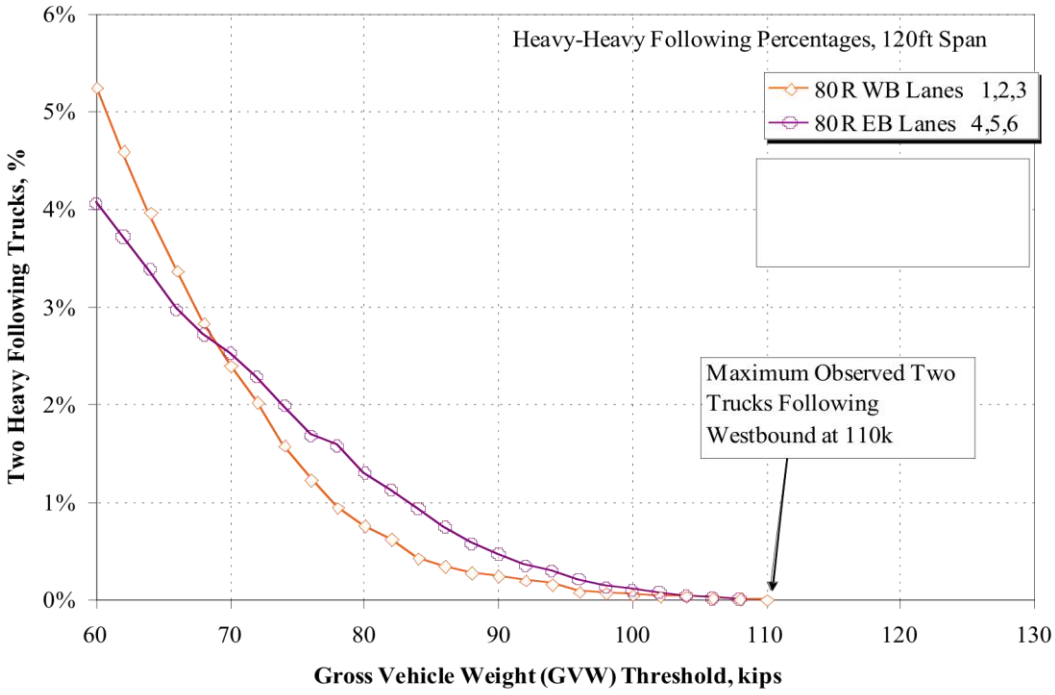

Figure 88. New Jersey WIM Site 80R: variation of following event statistics for two heavy trucks using different “heavy” weight thresholds for a span of 120 ft

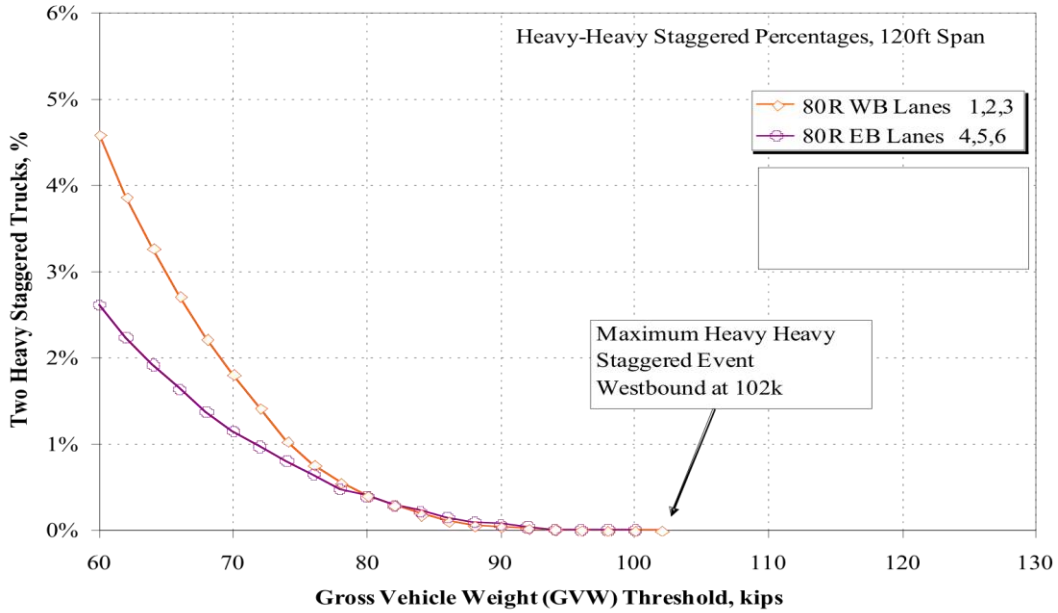

Figure 89. New Jersey WIM Site 80R: variation of staggered event statistics for two heavy trucks using different "heavy" weight thresholds for a span of 120 ft.

Table 15. New Jersey WIM Site 80R: summary of MP events involving two heavy trucks at different weight thresholds

120ft Span Threshold GVW, k	Heavy Side-by-Side Site 80R WB LN 1,2,3	Heavy Side-by-Side Site 80R EB LN 4,5,6	Heavy Staggered Site 80R WB LN 1,2,3	Heavy Staggered Site 80R EB LN 4,5,6	Heavy Following Site 80R WB LN 1,2,3	Heavy Following Site 80R EB LN 4,5,6
60	965	427	1727	811	1101	419
62	810	361	1454	695	963	384
64	654	299	1233	596	831	349
66	525	242	1023	509	707	307
68	412	194	836	427	595	281
70	324	166	682	356	503	260
72	238	131	535	302	425	235
74	168	99	390	251	332	205
76	123	73	287	201	259	174
78	87	58	208	148	200	163
80	55	42	152	123	161	134
82	37	31	111	91	132	116
84	22	24	71	71	91	97
86	16	19	41	47	74	77
88	9	12	23	31	60	60
90	3	5	16	22	52	49
92	1	4	10	13	43	37
94	1		6	5	35	31
96			3	2	18	22
98			2	2	15	14
100			2	2	10	10
102			2		8	8
104					8	4
106					5	2
108					2	1
110					1	
Total Base Events	**17735**	**14361**	**37574**	**31022**	**20950**	**10312**
Max Obs Wts (k)	**94**	**92**	**102**	**100**	**110**	**108**

Live Load Effects: Moments and Shears by Span Length

When designing or evaluating structures, the loads are first identified and then their effects are quantified. In live-load calibration, the bridge response is the underlying design factor—i.e., moments, shears, stresses, and deflections rather than truck weight. As every truck is unique in terms of configuration and axle loads, weight alone does not accurately describe the demand on a structure. The distribution of the weight must also be taken into account. Consider two trucks of equal gross weight *W*. One truck has five axles and overall length *L*. The other truck has five axles and an overall length of 1.5*L*. The two trucks have identical weights; however, it is clear that the shorter truck will cause a higher moment and shear on a given span than the longer truck. This point is evident when considering permit loads. A typical permit truck weighs much more than a legal truck. The main differentiation is that a permit configuration distributes the load over more axles and a longer distance. The opposite is true of certain fixed-load vehicles or mobile cranes. The crane configuration is often compact, with heavy axles causing a higher moment than similar configurations with similar weight. Nonetheless, permits and crane configurations are removed from the general truck data for calibration. When evaluating the effect of live load, the moment or shear demand of each truck must be considered. The load effects, specifically the moment or shears acting on specific members, are of the utmost interest.

The next section presents the moment and shear demands caused by the site-specific WIM data. The load effects are given in terms of a design load bias. Data from the Doremus Avenue Bridge WIM site operated by Rutgers University and New Jersey WIM stations, owned and operated by NJDOT were analyzed for their effect on the LRFD load factors. The following section presents the results of the load effect analysis using these site-specific WIM data sets. The observed and predicted data for simple moment based on the New Jersey WIM data are presented for the following New Jersey sites: 78B, 78D, 80R, 195, 287, A87, DOR12, DOR34, and DRM. These sites were selected for detailed analysis due to their proximity to the Port of Newark and their function as major truck routes in the greater New York metropolitan area.

Simple Moment: New Jersey WIM Data

Figure 90 displays the mean of the upper tail observing simple-span moments by span length based on the New Jersey WIM data subset. The upper tail is defined as the uppermost linear portion of the load effect data as plotted on the NPP. The upper tail mean simple-span moment for all the New Jersey WIM sites follows a similar trend. This is expected as each site is part of the same regional highway network and contains much of the same truck traffic. A common characteristic of the upper tail mean moments is that there were higher moment ratios for shorter spans. This is due to heavy, single, or groups of closely spaced axles acting on a short span. The HS20 design moment for short spans is governed by the design tandem pair of axles. The remaining shape of the plot is dictated by the truck configuration relative to the span length. For spans more

than 140 ft, the HS20 distributed lane loading controlled. The upper tail moments decrease linearly with larger spans more than 140 ft because the lane load moment was significantly greater than the single truck moment.

The plot in Figure 90 shows very large value of simple-span moment on the 20-ft span for the Doremus Avenue Bridge site. Initially, this aberration was thought to be an error in the WIM data. All processed WIM data was filtered to remove obvious data errors and impractical values of weights and axle spacings as well as permits. Further investigation revealed that the southbound lanes contained a number of overweight four-axle single-unit trucks (Figure 91) with axle weights of 14, 16, 38, and 38 kips for axles 1, 2, 3, and 4, respectively. The axle spacings for a typical truck are 17, 3.7, and 4 ft. This truck configuration contains three axles totaling more than 92 kips within a distance of 7.7 ft. The resulting moment on a 20-ft simple span is nearly equivalent to a single point load of 92 kips. When compared with the design values for the HS20, the moment ratio becomes 2.35 times HS20. Since these short, heavy vehicles are not permitted vehicles and do not contain obvious errors in weight or configuration, they must be included in the analysis. Their effect is most pronounced in the shorter spans because of the closely spaced heavy axles. In longer spans, their distinction is lost to longer, heavier semitrailer trucks. Heavy single axles are of special concern for pavement design, where a high concentration of load will cause severe rutting and cracking.

Figure 92 presents the coefficient of variation of upper tail moment for simple span, whereas Figure 93 shows the 75-year predicted moment ratio for NJ WIM sites. Similarly, the upper tail mean shear ratio and coefficient of variation, is shown in Figure 94 and Figure 95, respectively. Upper tail mean maximum negative moment ratio by span length and coefficient of variation is presented in Figure 96 and Figure 97, respectively. The 75-year predicated negative moment ratio is given in Figure 98.

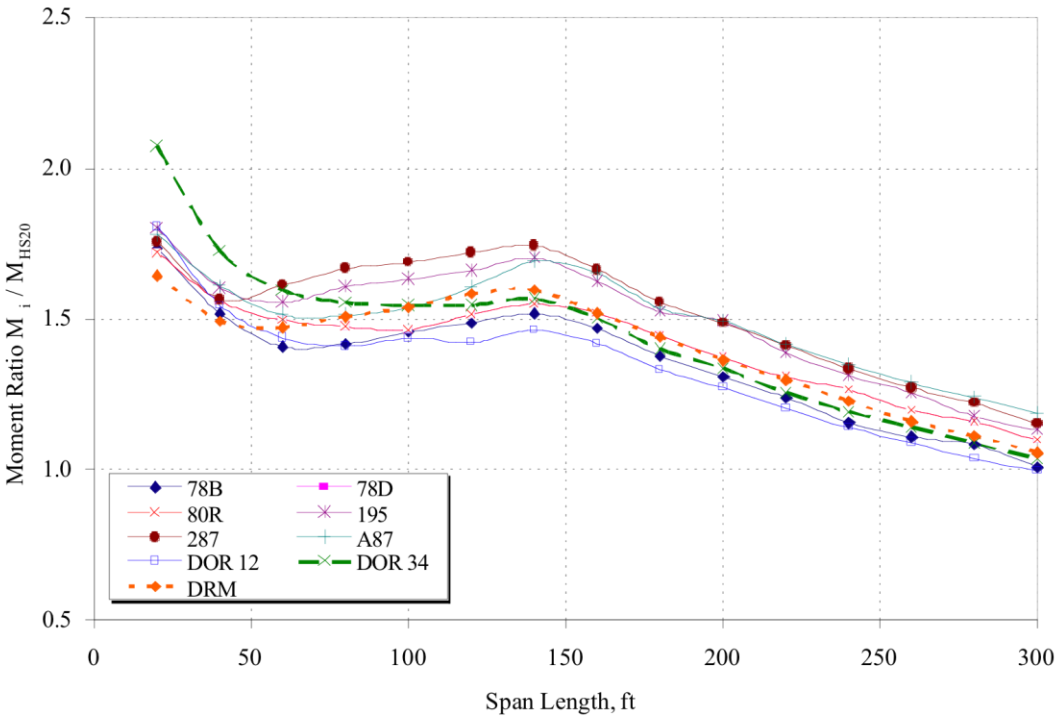

Figure 90. Upper tail mean moment ratio by simple span length for New Jersey WIM sites

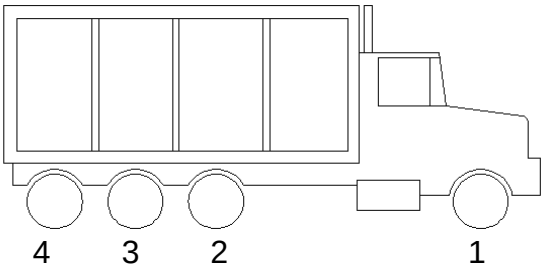

4-axle Single Unit Heavy Trucks			
W 1, k	13.4	S1, ft	15.3
W 2, k	20.8	S2, ft	3.6
W 3, k	39.8	S3, ft	4.1
W 4, k	37.6		
Total W, k	111.6		

Figure 91. Characteristics of short, heavy truck observed at the Doremus Avenue Bridge WIM site

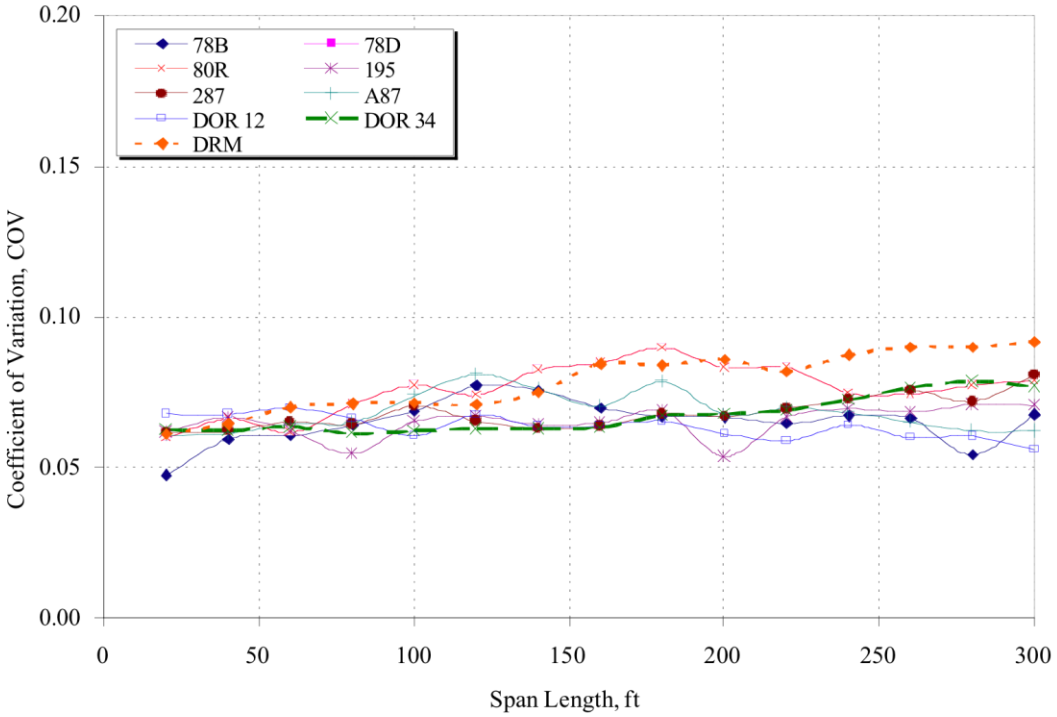

Figure 92. COV of upper tail moment by simple span for New Jersey WIM Sites

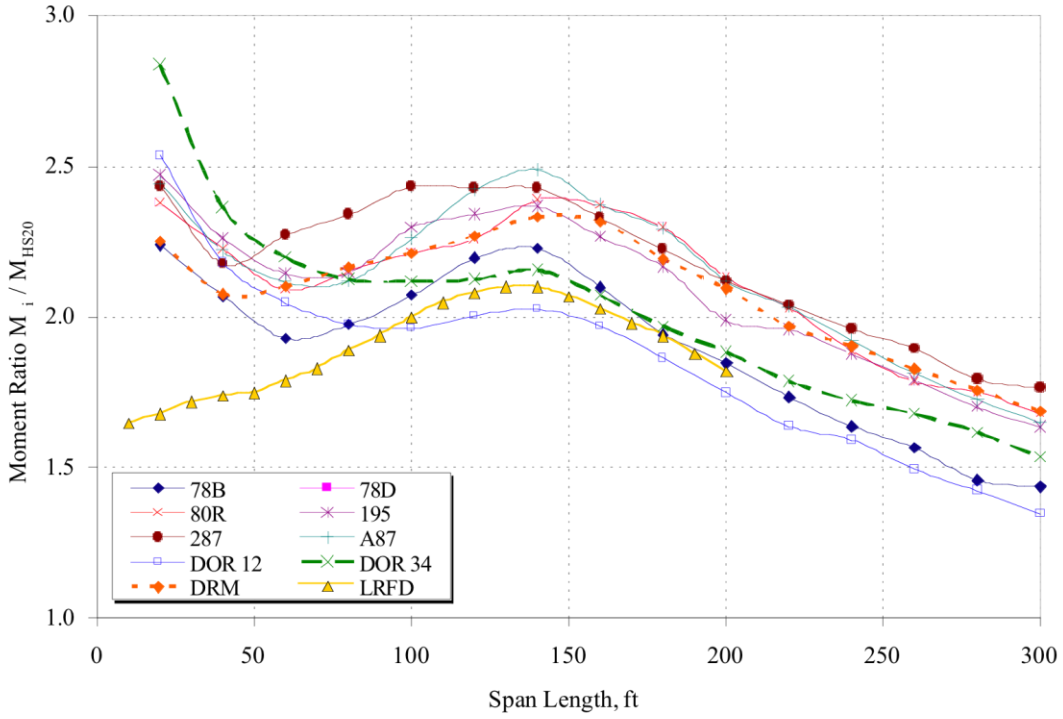

Figure 93. Seventy-five-year predicted moment ratio by simple span for New Jersey WIM sites

Simple Shear: New Jersey WIM Data

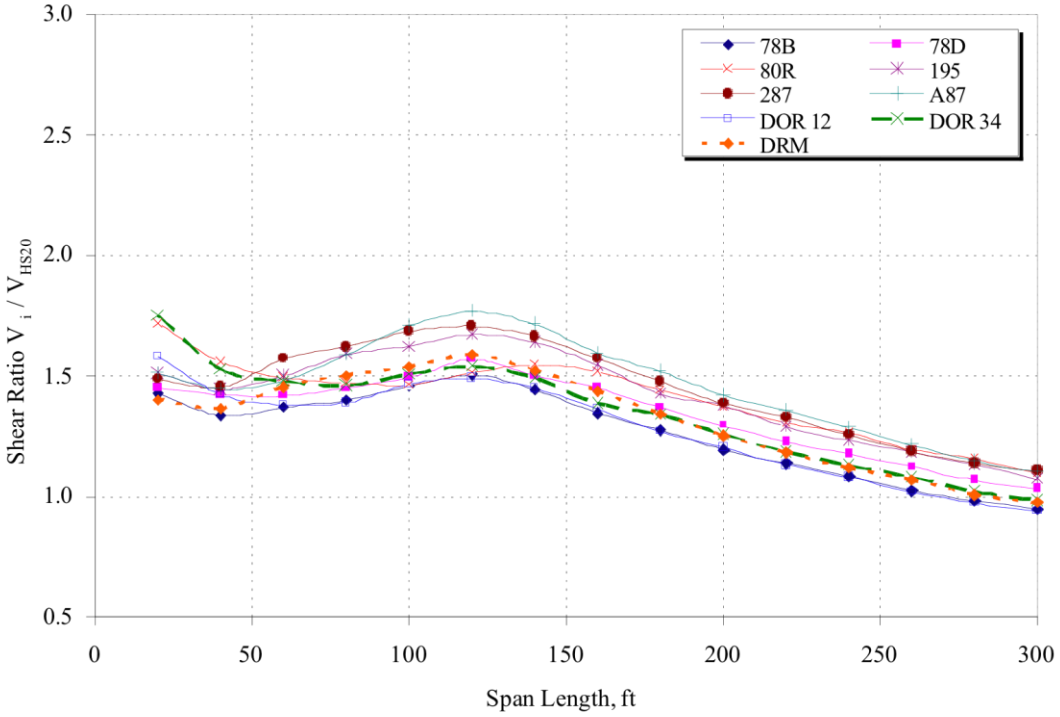

Figure 94. Upper tail mean shear ratio by simple span length for New Jersey WIM sites

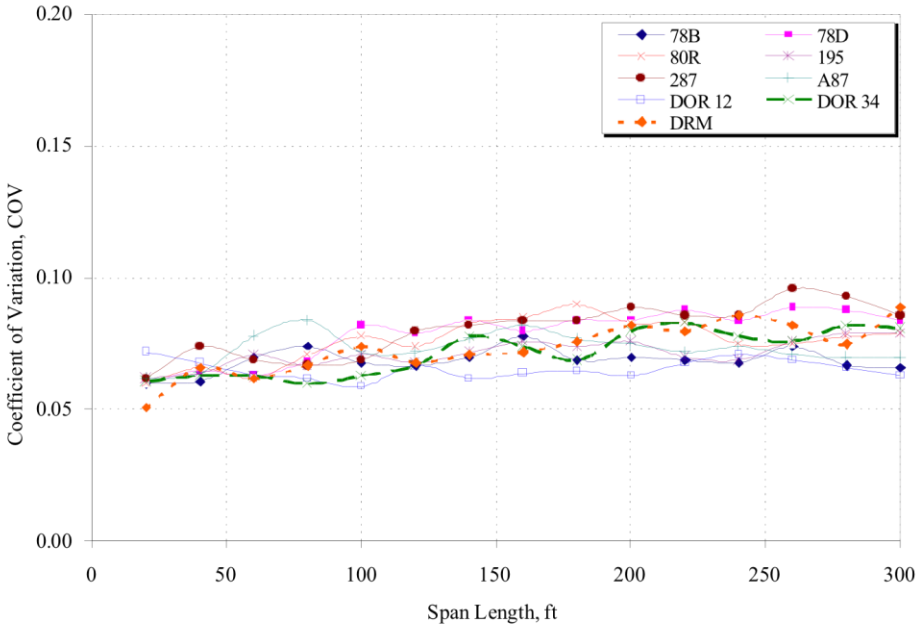

Figure 95. COV of upper tail shear by simple span for New Jersey WIM sites

Maximum Negative Moment on Two Continuous Spans: New Jersey WIM Data

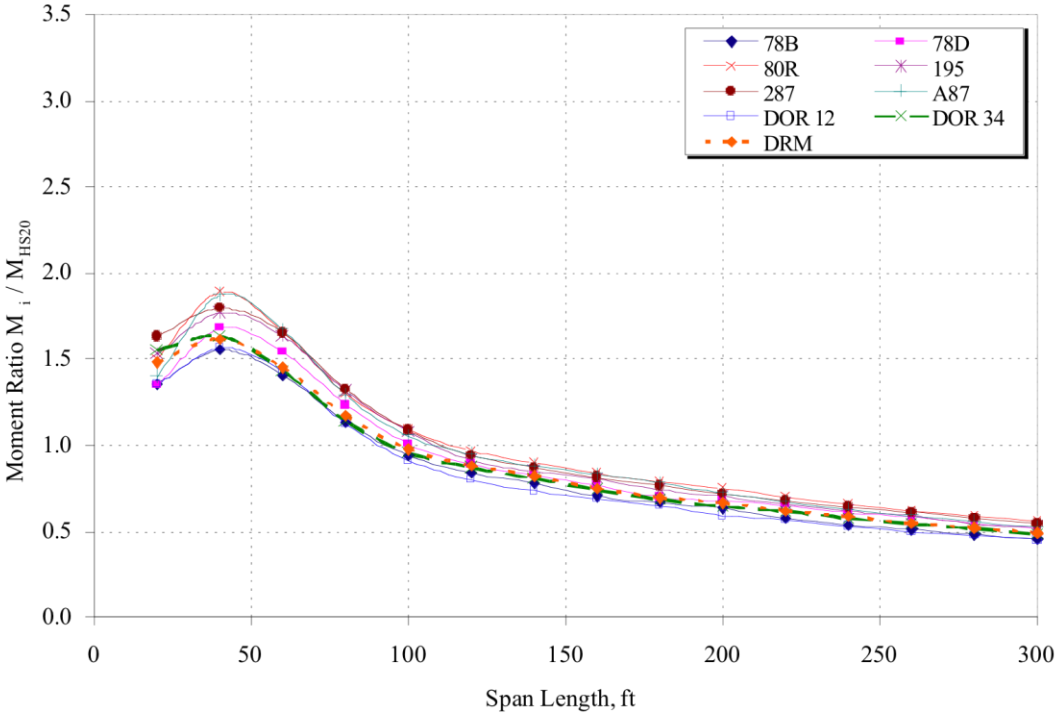

Figure 96. Upper tail mean maximum negative moment ratio by span length for New Jersey WIM sites

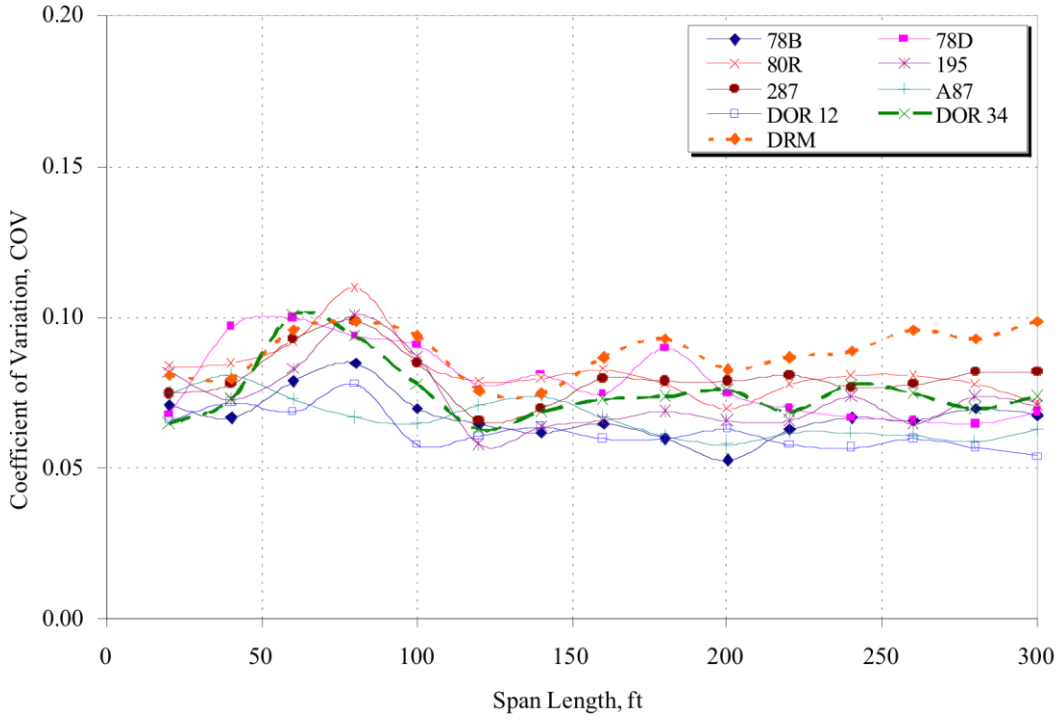

Figure 97. COV of upper tail negative moment by span for New Jersey WIM sites

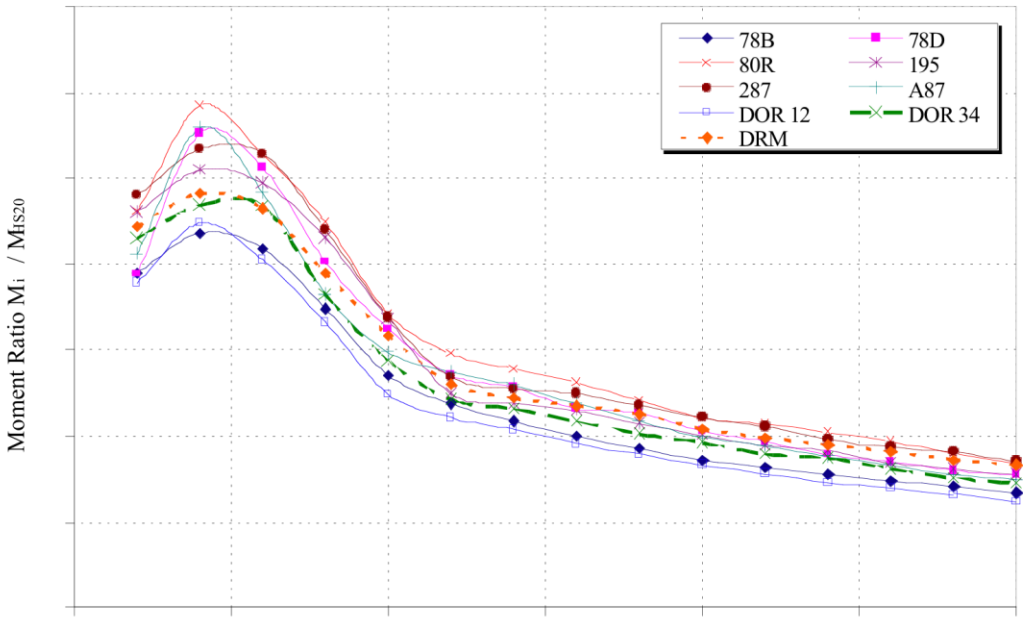

Figure 98. Seventy-five-year predicted negative moment ratio by span for New Jersey WIM sites

FATIGUE

Literature Review

In 1985, NCHRP Project 12-28, “Fatigue Evaluation Procedures for Steel Bridges,” was initiated. The goal of the principle investigators—Moses, Schilling, and Raju—was to develop fatigue design procedures that more accurately reflected fatigue-loading conditions. Probabilistic techniques were employed to ensure consistent levels of reliability. Also included in the recommendations was a means for evaluating existing bridges. A quantitative means of assessing remaining life was developed. Additionally, there were guidelines for engineers to develop site-specific fatigue design loads and account for future traffic volumes. New factors for load distribution, impact, truck superposition, and cycles per truck were introduced. Factors were developed to represent the typical or average effect of truck loading. Fatigue design was differentiated from static (ultimate) limit state design. Whereas exceeding the ultimate limit state would result in structural collapse, exceeding the fatigue limit state would simply result in a shortened life of the structural component. Corrective actions could be taken to extend the life or replace the structure before serious damage occurs. The end result of the shift from ultimate to a more tolerant limit state would be a more realistic, cost-efficient design philosophy.

The basis for the welded details needed in fatigue design was developed from laboratory testing of bridge elements. The tests conducted by Keating and Fisher (1985) were done for different samples at constant amplitude stress (*S*) ranges. The cycles to failure (*N*) were plotted on a representative *S*-*N* curve. There was significant scatter of the data; therefore, the allowable stress ranges were defined as two standard deviations below the mean stress. The current design *S*-*N* curves approximate the lower 95 percent confidence limits from test results. The mean *S*-*N* curves, therefore, provide a higher number of cycles.

Extensive work has been done on field-testing of bridges to determine remaining fatigue life. For the most part, the investigator installs strain gauges to key fatigue-prone detail locations on a bridge structure and monitors strain and stress levels for a given period of time. The cumulative damage is calculated based on Miner's rule, and along with the ADTT for the location, the fatigue life is calculated based on the recommendations of Moses et al. (1987) The remaining fatigue life is simply the total life minus the current service life of the structure.

Hahin, South, Mohammadi, and Polepeddi (1993) applied the new fatigue evaluation procedures proposed by Moses et al. to numerous bridges in Illinois. The experimental program consisted of instrumenting 15 representative steel bridges with strain gauges and monitoring stresses at critical details over a 3 to 8 hour period. Stress cycles were collected by using rainflow techniques. Stress cycles below 0.5 ksi were discarded as noise, and were considered a negligible contribution to fatigue damage. Short-term data were linearly extrapolated to a 24-hour period. Miner's Rule of linear damage accumulation was used along with fatigue strength coefficients and exponents based on the Munse et al. 50 percent mean data for structural details, given by:

$$N = c(S)^m \qquad \text{Eq. (20)}$$

where *S* is stress range (ksi), *c* is fatigue strength coefficient, *m* is fatigue strength exponent, and *N* is number of cycles to major crack formation or failure. The daily damage caused by truck traffic was also computed. Truck volume information was provided by the Illinois Department of Transportation. No indication was made of the truck weight distributions or superposition. Stress range cycles were linearly projected by multiplying the daily data out to 25 years. No consideration was made with regard to variability of the stress range cycles. The authors, however, do make provisions to account for truck volume and weight increases by compounding the number of cycles annually and increasing the stress magnitudes, respectively. The authors conclude that by increasing the truck weights 10 percent once and the truck volume 5 percent annually, fatigue damage becomes 4.5 times greater than with no volume or weight change over 25 years. The study is comprehensive with regard to the number of structures instrumented; however, little is known about the truck load spectra. Furthermore, only 3 to 8 hours of monitoring at three or four superstructure locations

was conducted for each site. Additional monitoring is needed to verify the assumption that the short test durations represent a typical day of loading. Also, additional gauge locations could have been added to determine load distributions for use in computer modeling of similar structures.

A subsequent study by Mohammadi, Guralnick, and Polepeddi (1998) incorporated more probabilistic treatment of fatigue damage. A beta distribution is assumed for the stress range, and a Weibull distribution is assumed for the fatigue resistance (Ang and Tang 1975). Different fatigue reliability target levels are 97.7 and 99.9 percent for redundant and nonredundant members, respectively. The bridge is said to have failed in fatigue when the sum of the Miner's Rule has reached unity. The authors express the expected damage as a statistical term:

$$E(D) = \int_0^{S_{max}} \frac{\overline{n}}{N(s)} f(s)ds \qquad \text{Eq. (21)}$$

where S is the stress range expressed as a continuous random variable with $f(s)$ as a probability density function and is the average number of cycles for all ranges, given by:

$$\overline{n} = \frac{c}{\int_0^{S_{max}} S^m f(s)ds} \qquad \text{Eq. (22)}$$

where c and m are empirical constants (Ang and Munse 1975). Finally, the fatigue reliability is expressed using Ang and Munse's (1975) equation:

$$L(n) = \exp\left\{-\left[\frac{\overline{n}}{n}\Gamma(1+\alpha)\right]^{1/\alpha}\right\} \qquad \text{Eq. (23)}$$

where $L(n)$ is fatigue reliability, Γ is gamma function, α is $\Omega^{1.08}$, Ω is uncertainty of fatigue life (0.54 for sections with cover plates), and n is the total number of cycles. A traffic growth factor is implemented similar to that in the Hahin (1993) paper and fatigue lives are computed. Results are similar to the 1993 paper. Again, no consideration was given to the truck weight distributions.

Nowak, Nassif, and Frank (1993) published the findings of a fatigue evaluation of a steel bridge. The bridge under study was instrumented to determine the remaining fatigue life. Strain gauges were installed so that fatigue critical members were monitored. Additionally, all girders in one span were instrumented to determine the load distribution. This was found to be crucial in understanding the actual versus assumed load distribution. Analytical results showed high stresses in the exterior girders, making those members most fatigue critical. However, the measured stresses were much less

than the calculated stresses. Sensors indicated that the connection of the floor beams to the exterior girder was behaving like a fixed-moment connection. Furthermore, the floor beam was responding as a beam fixed against rotation, but undergoing a relative displacement between the supports at the exterior and first interior girders.

After instrumenting the structure, test runs were conducted with a calibration truck of known weight. Knowing the truck gross weight and axle weight distribution is essential when comparing the experimental and analytical results. Bridge stress range data were collected continuously by using rainflow techniques for two weeks. Meanwhile, the traffic was recorded for 24 hours with a video camera. The video was later reviewed to determine the truck volumes and superposition (multiple presence). The ADTT was determined to be 11,334 in both directions, where less than 10 percent of trucks used the leftmost lane, and approximately every 20th (3 percent) to 25th (4 percent) truck is on the bridge simultaneously with another truck moving side by side in the same direction. In a manner similar to that described by Hahin et al. (1993), a minimum stress threshold of 0.5 ksi was used to eliminate possible signal–noise error.

Information on truck volumes from the opening of the bridge as well as projections 20 years into the future was given. A full fatigue life assessment was then conducted. Given the historical load data, the authors calculated the fatigue damage accumulated up to the time of testing and extrapolated 20 years into the future, considering traffic volume growth. The authors concluded that, despite a 25 percent increase in truck volumes, the bridge would be free of major fatigue cracking for at least 30 additional years. The Nowak et al. (1993) fatigue study provided a more complete analysis giving the calibration runs and information on truck superposition. The distribution of truck weights would have made the study more comprehensive and would have provided an opportunity for computer simulation of stress cycles. This study provides an important contribution to the fatigue study of bridges by proposing the following major steps:

1. Review the available drawings. Identify fatigue-prone components and details on the basis of experience. Special attention should be paid to distortion-induced fatigue.
2. Perform analysis to determine the load spectra for main girders (load distribution factors) and fatigue-prone details.
3. Instrument the bridge and take WIM measurements. Measure stress ranges under normal traffic flow.
4. Verify the accuracy of analytical girder distribution factors by comparing the measured load distribution.
5. Verify the calculated stress ranges by comparison with measured values.
6. Establish the cumulative distribution functions for stress range.
7. Estimate the fatigue resistance of the critical components and details.
8. Evaluate the fatigue performance of critical components by comparison of load and resistance.
9. Estimate the remaining fatigue life.

Laman and Nowak (1996) examined the truck weight distribution and stress response of five bridge sites in Michigan. The goal was to show the site-specific nature of truck loads and develop a representative fatigue load model. The bridges were instrumented with strain gauges and a WIM system. For each site, a truck of known weight was used to calibrate the sensors. Strain range cycles were collected for up to 3 weeks per site using the rainflow method.

The authors recommend the use of WIM systems as opposed to weigh station data for gathering truck weight distributions. It was found that the heaviest trucks were traveling on busy Interstate highways far from weigh stations (Laman 1996). The truck weight distribution was found to be strongly site specific. The difference between the highest and the lowest median value was approximately 40 percent, and the variation for the extreme GVW values was 100 percent. The equivalent truck weight ranged from 62.4 to 78 kips for the five locations.

It was found that 40 to 80 percent of the truck population was five-axle trucks. Furthermore, vehicles with three and four axles were configured similar to five-axle vehicles. When vehicles of similar configurations are grouped together, they represented 55 to 95 percent of the truck population.

The effect of span length on the number of cycles was also investigated. The number of cycles is much higher for shorter span bridges. This means that a bridge with a 15- to 30-ft span may experience two or more stress cycles per truck passage, accelerating the fatigue damage.

The primary conclusion of the study was the proposal of two fatigue design trucks: one three-axle truck and a four-axle truck. The fatigue damage would be assessed based on the fraction of 11-axle trucks and all other trucks by applying the four-axle and three-axle models, respectively. The primary contribution of this study was that truck weight distributions are strongly site specific. The truck records collected during the field monitoring were later entered into a simulation to determine the actual fatigue damage. The final fatigue models were also simulated across the bridges and compared with the actual truck fatigue. A comprehensive fatigue damage study includes the distribution of vehicle weights and types.

Bridge Monitoring for Fatigue

Evaluation of existing bridges for fatigue performance is important in the effort to address deteriorating infrastructure. The effort to prioritize bridge repair and rehabilitation options will highly depend on the identification of live loads and their

effects. Bridge live-load effects vary for different components and structural details. In many cases, analytical methods do not allow for an accurate estimation of load, in particular the load distribution and actual stress ranges. Structural health monitoring and field-testing can be very effective in evaluating bridge performance at the serviceability limits.

Field measurement of in-service structures is costly in terms of time and money. It is not practical to dedicate testing equipment to a single bridge for a long period of time. However, longer measurement periods yield a more complete picture of the load spectra. The ever-present question is: How long does one need to measure to accurately predict future fatigue damage? Moreover, prediction methods can be misleading if they are not based on rational and tested procedures. Therefore, there is a need to establish procedures for data collection and methods for reliable prediction of the remaining fatigue life of an existing bridge.

Knowing the complete load spectra for a bridge is an important aspect in fatigue prediction. To achieve the best description of the loading, one should monitor the structure for one year. The time-history data should contain the complete loading profile: stress ranges, number of cycles, times of occurrence, and mean cycle stresses. With the response of multiple sensors being recorded, the memory capacity of most data acquisition systems would be quickly exhausted. Thereafter, the time-history data collected is analyzed by using a rainflow counting algorithm to extract discrete stress cycles (ASTM E1049-85).

Although the complete time-history record is very useful, it is impractical and not necessary for fatigue evaluation. Fatigue damage depends only on the magnitude (stress range), number of respective cycles (at each range), and fatigue category for the detail in question. For complicated load histories, a representative means to convert variable amplitude signals to a count of closed-loop hysteresis was developed, termed rainflow cycle counting. The rainflow method of cycle counting, originally proposed by Matsuishi and Endo (1968), was analogous to rain falling down a pagoda roof. More recent cycle counting mechanisms are more efficient for real-time cycle counting (Socie and Downing 1982). Typically, rainflow data is stored in the stress-range-only format. The cycles are classified into a discrete number of categories, or bins, along with the number of cycles for each stress range. The stress-range-only format is the most compact in terms of data storage.

Experimental Program

More than 50 strain transducers were installed at various locations within the superstructure as indicated by the rectangles in Figure 99. The fatigue system consists of a Campbell CR9000 Datalogger connected to a total of 22 strain and 2 LVDT

deflection channels. A taut cable was installed from pier to pier in Span 3 to provide a reference for the LVDT mounted at the maximum moment position. The WIM system consists of the PAT DAW190 with two bending plates and one inductive loop per lane. The WIM and fatigue systems are linked via an RS422 serial connection. For each truck, the WIM system sends the vehicle information to the fatigue system. Therefore, the live loads and bridge stresses are known for each load event.

Traffic Data

Vehicle information including arrival time, lane, speed, axle weights, axle spacing, length, and class are stored by the WIM system for each truck. Figure **100** illustrates the daily vehicle count in all four lanes for a typical week comparing the Average Daily Traffic (ADT) and the Average Daily truck Traffic (ADTT). The WIM system has a real-time automated vehicle identification (AVI) port. For each identified truck, a stream of text data is generated and sent via a serial cable to the fatigue Datalogger. The WIMAVI data contains the same truck information as is contained in the WIM system, but also retains the timestamp to the nearest 1/100th second. Therefore, the position of a truck could be estimated with much greater accuracy than with a 1-second round off. For example, the position of a truck traveling at 72 km/h (45 mph) can be estimated to within ±20 m (66 ft) with a 1-second timestamp. The position of the same truck can be estimated to within 0.20 m (0.66 ft) with a 1/100th-second timestamp.

The weight distribution for the dominant truck type at the Doremus Avenue Bridge is illustrated in Figure 101. The Class 9—five-axle semi-trailer—accounts for more than 60 percent of all truck traffic at this location. The gross weight histogram shows two distinct peaks: empty and loaded. The empty population peaks at a weight of 20–25 kips. The loaded population peaks at a weight of 70–75 kips. Furthermore, the loaded and unloaded peaks for Lanes 3 and 4 southbound are greater than for the northbound direction. This indicates that heavier trucks are heading toward the port rather than out of the port on Doremus Avenue. It is possible that loaded trucks leaving the port use alternate routes such as the New Jersey Turnpike.

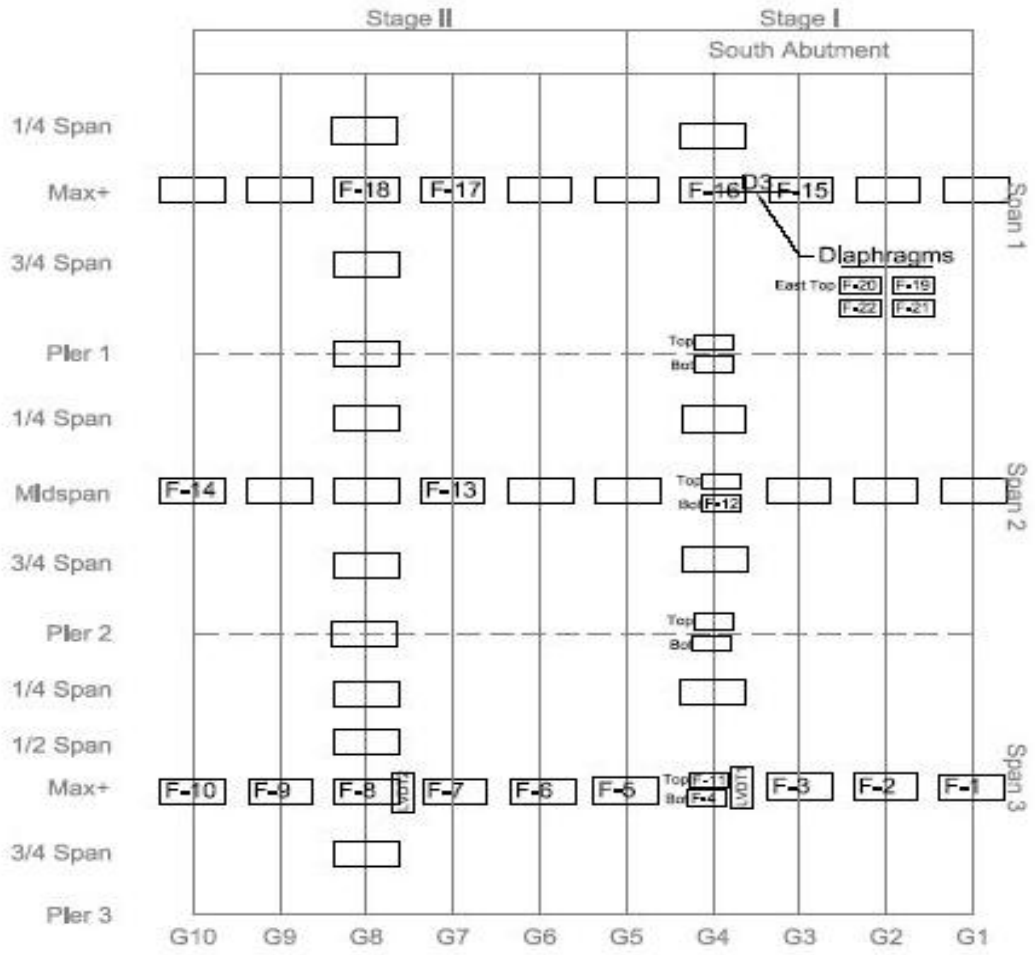

Figure 99. Doremus Avenue Bridge sensor arrangement

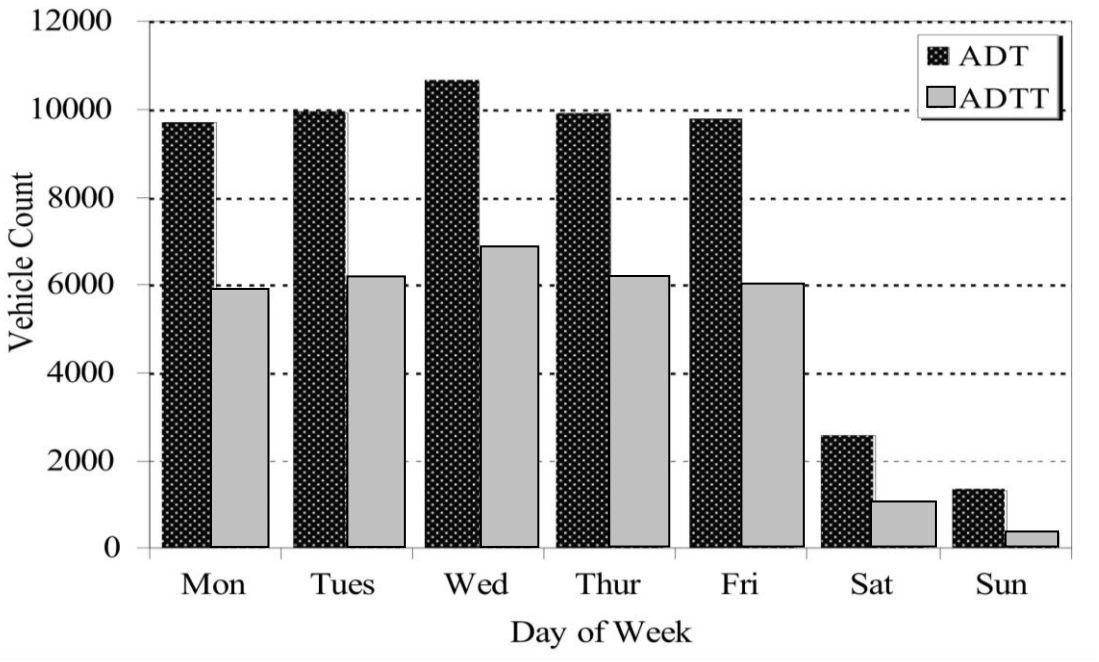

Figure 100. Traffic information for all four lanes of Doremus Avenue Bridge for a typical week

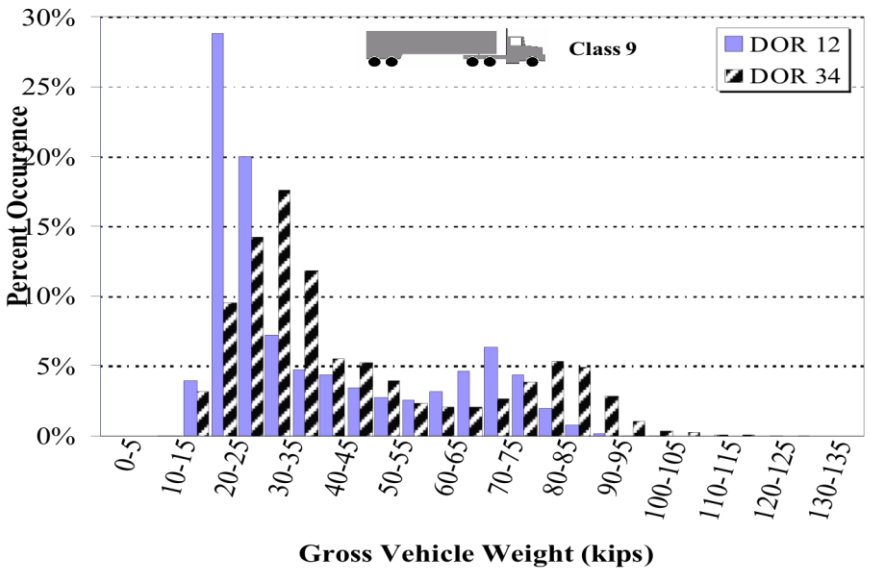

Figure 101. Gross weight distribution for five-axle (Class 9) trucks at Doremus Avenue Bridge

Trigger-Event Truck Data

A special data mode within the fatigue system was configured to capture the bridge response to heavy trucks. A table of trigger GVW is specified in the Datalogger program as shown in Table 16.

Table 16. Trigger thresholds of class and gross weight

Vehicle Class	Gross Weight,kips (kN)
4, 5, 6	55 (245)
7	66 (294)
8	77 (343)
9	88 (392)
10 to 15	100 (448)

If the WIM system signal shows a truck of a certain class exceeding the trigger GVW, the fatigue system begins recording a 14-second time history. These so-called trigger trucks are stored to a separate WIM file within the fatigue system. Trigger truck time history data is also useful for studying dynamic impact amplification, girder distribution, and deflection of the heaviest trucks on Doremus Avenue.

An extreme load event was captured by the WIM and fatigue systems on May 11, 2004. The WIM system reported a truck with a gross weight of more than 220,000 lb (Figure 102). The fatigue system was subsequently activated and strain data was captured (Figure 103). A truck that would have normally been suspected as an error was substantiated with the bridge stress record, which reached nearly 6 ksi. Considering that an HS20 design truck causes a stress of 2.2 ksi at this location, a truck of nearly three times HS20 was observed. This instance shows that a system of both traffic and bridge response data is valuable for tracking extreme truck loads. Later, local permit applications were reviewed for the area of Doremus Avenue. No matching legal permit configuration was found.

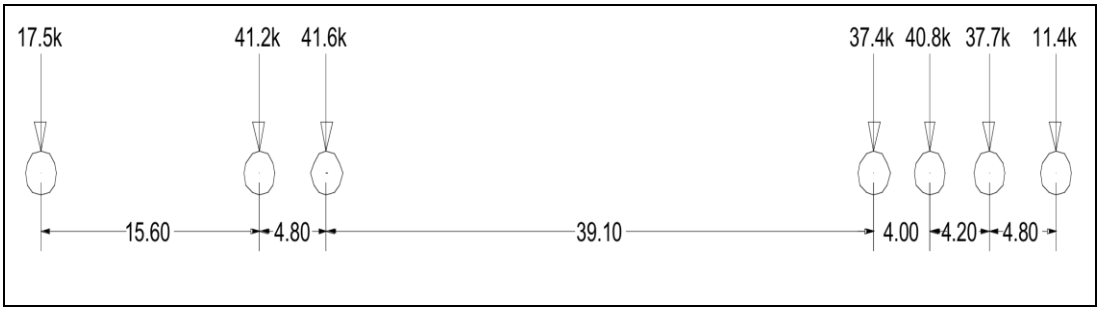

Figure 102. Extreme heavy truck observed at Doremus Avenue Bridge on 5/11/04 (weights are in kips, spacing in feet)

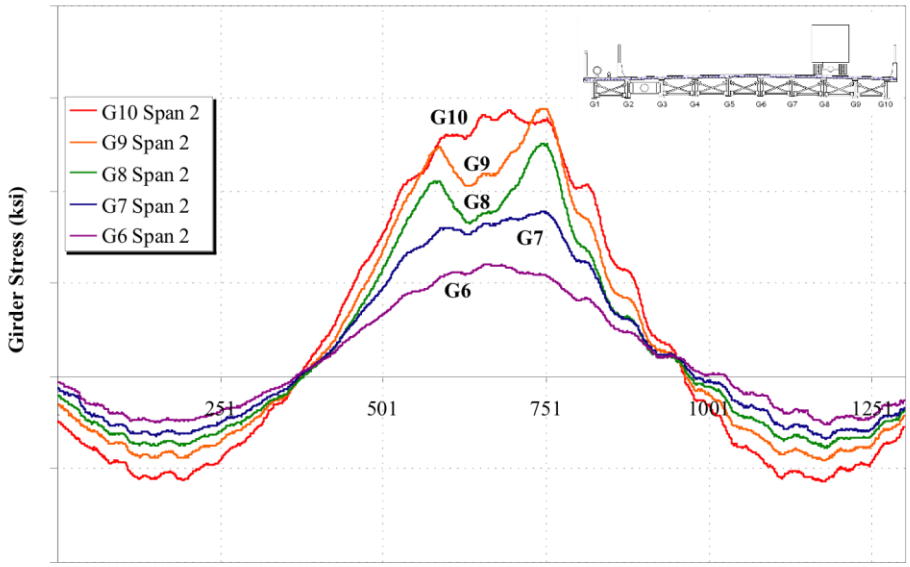

Figure 103. Measured stress history for Truck 3465 on 5/11/04 at Doremus Avenue Bridge

Bridge Modeling for Fatigue

Many methods are available for bridge modeling: finite element, grillage, semi-continuum (Jaeger and Bakht 1989), and beamline. For the application of numerous runs, the semi-continuum model is the most efficient model. The semi-continuum model has been widely used in previous truck load simulations (Laman and Ashbaugh 2000). Since the Doremus Avenue Bridge is composed of variable section plate girders, a weighted average method was used to obtain an effective moment of inertia for each girder. Unit loads were then applied to the semicontinuum model to generate an influence surface for the F-9 location (Figure 99). The model was run by using a time-lapse method to re-create the truck traffic on the bridge as it occurred. As mentioned previously, extensive live-load static and dynamic test results were used to verify this model for both strains and deflections. Using the timestamp and speed information contained in the WIM data, the axle loads are applied and the stresses are calculated for each 0.01-second time split. This procedure can be visualized as a truck animation where time is advanced in very small increments. A rainflow filter was applied to the output according to ASTM E1049-85 to extract stress cycles.

The field data and semi-continuum time-lapse model results are shown in Figure 104. The data set constitutes 1 week of WIM truck information and rainflow data. The location studied is the bottom flange of Girder 9, shown as F-9 in Figure **99**. This location is at the maximum positive moment position for Span 3. Additionally, a welded stiffener and attached cross frame are coincident at this location. The right wheels of trucks traveling in the northbound right lane pass directly over this location. Note that

the rainflow histogram shape and cycle counts are similar in Figure 104 for both the actual (left histogram) and the simulated data (right histogram). A lower threshold stress of 0.67 ksi (4.64 MPa) was imposed to eliminate erroneous and low-damage cycles. Relevant fatigue parameters for the rainflow histograms are presented in Table 17. The accumulated damage was calculated using the Palmgren-Miner Linear Damage Rule with an AASHTO LRFD fatigue detail of Category C using a detail constant, *A*, of 14.4 * 10^{11} MPa^3 (4.4 * 10^9 ksi^3). A total damage exceeding 1.0 represents the fatigue limit and therefore the structural detail is considered deficient or in need of repair.

To estimate the effect of truck superposition on fatigue, each truck in the WIM data was applied to the model independently. Figure 105 shows the effect of no truck superposition on the rainflow histogram. A reduction in the maximum stress range, Root-Mean-Cube (RMC) effective stress range, and overall cumulative damage was observed. Furthermore, the number of cycles above 0.67 ksi (4.64 MPa) was increased compared with the time-lapse model. Moreover, by neglecting truck superposition, events that were coincident are conservatively taken as independent, increasing the overall number of cycles.

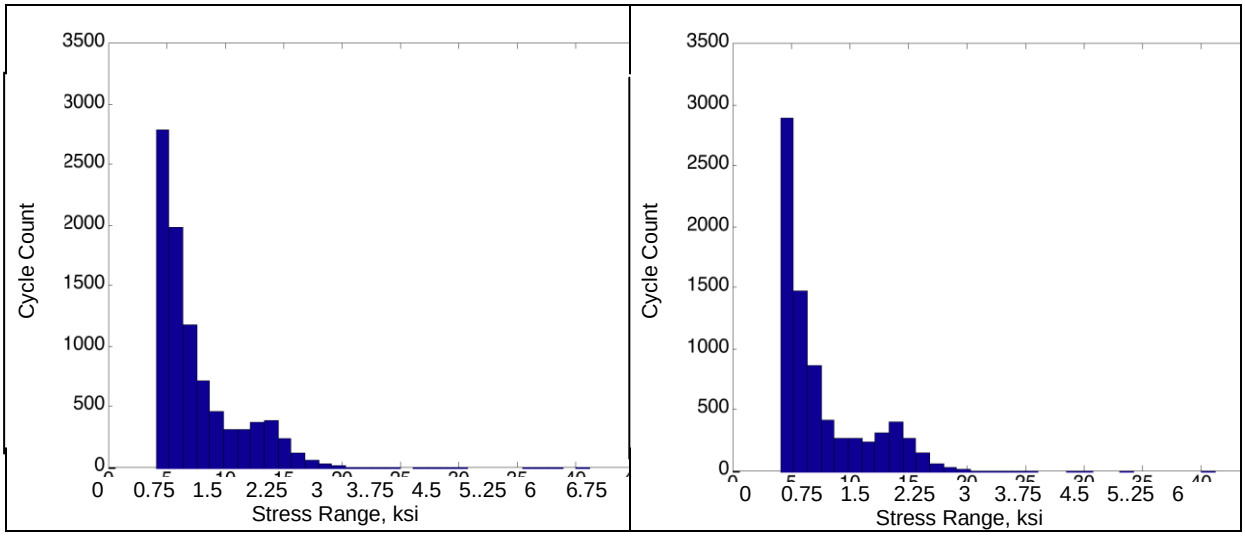

(a) (b)

Figure 104. One-week rainflow histograms for (a) field data and (b) semicontinuum model

Table 17. Fatigue parameters for field and model data

Parameter	Field Data	Time-Lapse Model	Model w/o Superposition
N cycles > 0.67 ksi (4.64 MPa)	9083	7794	7896
Max Stress, ksi (MPa)	5.88 (40.56)	5.88 (40.56)	5.55 (38.24)
RMC Stress, ksi (MPa)	1.34 (9.22)	1.37 (9.42)	1.31 (9.01)
Miner's Total Damage	$4.94 * 10^{-6}$	$4.53 * 10^{-6}$	$4.01* 10^{-6}$

Figure 104 shows that the semi-continuum model under predicts the peak and the midrange stress cycles. One possible reason is that the model considered only independent truck crossings, whereas the actual structure is subject to truck superposition. Depending on the coincident truck weight and location, the stresses would be increased. Based on the model results in, the omission of superposition results in a 4 percent decrease in the effective RMC stress range and 15 percent lower damage.

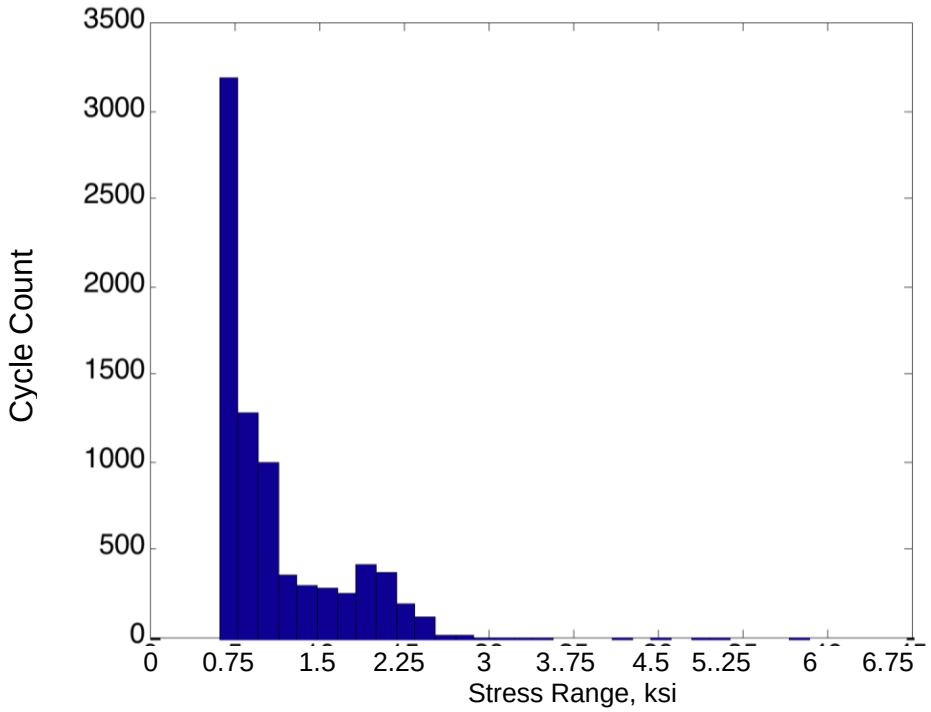

Figure 105. Results of semi-continuum simulation neglecting truck superposition.

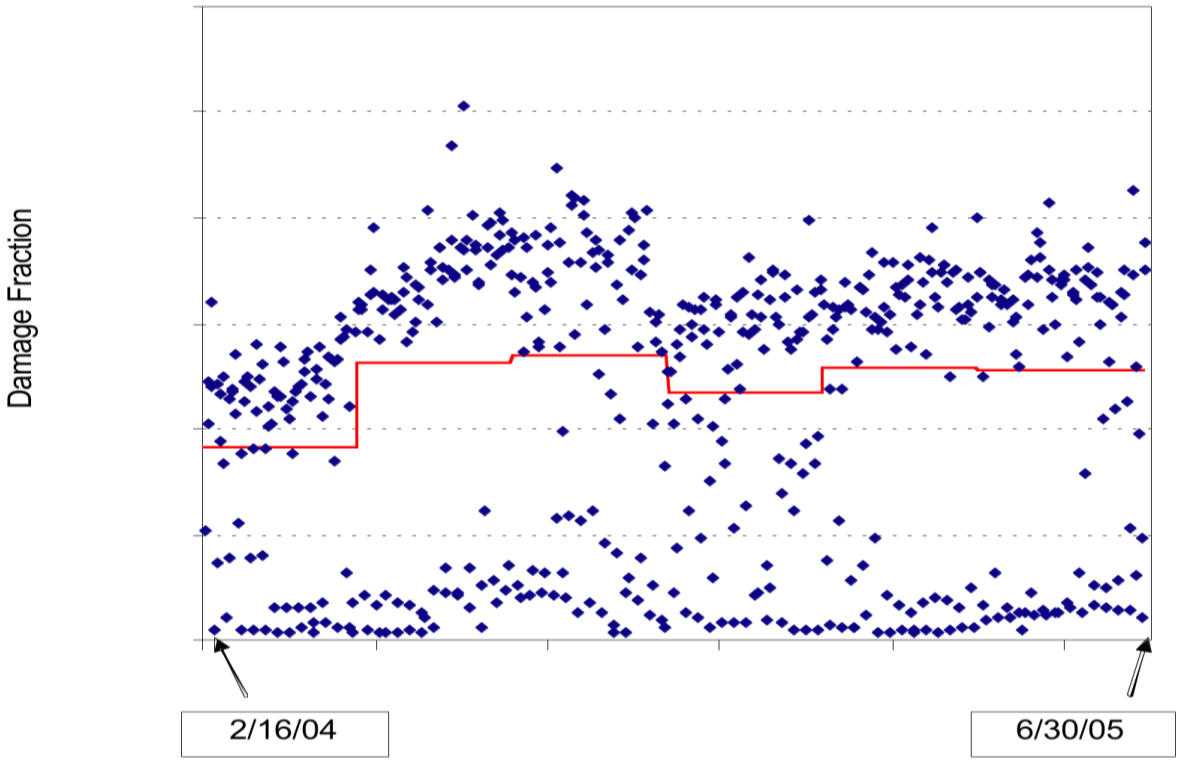

Figure 106. Daily fatigue damage for Doremus Bridge, Span 3, Girder 9 (data points) shown with 3-month equivalent blocks (solid line)

Damage Prediction

The monitoring of truck loads (WIM data) and bridge response (rainflow histograms) has continued for more than 2 years. Over this time, seasonal variations in damage are evident, as shown in Figure 106. The daily damage fraction was calculated from rainflow data using the Palmgren-Miner damage rule. The typical fatigue detail of the Doremus Avenue Bridge is transverse stiffeners welded to the bottom flange (Category B). The data shown covers a time span of 18 months, beginning in mid-February 2004 and extending through August 2005. A seasonal variation in the fatigue damage can be seen in Figure 106, where the damage surges in June 2004 and recedes in December 2004. Figure 106 also shows two distinct groups of data: a high-damage cluster and a low-damage cluster. The low-damage periods correspond to weekend days of low truck volume. Because weekdays account for the most fatigue damage, linear scaling of weekday stress ranges would result in a highly conservative remaining life prediction. For this reason, the minimum monitoring duration for fatigue damage should be a typical 7-day week. Further investigation shows that the truck volume at the Doremus Avenue Bridge tends to peak on Wednesdays, as shown in Figure 100. Fatigue damage also varies weekly and seasonally; however, 1 week can be considered the optimum short-term monitoring duration.

To account for the seasonality of fatigue damage, sampling could be done at intervals throughout the year. For example, given the periodic fluctuation shown in Figure 106 monitoring for 1 week every 3 months would be effective in capturing the seasonality. An example of 1-week measurements that represent the fatigue damage over a 3-month period is shown by the stepped solid line in **Figure** 106. The 75-year damage estimate using the intermittent 1-week sampling is shown in Table 18. Without prior stress data, determining when to monitor a bridge is difficult. One simple solution is to contact the state or local transportation authority with regard to stationary WIM data sites near the structure of interest. Since fatigue damage greatly depends on truck volume and weight, the WIM data is an indispensable resource. The NJDOT, for example, maintains 46 Strategic Highway Research Program (SHRP) WIM sites throughout the state. Given the WIM data, the researcher only to determine the truck volumes and equivalent RMC truck weights at intervals throughout a typical year to determine when to sample the stresses.

Given the short-term data, a methodology is needed to predict the future fatigue damage the structure will endure. Linear scaling is the simplest way to scale a current damage quantity to some future time. Linear scaling has been demonstrated by Hahin et al. (1993), who took brief strain readings at locations of critical fatigue details. The strain readings are stored as a rainflow histogram by the field computer. To determine the fatigue damage at some future time the engineer needs the following: the rainflow histogram of stresses, the fatigue detail constant, a linear damage rule (such as Palmgren-Miner), and the age of the bridge. Additional growth rates may be incorporated to account for an increase in truck volume. Hahin et al. sampled multiple bridges in Illinois for very brief periods, some as short as 8 hours. The future fatigue damage was estimated by linearly scaling to 1 day and then to 25 or more years. Growth rates for volume and truck weight increase were also included. A similar methodology was applied to the Doremus Avenue data. The linear damage from different durations of field measurement and linear estimates for Doremus Avenue are given in Table 18. The observed values for each duration were linearly scaled to provide an estimate of future fatigue damage.

The expected truck volume growth rate may also be considered for future damage estimation. Figure 107 shows the fatigue damage estimates for a bottom flange location on Span 3 Girder 9. The simple linear damage estimate is shown in the solid line, whereas the extrapolation with 4 percent growth is shown in the dashed curve. Despite the large increase in damage due to traffic growth, the detail is in little danger of fatigue cracking at 75 years. This is not surprising since the Doremus Avenue Bridge was designed according to the LRFD fatigue specifications with consideration for the high volume of port traffic. Rapid growth is expected for the Port Newark Container Terminal (PNCT). The PNCT container traffic in 2001 was 2.5 million 20-ft (6.1-m) equivalent units (TEU) and is expected to reach 5.3 million TEUs by 2015 (Nassif et al. 2002). Such rapid growth must be considered when making fatigue damage estimates for bridges in the surrounding region. Other factors, such as section loss due to

corrosion, may increase the damage rate. Periodically updating the prediction with traffic volume and inspection report data will help the engineer achieve a more accurate fatigue damage estimate.

Table 18. Simple linear extrapolation of field data given different data durations (Span 3, Girder 9)

		Observation Period					
		1 week	1 month	3 months	6 months	12 months	18 months
	Observed Damage	0.00002	0.00006	0.00017	0.00041	0.00082	0.00125
Prediction	In 5 years	0.00436	0.00385	0.00342	0.00408	0.00410	0.00416
	In 25 years	0.02182	0.01923	0.01712	0.02039	0.02050	0.02078
	In 75 years	0.06546	0.05770	0.05137	0.06118	0.06150	0.06233
	In 75 years using one week equivalent blocks	---	---	---	---	0.63750	0.06544

The effect of various data collection durations on the 75-year prediction of fatigue damage is given in Table 18. Data collected for 1 week, 1 month, 3 months, 6 months, and 8 months are linearly scaled to 75 years without consideration for growth. Data collection for up to 6 months is highly subject to seasonal fluctuations. Longer periods include the effect of both surges and recessions in damage and thus offer the best data set for fatigue predictions. The benefit of longer data collection is evident for the 75-year prediction in Table 18. As the collection duration increases, the predicted damage amount stabilizes to near 0.06. The data in Table 18 and show that, at its present state, the Doremus Avenue Bridge is in no danger of reaching the fatigue limit in the next 75 years. This is to be expected as the LRFD design specifications were used for the design.

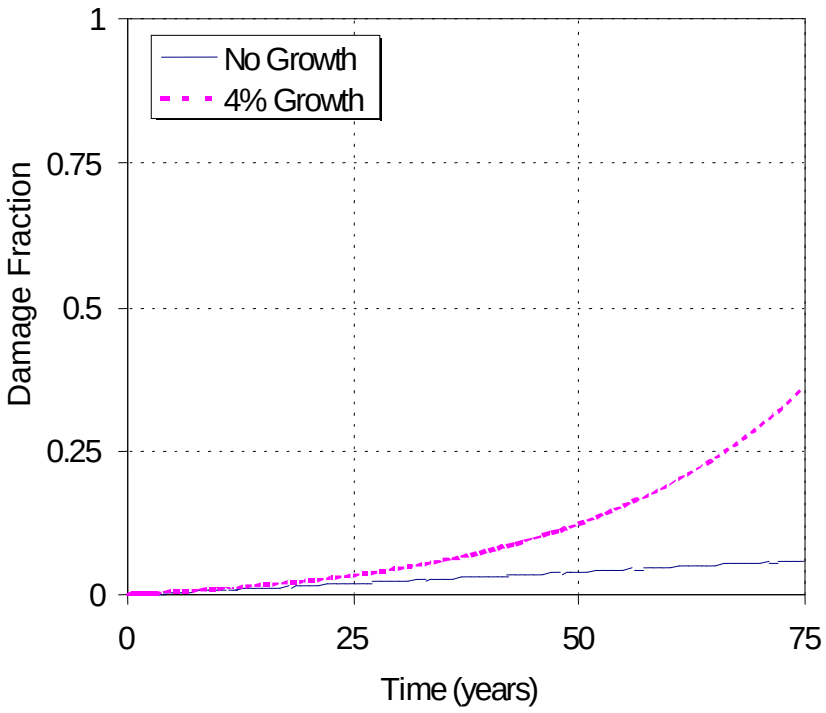

Figure 107. Fatigue damage estimates for Doremus Avenue, Span 3, Girder 9, bottom flange

Fatigue Summary

It is not practical to instrument and monitor a candidate bridge for periods greater than 1 month. Typically, managing agencies have a list of fatigue critical bridges that require further investigation. A testing or research organization cannot dedicate monitoring resources to one location for extended periods of time. Therefore, a compromise is needed between brief versus exhaustive monitoring. One solution is to monitor the bridge stresses at seasonal intervals. The sampling interval could be obtained from regional WIM data. For the case of the Doremus Avenue Bridge, the minimum monitoring duration was shown to be 1 week due to daily variations in truck volume. Furthermore, equivalent fatigue damage estimates can be made by sampling for 1 week every 3 months. Given the structural dimensions and properties of the Study Bridge and WIM data in the surrounding vicinity, a bridge model could be used to simulate stresses. Simulation using a structural model and WIM data has been shown to closely replicate the actual stress cycles. The implications of using bridge models with WIM data are tremendous: the ability to forecast the future fatigue damage more efficiently and spread monitoring resources over a larger population of structures. Simply input the properties of the structure and apply the known site-specific WIM truck information

to the model to generate a rainflow histogram of stresses. Quality control testing of the WIM data is obligatory. However, the quality control of the WIM data required to verify the procedure is far less extensive than instrumenting the entire bridge inventory owned by DOT. In this manner, most, if not all, the bridges under a state or local jurisdiction could be evaluated and reevaluated for fatigue by updating the WIM truck information for each site. Certain site characteristics such as traffic volume increase, truck weight increase, and girder section loss will accelerate fatigue damage. Site inspection data should be referenced to determine the extent of corrosion. Furthermore, more sophisticated extrapolation methods need to be investigated. These methods would account for the inherent scatter in the load (stress) spectra of the short-term data to yield a more realistic prediction of future fatigue damage.

RECOMMENDATIONS AND CONCLUSIONS

The primary objective of this study is to validate the AASHTO LRFD specifications through experimental and field-testing of the Doremus Avenue Bridge, New Jersey first AASHTO LRFD (1998) design. Several recommendations and conclusions are drawn from this research as follows:

Live-load Girder Distribution Factors (GDF) : The AASHTO LRFD live-load distribution factor (LDF) is proven to provide a more accurate LDF than the AASHTO Standard Specification based on field measurements and all three analytical methods conducted in this study: semi-continuum, grillage, and FE method. However, the AASHTO LRFD equation is complex with various unknown design parameters. Thus, new equations based on a simple "*S*-over" equation are proposed as part of this report that is shown in the executive summary of this report. It is recommended that the proposed equation be adopted in NJDOT design specification as an alternative to AASHTO LRFD.

Effective Flange Width: A more accurate and rational effective flange width (b_e) equation is also proposed. The proposed equation was calibrated using both laboratory and field measurements, as well as compared to available analytical methods. The proposed equation is shown in the executive summary of this report.

Deflection Limits: Truck traffic simulation based on the live load statistics developed and the Monte Carlo Method is found to produce bridge response similar to experimental measurements. The maximum 75-year deflection based on experimental and simulated results is estimated as one inch (24 mm). A live load deflection limit state function is defined. The resistance is taken as the deterministic Code (optional) limit of $L/800$ or $L/1000$ for the State of New Jersey. The static load effect is taken as the predicted maximum 75-year girder deflection. A reliability index of 6.02 and 3.75 is computed, respectively. With the inclusion of a 20% dynamic amplification factor, the

reliability indices reduce to 4.17 and 1.88, respectively. The assumption of normality for live load deflections is not supported and tends to underestimate the 75-year maximum value.

Dynamic Amplification Factor: In this study, the dynamic impact factor was measured and evaluated using detailed grillage models that include road roughness and truck models. The results were also compared to existing steel girder bridges in Michigan. For all tested bridges, the dynamic impact factors do not exceed 20 percent for heavy truck load with a minimum gross vehicle weight (GVW) of 60 kips.

Live Load: WIM measurements provide a comprehensive description of site-specific live load information. Since many drivers are not aware of their presence, records of overloaded vehicles are captured. Four percent of the Doremus WIM records from were observed to be overloaded trucks; GVW greater than legal limit of 80 kips.

5.1. Five dominant vehicle types are identified, which compose 92 percent of the truck population: 1) VT03 (Class 3: 2-axle, four-tire single unit trucks), VT10 (Class 6: 3-axle single unit trucks), VT19, VT20 (Class 7: both 4-axle single trailer trucks) and VT22 (Class 9: 5-axle single trailer trucks).

5.2. The GVWs of all dominant truck types correlate very well with WIM data obtained from the State of Michigan except for VT20, where more loaded trucks are observed in Michigan.

5.3. Statistics are computed for axle weights and spacings of dominant truck types. A better statistical description of axle weights for VT22 vehicles is obtained if the dataset is divided into unloaded (GVW < 60 kips) and loaded (GVW > 60 kips). Axle spacing 3 (AXS3) of VT22 should also be divided to two datasets; AXS3 < 16 ft and AXS3 >16 ft.

5.4. Multiple presence is affected by span length and volume of trucks. It is therefore site-specific and will generally vary from one site to another.

5.5. Multiple presence statistics are computed based on timestamp records of actual truck traffic. Three main traffic patterns are identified: single, following and side-by-side events. It is found that 66 percent of loading events are single trucks. Loading events are further classified with respect to vehicle class and total truck weight. The majority of trucks occurring simultaneously with another truck are light (GVW < 60 kips).

Fatigue: Fatigue resistance depends on type of detail, degree of corrosion and other deterioration. Load analysis requires the knowledge of load history (accumulated damage), current load spectra and prediction of future loads. The observed traffic stream is compared to the nominal fatigue evaluation model to gauge its effectiveness

in predicting fatigue damage at Doremus Avenue. The effect of measurement duration is also studied to determine the minimum sample size needed to make a stable and accurate fatigue life estimation. The procedures developed could be extended to simulate bridge live loads using site-specific weigh-in-motion (WIM) data applied to structural models. The resulting simulated stresses are then extrapolated, reducing or eliminating the need for labor-intensive field instrumentation.

REFERENCES

1. AASHTO, *Standard Specifications for Highway Bridges*. American Association State Highway and Transportation Officials, Washington, D.C., 1994
2. AASHTO-LRFD, *LRFD Specifications for Highway Bridges*. American Association State Highway and Transportation Officials, Washington, D.C.,1988
3. ABAQUS/Standard User's Manual. *Version 6.1, Hibbitt, Karlsson & Sorensen, Inc*. 2000
4. American Society for Testing and Materials. *E1049-85, Standard practices for cycle counting in fatigue analysis,* 1985
5. Bakht, B., and Pinjarkar, G. "Dynamic Testing of Highway Bridges." In *Transportation Research Record* 1223, 1989, pp 93-100
6. Ballard, R.F. Jr. "Method of Crosshole Seismic Testing" *Journal of Geotechnical Engineering Division, ASCE*, Vol. 102, No. GT 12, (1976), pp 1261-1273
7. Bathe, K.J. and Wilson, E.L. "Stability and Accuracy Analysis of Direct Integration Methods", *J. Earthquake Engrg Struct. Dyna* 1, (1973), pp 283-291
8. Biggs, J.M., Suer, H.S. and Louw, J.M. "Vibration of single Span Highway Bridges" *Transactions, ASCE*, Vol. 124, (1956), pp. 291-318
9. Billing, J.R. *Dynamic Tests of Bridges in Ontario, 1980 Data Capture, Test Procedure, and Data Processing*. Ministry of Transportation and Communication, Research and Development Reports, Vol. 26, 1982
10. Billing, J.R. "Dynamic Loading and Testing of Bridges in Ontario" *Canadian Journal of Civil Engineering*, Vol. 11, No. 4, December, (1984), pp 883-843.
11. Boothby, T. E. and Laman, J. A. (1999). "Cumulative Damage to Bridge Concrete Deck Slabs Due to Vehicle Loading," Journal of Bridge Engineering, Vol. 4, No. 1, February 1999
12. Bortsch, "Der Bauingenieur," p. 662.. 1921
13. Burke, M. P. (2001). "Superstructure Flexibility and Disintegration of Reinforced Concrete Deck Slabs: An LRFD Perspective," Transportation Research Record No. 1770, pp. 76-83, Paper No. 01-0132.

14. Cantieni, R. *Dynamic load tests on highway bridges in Switzerland: 60 years experience of EMPA*. *Tech. Rep. 211, Swiss Federal Lab. for Mat. Testing and Res*., Dubendorf, Switzerland, 1983

15. Cantieni, R. *Dynamic Behavior of Highway Bridges Under the Passage of Heavy Vehicles.* EMPA Report No. 220. EMPA, Dubendorf, Switzerland, 1992

16. Chatterjee, P.K., Datta, T.K., Surana, C.S. “Vibration of Continuous Bridges under Moving Vehicles” *Journal of Sound and Vibration*, Vol. 169, (1994), pp 619-632

17. Cook, J.P., "Composite Construction Methods," *John Wiley & Sons, New York*, 1977

18. Demitz, J. R., Mertz, D. R. and Gillespie, J. W. (2003). "Deflection Requirements for Bridges Constructed with Advanced Composite Materials," Journal of Bridge Engineering, Vol. 8, No. 2, March 2003

19. Elhebawey, M., Fu, C. C., Sahin, M. A., and Schelling, D. R., “Determination of Slab Participation from Weigh-In-Motion Bridge Testing,” *Journal of Bridge Engineering*, Vol. 4, No. 3, August 1999

20. Fancher, H., Ervin, R., MacAdam, C., and Winkler. “ Measurement and Representation of the Mechanical properties of truck leaf Springs” *Technical Paper Series 800905, Society of Automotive Engineers*, Warrendale, Pa., 1980

21. Federal Highway Administration (2001). “Traffic Monitoring Guide,” U.S. Department of Transportation, Office of Highway Policy Information.

22. Gindy, M. and Nassif, H. (2005a). “Application of Extreme Value Theory for the Prediction of Maximum Bridge Live Load Effects.” *Proceedings of the Ninth International Conference on Structural Safety and Reliability*, International Conference on Structural Safety and Reliability (ICOSSAR), Materials Damage, Bridges, and Buildings 3 Session, Rome, Italy, pp 1-7

23. Gindy, M. and Nassif, H. (2005b). “Reliability-Based Live Load Model for Serviceability Limit States.” *Proceedings of the Ninth International Conference on Structural Safety and Reliability*, International Conference on Structural Safety and Reliability (ICOSSAR), Life-Cycle Optimization, System Control 2 Session, Rome, Italy, pp 1-8

24. Gindy, M. and Nassif, H. (2007). “Prediction of Bridge Live Load Effects Based on the Theory of Extremes.” *Proceedings of the 10th International Conference on Applications of Statistics and Probability in Civil Engineering* (ICASP), Civil Engineering Risk and Reliability Association, Probabilistic and Statistical Prediction Session, Tokyo, Japan, pp 1-8

25. Green, M. F., Cebon, D., and Cole, D.J. "Effects of Vehicle Suspension Design on Dynamics of Highway Bridges", *ASCE, Journal of Structural Engineering*, Vol.121, (1995), pp 272-282

26. Gupta, R.K. and Traill-Nash, R.W. “Bridge Dynamic Loading Due to Road Surface Irregularities and Braking of Vehicle” *Earthquake Eng. Struct. Dynamics*, vol. 8, (1980), pp. 83-96

27. Hahin, C., South, J.M., Mohammadi, J., and Polpeddi, R.K. Accurate and Rapid Determination of Fatigue Damage in Steel Bridges. *Journal of Structural Engineering*. ASCE, 1993, **119**(1), 150-168

28. Hawk, H. and Ghali, A. “Dynamic Response of Bridges to Multiple Truck Loading” *Canadian Journal of Civil Engineering,* 8, (1981), pp 392-401

29. Hayes, M. D., Lesko, J. J., Haramis, J., Cousins, T. E., Gomez, J., and Masarelli, P. (2000). "Laboratory and Field Testing of Composite Bridge Superstructure," Journal of Composites for Construction, Vol. 4, No. 3, August 2000

30. Honda, H., Kobori, T., and Yamada, Y. “Dynamic Factor of Highway Steel Girder Bridges” *Proceedings, International Association of bridge and Structural Engineering*, P-98/86, Zurich, Switzerland, (May 1986), pp 57-75.

31. Humar, J.L., and Kashif, A.M. “Dynamic Response of Bridges under Traveling Loads" *Canadian Journal of Civil Engineering*, Vol. 20, 1994, pp 287-298.

32. Hwang, E.S. and Nowak, A.S. “Simulation of Dynamic Load for Bridges”, *J. Struct. Engrg. ASCE*, 117(5), 1991, pp 1413-1434.

33. Jaeger, L. G. and B. Bakht. “Multiple Presence Reduction Factors for Bridges” *Proc. Structures Congress, Structural Division, ASCE*, 1987, pp 47-59.

34. Karman, T. v., “Beitrage zur technischen Mechanik und technischen Physik,” Berlin, 1924

35. Laman, J. and Nowak, A. Fatigue-load model for girder bridges. *Journal of Structural Engineering*, ASCE, 1996, 122(7), 726-733.

36. Laman, J.A. and Ashbaugh, J.R. Highway network bridge fatigue damage potential of special truck configurations. *Transportation Research Record 1996*, pp. 81-92, 2000 (National Academy Press: Washington D.C.)

37. Liu, M. *A 3-D Dynamic Model For Bridge-Road-Vehicle System*. Unpublished Mater’s Thesis, Bradley University, Peoria, Illinois, 1996, 180p.

38. Matsuishi, M. and Endo, T. Fatigue of metals subjected to varying stress-fatigue lives under random loading, in *Preliminary Proceedings of the Kyushu District Meeting, pages 37-40. The Japan Society of Mechanical Engineers. In Japanese*, 1968

39. Metzer, W. ,“Die Mittragende Breite,” Luftfahrtforschung, 4, pp. 1-20 (in German), 1929)

40. Microsoft Terraserver Aerial Images: http://terrraserver.microsoft.com (accessed October 2005)

41. Moses, F., Schilling, C.G., and Raju, K.S. Fatigue evaluation procedures for steel bridges. *National Cooperative Highway Research Program Report 299*, 1987, (Transportation Research Board: Washington D.C.)

42. Mulcahy, N.L., Pulmano, V.A. and Traill-Nash, R.W. *Dynamic response of bridge decks to vehicle loads by the finite strip approach*. Proc. of 3rd Int. Conf. in Australia on FEM, The University of New South Wales, 1979

43. Nassif, H., Gucunski, N., Abu-Amra, T., Gindy, M., and Balic, M. *Analytical modeling and instrumentation planning of the Doremus Avenue Bridge*. Final Report, FHWA-NJ-2002-08, July 2002

44. Nassif, H. H. Liu, M. and Ertekin, A. "Model Validation for Bridge-Road-Vehicle Dynamic Interaction System" *ASCE Journal of Bridge Engineering*, 2002

45. Nassif, H. H. and Nowak, A.S. "Dynamic Load Spectra For Girder Bridges." *Journal of the Transportation Research Board*, No. 1476, TRB, National Research Council, Washington, D.C., 1995, pp 69-83.

46. Nassif, H.H. *Live Load Spectra For Girder Bridges*. Ph.D. Dissertation, The University of Michigan, Department of Civil and Environmental Engineering, 1993, p. 250

47. Newmark, N.M. “A Method of Computation for Structural Dynamics”, *J. Engrg. Mech., ASCE*, 85, 1959, pp 67-94

48. Nowak, A.S., Nassif, H.N., and DeFraine, L. “Effect of truck loads on bridges.” *Journal of Transportation Engineering*. 1993, **119**(6), 853-867

49. O’Connor, C., and Chan, T.H.T. “Dynamic Wheel Loads from Bridges Strains”, *Journal Structural Engineering, ASCE*, Vol. 114, 1988, pp 1703-1723

50. O’Connor, C., and Pritchard, R.W. “Impact Studies on Small Composite Girder Bridge” *Journal Structural Engineering, ASCE*, Vol. 111, 1985, pp 641-653

51. OHBDC. *Ontario Highway Bridge Design Code*. Ontario Ministry of Transportation, Ontario, Canada, 3rd Edition, 1993

52. Paultre, P., Chaalial, O., and Prouix, J. "Bridge Dynamics and Dynamic Amplification Factors - A Review of Analytical and Experimental Findings" *Canadian Journal of Civil Engineering*, Vol. 19, pp 260-278; and discussion Vol. 20, pp 876-878,1992

53. Paultre, P., Prouix, J., and Talbot, M. "Dynamic Testing Procedures for Highway Bridges Using Traffic Loads", *ASCE, Journal of Structural Engineering*, Vol. 121, 1995, pp 362-376

54. Roeder, C. W., Barth, K. and Bergman, A. (2002). "Improved Live Load Deflection Criteria for Steel Bridges," NCHRP Project 20- 7[133], Final Report, November 2002.

55. Savard M., Fafard M., Mallikarjuna, and Halchini C. *A Refined 3D Model for Bridge-Vehicle Systems*, 1994

56. Schule, “Mitteilungen der Eidgenossischen Materialprufungsanstalt,” Zurich, 1909

57. Socie, D.F. and Downing, S.D. “Simple rainflow counting algorithms.” *International Journal of Fatigue*, 1982, **4**(1), pp. 31-40

58. Swiss Association for Standardization. SIA 160, *Actions on Structures*. Swiss Society of Engineers and Architects, Zurich, 1989

59. Timoshenko, S., and Goodier, J.N., "Theory of Elasticity," *McGraw-Hill Book Company, Inc., New York*, 1951

60. Ugur, H.E. *Girder Distribution Factors for Skew Steel Girder bridges*. unpublished Master's Thesis, Bradley University, Peoria, Illinois, 1995, p.157

61. Veletsos, A. S., and Huang, T. "Analysis of Dynamic Response of Highway Bridges" *Journal of the engineering mechanics division, proceedings of ASCE*, Vol. 96, No. EM5, Ref. 35, (October 1970), pp 593-620

62. Wegmuller, A. W., "Overload Behavior of Composite Steel-Concrete Bridges," *Proceedings of the American Society of Civil Engineers*, Vol. 103, No. ST9, September 1977

63. Yang, Y.B., and Lin, B.-H. "Vehicle-bridge interaction analysis by dynamic condensation method" *J. Struct. Eng*., 121(11), 1636-1643," J. Struct. Eng., 1995